Hadronic molecules

Feng-Kun Guo[*]

CAS Key Laboratory of Theoretical Physics, Institute of Theoretical Physics,
Chinese Academy of Sciences, Beijing 100190, China
and School of Physical Sciences, University of Chinese Academy of Sciences,
Beijing 100049, China

Christoph Hanhart[†]

Institute for Advanced Simulation,
Institut für Kernphysik and Jülich Center for Hadron Physics,
Forschungszentrum Jülich, D-52425 Jülich, Germany

Ulf-G. Meißner[‡]

Helmholtz-Institut für Strahlen-und Kernphysik and Bethe Center for Theoretical Physics,
Universität Bonn, D-53115 Bonn, Germany
and Institute for Advanced Simulation, Institut für Kernphysik
and Jülich Center for Hadron Physics, Forschungszentrum Jülich, D-52425 Jülich, Germany

Qian Wang[§]

Helmholtz-Institut für Strahlen-und Kernphysik and Bethe Center for Theoretical Physics,
Universität Bonn, D-53115 Bonn, Germany

Qiang Zhao[‖]

Institute of High Energy Physics, Chinese Academy of Sciences, Beijing 100049, China,
School of Physical Sciences, University of Chinese Academy of Sciences, Beijing 100049, China,
and Theoretical Physics Center for Science Facilities, Chinese Academy of Sciences,
Beijing 100049, China

Bing-Song Zou[¶]

CAS Key Laboratory of Theoretical Physics, Institute of Theoretical Physics,
Chinese Academy of Sciences, Beijing 100190, China
and School of Physical Sciences, University of Chinese Academy of Sciences,
Beijing 100049, China

(published 8 February 2018)

A large number of experimental discoveries especially in the heavy quarkonium sector that did not meet the expectations of the until then very successful quark model led to a renaissance of hadron spectroscopy. Among various explanations of the internal structure of these excitations, hadronic molecules, being analogs of light nuclei, play a unique role since for those predictions can be made with controlled uncertainty. Experimental evidence of various candidates of hadronic molecules and methods of identifying such structures are reviewed. Nonrelativistic effective field theories are the suitable framework for studying hadronic molecules and are discussed in both the continuum and finite volumes. Also pertinent lattice QCD results are presented. Further, the production mechanisms and decays of hadronic molecules are discussed and comments are given on the reliability of certain assertions often made in the literature.

CONTENTS

[*]fkguo@itp.ac.cn
[†]c.hanhart@fz-juelich.de
[‡]meissner@hiskp.uni-bonn.de
[§]wangqian@hiskp.uni-bonn.de
[‖]zhaoq@ihep.ac.cn
[¶]zoubs@itp.ac.cn

I. INTRODUCTION

With the discovery of deuterium in 1931 and the neutron in 1932, the first bound state of two hadrons, i.e., the deuteron composed of one proton and one neutron, became known. The deuteron is very shallowly bound by a mere MeV per nucleon, i.e., it is located just below the neutron-proton continuum threshold. Furthermore, it has a sizable spatial extension. These two features can be used for defining a hadronic

molecule. A more precise definition will be given in the course of this review.

Then the first meson, the pion, as the carrier particle of the nuclear force proposed in 1935 by Yukawa was discovered in 1947, followed by the discovery of a second meson, the kaon, in the same year. Since then, many different hadrons have been observed. Naturally hadronic molecules other than the deuteron have been expected. The first identified meson-baryon molecule, i.e., the $\Lambda(1405)$ resonance composed of one kaon and one nucleon was predicted by Dalitz and Tuan (1959) and observed in the hydrogen bubble chamber at Berkeley in 1961 (Alston *et al.*, 1961) several years before the quark model was proposed. With the quark model developed in the early 1960s, it became clear that hadrons are not elementary particles, but composed of quarks and antiquarks. In the classical quark model, a baryon is composed of three quarks and a meson is composed of one quark and one antiquark. In this picture, the $\Lambda(1405)$ resonance is an excited state of a three-quark (*uds*) system with one quark in an orbital *P*-wave excitation. Ten years later, the theory of strong interactions, quantum chromodynamics (QCD), was proposed to describe the interactions between quarks as well as gluons. The gluons are the force carriers of the theory that also exhibit self-interactions due to the non-Abelian nature of the underlying gauge group $\text{SU}(3)_C$, where *C* denotes the color degree of freedom. In QCD the basic constituents of the hadrons are both quarks and gluons. Therefore, the structure of hadrons is more complicated than the classical quark model allows. There may be glueballs (which contain only valence gluons), hybrids (which contain valence quarks as well as gluons), and multiquark states (such as tetraquarks or pentaquarks). Note, however, that in principle the quark model also allows for certain types of multiquark states (Gell-Mann, 1964).

While the classical quark model is very successful in explaining properties of the spatial ground states of the flavor SU(3) vector meson nonet, baryon octet, and decuplet, it fails badly even for the lowest spatial excited states in both meson and baryon sectors.

In the meson sector, the lowest spatial excited SU(3) nonet is supposed to be the lowest scalar nonet which includes the $f_0(500)$, the $\kappa(800)$, the $a_0(980)$, and the $f_0(980)$. In the classical constituent quark model, these scalars should be $q\bar{q}(L = 1)$ states, where *L* denotes the orbital angular momentum, with the $f_0(500)$ as an $(u\bar{u} + d\bar{d})/\sqrt{2}$ state, the $a_0^0(980)$ as an $(u\bar{u} - d\bar{d})/\sqrt{2}$ state, and the $f_0(980)$ as mainly an $s\bar{s}$ state. This picture, however, fails to explain why the mass of the $a_0(980)$ is degenerate with the $f_0(980)$ instead of being close to the $f_0(500)$, as is the case of ρ and ω in the vector nonet. Instead, this kind of mass pattern can be easily understood in the tetraquark picture (Jaffe, 1977a) or in a scenario where these states are dynamically generated from the meson-meson interaction (Weinstein and Isgur, 1982; Janssen *et al.*, 1995; Oller, Oset, and Ramos, 2000), with the $f_0(980)$ and the $a_0(980)$ coupling strongly to the $\bar{K}K$ channel with isospins 0 and 1, respectively.

In the baryon sector, a similar phenomenon also seems to be happening (Zou, 2008). In the classical quark model, the lowest spatial excited baryon is expected to be a (*uud*) N^* state with one quark in an orbital angular momentum $L = 1$

state to have spin parity $1/2^-$. However, experimentally, the lowest negative parity N^* resonance is found to be the $N(1535)$, which is heavier than two other spatial excited baryons: the $\Lambda(1405)$ and the $N(1440)$. This is the long-standing mass reversal problem for the lowest spatial excited baryons. Furthermore, it is also difficult to understand the strange decay properties of the $N(1535)$, which seems to couple strongly to the final states with strangeness (Liu and Zou, 2006), as well as the strange decay pattern of another member of the $1/2^-$ nonet, the $\Lambda(1670)$, which has a coupling to $\Lambda\eta$ much larger than to NK and $\Sigma\pi$ according to its branching ratios listed in the tables in the Review of Particle Physics by the Particle Data Group (PDG) (Patrignani *et al.*, 2016). All these difficulties can be easily understood by assuming large five-quark components in them (Helminen and Riska, 2002; Liu and Zou, 2006; Zou, 2008) or considering them to be dynamically generated meson-baryon states (Kaiser, Siegel, and Weise, 1995; Oset and Ramos, 1998; Oller, Oset, and Ramos, 2000; Oller and Meißner, 2001; Inoue, Oset, and Vicente Vacas, 2002; Hyodo *et al.*, 2003; Garcia-Recio, Lutz, and Nieves, 2004; Magas, Oset, and Ramos, 2005; Huang *et al.*, 2007; Bruns, Mai, and Meißner, 2011).

No matter which configurations are realized in multiquark states, such as colored diquark correlations or colorless hadronic clusters, the mass and decay patterns for the lowest meson and baryon nonets strongly suggest that one must go beyond the classical, so-called quenched, quark model. The unquenched picture has been further supported by more examples of higher excited states in the light quark sector, such as the $f_1(1420)$ as a $K^*\bar{K}$ molecule (Törnqvist, 1994), and by many newly observed states with heavy quarks in the first decade of the new century, such as the $D_{s0}^*(2317)$ as a DK molecule or tetraquark state, or $X(3872)$ as a $D^*\bar{D}$ molecule or tetraquark state (Chen, Chen *et al.*, 2016). In fact, the possible existence of hadronic molecules composed of two charmed mesons was already proposed by Voloshin and Okun (1976) and supported by Törnqvist (1994) later within a one-pion exchange model.

Although many hadron resonances were proposed to be dynamically generated states from various hadron-hadron interactions or multiquark states, most of them cannot be clearly distinguished from classical quark model states due to tunable ingredients and possible large mixing of various configurations in these models. An example is the already mentioned $\Lambda(1405)$. Until 2010, i.e., 40 years after it was predicted and observed as the $\bar{K}N$ molecule, the PDG (Nakamura *et al.*, 2010) still claimed that "the clean Λ_c spectrum has in fact been taken to settle the decades-long discussion about the nature of the $\Lambda(1405)$—a true three-quark state or mere $\bar{K}N$ threshold effect—unambiguously in favor of the first interpretation." Only after many analyses of various relevant processes, the PDG (Patrignani *et al.*, 2016) now acknowledges the two-pole structure of the $\Lambda(1405)$ (Oller and Meißner, 2001) and thus a dynamical generation is most probable.

One way to unambiguously identify a multiquark state (including hadronic molecular configurations) is the observation of resonances decaying into a heavy quarkonium plus a meson with nonzero isospin made of light quarks or plus a baryon made of light quarks. Since 2008, several such states

have been claimed, six Z_c states, two Z_b states, and two P_c states; details on the experimental situation are given in the next section. Among these newly claimed states, the two P_c states are quite close to the predicted hadronic molecular states (Wu *et al.*, 2010; Wang *et al.*, 2011; Z.-C. Yang *et al.*, 2012; Xiao, Nieves, and Oset, 2013). However, many of those states are challenged by some proposed kinematic explanations, such as threshold cusp effects (Bugg, 2011; Swanson, 2015), triangle singularity effects (Chen, Liu, and Matsuki, 2013; Wang, Hanhart, and Zhao, 2013a; Guo *et al.*, 2015), etc. Some of these claims were challenged by Guo, Hanhart, Wang, and Zhao (2015) where strong support is presented that at least some of the signals indeed refer to S-matrix poles.

Further experimental as well as theoretical studies are necessary to settle the question which of the claimed states indeed exist. Nevertheless, the observation of at least some of these new states opens a new window for the study of multiquark dynamics. Together with many other newly observed states in the heavy quarkonium sector, they led to a renaissance of hadron spectroscopy. Among various explanations of the internal structure of these excitations, hadronic molecules, being analogs of the deuteron, play a unique role since for those states predictions can be made with controlled uncertainty, especially for the states with one or both hadrons containing heavy quark(s). In fact most of these observed exotic candidates are indeed closely related to open-flavor S-wave thresholds. To study these hadronic molecules, both nonrelativistic effective field theories (EFTs) and pertinent lattice QCD calculations are the suitable frameworks. Especially, Weinberg's famous compositeness criterion (Weinberg, 1963a, 1963b) (and extensions thereof), which pinned down the nature of the deuteron as a proton-neutron bound state, is applicable here. The pole location in the corresponding hadron-hadron scattering S matrix could also shed light on the nature of the resonances as extended hadronic molecules or compact states.

The revival of hadron spectroscopy is also reflected in a number of review articles. A few years ago, Klempt and collaborators gave two broad reviews on exotic mesons (Klempt and Zaitsev, 2007) and baryons (Klempt and Richard, 2010). Other more recent pertinent reviews include Brambilla *et al.* (2011), Olsen (2015), Chen, Chen *et al.* (2016), Hosaka *et al.* (2016), Oset *et al.* (2016), H.-X. Chen *et al.* (2017), Dong, Faessler, and Lyubovitskij (2017), Esposito, Pilloni, and Polosa (2017), Lebed, Mitchell, and Swanson (2017), and Olsen, Skwarnicki, and Zieminska (2018). Among various theoretical models for these new hadrons, we mainly cite those focusing on hadronic molecules and refer the interested reader to the previously mentioned comprehensive reviews for more references on other models.

This paper is organized as follows: In Sec. II, we discuss the experimental evidence for states that could possibly be hadronic molecules. In Sec. III, after a short review of the basic S-matrix properties, we give a general definition of hadronic molecules and discuss related aspects. Then, in Sec. IV, nonrelativistic effective field theories tailored to investigate hadronic molecules are formulated, followed by a brief discussion of hadronic molecules in lattice QCD in Sec. V. Section VI is devoted to the discussion of phenomenological manifestations of hadronic molecules, with a particular emphasis on clarifying certain statements from

the literature that have been used to dismiss certain states as possible hadronic molecules. We end with a short summary and outlook in Sec. VII. We mention that this field is very active and thus only references that appeared before April 2017 are included.

II. CANDIDATES OF HADRONIC MOLECULES: EXPERIMENTAL EVIDENCE

In this section we briefly review what is known experimentally about some of the most promising candidates for exotic states. Already the fact that those are all located close to some two-hadron continuum channels indicates that the two-hadron continuum is of relevance for their existence. We will show that many of those states are located near *S*-wave thresholds in both light and heavy hadron spectroscopy, which is not only a natural property of hadronic molecules, which are QCD bound states of two hadrons (a more proper definition will be given in Sec. III.B), but also a prerequisite for their identification as will be discussed in Sec. III. In the course of this review, we will present other arguments why many of these states should be considered as hadronic molecules and what additional experimental input is needed to further confirm this assignment.

In Tables I and II we present the current status for exotic candidates in the meson sector. Exotic candidates in the baryon sector are listed later in Table IV. Besides the standard properties we also quote for each state the nearest relevant *S*-wave threshold as well as its distance to that threshold. Note that only thresholds of narrow states are quoted since these are the only ones of relevance here (Guo and Meißner, 2011). Otherwise, the bound system would also be broad (Filin *et al.*, 2010). In addition, as a result of the centrifugal barrier one expects that if hadronic molecules exist, they should first appear in the *S* wave which is why in this review we do not consider *P* or higher partial waves although there is no principle reason for the nonexistence of molecular states in the *P* wave.

A. Light mesons

1. Scalars below 1 GeV

The lowest *S*-wave two-particle thresholds in the hadron sector are those for two pseudoscalar mesons, $\pi\pi$, πK, $\eta\pi$, and $K\bar{K}$. Those channels carry scalar quantum numbers. The pion pair is in either an isoscalar or an isotensor state, and the isovector state is necessarily in an odd partial wave. It turns out that there is neither a resonant structure in the isotensor $\pi\pi$ nor in the isospin $3/2$ πK *S*-wave; however, there are resonances observed experimentally in all other channels. According to the conventional quark model, a scalar meson of $q\bar{q}$ with $J^P = 0^+$ carries one unit of orbital angular momentum. Thus, the mass range of the lowest scalars is expected to

TABLE I. Mesons that contain at most one heavy quark that cannot be easily accommodated in the $q\bar{q}$ quark model. Their quantum numbers $I^G(J^{PC})$, masses, widths, the nearby *S*-wave thresholds, $m_{\text{threshold}}$, where we add in brackets $M - m_{\text{threshold}}$, and the observed decay modes are listed in order. The data without references are taken from the 2016 edition of the Review of Particle Physics (Patrignani *et al.*, 2016).

State	$I^G(J^{PC})$	M (MeV)	Γ (MeV)	S-wave threshold(s) (MeV)	Decay mode(s) [branching ratio(s)]
$f_0(500)^{\text{a}}$	$0^+(0^{++})$	449^{+22}_{-16}	550 ± 24	$\pi\pi(173^{+22}_{-16})$	$\pi\pi$ (dominant)
					$\gamma\gamma$
$\kappa(800)$	$\frac{1}{2}(0^+)$	682 ± 29	547 ± 24	$K\pi(48 \pm 29)$	πK
$f_0(980)$	$0^+(0^{++})$	990 ± 20	10–100	$K^+K^-(3 \pm 20)$	$\pi\pi$ (dominant)
				$K^0\bar{K}^0(-5 \pm 20)$	$K\bar{K}$
					$\gamma\gamma$
$a_0(980)$	$1^-(0^{++})$	980 ± 20	50–100	$K\bar{K}(-11 \pm 20)$	$\eta\pi$ (dominant)
					$K\bar{K}$
					$\gamma\gamma$
$f_1(1420)$	$0^+(1^{++})$	1426.4 ± 0.9	54.9 ± 2.6	$K\bar{K}^*(39.1 \pm 0.9)$	$K\bar{K}^*$ (dominant)
					$\eta\pi\pi$ (possibly seen)
					$\phi\gamma$
$a_1(1420)$	$1^-(1^{++})$	1414^{+15}_{-13}	153^{+8}_{-23}	$K\bar{K}^*(27^{+15}_{-13})$	$f_0(980)\pi$ (seen)
$X(1835)$	$?^?(0^{-+})$	$1835.8^{+4.0}_{-3.2}$	112 ± 40	$p\bar{p}(-40.7^{+4.0}_{-3.2})$	$p\bar{p}$
					$\eta'\pi\pi$
					$K^0_S K^0_S \eta$
$D^*_{s0}(2317)^+$	$0(0^+)$	2317.7 ± 0.6	< 3.8	$DK(-45.1 \pm 0.6)$	$D^+_s \pi^0$
$D_{s1}(2460)^+$	$0(1^+)$	2459.5 ± 0.6	< 3.5	$D^*K(-44.7 \pm 0.6)$	$D^{*+}_s \pi^0 [(48 \pm 11)\%]$
					$D^+_s \gamma [(18 \pm 4)\%]$
					$D^+_s \pi^+\pi^- [(4 \pm 1)\%]$
					$D^*_{s0}(2317)^+ \gamma [(4^{+5}_{-2})\%]$
$D^*_{s1}(2860)^+$	$0(1^-)$	2859 ± 27	159 ± 80	$D_1(2420)K(-59 \pm 27)$	DK
					D^*K

$^{\text{a}}$The mass and width are derived from the pole position quoted by Peláez (2016) via $\sqrt{s_p} = M - i\Gamma/2$.

TABLE II. Same as Table I but in the charmonium and bottomonium sectors. A blank in the fifth column means that there is no relevant nearby *S*-wave threshold.

State	$I^G(J^{PC})$	M (MeV)	Γ (MeV)	*S*-wave threshold(s) (MeV)	Observed mode(s) (branching ratios)
$X(3872)$	$0^+(1^{++})$	3871.69 ± 0.17	< 1.2	$D^{*+}D^- + \text{c.c.}(-8.15 \pm 0.20)$ $D^{*0}\bar{D}^0 + \text{c.c.}(0.00 \pm 0.18)$	$B \to K[\bar{D}^{*0}D^0](> 24\%)$ $B \to K[D^0\bar{D}^0\pi^0](> 32\%)$ $B \to K[J/\psi\pi^+\pi^-](> 2.6\%)$ $B \to K[J/\psi\pi^+\pi^-\pi^0]$ $p\bar{p} \to [J/\psi\pi^+\pi^-]...$ $pp \to [J/\psi\pi^+\pi^-]...$ $B \to K[J/\psi\omega](> 1.9\%)$ $B \to [J/\psi\gamma](> 6 \times 10^{-3})$ $B \to [\psi(2S)\gamma](> 3.0\%)$
$X(3940)$	$?^?(?^{??})$	3942.0 ± 9	37^{+27}_{-17}	$D^*\bar{D}^*(-75.1 \pm 9)$	$e^+e^- \to J/\psi[D\bar{D}^*]$
$X(4160)$	$?^?(?^{??})$	4156^{+29}_{-25}	139^{+110}_{-60}	$D^*\bar{D}^*(139^{+29}_{-25})$	$e^+e^- \to J/\psi[D^*\bar{D}^*]$
$Z_c(3900)$	$1^+(1^{+-})$	3886.6 ± 2.4	28.1 ± 2.6	$D^*\bar{D}(10.8 \pm 2.4)$	$e^+e^- \to \pi[D\bar{D}^* + \text{c.c.}]$ $e^+e^- \to \pi[J/\psi\pi]$
$Z_c(4020)$	$1(?^?)$	4024.1 ± 1.9	13 ± 5	$D^*\bar{D}^*(7.0 \pm 2.4)$	$e^+e^- \to \pi[D^*\bar{D}^*]$ $e^+e^- \to \pi[h_c\pi]$ $e^+e^- \to \pi[\psi'\pi]$
$Y(4260)$	$?^?(1^{--})$	4251 ± 9	120 ± 12	$D_1\bar{D} + \text{c.c.}(-38.2 \pm 9.1)$ $\chi_{c0}\omega(53.6 \pm 9.0)$	$e^+e^- \to J/\psi\pi\pi$ $e^+e^- \to \pi D\bar{D}^* + \text{c.c.}$ $e^+e^- \to \chi_{c0}\omega$ $e^+e^- \to X(3872)\gamma$
$Y(4360)$	$?^?(1^{--})$	4346 ± 6	102 ± 10	$D_1\bar{D}^* + \text{c.c.}(-85 \pm 6)$	$e^+e^- \to \psi(2S)\pi^+\pi^-$
$Y(4660)$	$?^?(1^{--})$	4643 ± 9	72 ± 11	$\psi(2S)f_0(980)(-33 \pm 21)$ $\Lambda_c^+\Lambda_c^-(70 \pm 6)$	$e^+e^- \to \psi(2S)\pi^+\pi^-$
$Z_c(4430)^+$	$?(1^+)$	4478^{+15}_{-18}	181 ± 31	$\psi(2S)\rho(17^{+15}_{-18})$	$B \to K[\psi(2S)\pi^+]$ $B \to K[J/\psi\pi^+]$
$Z_c(4200)^+$	$?(1^+)$	4196^{+35}_{-32}	370^{+100}_{-32}		$\bar{B}^0 \to K^-[J/\psi\pi^+]$
$Z_c(4050)^+$	$?(?^?)$	4051^{+24}_{-40}	82^{+50}_{-28}	$D^*\bar{D}^*(34^{+24}_{-40})$	$\bar{B}^0 \to K^-[\chi_{c1}\pi^+]$
$Z_c(4250)^+$	$?(?^?)$	4248^{+190}_{-50}	177^{+320}_{-70}	$\chi_{c1}\rho(-37^{+24}_{-50})$	$\bar{B}^0 \to K^-[\chi_{c1}\pi^+]$
$X(4140)$ (Aaij *et al.*, 2017a, 2017b)	$0^+(1^{++})$	$4146.5 \pm 4.5^{+4.6}_{-2.8}$	$83 \pm 21^{+21}_{-14}$	$D_s\bar{D}_s^*(-66.1^{+4.9}_{-3.2})$	$B^+ \to K^+[J/\psi\phi]$
$X(4274)$ (Aaij *et al.*, 2017a, 2017b)	$0^+(1^{++})$	$4273.3 \pm 8.3^{+17.2}_{-3.6}$	$56 \pm 11^{+8}_{-11}$	$D_s^*\bar{D}_s^*(-49.1^{+19.1}_{-9.1})$	$B^+ \to K^+[J/\psi\phi]$
$X(4500)$ (Aaij *et al.*, 2017a, 2017b)	$0^+(0^{++})$	$4506 \pm 11^{+12}_{-15}$	$92 \pm 21^{+21}_{-20}$	$D_{s0}^*(2317)\bar{D}_{s0}^*(2317)(-129^{+16}_{-19})$	$B^+ \to K^+[J/\psi\phi]$
$X(4700)$ (Aaij *et al.*, 2017a, 2017b)	$0^+(0^{++})$	$4704 \pm 10^{+14}_{-24}$	$120 \pm 31^{+42}_{-33}$	$D_{s0}^*(2317)\bar{D}_{s0}^*(2317)(69^{+17}_{-26})$	$B^+ \to K^+[J/\psi\phi]$
$Z_b(10610)$	$1^+(1^+)$	10607.2 ± 2.0	18.4 ± 2.4	$B\bar{B}^* + \text{c.c.}(4.0 \pm 3.2)$	$\Upsilon(10860) \to \pi[B\bar{B}^* + \text{c.c.}]$ $\Upsilon(10860) \to \pi[\Upsilon(1S)\pi]$ $\Upsilon(10860) \to \pi[\Upsilon(2S)\pi]$ $\Upsilon(10860) \to \pi[\Upsilon(3S)\pi]$ $\Upsilon(10860) \to \pi[h_b(1P)\pi]$ $\Upsilon(10860) \to \pi[h_b(2P)\pi]$
$Z_b(10650)$	$1^+(1^+)$	10652.2 ± 1.5	11.5 ± 2.2	$B^*\bar{B}^*(2.9 \pm 1.5)$	$\Upsilon(10860) \to \pi[B^*\bar{B}^*]$ $\Upsilon(10860) \to \pi[\Upsilon(1S)\pi]$ $\Upsilon(10860) \to \pi[\Upsilon(2S)\pi]$ $\Upsilon(10860) \to \pi[\Upsilon(3S)\pi]$ $\Upsilon(10860) \to \pi[h_b(1P)\pi]$ $\Upsilon(10860) \to \pi[h_b(2P)\pi]$

be higher than the lowest pseudoscalars or vectors of which the orbital angular momentum is zero. However, the lightest scalars have masses below those of the lightest vectors. Moreover, the mass ordering of the lightest scalars apparently violates the pattern of other $q\bar{q}$ nonets: Instead of having the isovectors be the lowest states, the isovector $a_0(980)$ states are almost degenerate with one of the isoscalar states $f_0(980)$, and those are the heaviest states in the nonet. The other isoscalar $f_0(500)$, also known as σ, has the lightest mass of the multiplet and an extremely large width. The strange scalar $K_0^*(800)$, also known as κ, has a large width as well. All these indicate some nontrivial substructure beyond a simple $q\bar{q}$ description.

The mass ordering of these lightest scalars is seen as strong evidence for the tetraquark scenario proposed by Jaffe (1977a, 1977b). Meanwhile, they can also be described as dynamically generated states through meson-meson scatterings (Pennington and Protopopescu, 1973; Au, Morgan, and Pennington, 1987; Morgan and Pennington, 1993). For a theoretical understanding of the $f_0(500)$ pole it is crucial to recognize that as a consequence of the chiral symmetry of QCD the scalar isoscalar $\pi\pi$ interaction is proportional to $(2s - M_\pi^2)/F_\pi^2$ at the leading order (LO) in the chiral expansion. Here $M_\pi(F_\pi)$ denotes the pion mass (decay constant). As a result, the LO scattering amplitude has already hit the unitarity bound for moderate energies necessitating some type of unitarization, which at the same time generates a resonance-like structure (Meißner, 1991). This observation, deeply nested in the symmetries of QCD, has indicated the significance of the $\pi\pi$ interaction for the light scalar mesons. The history and the modern developments regarding the $f_0(500)$ was recently reviewed by Peláez (2016). Similar to the isoscalar scalar $f_0(500)$ generated from the $\pi\pi$ scattering, the whole light scalar nonet appears naturally from properly unitarized chiral amplitudes for pseudoscalar-pseudoscalar scatterings (Oller, Oset, and Peláez, 1998, 1999; Gomez Nicola and Peláez, 2002). Similar conclusions also follow from more phenomenological studies (Weinstein and Isgur, 1990; Janssen *et al.*, 1995). One of the most interesting observations about $a_0(980)$ and $f_0(980)$ is that their masses are almost exactly located at the $K\bar{K}$ threshold. The closeness of the $K\bar{K}$ threshold to $a_0(980)$ and $f_0(980)$ and their strong S-wave couplings make both states good candidates for $\bar{K}K$ molecular states (Weinstein and Isgur, 1990; Baru *et al.*, 2004).

2. Axial vectors $f_1(1420)$, $a_1(1420)$, and implications of the triangle singularity

The S-wave pseudoscalar meson pair scatterings can be extended to S-wave pseudoscalar-vector scatterings and vector-vector scatterings where again dynamically generated states can be investigated. The S-wave pseudoscalar-vector scatterings can access the quantum numbers $J^P = 1^+$, while the vector-vector scatterings give $J^P = 0^+$, 1^+, and 2^+. This suggests that some of the states with those quantum numbers can be affected by the S-wave open thresholds if their masses are close enough to the thresholds. Or it might be possible that such scatterings can dynamically generate states as discussed in the literature (Lutz and Kolomeitsev, 2004b; Roca, Oset, and Singh, 2005; Geng and Oset, 2009). Note that not all

states found in these studies survive once a more sophisticated and realistic treatment as outlined by Gülmez, Meißner, and Oller (2017) is utilized.

In addition, the quark model also predicts regular $q\bar{q}$ states in the same mass range such that it appears difficult to identify the most prominent structure of the states.

Let us focus on the lowest 1^{++} mesons. Despite the fact that these states could be dynamically generated from the resummed chiral interactions (Lutz and Kolomeitsev, 2004b; Roca, Oset, and Singh, 2005), there are various experimental findings consistent with a usual $q\bar{q}$ nature of the members of the lightest axial nonet $f_1(1420)$, $f_1(1285)$, $a_1(1260)$, and $K_{1A}(1^3P_1)$ (Patrignani *et al.*, 2016). However, two recent experimental observations expose novel features in their decay mechanisms which illustrate the relevance of their couplings to the two-meson continua. The BESIII Collaboration observed an anomalously large isospin symmetry breaking in $\eta(1405)/\eta(1475) \to 3\pi$ (Ablikim *et al.*, 2012), which could be accounted for by the so-called triangle singularity (TS) mechanism as studied by Aceti *et al.* (2012) and Wu *et al.* (2012). This special threshold phenomenon arises in triangle (three-point loop) diagrams with special kinematics detailed in Sec. IV.A. Physically, it emerges when all the involved vertices in the triangle diagram can be interpreted as classical processes. For it to happen, one necessary condition is that all intermediate states in the triangle diagram, $\bar{K}K^*(K)$ + c.c. for the example at hand, should be able to reach their on-shell condition simultaneously. As a consequence, the $f_1(1420)$, which is close to the $\bar{K}K^*$ threshold and couples to $\bar{K}K^*$ in an S-wave as well, should also have large isospin violations in $f_1(1420) \to 3\pi$. This contribution has not been included in the BESIII analysis (Ablikim *et al.*, 2012). However, a detailed partial-wave analysis suggests the presence of the $f_1(1420)$ contribution via the TS mechanism (Wu *et al.*, 2013). Moreover, the TS mechanism predicts structures in different C parity and isospin (or G parity) channels via the $\bar{K}K^*(K)$ + c.c. triangle diagrams. The $f_1(1420)$ was speculated a long time ago to be a $\bar{K}^*K$ molecule from a dynamical study of the $K\bar{K}\pi$ three-body system (Longacre, 1990).

Apart from the $I = 0$, $J^{PC} = 1^{++}$ state $f_1(1420)$, one would expect that the TS will cause enhancements in $I = 1$ channels with $C = \pm$. It provides a natural explanation for the newly observed $a_1(1420)$ by the COMPASS Collaboration (Adolph *et al.*, 2015) in $\pi^- p \to \pi^- \pi^- \pi^+ p$ and $\pi^- \pi^0 \pi^0 p$ (Mikhasenko, Ketzer, and Sarantsev, 2015; Liu, Oka, and Zhao, 2016). It should be noted that Aceti, Dai, and Oset (2016), Cheng, Xie, and Cao (2016), and Debastiani, Aceti *et al.* (2017) proposed the $a_1(1420)$ enhancement to be caused by the $a_1(1260)$ together with the TS mechanism and similarly $f_1(1420)$ is produced by $f_1(1285)$. However, as shown by the convincing experimental data from MARK-III, BESII, BESIII, and the detailed partial-wave analysis of Wu *et al.* (2013), the $f_1(1420)$ matches the behavior of a genuine state in the $K\bar{K}\pi$ channel that is distorted in other channels by an interference with the TS. This appears to be a more consistent picture to explain the existing data and underlying mechanisms (Zhao, 2017). These issues are discussed further in Sec. VI.

B. Open heavy-flavor mesons

Since 2003, quite a few open heavy-flavor hadrons have been observed experimentally. Some of them are consistent with the excited states predicted in the potential quark model, while the others are not [for a recent review, see H.-X. Chen *et al.* (2017)]. Particular interest has been paid to the positive-parity charm-strange mesons $D_{s0}^*(2317)$ and $D_{s1}(2460)$ observed in 2003 by the *BABAR* (Aubert *et al.*, 2003) and CLEO (Besson *et al.*, 2003) Collaborations. The masses of $D_{s0}^*(2317)$ and $D_{s1}(2460)$ are below the DK and D^*K thresholds, respectively, by about the same amount, only 45 MeV (see Table I and reference therein), which makes them natural candidates for hadronic molecules (Barnes, Close, and Lipkin, 2003; Szczepaniak, 2003; van Beveren and Rupp, 2003; Hofmann and Lutz, 2004; Kolomeitsev and Lutz, 2004; Guo, Shen *et al.*, 2006; Faessler *et al.*, 2007; Flynn and Nieves, 2007; Gamermann *et al.*, 2007; Guo, Shen, and Chiang, 2007; Cleven *et al.*, 2011b; Wu and Zhao, 2012; Cleven, Grießhammer *et al.*, 2014; Albaladejo, Jido *et al.*, 2016), while also other explanations such as P-wave $c\bar{s}$ states and tetraquarks exist in the literature. We will return to the properties of these states occasionally in this review. Here we collect the features supporting the DK/D^*K molecular hypothesis as follows:

- Their masses are about 160 and 70 MeV, respectively, below the predicted 0^+ and 1^+ charm-strange mesons by the Godfrey-Isgur quark model (Godfrey and Isgur, 1985; Di Pierro and Eichten, 2001), making them not easy to be accommodated by the conventional $c\bar{s}$ states.
- The mass difference between these two states is equal to the energy difference between the corresponding $D^{(*)}K$ thresholds. This appears to be a natural consequence in the hadronic molecular scenario, since the involved interaction is approximately heavy quark spin symmetric (Guo, Hanhart, and Meißner, 2009a).
- The small widths of both $D_{s0}^*(2317)$ and $D_{s1}(2460)$ can be understood only if they are isoscalar states,[1] for then, since both of them are below the DK/D^*K thresholds, the only possible hadronic decay modes are the isovector channels $D_s^+\pi^0$ and $D_s^{*+}\pi^0$, respectively. The molecular nature together with the proximity to the DK/D^*K thresholds leads to a prediction for the width of the states above 100 keV while other approaches give a width of about 10 keV (Colangelo and De Fazio, 2003; Godfrey, 2003). These issues are discussed in detail in Secs. V.D and VI.A.3.
- Their radiative decays, i.e., $D_{s0}^*(2317) \to D_s\gamma$ and $D_{s1}(2460) \to D_s^{(*)}\gamma$, and production in B decays proceed via short-range interactions (Lutz and Soyeur, 2008; Cleven, Grießhammer *et al.*, 2014; Chen, Huo, and Zhao, 2015). They are therefore insensitive to the molecular component of the states.
- As will be discussed in Secs. III.B and V.D, the DK scattering length extracted from LQCD calculations (L. Liu *et al.*, 2013) is compatible with the result extracted in the molecular scenario for $D_{s0}^*(2317)$ based on Weinberg's compositeness theorem.

The $D_{sJ}(2860)$ observed by the *BABAR* Collaboration (Aubert *et al.*, 2006a) presents another example of an interesting charm-strange meson. It decays into both DK and D^*K with similar branching fractions (Patrignani *et al.*, 2016). One notices that the difference between the $D_{sJ}(2860)$ mass and the $D_1(2420)K$ threshold is similar to that between the $D_{s0}^*(2317)$ and DK. Assuming the $D_{s0}^*(2317)$ to be a DK hadronic molecule, an S-wave $D_1(2420)K$ bound state with quantum numbers $J^P = 1^-$ was predicted to have a mass 2870 ± 9 MeV, consistent with that of the $D_{sJ}(2860)$, in Guo and Meißner (2011), where the ratio of its partial widths into the DK and D^*K also gets naturally explained. As a result of heavy quark spin symmetry (HQSS), a $D_2(2460)K$ hadronic molecule with $J^P = 2^-$ and a mass of around 2.91 GeV was predicted by Guo and Meißner (2011). A later analysis by the LHCb Collaboration suggests that this structure corresponds to two states: $D_{s1}^*(2860)$ with $J^P = 1^-$ and $D_{s3}^*(2860)$ with $J^P = 3^-$ (Aaij *et al.*, 2014b). Regular $c\bar{s}$ interpretations for these two states have been summarized in H.-X. Chen *et al.* (2017).

The most recently reported observation of an exotic singly heavy meson candidate is a narrow structure in the $B_s^0\pi^{\pm}$ invariant mass distribution, named $X(5568)$, by the D0 Collaboration (Abazov *et al.*, 2016). Were it a hadronic state, it would be an isovector meson containing four different flavors of valence quarks ($\bar{b}s\bar{u}d$). However, the peak is located at only about 50 MeV above the $B_s\pi$ threshold. The existence of a tetraquark, whether or not being a hadronic molecule, at such a low mass is questioned from the quark model point of view by Burns and Swanson (2016), and, more generally, from chiral symmetry and heavy quark flavor symmetry in Guo, Meißner, and Zou (2016). Both the LHCb (Aaij *et al.*, 2016b) and CMS (Sirunyan *et al.*, 2017) Collaborations quickly reported negative results on the existence of $X(5568)$ in their data sets. An alternative explanation for the $X(5568)$ observation is necessary. One possibility is provided by Yang, Wang, and Meißner (2017). Because of these controversial issues with the $X(5568)$, we will not discuss this structure any further.

C. Heavy quarkoniumlike states: *XYZ*

The possibility of hadronic molecules in the charmonium mass region was suggested by Voloshin and Okun (1976) and De Rujula, Georgi, and Glashow (1977) only a couple of years after the "November revolution" due to the discovery of the J/ψ. Such an idea became popular after the discovery of the famous $X(3872)$ by Belle in 2003 (Choi *et al.*, 2003).

Since then, numerous other exotic candidates have been found in the heavy quarkonium sector as listed in Table II. In fact, it is mainly due to the observation of these structures that the study of hadron spectroscopy experienced a renaissance. The naming scheme currently used in the literature for these XYZ states assigns isoscalar $J^{PC} = 1^{--}$ states as Y and the isoscalar (isovector) states with other quantum numbers are named as $X(Z)$. Note that the charged heavy quarkoniumlike states $Z_c(3900)^{\pm}$, $Z_c(4020)^{\pm}$, $Z_b(10610)^{\pm}$, $Z_b(10650)^{\pm}$, and $Z_c(4430)^{\pm}$ are already established as being exotic, since they should contain at least two quarks and two antiquarks with the hidden pair of $c\bar{c}$ or $b\bar{b}$ providing the dominant parts of their masses.
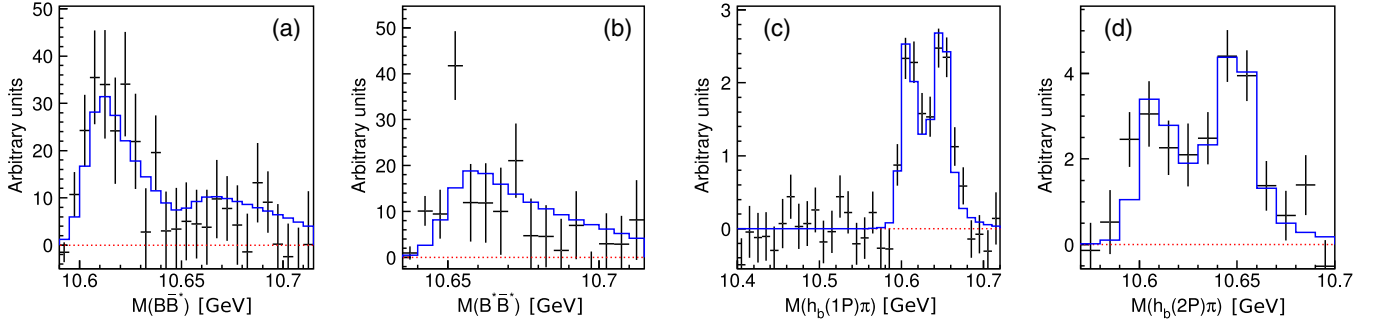
---

[1] A negative result was reported in a search for the isospin partner of the $D_{s0}^*(2317)$ (Choi *et al.*, 2015).

FIG. 1. *S*-wave open-charm thresholds and candidates for exotic states in the charmonium sector. The solid (red) (dashed blue) horizontal lines indicate the thresholds for nonstrange (strange) meson pairs. Two additional thresholds involving a charmonium $\chi_{c0}\omega$ and $\psi' f_0(980)$ are also shown as dotted green lines. The exotic candidates are listed as black dots and green triangles with the latter marking the states to be discussed here. Here D_{s0}, D_{s1}, D'_{s1}, and D_{s2} mean $D^*_{s0}(2317)$, $D_{s1}(2460)$, $D_{s1}(2536)$, and $D_{s2}(2573)$, respectively. All masses take the central values given in Patrignani *et al.* (2016).

In the heavy quarkonium mass region, there are quite a few *S*-wave thresholds opened by narrow heavy-meson pairs. In the charmonium mass region, the lowest-lying thresholds are $D\bar{D}$, $D\bar{D}^*$, and $D^*\bar{D}^*$. They are particularly interesting for understanding the *X* and *Z* states which can couple to them in an *S* wave. The relevant quantum numbers are thus $J^{PC} = 1^{+-}$ and $(0, 1, 2)^{++}$ (for more details, see Sec. IV.B). The *S*-wave thresholds for the *XYZ* exotic candidates are also shown in Table II. In addition, the exotic candidates in the charmonium sector and the *S*-wave open-charm thresholds are shown in Fig. 1. Here the thresholds involving particles with a large width $\gtrsim 100$ MeV have been neglected.

Since only *S*-wave hadronic molecules with small binding energies are well defined (Sec. III.B), in the following, we will focus on those candidates, i.e., $X(3872)$, $Z_c(3900)$, $Z_c(4020)$, and $Y(4260)$ in the charmonium sector and $Z_b(10610)$ and $Z_b(10650)$ in the bottomonium sector. All of them have

extremely close-by *S*-wave thresholds except for the $Y(4260)$, as will be discussed. For the experimental status and phenomenological models of other exotic candidates, we refer to several recent reviews (Swanson, 2006; Eichten *et al.*, 2008; Brambilla *et al.*, 2014; Esposito, Guerrieri, Piccinini *et al.*, 2015; Chen, Chen *et al.*, 2016; Richard, 2016; Esposito, Pilloni, and Polosa, 2017; Lebed, Mitchell, and Swanson, 2017; Olsen, Skwarnicki, and Zieminska, 2018) and references therein.

1. $X(3872)$

In 2003, the Belle Collaboration reported a narrow structure $X(3872)$ in the $J/\psi\pi^+\pi^-$ invariant mass distribution in the $B^\pm \to K^\pm J/\psi\pi^+\pi^-$ (Choi *et al.*, 2003) process. It was confirmed shortly after by *BABAR* (Aubert *et al.*, 2005c, 2008) in e^+e^- collisions, and by CDF (Acosta *et al.*, 2004; Abulencia *et al.*, 2006, 2007; Aaltonen *et al.*, 2009) and D0 (Abazov *et al.*, 2004) in $p\bar{p}$ collisions. Recently LHCb also confirmed its production in pp collisions (Aaij *et al.*, 2012, 2013, 2014a, 2015c) and pinned down its quantum numbers to $J^{PC} = 1^{++}$, which are consistent with the observations of its radiative decays (Abe *et al.*, 2005; Aubert *et al.*, 2006b; Bhardwaj *et al.*, 2011) and multipion transitions (Abe *et al.*, 2005; Abulencia *et al.*, 2006; del Amo Sanchez *et al.*, 2010). The negative result of searching for its charged partner in *B* decays (Aubert *et al.*, 2005b) indicates that the $X(3872)$ is an isosinglet state.

The most salient feature of the $X(3872)$ is that its mass coincides exactly with the $D^0\bar{D}^{*0}$ threshold[2] (Patrignani *et al.*, 2016)

$$M_{D^0} + M_{D^{*0}} - M_{X(3872)} = 0.00 \pm 0.18 \text{ MeV}, \qquad (1)$$

which indicates the important role of the $D^0\bar{D}^{*0}$ in the $X(3872)$ dynamics. That this should be the case can be seen most clearly from the large branching fraction (Gokhroo *et al.*, 2006; Aushev *et al.*, 2010) (see Table II)

$$\mathcal{B}(X(3872) \to \bar{D}^0 D^0 \pi^0) > 32\%, \qquad (2)$$

although the $X(3872)$ mass is so close to the $D^0\bar{D}^{*0}$ and $\bar{D}^0 D^0\pi^0$ thresholds. These experimental facts lead naturally to the interpretation of the $X(3872)$ as a $D\bar{D}^*$ hadronic molecule[3] (Törnqvist, 2003), which had been predicted by Törnqvist

---

[2]Here we use the updated "OUR AVERAGE" values in PDG2016 for the masses: $M_{D^0} = 1864.84 \pm 0.05$ MeV, $M_{D^{*0}} = 2006.85 \pm 0.05$ MeV, and $M_X = 3871.69 \pm 0.17$ MeV from the $J/\psi\pi^+\pi^-$ and $J/\psi\omega$ modes (Patrignani *et al.*, 2016).

[3]See also Close and Page (2004), Pakvasa and Suzuki (2004), Swanson (2004a, 2004b), Törnqvist (2004), Voloshin (2004b), Wong (2004), AlFiky, Gabbiani, and Petrov (2006), Braaten and Lu (2007), Fleming *et al.* (2007), Ding, Liu, and Yan (2009), Dong *et al.* (2009), Lee *et al.* (2009, 2011), Liu *et al.* (2009), Zhang and Huang (2009), Gamermann *et al.* (2010), Wang, Deng, and Chen (2010), Mehen and Springer (2011), Nieves and Valderrama (2011, 2012), Li and Zhu (2012), Sun, Liu *et al.* (2012), Sun, Luo *et al.* (2012), Guo *et al.* (2013a), Hidalgo-Duque *et al.* (2013), N. Li *et al.* (2013), Wang and Wang (2013), Yamaguchi *et al.* (2013), Guo, Hidalgo-Duque *et al.* (2014), He (2014), Zhao, Ma, and Zhu (2014), Baru *et al.* (2015a, 2015b), Jansen, Hammer, and Jia (2015), Karliner and Rosner (2015a), Molnar, Luiz, and Higa (2016), and Y.-C. Yang *et al.* (2017).

FIG. 2. Measured line shapes of the two Z_b states in the $B\bar{B}^*$, $B^*\bar{B}^*$, and $h_b(1P, 2P)\pi$ channels (Garmash *et al.*, 2016) and a fit using the parametrization of Hanhart *et al.* (2015) and Guo, Hanhart *et al.* (2016).

with the correct mass a decade earlier (Törnqvist, 1994). As discussed in Sec. VI, precise measurements of the partial widths of the processes $X(3872) \to D^0\bar{D}^0\pi^0$ and $X(3872) \to D^0\bar{D}^0\gamma$ are particularly important in understanding the long-distance structure of the $X(3872)$. In the $D^0\bar{D}^{*0}$ hadronic molecular scenario, one gets a tremendously large $D^0\bar{D}^{*0}$ scattering length of ≥ 10 fm, cf. Eq. (18). However, a precision measurement of its mass is necessary to really distinguish a molecular $X(3872)$ from a tetraquark scenario (Maiani *et al.*, 2005; Esposito, Guerrieri, Piccinini *et al.*, 2015). This will be discussed further in Secs. III.B.3 and III.C.

Other observables are also measured which could be sensitive to the internal structure of the $X(3872)$. The ratio of branching fractions

$$R^I \equiv \frac{\mathcal{B}(X(3872) \to J/\psi\pi^+\pi^-\pi^0)}{\mathcal{B}(X(3872) \to J/\psi\pi^+\pi^-)}$$

was measured to be $1.0 \pm 0.4 \pm 0.3$ by Belle (Abe *et al.*, 2005) and 0.8 ± 0.3 by *BABAR* (del Amo Sanchez *et al.*, 2010). The value about unity means a significant isospin breaking because the three and two pions are from the isoscalar ω (Abe *et al.*, 2005; del Amo Sanchez *et al.*, 2010) and from the isovector ρ (Abulencia *et al.*, 2006), respectively. Notice that there is a strong phase space suppression on the isospin conserved three-pion transition through the $J/\psi\omega$ channel. The fact that the molecular scenario of $X(3872)$ provides a natural explanation for the value of R^I will be discussed in Sec. VI.A.3.

The experimental information available about the radiative decays of the $X(3872)$ is (Aaij *et al.*, 2014a)

$$\frac{\mathcal{B}(X(3872) \to \psi'\gamma)}{\mathcal{B}(X(3872) \to J/\psi\gamma)} = 2.46 \pm 0.64 \pm 0.29. \quad (3)$$

A value larger than 1 for this ratio was argued to favor the $\chi_{c1}(2^3P_1)$ interpretation (Swanson, 2004a) over the $D^0\bar{D}^{*0}$ hadronic molecular picture. This, however, is not the case (Mehen and Springer, 2011; Guo, Hanhart, Kalashnikova *et al.*, 2015) as will be demonstrated in Sec. VI.

The production rates of $X(3872)$ in B^0 and B^- decays was measured by *BABAR* (Aubert *et al.*, 2006c), i.e.,

$$\frac{\mathcal{B}(B^0 \to X(3872)K^0 \to J/\psi\pi^+\pi^-K^0)}{\mathcal{B}(B^- \to X(3872)K^- \to J/\psi\pi^+\pi^-K^-)}$$
$$= 0.50 \pm 0.30 \pm 0.05. \quad (4)$$

We show in Sec. VI that this value is also consistent with a molecular nature of the $X(3872)$.

One expects mirror images of charmoniumlike states to be present in the bottomonium sector. The Z_c and Z_b states discussed in the next section suggest that such phenomena do exist. The analog of the $X(3872)$ in the bottom sector X_b has not yet been identified. A search for the X_b was carried out by the CMS Collaboration, but no signal was observed in the $\Upsilon\pi^+\pi^-$ channel (Chatrchyan *et al.*, 2013b). However, as pointed out by Guo *et al.* (2013a) before the experimental results and stressed again by Guo *et al.* (2014b) and Karliner and Rosner (2015b) afterward, the $X_b \to \Upsilon\pi^+\pi^-$ decay requires an isospin breaking which should be strongly suppressed due to the extremely small mass differences between the charged and neutral bottomed mesons and the large difference between the $B\bar{B}^*$ threshold and the $\Upsilon(1S)\omega$ and $\Upsilon(1S)\rho$ thresholds. In contrast, other channels such as $X_b \to \Upsilon\pi^+\pi^-\pi^0$, $X_b \to \chi_{bJ}\pi^+\pi^-$ (Guo *et al.*, 2013a, 2014b; Karliner and Rosner, 2015b), and $X_b \to \gamma\Upsilon(nS)$ (Li and Wang, 2014) should be a lot more promising for an X_b search.

2. $Z_b(10610)$, $Z_b(10650)$ and $Z_c(3900)$, $Z_c(4020)$

From an analysis of the $\Upsilon(10860) \to \pi^+\pi^-(b\bar{b})$ processes in 2011 the Belle Collaboration reported the discovery of two charged states decaying into $\Upsilon(nS)\pi$ with $n = 1, 2$, and 3 and $h_b(mP)\pi$ with $m = 1$ and 2 (Bondar *et al.*, 2012). Their line shapes in a few channels are shown in Fig. 2. A later analysis at the same experiment allowed for an amplitude analysis where the quantum numbers $I^G(J^P) = 1^+(1^+)$ were strongly favored (Garmash *et al.*, 2015).[4] This together with the fact that the $Z_b(10610)$ and $Z_b(10650)$ have masses very close to

_____

[4] The existence of an isovector $b\bar{b}q\bar{q}$ state with exactly these quantum numbers was speculated a long time ago for explaining the puzzling $\Upsilon(3S) \to \Upsilon(1S)\pi\pi$ transition (Voloshin, 1983; Anisovich *et al.*, 1995). The Z_b effects in dipion transitions among Υ states were recently reanalyzed using the dispersion technique by Y.-H. Chen *et al.* (2016, 2017).

TABLE III. The reported branching fractions of the known decay modes of $Z_b(10610)^+$ and $Z_b(10650)^+$ (Garmash *et al.*, 2016) with the statistical and systematical uncertainties in order.

Channel	$\mathcal{B}$ of $Z_b(10610)$ (%)	$\mathcal{B}$ of $Z_b(10650)$ (%)
$\Upsilon(1S)\pi^+$	$0.54^{+0.16+0.11}_{-0.13-0.08}$	$0.17^{+0.07+0.03}_{-0.06-0.02}$
$\Upsilon(2S)\pi^+$	$3.62^{+0.76+0.79}_{-0.59-0.53}$	$1.39^{+0.48+0.34}_{-0.38-0.23}$
$\Upsilon(3S)\pi^+$	$2.15^{+0.55+0.60}_{-0.42-0.43}$	$1.63^{+0.53+0.39}_{-0.42-0.28}$
$h_b(1P)\pi^+$	$3.45^{+0.87+0.86}_{-0.71-0.63}$	$8.41^{+2.43+1.49}_{-2.12-1.06}$
$h_b(2P)\pi^+$	$4.67^{+1.24+1.18}_{-1.00-0.89}$	$14.7^{+3.2+2.8}_{-2.8-2.3}$
$B^+\bar{B}^{*0}+\bar{B}^0 B^{*+}$	$85.6^{+1.5+1.5}_{-2.0-2.1}$	$\cdots$
$B^{*+}\bar{B}^{*0}$	$\cdots$	$73.7^{+3.4+2.7}_{-4.4-3.5}$

FIG. 3. The missing mass spectra for $h_b(1P)\pi^+\pi^-$ and $h_b(2P)\pi^+\pi^-$ channels in the $\Upsilon(11020)$ region. The solid and dashed histograms are the fits with the Z_b signal fixed from the $\Upsilon(10860)$ analysis and with only a phase space distribution, respectively. From Abdesselam *et al.*, 2016.

the $B\bar{B}^*$ and $B^*\bar{B}^*$ thresholds, respectively, makes both excellent candidates for hadronic molecules (Bondar *et al.*, 2011).[5] This statement finds further support in the observation that both states also decay by far most probably into $B\bar{B}^*$ and $B^*\bar{B}^*$ (Garmash *et al.*, 2016) (see Table III).[6] The neutral partner is so far observed only for the lighter state (Krokovny *et al.*, 2013). Recently, the Belle Collaboration reported the invariant mass distributions of $h_b(1P)\pi$ and $h_b(2P)\pi$ channels at $\Upsilon(11020)$ energy region (Abdesselam *et al.*, 2016) (see Fig. 3), showing a resonant enhancement in the Z_b mass region. However, due to the limited statistics it is impossible to judge whether there are two peaks or just one.

Employing sums of BW functions for the resonance signals the experimental analyses gave masses for both Z_b states slightly above the corresponding open-flavor thresholds together with narrow widths. It seems in conflict with the hadronic molecular picture and was claimed to be consistent with the tetraquark approach (Esposito, Pilloni, and Polosa, 2016). It is therefore important to note that a recent analysis based on a formalism consistent with unitarity and analyticity leads for both states to below-threshold pole positions (Hanhart *et al.*, 2015; Guo, Hanhart *et al.*, 2016).[7]

A few years after the discovery of $Z_b(10610)$ and $Z_b(10650)$ in the Belle experiment, the BESIII and Belle

---

[5]See also Cleven *et al.* (2011a), Sun *et al.* (2011), Zhang, Zhong, and Huang (2011), Danilkin, Orlovsky, and Simonov (2012), Ohkoda *et al.* (2012b), Y. Yang *et al.* (2012), Dong *et al.* (2013a), Li, Shao *et al.* (2013), Wang and Huang (2014), Z.-G. Wang (2014), Dias, Aceti, and Oset (2015), and Karliner and Rosner (2015a).

[6]The branching fractions were measured by assuming that these channels saturate the decay modes and using the Breit-Wigner (BW) parametrization for the Z_b structures (Garmash *et al.*, 2016). However, there could be non-negligible modes such as the $\eta_b\rho$, and the branching fractions measured in this way for near-threshold states should not be used to calculate partial widths by simply multiplying with the BW width. This point was discussed by Y.-H. Chen *et al.* (2016) for the Z_b case.

[7]Note that this, however, does not exclude the possibility of above-threshold poles. In the parametrization used, the contact terms are taken to be constants. The possibility of getting an above-threshold pole is available once energy dependence is allowed in the contact terms. Nevertheless, the analyses at least show that the below-threshold-pole scenario is consistent with the current data.
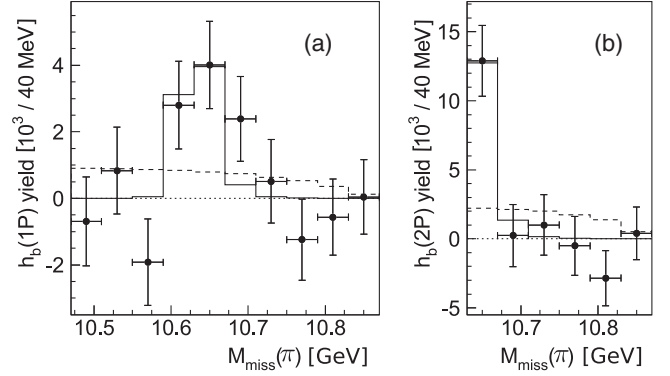
Collaborations almost simultaneously claimed the observation of a charged state in the charmonium mass range $Z_c(3900)$ (Ablikim *et al.*, 2013a; Z. Q. Liu *et al.*, 2013). It was shortly after confirmed by a reanalysis of CLEO-c data (Xiao *et al.*, 2013), and its neutral partner was also reported by Xiao *et al.* (2013) and Ablikim *et al.* (2015e). Soon after these observations, the BESIII Collaboration reported the discovery of another charged state $Z_c(4020)$ (Ablikim *et al.*, 2013b), and its neutral partner was reported by Ablikim *et al.* (2014c). These charmoniumlike states show in many respects similar features as the heavier bottomoniumlike states discussed previously, although there are also some differences. On the one hand, while the $Z_c(3900)$ is seen in the $J/\psi\pi$ channel and $Z_c(4020)$ is seen in $h_c\pi$, there is no clear signal of $Z_c(4020)$ in $J/\psi\pi$ and $Z_c(3900)$ in $h_c\pi$, although in the latter case there might be some indications of $Z_c(3900) \to h_c\pi$. This pattern might reflect a strong mass dependence of the production mechanism (Wang, Hanhart, and Zhao, 2013b). On the other hand, in analogy to $Z_b(10610)$ and $Z_b(10650)$, $Z_c(3900)$ and $Z_c(4020)$ have masses very close to the $D\bar{D}^*$ and $D^*\bar{D}^*$ thresholds, respectively, and they couple most prominently to these open-flavor channels regardless of the significant phase space suppression (Ablikim *et al.*, 2014a, 2014b, 2015c, 2015d). The two Z_c states are also widely regarded as hadronic molecules (Dong *et al.*, 2013b; Guo *et al.*, 2013a; He *et al.*, 2013; Ke, Wei, and Li, 2013; Li, 2013; Voloshin, 2013; Wang, Hanhart, and Zhao, 2013a; Wilbring, Hammer, and Meißner, 2013; Zhang, 2013; Cui *et al.*, 2014; W. Chen *et al.*, 2015; Karliner and Rosner, 2015a; Gong, Guo *et al.*, 2016).

Analogous to the Z_b case, the experimental analyses of the two Z_c states based on sums of BW distributions result in masses above the continuum thresholds as well. However, this does not allow the correct extraction of the pole locations. In order to obtain reliable pole locations an analysis in the spirit of Hanhart *et al.* (2015) and Guo, Hanhart *et al.* (2016) is necessary for these charmoniumlike states. Such an analysis was done for the $Z_c(3900)$ by Albaladejo, Guo *et al.* (2016). By fitting to the available BESIII data in the $Y(4260) \to J/\psi\pi^+\pi^-$ (Ablikim *et al.*, 2013a) and the $Y(4260) \to J/\psi\pi^+\pi^-$ (Ablikim *et al.*, 2015a) modes, it was found that
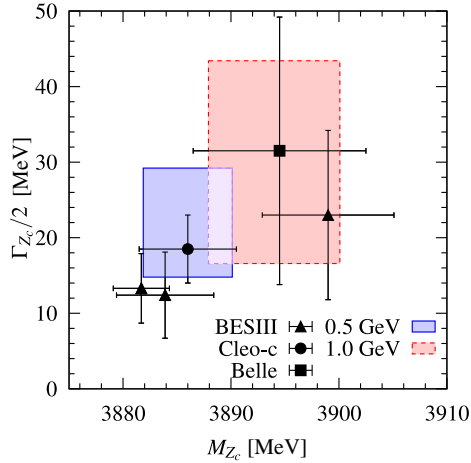
FIG. 4. The poles determined by Albaladejo, Guo *et al.* (2016) (0.5 and 1.0 GeV refer to the cutoff values used therein) in comparison with the mass and width values for the $Z_c(3900)$ reported by Ablikim *et al.* (2013a, 2014b, 2015a), Z. Q. Liu *et al.* (2013), and Xiao *et al.* (2013). From Albaladejo, Guo *et al.*, 2016.

the current data are consistent with either an above-threshold resonance pole or a below-threshold virtual state pole. A comparison of the resonance pole obtained therein with various determinations in experimental papers is shown in Fig. 4.

3. $Y(4260)$ and other vector states

At present, the vector channel with $J^{PC} = 1^{--}$, in both the bottomonium and the charmonium sector, is the best investigated one experimentally, since it can be accessed directly in e^+e^- annihilations. Note that a pair of ground-state open-flavor mesons, such as $D\bar{D}$, $D\bar{D}^* + $ c.c., $D^*\bar{D}^*$, $D_s\bar{D}_s$, etc., carry positive parity in the S wave and thus cannot be directly accessed in e^+e^- annihilations. Accordingly, if the S-wave hadronic molecules exist in the vector channel, they should be formed (predominantly) by constituents different from them. In particular, it suggests that the S-wave molecular states in the vector channel should be heavier than those thresholds opened by a pair of ground-state $D^{(*)}$ mesons.

As the first Y state, the $Y(4260)$ was observed by the *BABAR* Collaboration in the $J/\psi\pi^+\pi^-$ channel in the initial state radiation (ISR) process $e^+e^- \to \gamma_{\rm ISR}J/\psi\pi^+\pi^-$ (Aubert *et al.*, 2005a). The fitted mass and width are $4259 \pm 8^{+2}_{-6}$ MeV and 50–90 MeV, respectively. It was confirmed by CLEO-c (He *et al.*, 2006), Belle (Yuan *et al.*, 2007), and an additional analysis of *BABAR* (Lees *et al.*, 2012) with, however, mass values varying in different analyses. We note that a recent combined analysis of the BESIII data in four different channels $e^+e^- \to \omega\chi_{c0}$ (Ablikim *et al.*, 2016a), $\pi^+\pi^-h_c$ (Ablikim *et al.*, 2017b), $\pi^+\pi^-J/\psi$ (Ablikim *et al.*, 2017c), and $D^0D^{*-}\pi^+ + $ c.c. (Yuan, 2017) gives a mass of $4219.6 \pm 3.3 \pm 5.1$ MeV and a width of $56.0 \pm 3.6 \pm 6.9$ MeV (Gao, Shen, and Yuan, 2017).

The $Y(4260)$ was early recognized as a good candidate for an exotic state since there are no quark model states predicted around its mass. Moreover, it does not show a strong coupling
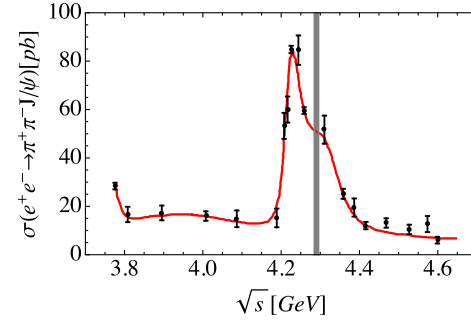
FIG. 5. The cross section of $e^+e^- \to \pi^+\pi^-J/\psi$ for center-of-mass energies from 3.77 to 4.6 GeV (Ablikim *et al.*, 2017c). It shows a clear shoulder around the $D_1\bar{D}$ threshold (marked by the vertical gray band) as predicted by Cleven, Wang *et al.* (2014). The solid red curve is from the analysis of BESIII (Ablikim *et al.*, 2017c). A comparison of these data with the BESIII scan data can be found in Gao, Shen, and Yuan (2017).

to $D\bar{D}$ as generally expected for vector $c\bar{c}$ states, and it does not show up as a pronounced enhancement in the inclusive cross sections for $e^+e^- \to$ hadrons (or the famous R value plot). It is still believed to be a prime candidate for a hybrid state (Close and Page, 2005) [for a recent discussion see Kalashnikova and Nefediev (2016)] or a hadrocharmonium state (Dubynskiy and Voloshin, 2008; Li and Voloshin, 2014). However, it is also suggested to be a $D_1(2420)\bar{D}$ molecular state (Ding, 2009; G. Li and Liu, 2013; M.-T. Li *et al.*, 2013; Wang, Hanhart, and Zhao, 2013a; Cleven, Wang *et al.*, 2014; X.-G. Wu *et al.*, 2014) [the hadrocharmonium picture and the molecular picture are contrasted by Wang *et al.* (2014)]. This picture is further supported by the fact that the recent high-statistics data from BESIII (Ablikim *et al.*, 2017c) (see Fig. 5) show an enhancement at the $D_1(2420)\bar{D}$ threshold in the $J/\psi\pi\pi$ channel.[8] The observations of $Z_c(3900)\pi$ (Sec. II.C.2) and $X(3872)\gamma$ (Ablikim *et al.*, 2014d) in the mass region of the $Y(4260)$ provide further support for a sizable $D_1(2420)\bar{D}$ component in its wave function as discussed in Sec. VI. The suppression of an S-wave production, in the heavy quark limit, of the 1^{--} $D_1(2420)\bar{D}$ pair in e^+e^- collisions (Eichten *et al.*, 1978, 1980; Li and Voloshin, 2013) could be the reason for the dip around the $Y(4260)$ mass in the inclusive cross section of $e^+e^- \to$ hadrons (Wang *et al.*, 2014). In addition, the data from Belle in $e^+e^- \to \bar{D}D^*\pi$ (Pakhlova *et al.*, 2009) and from BESIII on $e^+e^- \to h_c\pi\pi$ (Ablikim *et al.*, 2017b), $\chi_{c0}\omega$ (Ablikim *et al.*, 2015f) are highly nontrivial (Fig. 6) and are claimed to be consistent with the molecular picture (Cleven, Wang *et al.*, 2014; Cleven and Zhao, 2017). A combined analysis of the BESIII data in different channels was presented by Gao, Shen, and Yuan (2017).

The absence of a signal for $Y(4260)$ in $J/\psi K\bar{K}$ (He *et al.*, 2006; Yuan *et al.*, 2008; Shen *et al.*, 2014) questions the tetraquark picture of $Y(4260)$ with a diquark-antidiquark

---

[8]In this context note that the hybrid picture also predicts a large coupling of $Y(4260)$ to $D_1(2420)\bar{D}$ (Barnes, Close, and Swanson, 1995; Close and Page, 2005; Kou and Pene, 2005), which could be interpreted as the necessity of considering $D_1\bar{D}$ as a component.
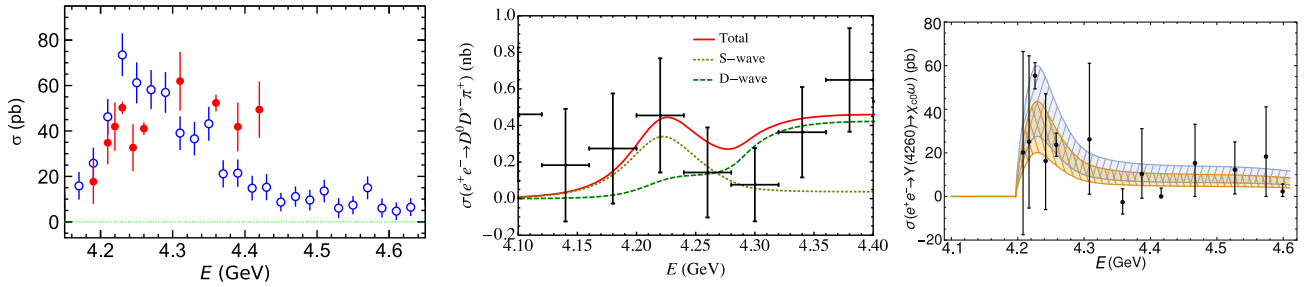
FIG. 6. The left plot shows the cross sections of the $e^+e^- \to h_c\pi\pi$ (solid red circles) from BESIII (Ablikim *et al.*, 2013b) and the $e^+e^- \to J/\psi\pi\pi$ (hollow blue circles) from Belle (Z. Q. Liu *et al.*, 2013) (note that the recent BESIII data for $e^+e^- \to J/\psi\pi\pi$ have much smaller errors as shown in Fig. 5). From Yuan, 2014. The middle one is the line shape for the $D\bar{D}^*\pi$ channel within the $D_1\bar{D}$ molecular picture (Cleven, Wang *et al.*, 2014) compared to the Belle data (Pakhlova *et al.*, 2009). The predicted line shape is similar to the solid line of the right panel of Fig. 10 with unstable constituent in Sec. III [note that an updated analysis can be found in Qin, Xue, and Zhao (2016) and the new data from BESIII can be found in Gao, Shen, and Yuan (2017)]. The right plot is the line shape of $e^+e^- \to \chi_{c0}\omega$ measured by BESIII (Ablikim *et al.*, 2015f) and the bands are theoretical calculations in the $D_1\bar{D}$ molecular picture (Cleven and Zhao, 2017).

$[cs][\bar{c}\,\bar{s}]$ configuration (Esposito, Guerrieri, Piccinini *et al.*, 2015). In addition, the ground state in the tetraquark picture (Esposito, Guerrieri, Piccinini *et al.*, 2015) $Y(4008)$ is not confirmed by the recent high-statistics data from BESIII (Ablikim *et al.*, 2017c). Meanwhile, the cross sections for $e^+e^- \to \psi'\pi\pi$ (Aubert *et al.*, 2007; Wang *et al.*, 2007), $\eta J/\psi$ (Ablikim *et al.*, 2016b), $\eta J/\psi$, and $\pi^0 J/\psi$ (Ablikim *et al.*, 2015b) do not show any structure around the $Y(4260)$ energy region. It remains to be seen if these findings allow for further conclusions on the nature of the $Y(4260)$.

It is interesting to observe that some properties of the $Y(4260)$, such as its proximity and strong coupling to the $D_1\bar{D}$ threshold, are mirror imaged by the $\Upsilon(11020)$ in the bottomonium sector (Bondar and Voloshin, 2016). Belle II appears to be an ideal instrument to investigate this connection in more detail in the future (Bondar, Mizuk, and Voloshin, 2017).

Searching for new decay modes of the $Y(4260)$, *BABAR* scanned the line shapes of $e^+e^- \to \psi(2S)\pi^+\pi^-$ and found a new structure, named $Y(4360)$ with a mass of 4324 ± 24 MeV and a width of 172 ± 33 MeV (Aubert *et al.*, 2007). In the same year, the Belle Collaboration (Wang *et al.*, 2007) analyzed the same process and found two resonant structures: a lower one consistent with $Y(4360)$ and a higher one, named $Y(4660)$, with a mass of $4664 \pm 11 \pm 5$ MeV and a width of $48 \pm 15 \pm 3$ MeV. A combined fit (Liu, Qin, and Yuan, 2008) to the cross sections of the process $e^+e^- \to \psi(2S)\pi^+\pi^-$ from both *BABAR* and Belle gives the parameters for the two resonances $M_{Y(4360)} = 4355^{+9}_{-10} \pm 9$, $\Gamma_{Y(4360)} = 103^{+17}_{-15} \pm 11$ and $M_{Y(4660)} = 4661^{+9}_{-8} \pm 6$, $\Gamma_{Y(4660)} = 42^{+17}_{-12} \pm 6$ MeV for $Y(4360)$ and $Y(4660)$, respectively. The fit at the same time provides an upper limit for $\mathcal{B}(Y(4260) \to \psi(2S)\pi^+\pi^-)\Gamma_{e^+e^-}$ as 4.3 eV. Those measurements were updated by Wang *et al.* (2015). Later on the Belle Collaboration found a structure in the $\Lambda_c^+\Lambda_c^-$ channel with a peak position 30 MeV lower than that of $Y(4660)$ (Pakhlova *et al.*, 2008), which might either point at an additional state, called $Y(4630)$, or, be an additional decay channel of the $Y(4660)$ (Cotugno *et al.*, 2010; Guo, Haidenbauer *et al.*, 2010). The latter is the view taken in the 2016 Review of

Particle Physics (Patrignani *et al.*, 2016). Of particular interest to this review is the observation of Guo, Haidenbauer *et al.* (2010) that within the $\psi' f_0(980)$ hadronic molecular picture (Guo, Hanhart, and Meißner, 2008; Wang and Zhang, 2010b) the line shape of $Y(4630)$ in the $\Lambda_c^+\Lambda_c^-$ channel could be understood as the signal of $Y(4660)$ with the $\Lambda_c^+\Lambda_c^-$ final state interaction. As a byproduct, Guo, Hanhart, and Meißner (2009a) predicted the properties of its spin partner, an $\eta_c' f_0(980)$ hadronic molecule, at around 4.61 GeV.

As stressed by Wang, Hanhart, and Zhao (2013b) and Bondar and Voloshin (2016) the production of $Z_c(3900)$ and $Z_c(4020)$ in the mass region of $Y(4260)$ and $Y(4360)$ as well as that of $Z_b(10610)$ and $Z_b(10650)$ in the mass region of $\Upsilon(10860)$ and $\Upsilon(11020)$, respectively, is sensitive to the TS mechanism. A peculiar feature of such a mechanism is that whether peaks appear in certain invariant mass distributions depends strongly on the kinematics. The recent observation of a peak in the $\psi'\pi$ invariant mass distribution by the BESIII Collaboration (Ablikim *et al.*, 2017a) shows exactly this behavior. The correlations between the initial S-wave thresholds and the final S-wave thresholds could be a key for understanding the rich phenomena observed in this energy region (Liu, Oka, and Zhao, 2016).

D. Baryon candidates for hadronic molecules

We now switch to the experimental evidence for hadronic molecules in the baryon sector. In analogy to the meson sector we focus on states which are located close to S-wave thresholds of narrow meson-baryon pairs.[9] In the light baryon spectrum the $\Lambda(1405)$ has been broadly discussed as a $\bar{K}N$ molecular state. A few charm baryons discovered in recent years are close to S-wave thresholds, and they have been suggested to be hadronic molecules in the literature. The recently observed $P_c(4450)$ and $P_c(4380)$ have also been proposed to be hadronic molecules with hidden charm.

---

[9]Note that also $P_{11}(1440)$ was proposed to have a prominent $f_0(500)N$ substructure (Krehl *et al.*, 2000). However, the large width of the $f_0(500)$ prohibits a model-independent study of this claim.

TABLE IV. The same as Table I but in the baryon sector.

State	$I(J^P)$	M (MeV)	Γ (MeV)	S-wave threshold(s) (MeV)	Observed mode(s) (branching ratios)
$\Lambda(1405)$	$0(\frac{1}{2}^-)$	$1405.1^{+1.3}_{-1.0}$	50.5 ± 2.0	$N\bar{K}(-29.4^{+1.3}_{-1.0})$ $\Sigma\pi(76.2^{+1.3}_{-1.0})$	$\Sigma\pi(100\%)$
$\Lambda(1520)$	$0(\frac{3}{2}^-)$	1519.5 ± 1.0	15.6 ± 1.0	$\Sigma(1385)^-\pi^+(-7.3 \pm 1.1)$ $\Sigma(1385)^+\pi^-(-2.9 \pm 1.1)$ $\Sigma(1385)^0\pi^0(0.8 \pm 1.4)$	$N\bar{K}(45 \pm 1)\%$ $\Sigma\pi(42 \pm 1)\%$ $\Lambda\pi\pi(10 \pm 1)\%$
$\Lambda(1670)$	$0(\frac{1}{2}^-)$	≈ 1670	≈ 35	$\Lambda\eta(4)$	$N\bar{K}(20\text{–}30)\%$ $\Sigma\pi(25\text{–}55)\%$ $\Lambda\eta(10\text{–}25)\%$
$\Lambda_c(2595)$	$0(\frac{1}{2}^-)$	2592.25 ± 0.28	2.6 ± 0.6	$\Sigma_c(2455)^{++}\pi^-(-1.04 \pm 0.31)$ $\Sigma_c(2455)^0\pi^+(-0.82 \pm 0.31)$ $\Sigma_c(2455)^+\pi^0(4.62 \pm 0.49)$	$\Sigma_c(2455)^{++}\pi^-(24 \pm 7)\%$ $\Sigma_c(2455)^0\pi^+(24 \pm 7)\%$ $\Lambda_c^+\pi^+\pi^-3-\text{body}(18 \pm 10)\%$
$\Lambda_c(2625)$	$0(\frac{3}{2}^-)$	2628.11 ± 0.19	< 0.97	$\Sigma_c(2455)\pi(36.53 \pm 0.24)$	$\Lambda_c^+\pi^+\pi^-(67\%)$ $\Sigma_c(2455)^{++}\pi^-(< 5\%)$ $\Sigma_c(2455)^0\pi^+(< 5\%)$
$\Lambda_c(2880)$	$0(\frac{5}{2}^+)$	2881.53 ± 0.35	5.8 ± 1.1	$ND^*(-65.91 \pm 0.35)$	$\Lambda_c^+\pi^+\pi^-$ $\Sigma_c(2455)^{0,++}\pi^\pm$ $\Sigma_c(2520)^{0,++}\pi^\pm$ pD^0
$\Lambda_c(2940)$ Aaij *et al.* (2017d)	$0(\frac{3}{2}^-)$	$2939.3^{+1.4}_{-1.5}$	17^{+8}_{-6}	$ND^*(-8.1^{+1.4}_{-1.5})$	$\Sigma_c(2455)^{0,++}\pi^\pm$ pD^0
$\Sigma_c(2800)$	$1(?^?)$	2800^{+5}_{-4}	70^{+23}_{-15}	$ND(-6 \pm 5)$	$\Lambda_c^+\pi$
$\Xi_c(2970)$	$\frac{1}{2}(?^?)$	2969.4 ± 1.7	19.0 ± 3.9	$\Sigma_c(2455)K(20.2 \pm 1.7)$	$\Lambda_c^+\bar{K}\pi$ $\Sigma_c(2455)\bar{K}$ $\Xi_c2\pi$ $\Xi_c(2645)\pi$
$\Xi_c(3055)$	$?(?^?)$	3055.1 ± 1.7	11 ± 4	$\Sigma_c(2520)K(41.1 \pm 1.7)$ $\Xi_c(2970)\pi(-52.3 \pm 2.4)$	
$\Xi_c(3080)$	$\frac{1}{2}(?^?)$	3078.4 ± 0.7	5.0 ± 1.3	$\Sigma_c(2520)K(64.4 \pm 0.7)$ $\Xi_c(2970)\pi(-29.0 \pm 1.8)$	$\Lambda_c^+\bar{K}\pi$ $\Sigma_c(2455)\bar{K}$ $\Sigma_c(2520)\bar{K}$
$P_c(4380)$ Aaij *et al.* (2015b)	$\frac{1}{2}(\frac{3}{2}^?/\frac{5}{2}^?)$	$4380 \pm 8 \pm 29$	$205 \pm 18 \pm 86$	$\Sigma_c(2520)\bar{D}\ (-6 \pm 30)$ $\Sigma_c(2455)\bar{D}^*\ (-82 \pm 30)$	$J/\psi p$
$P_c(4450)$ Aaij *et al.* (2015b)	$\frac{1}{2}(\frac{3}{2}^?/\frac{5}{2}^?)$	$4449.8 \pm 1.7 \pm 2.5$	$39 \pm 5 \pm 19$	$\chi_{c1}p\ (0.9 \pm 3.0)$ $\Lambda_c(2595)\bar{D}\ (-9.9 \pm 3.0)$ $\Sigma_c(2520)\bar{D}^*\ (-77.2 \pm 3.0)$ $\Sigma_c(2520)\bar{D}\ (64.2 \pm 3.0)$ $\Sigma_c(2455)\bar{D}^*\ (-12.3 \pm 3.0)$	$J/\psi p$

1. Candidates in the light baryon sector

The $\Lambda(1405)$ was discovered in the $\pi\Sigma$ subsystems of $Kp \to \Sigma\pi\pi$ (Alston *et al.*, 1961) [see also Kim (1965) and Hemingway (1985)]. Further experimental information about this state comes from old scattering data (Humphrey and Ross, 1962; Watson, Ferro-Luzzi, and Tripp, 1963; Sakitt *et al.*, 1965; Ciborowski *et al.*, 1982) complemented by the recent $\bar{K}N$ threshold amplitude extracted from data on kaonic hydrogen (Bazzi *et al.*, 2011, 2012) as well as the older so-called threshold ratios (Tovee *et al.*, 1971; Nowak *et al.*, 1978). There are further data on $\Sigma\pi$ distributions from $pp \to \Sigma^\pm\pi^\mp K^+ p$ (Zychor *et al.*, 2008; Agakishiev *et al.*, 2013), the photoproduction $\gamma p \to K^+\Sigma\pi$ (Moriya *et al.*, 2014), and additional reactions. It appears also feasible that

high-energy experiments such as *BABAR*, Belle, BESIII, CDF, D0, and LHCb investigate the $\Lambda(1405)$ via the decays of heavy hadrons such as $\Lambda_b \to J/\psi\Lambda(1405)$ (Roca *et al.*, 2015). Note that a signal of $\Lambda(1405)$ was clearly visible in an analysis of $\Lambda_b \to J/\psi Kp$ performed by the LHCb Collaboration (Aaij *et al.*, 2015b).

The $\Lambda(1405)$ has strangeness $S = -1$ with $I(J^P) = 0(1/2^-)$ and a mass about 30 MeV (see Table IV) below the $\bar{K}N$ threshold. Note that a direct experimental determination of the spin-parity quantum numbers was given only recently by the CLAS Collaboration (Moriya *et al.*, 2014). Since its mass is smaller than that of the nucleon counterpart $N(1535)1/2^-$ and the mass difference from its spin-splitting partner state $\Lambda(1520)\ I(J^P) = 0(3/2^-)$ is larger than that between $N(1535)1/2^-$ and $N(1520)3/2^-$, it can hardly be

accepted by the conventional three-quark picture of the constituent quark model (Hyodo and Jido, 2012). It is fair to say that the $\Lambda(1405)$ was most probably the first exotic hadron observed (Alston *et al.*, 1961). The theoretical aspects of the $\Lambda(1405)$ will be discussed in Sec. VI.D.

2. Candidates in the charm baryon sector

The two light quarks in a charm baryon can be in either the symmetric sextet or antisymmetric antitriplet representation of SU(3). Since the color wave function is totally antisymmetric, the spin-flavor-space wave functions must be symmetric. Hence the light-quark system in the *S*-wave flavor sextet (antitriplet) has spin 1 (0). After combining with a heavy quark, the sextet and antitriplet give the $B_6(1/2^+)$, $B_6^*(3/2^+)$, and $B_{\bar{3}}(1/2^+)$ baryon multiplets, respectively, as (Yan *et al.*, 1992)

$$B_6 = \begin{pmatrix} \Sigma_c(2455)^{++} & \frac{1}{\sqrt{2}}\Sigma_c(2455)^+ & \frac{1}{\sqrt{2}}\Xi_c'^+ \\ \frac{1}{\sqrt{2}}\Sigma_c(2455)^+ & \Sigma_c(2455)^0 & \frac{1}{\sqrt{2}}\Xi_c'^0 \\ \frac{1}{\sqrt{2}}\Xi_c'^+ & \frac{1}{\sqrt{2}}\Xi_c'^0 & \Omega_c^0 \end{pmatrix},$$

$$B_6^* = \begin{pmatrix} \Sigma_c(2520)^{++} & \frac{1}{\sqrt{2}}\Sigma_c(2520)^+ & \frac{1}{\sqrt{2}}\Xi_c(2645)^+ \\ \frac{1}{\sqrt{2}}\Sigma_c(2520)^+ & \Sigma_c(2520)^0 & \frac{1}{\sqrt{2}}\Xi_c(2645)^0 \\ \frac{1}{\sqrt{2}}\Xi_c(2645)^+ & \frac{1}{\sqrt{2}}\Xi_c(2645)^0 & \Omega_c(2770)^0 \end{pmatrix},$$

$$B_{\bar{3}} = \begin{pmatrix} 0 & \Lambda_c^+ & \Xi_c^+ \\ -\Lambda_c^+ & 0 & \Xi_c^0 \\ -\Xi_c^+ & -\Xi_c^0 & 0 \end{pmatrix}.$$

All the ground-state charm baryons within these three multiplets have been well established in experiments (Patrignani *et al.*, 2016). Among the other charm baryons, $\Lambda_c(2765)$, $\Xi_c(2815)$, and $\Xi_c(3123)$ are not well established from the experimental analysis (Patrignani *et al.*, 2016). The *P*-wave $1/2^-$ and $3/2^-$ antitriplet states are identified as $[\Lambda_c(2595)^+, \Xi_c(2790)^+, \Xi_c(2790)^0]$ (Cheng and Chua, 2007, 2015) and $[\Lambda_c(2625)^+, \Xi_c(2815)^+, \Xi_c(2815)^0]$, respectively (Cheng and Chua, 2015). Among the remaining charm baryons, the $\Lambda_c(2880)^+$ has a definite spin of $5/2$ (Patrignani *et al.*, 2016; Aaij *et al.*, 2017d) and the quantum numbers of the $\Lambda_c(2940)^+$ were measured to be $J^P = 3/2^-$ (Aaij *et al.*, 2017d). Besides these two charm baryons, LHCb also measured another charm baryon $\Lambda_c(2860)^+$ which is consistent with the predication of the orbital *D*-wave Λ_c^+ excitation (Chen, Mao *et al.*, 2016; Chen, Liu, and Zhang, 2017; B. Chen *et al.*, 2017). The only available information of other measured charm baryons is their masses and some of their decay modes. For recent reviews on the heavy baryons, see Klempt and Richard (2010) and H.-X. Chen *et al.* (2017).

Although the $\Lambda_c(2595)^+$ may be accommodated as a regular three-quark baryon in quark models (Copley, Isgur, and Karl, 1979; Pirjol and Yan, 1997; Tawfiq, O'Donnell, and Korner, 1998; Zhu, 2000; Blechman *et al.*, 2003; Migura *et al.*, 2006; Zhong and Zhao, 2008), one cannot neglect one striking feature of it (Hyodo, 2013b) which could provide other potential interpretations: It lies between the $\Sigma_c(2455)^+\pi^0$ and $\Sigma_c(2455)^0\pi^+$, $\Sigma_c(2455)^{++}\pi^-$ thresholds

as shown in Table IV. Thus, the $\Lambda_c(2595)$ is proposed as a dynamically generated state of the nearby $\Sigma_c(2455)\pi$ coupling with other possible higher channels (Lutz and Kolomeitsev, 2004a; Hofmann and Lutz, 2005; Mizutani and Ramos, 2006; Garcia-Recio *et al.*, 2009, 2015; Jimenez-Tejero, Ramos, and Vidana, 2009; Haidenbauer *et al.*, 2011; Romanets *et al.*, 2012; Liang *et al.*, 2015; Lu *et al.*, 2015; Long, 2016; Lu, Chen *et al.*, 2016), such as ND, ND^*, etc. The strong coupling between the $\Lambda_c(2595)$ and $\Sigma_c(2455)\pi$ channels even leads to a prediction of the existence of a three-body $\Sigma_c\pi\pi$ resonance in Long (2016) and Long, Wang, and Lyu (2017). The analysis by Guo and Oller (2016b), however, indicates that the compositeness of $\Sigma_c(2455)^+\pi^0$ is smaller than 10% leaving $\Lambda_c(2595)$ dominated by either other heavier hadronic channels (such as ND and ND^*) or compact quark-gluon structures. Some other charm baryons, such as $\Lambda_c(2880)$ (Lutz and Kolomeitsev, 2004a), $\Lambda_c(2940)$ (He *et al.*, 2007, 2010; Ortega, Entem, and Fernandez, 2013; Zhang, 2014; Zhao, Huang, and Ping, 2017), and $\Sigma_c(2800)$ (Jimenez-Tejero, Ramos, and Vidana, 2009; Jimenez-Tejero *et al.*, 2011; Zhang, 2014), have also been considered as dynamically generated states from meson-baryon interactions. In particular, the $\Lambda_c(2940)^+$ is very close to the ND^* threshold —it even overlaps with the threshold if using the recent LHCb measurement (Aaij *et al.*, 2017d), and it can couple to ND^* in an *S* wave. Both are favorable features for treating it as an ND^* hadronic molecule (Ortega, Entem, and Fernandez, 2013; Zhao, Huang, and Ping, 2017).

3. Pentaquarklike structures with hidden charm

Recently, LHCb reported two pentaquarklike structures $P_c(4380)^+$ and $P_c(4450)^+$ in the $J/\psi p$ invariant mass distribution of $\Lambda_b \to J/\psi pK^-$ (Aaij *et al.*, 2015b). Their masses (widths) are $4380 \pm 8 \pm 29$ MeV ($205 \pm 18 \pm 86$ MeV) and $4449.8 \pm 1.7 \pm 2.5$ MeV ($39 \pm 5 \pm 19$ MeV), respectively. In this analysis the Λ^* states that appear in the crossed channel were parametrized via BW functions. The LHCb analysis reported preference of the spin-parity combinations $(3/2^-, 5/2^+)$, $(3/2^+, 5/2^-)$, or $(5/2^+, 3/2^-)$ for these two states, respectively. The branching ratio for $\Lambda_b \to J/\psi pK^-$ was also measured (Aaij *et al.*, 2016d).

The data for the Cabibbo suppressed process $\Lambda_b \to J/\psi p\pi^-$ are consistent with the existence of these two P_c structures (Aaij *et al.*, 2016a). The same experiment also published a measurement of $\Lambda_b^0 \to \psi(2S)pK^-$, but no signals for the P_c states were observed due to either the low statistics or their absence in the $\psi(2S)p$ channel (Aaij *et al.*, 2016c).

The production mechanism and the decay pattern imply a five-quark content of these two states with three light quarks and a hidden heavy $c\bar{c}$ component if they are hadronic states. In fact, pentaquarklike states with hidden charm have been predicted in the right mass region as dynamically generated in meson-baryon interactions a few years before the LHCb discovery (Wu *et al.*, 2010, 2011). There are several thresholds in the mass region of the two P_c structures, namely, $\chi_{c1}p$, $\Sigma_c(2520)\bar{D}$, $\Sigma_c(2455)\bar{D}^*$, $\Lambda_c(2595)\bar{D}$, and $\Sigma_c(2520)\bar{D}^*$ (see Table IV), although not all of them couple in *S* waves to the reported preferred quantum numbers, suggesting different interpretations of the two P_c states, such as $\Sigma_c(2455)\bar{D}^*$,

$\Sigma_c(2520)\bar{D}$, or $\Sigma_c(2520)\bar{D}^*$ hadronic molecules (Chen, Chen *et al.*, 2015; R. Chen *et al.*, 2015; Karliner and Rosner, 2015a; Roca, Nieves, and Oset, 2015; Chen, Cui *et al.*, 2016; He, 2016; Shimizu, Suenaga, and Harada, 2016; Ortega, Entem, and Fernández, 2017). It has been suggested that their decay patterns could be used to distinguish among various hadronic molecular options (Lü and Dong, 2016; Shen *et al.*, 2016; G.-J. Wang *et al.*, 2016; Lin *et al.*, 2017). There are also other dynamical studies with different channel bases (Azizi, Sarac, and Sundu, 2017; Geng, Lu, and Valderrama, 2017; Xiao, 2017; Yamaguchi and Santopinto, 2017).

The extreme closeness of the $P_c(4450)$ to the $\chi_{c1}p$ threshold and to a TS from a $\Lambda^*(1890)\chi_{c1}p$ triangle diagram was pointed out by Guo *et al.* (2015). Bayar *et al.* (2016) stressed that the $\chi_{c1}p$ needs to be in an S wave so as to produce a narrow observable peak in the $J/\psi p$ invariant mass distribution, and correspondingly J^P needs to be $1/2^+$ or $3/2^+$. This TS and other possible relevant TSs are also discussed by Guo *et al.* (2016) and Liu, Wang, and Zhao (2016). It is worthwhile to emphasize that the existence of TSs in the P_c region does not exclude a possible existence of pentaquark states whether or not they are hadronic molecules. Meißner and Oller (2015) investigated the possibility that the $P_c(4450)$ could be a $\chi_{c1}p$ molecule.

In order to confirm the existence of the two P_c states and distinguish them from pure kinematic singularities, cf. discussions in Sec. VI.A.4, one can either search for them in other processes, such as $\Lambda_b \to \chi_{c1}pK^-$ (Guo *et al.*, 2015), photoproduction (Kubarovsky and Voloshin, 2015, 2016; Wang, Liu, and Zhao, 2015; Gryniuk and Vanderhaeghen, 2016; Hiller Blin *et al.*, 2016; Huang *et al.*, 2016; Karliner and Rosner, 2016), heavy ion collisions (R.-Q. Wang *et al.*, 2016), pion-nucleon reactions (Kim, Kim, and Hosaka, 2016; Liu and Oka, 2016b; Lin *et al.*, 2017), or search for their strange (Feijoo *et al.*, 2015, 2016; Chen, Liu, and Zhu, 2016; Lu, Wang *et al.*, 2016; Ramos, Feijoo, and Magas, 2016), neutral (Lebed, 2015; Lü *et al.*, 2016) and bottomonium (Xiao and Meißner, 2015) partners. The $\Lambda_b \to \chi_{c1}pK^-$ decay process has been observed at the LHCb experiment (Aaij *et al.*, 2017c).

III. IDENTIFYING HADRONIC MOLECULES

Hadronic molecules are analogs of light nuclei, most notably the deuteron. They can be treated to a good approximation as composite systems made of two or more hadrons which are bound together via the strong interactions. In this section the general notion of a molecular state is introduced. As demonstrated for near-threshold bound states this picture can be put into a formal definition that even allows one to relate observables directly to the probability to find the molecular component in the bound state wave function. However, it appears necessary to work with a more general notion of hadronic molecules as also resonances can be of molecular nature in the sense formulated above. Before we proceed it appears necessary to review some general properties of the S matrix. In this section the terminology of a bound state, a virtual state, and a resonance is discussed for these notions are heavily used throughout this review.

A. Properties of the S matrix

The unitary operator that connects asymptotic *in* and *out* states is called the S matrix. It is an analytic function in the Mandelstam plane up to its branch points and poles. The S matrix is the quantity that encodes all physics about a certain scattering or production reaction. In general it is assumed that the S matrix is analytic up to the following:

- *Branch points*, which occur at each threshold. On the one hand, there are the so-called right-hand cuts starting from the branch points at the thresholds for an s-channel kinematically allowed process (e.g., at the $\bar{K}K$ threshold in the $\pi\pi$ scattering amplitude). On the other hand, when reactions in the crossed channel become possible one gets the left-hand cuts, which are usually located in the unphysical region for the reaction studied but may still significantly influence, e.g., the energy dependence of a reaction cross section. Branch points can also be located inside the complex plane of the unphysical Riemann sheets: This is possible when the reaction goes via an intermediate state formed by one or more unstable states. It is clear that these threshold branch points and cuts are kinematically determined and happen at the loop level of Feynman diagrams.

  In general, a loop Feynman diagram with more than two intermediate particles has more complicated kinematical singularities. They are called Landau singularities (Landau, 1959); see, e.g., Eden *et al.* (1966), Chang (1983), and Gribov, Dokshitzer, and Nyiri (2009). For instance, in triangle diagrams the branch points of two intermediate pairs can be very close to the physical region simultaneously, and such a situation gives rise to the so-called triangle singularity already introduced in Sec. II. We return to those in Sec. IV.A.1.[10]

- *Poles*, which appear due to the interactions inherited in the dynamics of the underlying theory. Depending on the locations, poles can be further classified as follows:

  (i) *Bound states*, which appear as poles on the physical sheet. By causality they are only allowed to occur on the real s axis below the lowest threshold. The deuteron in the isospin-0 and spin-1 proton-neutron system, which can be regarded as the first established hadronic molecule, is a nice example.

  (ii) *Virtual states*, which appear on the real s axis, however, on the unphysical Riemann sheet. A well-known example in nuclear physics is the pole in the isospin-1 and spin-0 nucleon-nucleon scattering. It is within 1 MeV from the threshold and drives the scattering length to a large value of about 24 fm.

  (iii) *Resonances*, which appear as poles on an unphysical Riemann sheet close to the physical one. There is no restriction for the location of

---

[10]The Landau singularity can even be a pole if the one-loop Feynman diagram has at least five intermediate particles (Gribov, Dokshitzer, and Nyiri, 2009). However, this case is irrelevant for us and will not be considered.
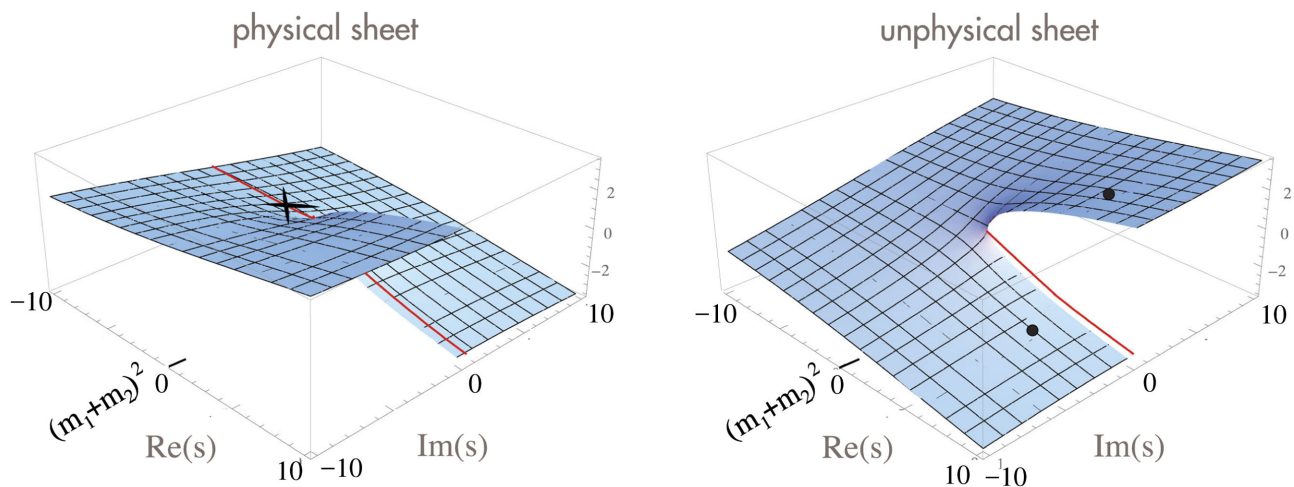
FIG. 7. The imaginary part of a typical single-channel amplitude in the complex s plane. The solid dots indicate allowed positions for resonance poles, the cross for a bound state. The solid line is the physical axis (shifted by $i\epsilon$ into the physical sheet). The two sheets are connected smoothly along their discontinuities.

poles on the unphysical sheets. Yet, Hermitian analyticity requires that, if there is a pole at some complex value of s there must be another pole at its complex conjugate value s^*. Normally, the pole with a negative imaginary part is closer to the physical axis and thus influences the observables in the vicinity of the resonance region more strongly. However, at the threshold both poles are always equally important. This is illustrated in Fig. 7.

For a discussion of the analytic structure of the S matrix with a focus on scattering experiments see Döring *et al.* (2009) and references therein. Any of these singularities leads to some structure in the observables. In a partial wave decomposed amplitude additional singularities not related to resonance physics may emerge as a result of the partial-wave projection. For a discussion see, e.g., Höhler (1983).

From this classification, it is clear that the branch points are kinematical so that they depend completely on the masses of the involved particles in a certain physical process, while the poles are of dynamical origin so that they should appear in many processes as long as they are allowed by quantum numbers.

We call a structure observed experimentally a state if and only if the origin of this structure is a pole in the S matrix due to dynamics. On the one hand, this definition is quite general as it allows us to also call the mentioned pole in the isovector nucleon-nucleon scattering a state. From the point of view of QCD, this definition appears to be quite natural since it takes only a marginal change in the strength of the two-hadron potential (e.g., via a small change in quark masses) to switch from a shallow bound state to a near-threshold virtual state, and both leave a striking imprint in observables (we return to this in Sec. III.C). For example, various lattice QCD groups observed the dineutron to become a bound state at quark masses heavier than the physical value (Yamazaki *et al.*, 2012, 2015; Beane *et al.*, 2013; Berkowitz *et al.*, 2017). On the other hand, if a structure in the data finds its origin purely in a

kinematical singularity without a nearby pole, it would not be called a state. There is currently a heated discussion going on in the literature whether some of the XYZ states are just threshold cusps or triangle singularities (Bugg, 2004; Chen and Liu, 2011; Chen, Liu, and Matsuki, 2013; Swanson, 2015, 2016; Gong, Pang *et al.*, 2016; Pilloni *et al.*, 2017). It should be stressed, however, that pronounced near-threshold signals in the continuum channel related to that threshold must find their origin in a nearby pole (Guo, Hanhart, Wang, and Zhao, 2015).

In the physical world, basically all candidates for hadronic molecules, except for nuclei, can decay strongly and thus cannot be bound states in the rigorous sense of the word, since the lowest threshold is defined by the production threshold of the decay products. However, it still appears justified to call the $f_0(980)$ a $K\bar{K}$ bound state, or a quasibound state in a more rigorous sense, if the corresponding pole is located on the physical sheet for the two-kaon system, or a virtual state if it is on the unphysical sheet for the two-kaon system, although the lowest threshold is the two-pion threshold.

B. Definition of hadronic molecules

In order to proceed it is necessary to first define the notion of a molecular state. Naively one might be tempted to argue that if data can be described by a model where all interactions between continuum states come from s-channel pole terms, the resulting states have to be interpreted as "elementary" states. However, as we discuss, this is in general not correct. Analogously, a model that contains only nonpole interactions can still at the end lead to a pole structure of the S matrix that needs to be interpreted as nonmolecular. The origin of the failure of intuition in these circumstances is the fact that a hadronic description of hadron dynamics can only be understood in the sense of an effective field theory with limited range of applicability. In particular the very short-ranged parts of the wave function as well as the interaction potential are

model dependent and cannot be controlled within the hadronic prescription.

However, at least for near-threshold bound states (the term "near" will be quantified in the next section) there is a unique property of the wave function of a molecular state as long as it is formed by a (nearly) stable particle pair in an S wave: The fact that this particle pair can almost go on shell leaves an imprint with observable consequences in the analytic structure of the corresponding amplitude, a feature absent to all other possible substructures. In fact, as a consequence of this feature, hadronic molecules can be extended. To see this observe that a bound state wave function at large distances scales as $\exp(-\gamma r)/r$, where r is the distance between the constituents and γ denotes the typical momentum scale defined via

$$\gamma = \sqrt{2\mu E_B}, \qquad (5)$$

where $\mu = m_1 m_2/(m_1 + m_2)$ denotes the reduced mass of the two-hadron system and

$$E_B = m_1 + m_2 - M \qquad (6)$$

the binding energy of the state with mass M (note that we chose E_B positive so that the bound state is located at $E = -E_B$ with E the energy relative to the threshold). Thus, the size R of a molecular state is given by $R \sim 1/\gamma$. Accordingly, if $X(3872)$ with a binding energy of less than 200 keV with respect to the $D^0 \bar{D}^{*0}$ threshold were a molecule, it would be at least as large as 10 fm. For a review of properties of systems with large scattering length see Braaten and Hammer (2006).

All of these issues will be discussed in detail in the following sections. The arguments start in Sec. III.B.1 from the classic definition introduced by Weinberg to model independently capture the nature of the deuteron as a proton-neutron bound state. A detailed discussion of the derivation will allow us to explain at the same time the limitations of this definition. Then in Sec. III.B.2 it is demonstrated that the Weinberg criterion is actually identical to the pole counting arguments by Morgan. In Sec. III.B.3 the generalization of the arguments to resonances is prepared by a detailed discussion of pole trajectories that emerge when some strength parameter that controls the location of the S-matrix poles varies. The compositeness criteria for resonances are briefly discussed in Sec. III.B.4.

1. The Weinberg compositeness criterion

We start from the following ansatz for the physical wave function of a bound state (Weinberg, 1965):

$$|\Psi\rangle = \begin{pmatrix} \lambda |\psi_0\rangle \\ \chi(\boldsymbol{k})|h_1 h_2\rangle \end{pmatrix}, \qquad (7)$$

where $|\psi_0\rangle$ denotes the compact component of the state and $|h_1 h_2\rangle$ its two-hadron component. Here compact denotes an object whose size is controlled by the confinement radius $R_{\text{conf}} < 1$ fm. Thus this component is assumed to be more

compact than $R \sim 1/\gamma$, which denotes the characteristic size of a shallow bound state.[11] In addition, $\chi(\boldsymbol{k})$ is the wave function of the two-hadron part, where $\boldsymbol{k}$ denotes the relative momentum of the two particles. In this parametrization, by definition λ quantifies the contribution of the compact component of the wave function to the physical wave function of the state. Accordingly λ^2 denotes the probability to find the compact component of the wave function in the physical state, which corresponds to the wave function renormalization constant Z in quantum field theory. Thus, the goal is to relate λ to observables.

In order to proceed one needs to define the interaction Hamiltonian. As shown by Weinberg (1963b) under general conditions one may write

$$\hat{\mathcal{H}}|\Psi\rangle = E|\Psi\rangle, \qquad \hat{\mathcal{H}} = \begin{pmatrix} \hat{H}_c & \hat{V} \\ \hat{V} & \hat{H}_{hh}^0 \end{pmatrix}. \qquad (8)$$

Equation (8) exploits the observation that it is possible by a proper field redefinition to remove all hadron-hadron interactions from the theory and to cast them into ψ_0 (Weinberg, 1963a, 1963b). Then the two-hadron Hamiltonian is given simply by the kinetic term $\hat{H}_{hh}^0 = k^2/(2\mu)$, where $\mu = m_1 m_2/(m_1 + m_2)$ denotes the reduced mass of the two-hadron system and m_i denotes the mass of hadron h_i. Introducing the transition form factor,

$$\langle \psi_0 | \hat{V} | h_1 h_2 \rangle = f(\boldsymbol{k}), \qquad (9)$$

one finds the wave function in momentum space as

$$\chi(\boldsymbol{k}) = \lambda \frac{f(\boldsymbol{k})}{E - k^2/(2\mu)}. \qquad (10)$$

The wave function of a physical bound state needs to be normalized to have a probabilistic interpretation. We thus get

$$1 = \langle \Psi | \Psi \rangle = \lambda^2 \langle \psi_0 | \psi_0 \rangle + \int \frac{d^3 k}{(2\pi)^3} |\chi(\boldsymbol{k})|^2 \langle h_1 h_2 | h_1 h_2 \rangle$$

$$= \lambda^2 \left\{ 1 + \int \frac{d^3 k}{(2\pi)^3} \frac{f^2(\boldsymbol{k})}{[E_B + k^2/(2\mu)]^2} \right\}. \qquad (11)$$

As mentioned, λ^2 is in fact the wave function renormalization constant Z, since the integral in the last line of Eq. (11) is nothing but the energy derivative of the self-energy. Because of the positivity of the integral, λ^2 is bound in the range between 0 and 1 and thus allows for a physical probabilistic interpretation for a bound state.

At this point a comment is necessary: in many textbooks on quantum field theory it is written that the wave function renormalization constant Z is scheme dependent and is to be used to absorb the ultraviolet (UV) divergence of the vertex corrections. Clearly this is correct. However, the scheme dependence and UV divergence are only for the terms analytic in E. What we find here is the LO piece of Z in

---

[11]Actually, we define the notion "shallow" by the request of $R > R_{\text{conf}}$, which translates into $E_B < 1/(2\mu R_{\text{conf}}^2)$.

an energy expansion around the threshold,[12] and as this piece is proportional to $\sqrt{E}$ it cannot be part of the Lagrangian. Thus, the Weinberg criterion as outlined is based explicitly on the presence of the two-particle cut which is responsible for the appearance of the square root, whose presence is a distinct feature of the two-hadron component.

The integral in Eq. (11) converges if $f(\mathbf{k})$ is a constant. The denominator contains solely model-independent parameters, while the momentum dependence of the numerator is controlled by the relevant momentum range of the vertex function that may be estimated by β, the inverse range of forces. Thus, if $\beta \gg \gamma$, the integral can be evaluated model independently for the case of S-wave coupling which implies the constant $g_0 = f(0)$ as the LO piece of $f(\mathbf{k})$.[13] Then one finds

$$1 = \lambda^2 \left[1 + \frac{\mu^2 g_0^2}{2\pi\sqrt{2\mu E_B}} + \mathcal{O}\left(\frac{\gamma}{\beta}\right) \right]. \qquad (12)$$

From this we find the desired relation, namely,

$$g_0^2 = \frac{2\pi\gamma}{\mu^2} \left(\frac{1}{\lambda^2} - 1\right), \qquad (13)$$

which provides a relation between λ^2, the probability of finding the compact component of the wave function inside the physical wave function, and g_0, the bare coupling constant of the physical state to the continuum, or λg_0, the physical coupling constant.

The quantity g_0 also appears in the physical propagator of the bound state since the self-energy is given by

$$\Sigma(E) = -\int \frac{d^3 k}{(2\pi)^3} \frac{f^2(\mathbf{k})}{E - k^2/(2\mu) + i\epsilon}$$
$$= \Sigma(-E_B) + ig_0^2 \frac{\mu}{2\pi} \sqrt{2\mu E + i\epsilon} + \mathcal{O}\left(\frac{\gamma}{\beta}\right). \qquad (14)$$

We may therefore write for the T matrix of the two continuum particles whose threshold is close to the location of the bound state,

$$T_{\mathrm{NR}}(E) = \frac{g_0^2}{E - E_0 + \Sigma(E)} + \text{(nonpole terms)}, \qquad (15)$$

where the subscript "NR" is a reminder of the nonrelativistic normalization. As long as the pole is close to the threshold, the amplitude near threshold should be dominated by the pole term (the nonpole terms are again controlled quantitatively by the range of forces). Using $E_B = -E_0 + \Sigma(-E_B) - g_0^2\mu\gamma/(2\pi)$, which absorbs the (divergent) leading contribution of the real part into the bare pole energy and at the same time takes care of the fact that the analytic continuation of the momentum term also contributes at the pole,[14] we get

$$T_{\mathrm{NR}}(E) = \frac{g_0^2}{E + E_B + g_0^2\mu/(2\pi)(ik + \gamma)}, \qquad (16)$$

where we introduced the two-hadron relative momentum $k = \sqrt{2\mu E}$. Note that Eq. (16) is nothing but the one-channel version of the well-known Flatté parametrization (Flatté, 1976). Thus, a measurement of near-threshold data allows one in principle to measure the composition of the bound state wave function, in line with the effective field theory analysis discussed in Sec. VI, although in practice a reliable extraction of the coupling might be hindered by a scale invariance of the Flatté parametrization that appears for large couplings (Baru *et al.*, 2005). The phenomenological implications especially of Eq. (13) on Eq. (16) and generalizations thereof will be discussed in Sec. III.C.

To make the last statement explicit we match Eq. (16) onto the effective range expansion

$$T_{\mathrm{NR}}(E) = -\frac{2\pi}{\mu} \frac{1}{1/a + (r/2)k^2 - ik}, \qquad (17)$$

and find

$$a = -2\frac{1-\lambda^2}{2-\lambda^2}\left(\frac{1}{\gamma}\right) + \mathcal{O}\left(\frac{1}{\beta}\right),$$
$$r = -\frac{\lambda^2}{1-\lambda^2}\left(\frac{1}{\gamma}\right) + \mathcal{O}\left(\frac{1}{\beta}\right). \qquad (18)$$

Thus, for a pure molecule ($\lambda^2 = 0$) one finds that the scattering length gets maximal $a = -1/\gamma$, and in addition $r = \mathcal{O}(1/\beta)$, where the latter term is typically positive, while for a compact state ($\lambda^2 = 1$) one gets $a = -\mathcal{O}(1/\beta)$ (in the presence of a bound state the scattering length is necessarily negative within the sign convention chosen here) and $r \to -\infty$. These striking differences have severe implications on the line shapes of near-threshold states as discussed in Sec. III.C.

It is illustrative to apply the Weinberg criterion to the deuteron, basically repeating the analysis presented already by Weinberg (1965). The scattering length and effective range extracted from proton-neutron scattering data in the deuteron channel are (Klarsfeld, Martorell, and Sprung, 1984)

$$a = -5.419(7) \text{ fm} \quad \text{and} \quad r = 1.764(8) \text{ fm}, \qquad (19)$$

where the sign of the scattering length was adapted to the convention employed here. Furthermore, the deuteron binding energy reads (Van Der Leun and Alderliesten, 1982)[15]

$$E_B = 2.22 \text{ MeV} \Rightarrow \gamma = 45.7 \text{ MeV} = 0.23 \text{ fm}^{-1}. \qquad (20)$$

On the other hand, in case of the deuteron the range of forces is provided by the pion mass—accordingly the range corrections that appear in Eqs. (18) may in this case be estimated via

---

[12]More discussion on this point can be found in Sec. IV.B.

[13]Note that in some works a model for the form factor $f(\mathbf{k})$ is employed (Faessler *et al.*, 2007).

[14]When E takes real values, the square root on the first sheet is defined by $\sqrt{2\mu E + i\epsilon} = +i\sqrt{-2\mu E}\theta(-E) + \sqrt{2\mu E}\theta(E)$.

[15]The reference quotes $E_B = 2.224\,575(9)$ MeV; however, for the analysis here such a high accuracy is not necessary.

$$\frac{1}{\beta} \sim \frac{1}{M_\pi} \simeq 1.4 \text{ fm}. \qquad (21)$$

Thus the effective range is of the order of the range corrections (and positive) as required by the compositness criterion for a molecular state. Using $\lambda^2 = 0$ in the expression for the scattering length we find

$$a_{\text{mol}} = -(4.3 \pm 1.4) \text{ fm} \qquad (22)$$

also consistent with Eq. (19). Based on these considerations Weinberg concluded that the deuteron is indeed composite.

As mentioned, a location of a molecular state very near a threshold is quite natural, while a near-threshold compact state is difficult to accomplish (Jaffe, 2007; Hanhart, Peláez, and Ríos, 2014). This can now be illustrated on the basis of Eqs. (17) and (18). By construction for $k = i\gamma$ the T matrix develops a pole which may be read off from Eq. (17):

$$\gamma = -\frac{1}{a} + \frac{\gamma^2 r}{2}. \qquad (23)$$

For a (nearly) molecular state $a \simeq -1/\gamma$ and $r \sim \mathcal{O}(1/\beta)$. Thus, for this case Eq. (23) is largely saturated by the scattering length term, and the range term provides only a small correction. However, for a predominantly genuine state we have $-1/a \simeq \beta \gg \gamma$ and $r \to -\infty$. Thus in this case a subtle fine-tuning between the range term and the scattering length term appears necessary for the pole to be located very near threshold.

While the low-energy scattering of the hadrons that form the bound state is controlled by the scattering length and effective range, production reactions are sensitive to the residue of the bound state pole, which serves as the effective coupling constant, to be called g_{eff}, squared of the bound state to the continuum. It is simply given by the bare coupling constant g_0^2 previously introduced multiplied by the wave function renormalization constant Z, which is λ^2 as explained,

$$g_{\text{NR}}^2 \equiv Z g_0^2 = \frac{2\pi\gamma}{\mu^2}(1 - \lambda^2). \qquad (24)$$

After switching to a relativistic normalization by multiplying with $(\sqrt{2m_1}\sqrt{2m_2}\sqrt{2M})^2$, and dropping terms of the order of (E_B/M), we thus get

$$\frac{g_{\text{eff}}^2}{4\pi} = 4M^2\left(\frac{\gamma}{\mu}\right)(1 - \lambda^2). \qquad (25)$$

What is interesting about Eq. (25) is that it is bounded from above: The effective coupling constant of a bound system to the continuum gets maximal for a pure two-hadron bound state. Since $1 - \lambda^2$ is the probability of finding the two-hadron composite state component in the physical wave function, it is sometimes called "compositeness." Using Eq. (18), the effective coupling can be expressed in terms of the scattering length

$$\frac{g_{\text{eff}}^2}{4\pi} = \frac{4M^2}{\mu}\frac{-a\gamma}{a + 2/\gamma}, \qquad (26)$$

which reduces to $-4M^2/\mu a$ in the limit of $\lambda^2 = 0$, reflecting the universality of an S-wave system with a large scattering length (Braaten and Hammer, 2006).

Before closing this section some comments are necessary.

• The approach allows for model-independent statements only for S waves, since otherwise in the last integral of Eq. (11) there appears in the numerator of the integrand an additional factor k^{2L} from the centrifugal barrier. Accordingly, the integral can no longer be evaluated model independently without introducing additional parameters (regulator) to cope with the UV divergence.

• For the same reason the continuum channel needs to be a two-body channel, since otherwise the momentum dependence of the phase space calls for an additional suppression of the integrand.

• The binding momentum must be small compared to the inverse range of forces, since otherwise the range corrections get larger than the terms that contain the structure information.

• For the applicability of the formalism as outlined and an unambiguous probabilistic interpretation, the state studied must be a bound state, since otherwise the normalization condition of Eq. (11) is not applicable which is at the very heart of the derivation. However, nowadays there exist generalizations of the Weinberg approach also to resonances which will be discussed in Sec. III.B.4.

• The constituents that form the bound state must be narrow, since otherwise the bound system would also be broad (Filin *et al.*, 2010; Guo and Meißner, 2011).

For a long time it seemed that the conditions were satisfied only by the deuteron and Weinberg therefore closed his paper with the phrase (Weinberg, 1965): "One begins to suspect that Nature is doing her best to keep us from learning whether the "elementary" particles deserve that title." However, as outlined in the Introduction, there are now various near-threshold states confirmed experimentally that appear to be consistent with those criteria, such as $X(3872)$, $D_{s0}^*(2317)$ and less rigorously $f_0(980)$ and others.

For illustration we compare what is known about the effect of the $D_{s0}^*(2317)$ on DK scattering to the Weinberg criterion. Clearly, DK scattering cannot be measured directly in experiment, however, it can be studied in lattice QCD using the so-called Lüscher method (Lüscher, 1991). The first study using this method for the DK system was presented by Mohler *et al.* (2013). The scattering length and effective range extracted in this work for the lowest pion mass ($M_\pi = 156$ MeV) are $-(1.33 \pm 0.20)$ and (0.27 ± 0.17) fm, respectively. This number is to be compared to the Weinberg prediction for a purely molecular state of $a = -(1 \pm 0.3)$ fm and $r \sim 0.3$ fm, where the inverse ρ mass was assumed for the range of forces and we used the fact that for molecular states the effective range is positive and of the order of the range of forces. Scattering lengths of the same size were also extracted from a study of the scattering of the light pseudoscalars off D mesons using unitarized chiral perturbation theory (L. Liu *et al.*, 2013). Thus from both chiral dynamics on the hadronic level

and lattice QCD there are strong indications that $D^*_{s0}(2317)$ indeed is a DK molecule. The lattice aspects will be further discussed in Sec. V. Clearly, a direct experimental confirmation of the molecular assignment for $D^*_{s0}(2317)$ is desirable. A possible observable could be the hadronic width of $D^*_{s0}(2317)$ as discussed in Sec. VI.A.3.

So far we focused only on bound states. However, also very near-threshold poles on the second sheet not accompanied by a first sheet pole, so-called virtual states, leave a striking imprint in observables; cf. Sec. III.A. A T matrix that has its pole on the second, instead of on the first, sheet reads, in distinction to Eq. (16),

$$T_{\mathrm{NR}}(E) = \frac{g_0^2}{E + E_v + g_0^2 \mu/(2\pi)(ik - \gamma)}, \qquad (27)$$

where now the virtual pole is located on the second sheet at $E = -E_v$, with $E_v > 0$ and we still use γ to denote $\sqrt{2\mu E_v}$. Here we use the fact that on the second sheet below threshold the momentum is $-i|\sqrt{2\mu E}|$.

2. The pole counting approach

One of the classic approaches put forward to distinguish molecular states from genuine ones is the so-called pole counting approach (Morgan, 1992), which can be summarized as follows: A bound state that is dominated by its compact component (in the language of the previous section this implies λ^2 close to 1) manifests itself in two near-threshold singularities (one on the first sheet, one on the second) while a predominantly molecular bound state gives rise only to a single near-threshold pole on the first sheet.

To see that these criteria actually map perfectly on the Weinberg criterion it is sufficient to observe that the poles of Eq. (17) are given by

$$k_{1/2} = \frac{i}{r} \pm \sqrt{-\frac{1}{r^2} - \frac{2}{ar}}. \qquad (28)$$

Based on the sign convention employed in this work, cf. Eq. (17), in the presence of a bound state the scattering length is negative. In addition, keeping only the leading terms for both the scattering length a and the effective range r as shown in Eqs. (18), one obtains

$$k_1 = i\gamma, \qquad k_2 = -i\gamma\left(\frac{2 - \lambda^2}{\lambda^2}\right). \qquad (29)$$

Thus it is easy to see that k_1 and k_2 are positive and negative imaginary numbers, respectively, which implies that the former is a pole on the first Riemann sheet (a bound state pole), while the latter is located on the second sheet. When λ approaches 0, which implies that the molecular component of the state becomes increasingly important, the second pole disappears toward negative imaginary infinity, which leaves k_1 as the only relevant pole. In particular one gets from this for the asymmetry of the pole locations

$$\frac{|k_1| - |k_2|}{|k_1| + |k_2|} = \lambda^2 - 1. \qquad (30)$$

Thus the asymmetry of the pole locations is a direct measure of the amount of molecular admixture in the bound state wave function (as defined within the Weinberg approach) in line with the findings of Morgan (1992). The close relation between the two approaches was first observed by Baru *et al.* (2004).

3. Remarks about pole trajectories

QCD is characterized by a small number of parameters, namely, the quark masses, the number of colors (N_c), and Λ_{QCD} (the running coupling constant). Accordingly those parameters completely determine the hadron spectrum. With advanced theoretical tools it became possible recently to investigate the movement of the QCD poles as QCD parameters are varied. There exist studies for varying quark masses as well as varying numbers of colors N_c—both of them allowing for deeper insight into the structure of the investigated states.

Studies that vary the number of colors are available mostly for light quark systems. For a recent review, see Peláez (2016). In order to connect the N_c dependence of a given state in the spectrum to QCD by Peláez (2016) a unitarized version of chiral perturbation theory, the so-called inverse amplitude method, is employed, where the fact is exploited that the leading N_c behavior of the low-energy constants (LECs) is known. Thus, once the unitarized amplitudes are fitted to phase shifts, it is possible to investigate the impact of a varying N_c by proper rescaling of these LECs. This kind of study was pioneered by the work of Peláez (2004), where it was demonstrated that the N_c scaling of the vector mesons ρ and K^* is in line with expectations for $\bar{q}q$ states; however, that of $f_0(500)$ and $K_0^*(800)$ is completely at odds with them. While the N_c studies allow one to distinguish the quark content of different states, they do not allow one to disentangle hadronic molecules from other four-quark structures. In addition, both mentioned resonances are very broad and as such do not allow one to straightforwardly quantify their molecular component following the approach of the previous section.

Existing studies where quark masses are varied allow for a more direct contact to the discussion of the previous section. Understanding the quark mass dependence of hadrons with different composition is not only interesting for its own sake, it is also important since lattice QCD studies can be performed at arbitrary quark masses (and in fact are often performed at enlarged quark masses for practical reasons). Thus, as soon as we can relate certain pole trajectories to the structure of the hadron it becomes feasible to "measure" the nature of the state using lattice QCD. More direct methods to use the lattice to determine the nature of certain hadrons will be discussed in Sec. V.

Let us consider pole trajectories of resonances as some generic strength parameter is varied. Here we follow the presentation of Hanhart, Peláez, and Ríos (2014). In this work it was shown that in the presence of a pole the one-channel S matrix can be written as (for simplicity assuming the masses of the continuum particles to be equal)
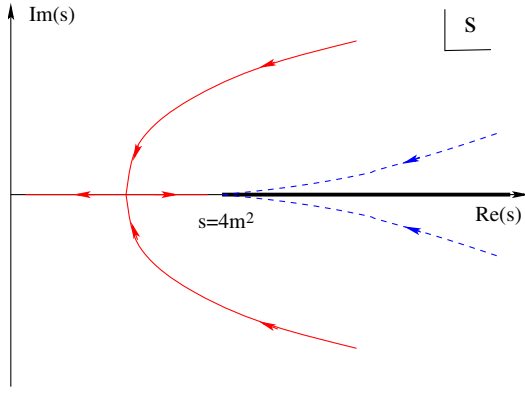
FIG. 8. Typical pole trajectories for S waves (solid red lines) and for higher partial waves (dashed blue lines) in the second sheet of the complex s plane. The thick line denotes the branch cut.

$$S = \frac{(k - k_p - i\xi)(k + k_p - i\xi)}{(k - k_p + i\xi)(k + k_p + i\xi)}$$
$$= \frac{k^2 - (k_p^2 + \xi^2) - 2ik\xi}{k^2 - (k_p^2 + \xi^2) + 2ik\xi}$$
$$= \frac{s - s_0 - 4i(s - 4m^2)^{1/2}\xi}{s - s_0 + 4i(s - 4m^2)^{1/2}\xi}, \quad (31)$$

where $\xi \geq 0$. The unimodular form of Eq. (31) is because of the unitarity of the S matrix. This parametrization accounts for the fact that if the S matrix has a pole at some complex momentum on the second sheet $k_p - i\xi$, it also has to have a pole $-k_p - i\xi$, which is the realization of the Schwarz reflection principle in momentum space, and that any pole on the second sheet is accompanied by a zero on the first. As shown by the last equality, the momentum space expression can be straightforwardly mapped onto the s plane, where $s_0 = 4(k_p^2 + \xi^2 + m^2)$ was introduced. In the s plane the Schwarz reflection principle calls for poles at complex conjugate points.

To investigate the general behavior of the pole trajectories it is sufficient to vary the parameter k_p^2 from some finite positive value to some finite negative value. Typical trajectories are shown in Fig. 8. The trajectories for S waves are depicted by the solid lines and for higher partial waves by the dashed lines. As long as k_p^2 is positive (k_p is real), Eq. (31) develops two complex conjugate poles for all partial waves. When k_p^2 decreases, the poles approach each other and eventually, for $k_p^2 = 0$, meet on the real axis. One of the poles switches to the first sheet at the point where $k_p^2 + \xi^2 = 0$, which is the threshold and at least for S waves requires a negative value of k_p^2 (k_p is imaginary).

The first nontrivial observation that can be read off Eq. (31) and Fig. 8 straightforwardly is that S waves and higher partial waves behave very differently: The reason for this is the centrifugal barrier that forces one to introduce a momentum dependence into ξ according to

$$\xi(k) = \tilde{\xi}k^{2L}. \quad (32)$$

This has a striking impact on the pole trajectories: For any $L > 0$ the ξ term is zero at $k = 0$ and therefore the point where the two pole trajectories meet ($k_p^2 = 0$) coincides with $k = 0$ which denotes the threshold. This is different for S waves: in this case the poles can meet somewhere below the threshold. Then, when k_p^2 is decreased further to negative values, both poles move away from the meeting point, such that one approaches the threshold while the other one goes away from the threshold. This behavior can easily be interpreted via the pole counting approach: The farther away from the threshold the point is located where the two trajectories meet (this point is determined by the value of ξ at the point where $k_p^2 = 0$), the more asymmetric are the two poles once one of them has switched to the first sheet, and thus the molecular component of the state is more pronounced.

To make more explicit the connection between the trajectories and the molecular nature of the states we study the scattering length and the effective range that emerge from Eq. (31):

$$a = -\frac{2\xi}{\xi^2 + k_p^2}, \qquad r = -\frac{1}{\xi}. \quad (33)$$

If we now use the fact that the binding momentum $\gamma = \kappa_p - \xi$, where $\kappa_p = ik_p$, we can read off the following from the previous equations and Eq. (18):

$$\lambda^2 = 1 - \frac{\xi}{\kappa_p}. \quad (34)$$

To see the implications of Eq. (34) we parametrize the relevant quantities via

$$\gamma = \epsilon\delta, \qquad \xi = \delta, \qquad \kappa_p = (1 + \epsilon)\delta \rightarrow \lambda^2 = \frac{\epsilon}{1 + \epsilon}, \quad (35)$$

where $\delta > 0$ and $\epsilon > 0$. Here it was already used that for a bound state to exist with a finite binding energy κ_p must exceed ξ. A vanishing binding momentum ($\gamma \rightarrow 0$) can be achieved by either $\epsilon \rightarrow 0$ for finite δ, which immediately implies that $\lambda^2 \rightarrow 0$, so that the state is purely molecular, or $\delta \rightarrow 0$ for finite ϵ. This case allows for a compact admixture of the very near-threshold pole, however, at the price of an extreme fine-tuning of κ_p and ξ as both then need to go to zero simultaneously. This is the same kind of fine-tuning already observed for nonmolecular near-threshold states below Eq. (23) from a different perspective.

As an example Hanhart, Peláez, and Ríos (2014) explicitly demonstrated that the pole trajectories of the $f_0(500)$ meson as well as the ρ meson that emerge when the quark masses are varied can be easily parametrized in terms of the parameters ξ and κ_p previously introduced. In particular it was shown that while ξ changes only mildly in the parameter range studied, k_p^2 changes a lot and in particular ξ is sizable at the point where k_p^2 is zero in the $f_0(500)$ channel. Accordingly Hanhart, Peláez, and Ríos (2014) concluded that, at least for unphysically large quark masses, the $f_0(500)$ meson behaves like a hadronic molecule.

What should be clear from these considerations is that states born off hadron-hadron dynamics with poles above the relevant threshold are necessarily broad; after all their coupling to this continuum channel is maximal. This should also be clear from the pole trajectories illustrated in Fig. 8. An example for such a scenario is the very broad $f_0(500)$ most probably generated by nonperturbative $\pi\pi$ interactions. Such a property is in contrast to the tetraquark picture advocated by Esposito, Pilloni, and Polosa (2016), where they argued that tetraquarks that are visible in experiment must be narrow and slightly above threshold. It is therefore important that the pole locations of exotic candidates are determined with high precision.

4. Generalizations to resonances

The first work where the Weinberg approach was generalized to resonances was by Baru *et al.* (2004), where the spectral density was employed to supplement the parameter λ^2 introduced for bound states. The subject was later elaborated in various papers (Aceti and Oset, 2012; Hyodo, Jido, and Hosaka, 2012; Hyodo, 2013a, 2013b; Sekihara, Hyodo, and Jido, 2015; Guo and Oller, 2016a; Kang, Guo, and Oller, 2016; Xiao and Zhou, 2016, 2017a, 2017b; Sekihara, 2017); however, what is common to all of them is that a quantitative, probabilistic extraction of the level of compositeness is not possible rigorously as soon as one moves to resonances. The reason is that states that belong to poles on the second sheet are not normalizable and as such one loses the condition of Eq. (11) that is crucial for the probabilistic interpretation.

However, it still appears reasonable to take over the key finding of Sec. III.B, namely, that the coupling of a state is larger for a larger molecular component, also to resonance states. As we will see, in certain situations this leads to quite striking observable consequences. When being translated to an effective field theory this observation implies that for molecular states loop contributions always appear already at LO. The resulting power counting will be detailed in Sec. IV.

When the state of interest is located below the production threshold of the two hadrons that possibly form the molecular state, one can still distinguish between quasibound states and virtual states, depending on whether the leading pole is located on the first or the second sheet with respect to the mentioned two-hadron system. The phenomenological implications of this are discussed in Sec. III.C.

C. Characteristic line shapes of hadronic molecules

Besides the deuteron all other (candidates for) hadronic molecules are unstable. Then the scattering T matrix needs to be modified compared to the form discussed in Sec. III.B. In particular, Eq. (16) now reads

$$T_{\text{in}}(E) = \frac{g^2/2}{E - E_r + (g^2/2)(ik + \gamma) + i\Gamma_0/2}, \quad (36)$$

where $E = k^2/(2\mu)$ and Γ_0 accounts for inelasticities not related to the channel whose threshold is nearby. Those channels will be called inelastic channels. We also changed the parameter that controls the pole location from E_B to $-E_r$
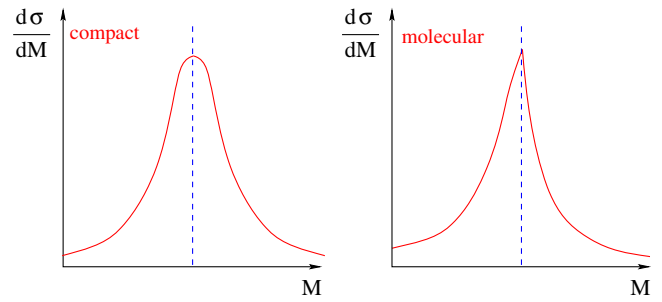
FIG. 9. Typical near-threshold line shapes that emerge for compact (left panel) and molecular states (right panel). The dashed perpendicular lines indicate the location of the threshold. The x axis shows $M = m_1 + m_2 + E$.

since it now refers to a resonance instead of a bound state. Following the logic of the previous sections in the near-threshold regime the dominant momentum dependence for molecular states comes from the term proportional to g^2 which is very large in this case; cf. Eq. (13). On the contrary, for compact states the k^2 term controls the momentum dependence. As a result of this in the former case the line shape of the state that appears in any of the inelastic channels is asymmetric while in the latter it is symmetric. The two scenarios are sketched in Fig. 9. In addition, the line shape for the molecular state shows a visible nonanalyticity at the two-particle threshold which would be much weaker in the other case.[16] Its presence follows directly from Eq. (36), since

$$\frac{\partial T_{\text{in}}(E)}{\partial E} \propto -\frac{1 + (ig^2/2)(\partial k/\partial E)}{[E - E_r + g^2/2(ik + \gamma) + i\Gamma_0/2]^2}, \quad (37)$$

with $\partial k/\partial E = \sqrt{\mu/2E}$. It is this derivative that is not continuous when the energy crosses zero, the location of the threshold. One might expect from this discussion that the coupling g^2 can be read off from the line shape directly allowing for a direct interpretation of the structure of the underlying state. However, a scale invariance of Eq. (37) for the line shape appears as soon as the g^2 term dominates, and it hinders a quantitative study in practice (Baru *et al.*, 2005). In addition, even for large values of g^2 the nonanalyticity might not show up in the line shape since its visibility depends in addition on a subtle interplay of E_r, Γ_0, and γ.

It was already mentioned at the end of Sec. III.B.2 that also near-threshold virtual poles leave a striking impact on observables. In the presence of inelastic channels a virtual state always leads to a peak of the line shape exactly at the threshold while a near-threshold bound state still has strength even below the threshold. For very near-threshold states such as the $X(3872)$ these two scenarios might be difficult to disentangle.

As first stressed by Braaten and Lu (2007) the line shapes in the elastic channel might well be interesting if at least one of the constituents of the system studied is unstable so that some

---

[16]It is completely absent only if the coupling between the state with the two hadrons vanishes. However, in this case the T matrix given in Eq. (36) vanishes as well.

strength of the amplitude leaks into the region below the threshold.[17] To be concrete: If a state is located near the threshold of particles A and B and A decays to a and b, then the spectra in the abB channel need to be studied both below and above the nominal AB threshold. To implement the necessary changes, in the formulas for narrow constituents one may simply replace the momentum k in Eq. (36) by (Braaten and Lu, 2007)

$$k_{\text{eff}} = \sqrt{\mu}\sqrt{\sqrt{E^2 + \Gamma^2/4} + E}$$
$$+ i\sqrt{\mu}\sqrt{\sqrt{E^2 + \Gamma^2/4} - E}, \qquad (38)$$

where Γ denotes the width of the unstable constituent, and μ is the reduced mass of the two-hadron system evaluated using the mass of the unstable state. In addition, the subtraction term γ needs to be replaced by

$$\gamma_{\text{eff}} = \pm\sqrt{\mu}\sqrt{\sqrt{E_r^2 + \Gamma^2/4} - E_r}, \qquad (39)$$

where the upper sign leads to a (quasi)bound state while the lower one to a virtual state. Clearly, for $\Gamma \to 0$ these expressions nicely map on those used for k and γ above for $E_r < 0$. Equations (38) and (39) hold as long as the line shape for the unstable constituent is well described by a BW distribution, namely, for $\Gamma/2 \ll m_A - m_a - m_b$. As soon as the energy dependence of Γ starts to matter, more sophisticated expressions need to be used; cf. Hanhart, Kalashnikova, and Nefediev (2010). For simplicity we here use the expressions previously given. The resulting line shapes in the elastic channel are shown for various values of Γ in Fig. 10, where we used the parameters

$$E_r = -0.5 \text{ MeV}, \quad \Gamma_0 = 1.5 \text{ MeV}, \quad g^2 = 0.1, \quad \mu = 0.5. \qquad (40)$$

The left panel shows the results for the (quasi)bound state ($\gamma_{\text{eff}} > 0$), and the right one is for the virtual state ($\gamma_{\text{eff}} < 0$). Above the nominal two-hadron channel ($E = 0$) the spectra in the left and right panels look very much alike, however, for $\Gamma > 0$ drastic differences appear between the two cases for negative values of E.

Following the Weinberg criterion, for the bound state case it is the relative height of the peak for $E < 0$ and the bump for $E > 0$ which are difficult to distinguish for the largest value of Γ, that is a measure of the molecular admixture of the studied state. Therefore a high-resolution measurement of the line shape of $X(3872)$ would be valuable to deduce its nature (Braaten and Lu, 2007; Hanhart *et al.*, 2007a; Hanhart, Kalashnikova, and Nefediev, 2010; Meng *et al.*, 2015; Kang and Oller, 2017).

In this context it is interesting to note that a line shape similar to the one shown in the left panel of Fig. 10 was also predicted for $Y(4260) \to D^*\pi\bar{D}$ under the assumption that
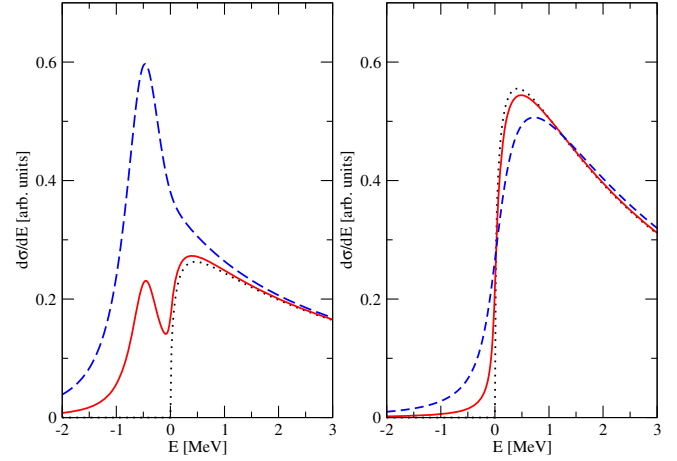
FIG. 10. Line shapes that emerge for a bound state (left panel) and for a virtual state (right panel) once one of the constituents is unstable. The dotted, solid, and dashed lines show the results for $\Gamma = 0$, 0.1, and 1 MeV, respectively. The other parameters of the calculation are given in Eq. (40).

$Y(4260)$ is a $D_1\bar{D}$ molecular state [note that $D^*\pi$ is the most prominent decay channel of $D_1(2420)$] (Wang *et al.*, 2014); see the middle panel of Fig. 6. A similar line shape also shows up in the calculation of Debastiani, Aceti *et al.* (2017) for the $f_1(1285)$ strongly coupled to $K^*\bar{K}$.

Everything stated so far had the implicit assumption that there are at most two near-threshold poles on the two relevant sheets. The possible line shapes change dramatically as soon as additional poles are located in the near-threshold regime as discussed by Artoisenet, Braaten, and Kang (2010), Baru *et al.* (2010), and Hanhart, Kalashnikova, and Nefediev (2011).

D. Heavy quark spin symmetry

In the limit of infinitely heavy quarks, the spin of heavy quarks decouples from the system and is conserved individually. As a result, the total angular momentum of the light degrees of freedom becomes a good quantum number as well. This gives rise to the so-called HQSS (Isgur and Wise, 1989). In the real world quarks are not infinitely heavy; however, heavy quark effective field theory allows one to systematically include corrections that emerge from finite quark masses in a systematic expansion in Λ_{QCD}/M_Q, where M_Q denotes the heavy quark mass. For an extensive review see Neubert (1994). HQSS is the origin for the near degeneracy of D^* and D as well as B^* and B. Similarly, it also straightforwardly predicts multiplets of hadronic molecules made of a heavy hadron or heavy quarkonium and light hadrons (Guo, Hanhart, and Meißner, 2009a; Yamaguchi *et al.*, 2015) and of hadroquarkonium as well (Cleven *et al.*, 2015). In addition, HQSS allows one to predict ratios of different transitions involving heavy hadrons in the same spin multiplet, and, in particular, transitions of hadronic molecules. Examples for those predictions can be found in Fleming and Mehen (2008, 2012) where the decays of the $X(3872)$ into the final states $\chi_{cJ}\pi$ and $\chi_{cJ}\pi\pi$ are discussed in the XEFT framework which will be discussed in Sec. IV.A. The ratios among various decays of the $Z_b(10610)$ and $Z_b(10650)$ into $h_b(mP)\pi$ and $\chi_{bJ}(mP)\gamma$ (from

---

[17]At the same time the nonanalyticity gets smeared out.

the neutral Z_b states) were computed in both XEFT (Mehen and Powell, 2011) and NREFT$_I$ (Cleven *et al.*, 2013) frameworks to be discussed in the next section. They are consistent with the result solely based on the HQSS (Ohkoda *et al.*, 2012a). For other predictions based on HQSS on the radiative and strong decays of hadronic molecules in the heavy quarkonium sector, see Ma *et al.* (2014, 2015).

In special cases HQSS also allows one to make predictions for bound systems of two or more heavy mesons (Mehen and Powell, 2011; Voloshin, 2011; Nieves and Valderrama, 2012; Guo *et al.*, 2013a; Liu, 2013; Baru *et al.*, 2016) since certain potentials get linked to each other. This will be discussed in Sec. IV.B.

IV. NONRELATIVISTIC EFFECTIVE FIELD THEORIES

All the candidates for hadron resonances, and, in particular, the candidates of hadronic molecules, which are the focus of this review, were discovered via their strong decays into other hadrons. Therefore, to understand these structures also requires a study of their decays. Because of the nonperturbative nature of QCD at hadronic energy scales, a first-principle calculation of the spectrum of hadronic resonances at the level of quarks and gluons can be done only using lattice QCD. Although there has been tremendous progress in lattice QCD, a reliable calculation of the full hadronic resonance spectrum for physical quark masses is still out of reach. In addition, even if such calculations were available, the interpretation of the emerging spectra still requires additional theoretical analyses.

Only in the special case discussed in Sec. III, i.e., for shallow bound states coupling in an S wave to a nearby continuum channel comprised of two stable or at least narrow hadrons, one finds a direct and physical interpretation for the leading and nonanalytic contribution of the wave function renormalization constant Z as the (normalizable) probability to find the continuum contribution in the physical state. Because of the closeness of the threshold to the mass of the physical composite state, such systems are ideal objects to apply the concept of EFTs, which makes use of the separation of scales and which per definition include a cutoff (Lepage, 1990). Of particular relevance here are the nonrelativistic EFTs (NREFTs). Note that the general principles underlying any EFT are formulated in Weinberg's paper on phenomenological Lagrangians (Weinberg, 1979).

As mentioned in Sec. III, hadronic molecules are located close to some strongly coupled thresholds. We denote the low-energy (low-momentum) scale characterizing such a system, given by the binding energy (binding momentum) defined in Eq. (6) [Eq. (5)], generically by Q. All other hadronic scales that we collectively label as Λ are thus regarded as hard. This enables one to construct a perturbation theory in Q/Λ, which for near-threshold states should be a small number. As will become clear, it depends on the system which scale is appropriate for Λ. For example, when investigating the $f_0(980)$ as a candidate for a $\bar{K}K$ molecular state, the inverse range of forces, the natural candidate for Λ, is given by the mass of the allowed lightest exchange meson, the rho meson. A phenomenologically adequate value for the binding energy is 10 MeV. It corresponds to a binding momentum of 70 MeV, and thus $Q/\Lambda \sim 1/10$ is a good expansion parameter.[18] Furthermore, the closeness to threshold also means that the constituent hadrons can be treated nonrelativistically.

As discussed in the preceding section, the most interesting information about the structure of a near-threshold state is contained in its coupling strength to the threshold channel, which measures the probability of finding the two-body bound state component in the physical state. This is consistent with the intuition that a state is the more composite the larger its coupling to the continuum. As shown in Eq. (25), for a bound state the coupling reaches its maximal value, if the physical state is purely an S-wave bound state, $\lambda^2 = 0$. Hence, it is important to extract the value of the coupling constant for understanding the nature of near-threshold structures. In addition, a large coupling implies the prominence of hadronic loops not only in the formation of the state but also in transitions and decays. In this section, we discuss the NREFT formalism which is a natural framework for studying the transitions involving hadronic molecules with a small energy release. It can also be used to compute the universal long-distance part of the production and decay processes of hadronic molecules, which will be discussed in Sec. VI.

The analytic structure of the three-point scalar loop integral (including the TS) will be discussed in Sec. IV.A.1. The power counting rules for the NREFT treating all intermediate particles on the same footing will be detailed in Sec. IV.A.2. We denote such a theory as NREFT$_I$. When one of the intermediate particles is much more off shell than the others, it can be integrated out from NREFT$_I$ and one gets another effective field theory, here called NREFT$_{II}$, which was originally introduced as XEFT to study the properties of the $X(3872)$. The XEFT and its relation to NREFT$_I$ will be discussed in Secs. IV.A.3 and IV.A.4. Section IV.B is devoted to a description of the formation of hadronic molecules.

The formation of hadronic molecules can be viewed as a result of nonperturbative hadron-hadron interactions. It is therefore natural to ask if there is also an impact of hadron loops on the properties of more regular excited hadrons. Indeed, for certain transitions the effective field theory NREFT$_I$ predicts prominent loop effects. As examples, we discuss single-pion or eta transitions and hindered $M1$ transitions between heavy quarkonia in Sec. IV.C. It will become clear that whether the hadron-loop effects are important for properties of an excited hadron is process dependent. In particular, the location of an excited hadron close to a threshold is a necessary but not a sufficient condition.

A. Power counting schemes

As demonstrated in Sec. III, the decisive feature of molecular states as compared to more compact structures is

---

[18]The subtle interplay of scales in molecular transitions was discussed by Hanhart *et al.* (2007b) on the example of decays of the $f_0(980)$.
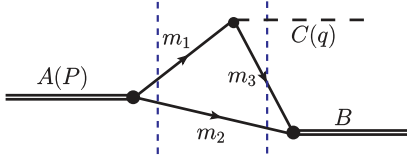
FIG. 11. A triangle diagram illustrating the long-distance contribution to the transition between two heavy particles A and B with the emission of a light particle C. The two vertical dashed lines denote the two relevant cuts.

the prominence of a two-hadron cut. In some decays the cuts induced by intermediate particles might also matter. To illustrate this point, we start this section by a discussion of the analytic structure of three-point loop functions. This will shed light on the NREFT power counting as well.

1. Analytic structure of the three-point loop integral

If a hadronic molecule has at least one unstable constituent, it can decay directly through the decays of that unstable particle when phase space allows. It can also decay into another heavy particle with a mass of the same order by emitting light particles such as pions or photons from its constituents. The mechanism for a transition accompanied by the emission of a single light particle is depicted in Fig. 11. In the figure the two vertical dashed lines show the relevant branch cuts: They correspond to the time slices at which the intermediate particles can go onto their mass shells.

We denote the intermediate particles as $M_{1,2,3}$ with masses $m_{1,2,3}$, and the external particles as A, B, C with masses $m_{A,B,C}$, as shown in Fig. 11. If all intermediate particles are nonrelativistic we can formulate a power counting based on the velocities of the intermediate particles. Let us start from the scalar triangle loop integral

$$I(q) = i \int \frac{d^4l}{(2\pi)^4} \frac{1}{(l^2 - m_1^2 + i\epsilon)[(P-l)^2 - m_2^2 + i\epsilon][(l-q)^2 - m_3^2 + i\epsilon]}$$
$$\simeq \frac{i}{N_m} \int \frac{dl^0 d^3\boldsymbol{l}}{(2\pi)^4} \frac{1}{[l^0 - T_1(|\boldsymbol{l}|) + i\epsilon][P^0 - l^0 - T_2(|\boldsymbol{l}|) + i\epsilon][l^0 - E_C - T_3(|\boldsymbol{l} - \boldsymbol{q}|) + i\epsilon]}, \quad (41)$$

where $\epsilon = 0^+$, $N_m = 8m_1 m_2 m_3$, $T_i(p) = p^2/2m_i$ denotes the kinetic energy for a heavy meson with mass m_i, and E_C denotes the energy of the particle C in the rest frame of the initial particle A. The second line is obtained by treating all the intermediate states nonrelativistically in the rest frame of the initial particle. Performing the contour integration over l^0, one gets a convergent integral over the three-momentum. Defining $\mu_{ij} = m_i m_j/(m_i + m_j)$, $b_{12} = m_1 + m_2 - m_A$, and $b_{23} = m_2 + m_3 + E_C - m_A$, one has

$$I(q) \simeq \frac{4\mu_{12}\mu_{23}}{N_m} \int \frac{d^3\boldsymbol{l}}{(2\pi)^3} \left[(l^2 + c_1 - i\epsilon)\left(l^2 + c_2 - \frac{2\mu_{23}}{m_3}\boldsymbol{l} \cdot \boldsymbol{q} - i\epsilon\right) \right]^{-1}, \quad (42)$$

where $c_1 = 2\mu_{12}b_{12}$ and $c_2 = 2\mu_{23}b_{23} + (\mu_{23}/m_3)q^2$ with $q \equiv |\boldsymbol{q}|$. The two terms in the denominator of the integrand contain a unitary cut each, as indicated by the vertical dashed lines in Fig. 11. The other two-body cut crossing the lines of M_1 and M_3 corresponds to the case in which the particle M_3 is propagating back in time (we assume implicitly that it is M_1 and not M_2 that can decay to M_3 and C in near on-shell kinematics). This is a relativistic effect which is neglected here. The intermediate particles M_1 and M_2 are on shell when $l^2 + c_1 = 0$; M_2 and M_3 (as well as C) are on shell for $l^2 + c_2 - 2\mu_{23}\boldsymbol{l} \cdot \boldsymbol{q}/m_3 = 0$. Accordingly, $\sqrt{|c_1|}$ and $\sqrt{|c_2|}$ define two different momentum scales where the corresponding intermediate states go on shell. Their values depend on all of the masses involved and may be very different from each other. For the nonrelativistic approximation to hold both must be small compared to m_i ($i = 1, 2, 3$).

The integral of Eq. (42) can be presented in closed form (Guo *et al.*, 2011; Mehen, 2015)

$$I(q) = \mathcal{N} \frac{1}{\sqrt{a}} \left[\arctan\left(\frac{c_2 - c_1}{2\sqrt{a(c_1 - i\epsilon)}} \right) - \arctan\left(\frac{c_2 - c_1 - 2a}{2\sqrt{a(c_2 - a - i\epsilon)}} \right) \right] \quad (43)$$

$$= \mathcal{N} \frac{1}{\sqrt{a}} \left[\arcsin\left(\frac{c_2 - c_1}{\sqrt{(c_2 - c_1)^2 + 4ac_1 - i\epsilon}} \right) - \arcsin\left(\frac{c_2 - c_1 - 2a}{\sqrt{(c_2 - c_1)^2 + 4ac_1 - i\epsilon}} \right) \right], \quad (44)$$

where $\mathcal{N} = \mu_{12}\mu_{23}/(2\pi m_1 m_2 m_3)$ and $a = (\mu_{23}/m_3)^2 q^2$. Especially Eq. (44) highlights the presence of a special singularity at

$$(c_2 - c_1)^2 + 4ac_1 = 0. \quad (45)$$

When rewriting the inverse trigonometric functions in terms of logarithms, one finds that this is a logarithmic divergence. The solution of Eq. (45) gives the leading Landau singularity (Landau, 1959) [for early or recent reviews, see Chang (1983), Eden *et al.* (1966), and Aitchison (2015)] for a triangle diagram, also called triangle singularity, evaluated in nonrelativistic kinematics (Guo, Meißner, and Shen, 2014). The singularity location is slightly shifted from that found by solving the relativistic Landau equation. A comparison for a specific example can

be found in the appendix of Guo, Meißner, and Shen (2014).

Being nonlinear in all of the involved masses, Eq. (45) as well as the Landau equation allows for different solutions. However, a direct evaluation of the loop integral reveals that only in a very restricted kinematics one of the solutions produces an observable effect, namely, when this solution is located on the physical boundary, i.e., the upper edge of the branch cut in the first Riemann sheet or alternatively the lower edge of the branch cut in the second (Schmid, 1967); see Fig. 7. In this case, the TS can produce a narrow peak in the invariant mass distribution, which may even mimic a resonance. This effect was already indicated in Sec. II.A.2 and will be further illustrated in Sec. VI.A.4. We therefore discuss now under which circumstances the singularity appears on the physical boundary. This case is contained in the Coleman-Norton theorem (Coleman and Norton, 1965) [for triangle diagrams see Bronzan (1964)]. The physical picture becomes most transparent using the simple triangle singularity equation derived by Bayar *et al.* (2016):

$$q_{\text{on}+} = q_{a-}, \qquad (46)$$

where $q_{\text{on}+}$ is the center-of-mass (c.m.) momentum of particles M_1 and M_2 when they are on shell, and q_{a-} is the momentum of particle M_2 in the rest frame of A when M_2 and M_3 are on shell (being on shell is necessary but not sufficient to define q_{a-}). One finds

$$q_{\text{on}+} = \frac{1}{2m_A} \sqrt{\lambda(m_A^2, m_1^2, m_2^2)},$$
$$q_{a-} = \gamma(\beta E_2^* - p_2^*), \qquad (47)$$

where

$$E_2^* = \frac{m_B^2 + m_2^2 - m_3^2}{2m_B}, \qquad p_2^* = \frac{\sqrt{\lambda(m_B^2, m_2^2, m_3^2)}}{2m_B}, \qquad (48)$$

are the energy and the magnitude of the three-momentum of particle M_2 in the rest frame of particle B, i.e., the c.m. frame of the (M_2, M_3) system, respectively, $\beta = q/E_B$ is the magnitude of the velocity of particle B in the rest frame of A, and $\gamma = 1/\sqrt{1 - \beta^2} = E_B/m_B$ is the Lorentz boost factor. Equation (46) is the condition for the amplitude $I(q)$ to have a TS on the physical boundary. Note that if particle M_1 can go on shell simultaneously with M_3 and C, it must be unstable. Consequently, its width moves the logarithmic divergence into the complex plane and the physical amplitude becomes finite.

Let us consider the kinematical region where the momentum of particle M_2 is positive so that Eq. (46) can be satisfied: $p_2 = q_{a-} = \gamma(\beta E_2^* - p_2^*) > 0$. Then $p_3 = \gamma(\beta E_3^* + p_2^*)$ (where E_3^* is the energy of particle M_3 in the rest frame of particle B), the momentum of particle M_3 in the rest frame of the initial particle is positive as well. This means that particles M_2 and M_3 move in the same direction in that frame. The corresponding velocities are given by

$$\beta_2 = \beta \frac{E_2^* - p_2^*/\beta}{E_2^* - \beta p_2^*}, \qquad \beta_3 = \beta \frac{E_3^* + p_2^*/\beta}{E_3^* + \beta p_2^*}. \qquad (49)$$

It is easy to see that $p_2 > 0$ leads to

$$\beta_3 > \beta > \beta_2, \qquad (50)$$

which means that particle M_3 moves faster than M_2 and in the same direction in the rest frame of the initial particle A. This, together with the requirement that all intermediate particles are on their mass shells, gives the condition for having a TS on the physical boundary. This is in fact the Coleman-Norton theorem (Coleman and Norton, 1965) applied to the triangle diagram: the singularity is on the physical boundary if and only if the diagram can be interpreted as a classical process in spacetime. For other discussions about TSs using the Mandelstam variables, see Szczepaniak (2015) and Liu, Oka, and Zhao (2016) and references therein.

To finish this section, we point out again that the TS mechanism has been around for more than half a century, but only in recent years has become a viable tool in hadron physics phenomenology due to the data discussed in this review. In fact, many of the calculations outlined in which the TS plays a dominant role can be and often are done without recourse to an EFT. Still, in a broader view it can nicely be embedded in the framework outlined here. In any case, whenever the TS can play a role it has to be included.

2. NREFT$_{\text{I}}$

A key component for any EFT is the power counting in terms of some dimensionless small quantity, which allows for a systematic expansion and an estimate for the uncertainty of the calculation caused by the truncation of the series at some finite order. The natural small quantity in nonrelativistic systems is the velocity v (measured in units of the speed of light) which is much smaller than 1 by assumption.

As mentioned in Sec. IV.A.1, triangle diagrams with all three intermediate particles being nonrelativistic in fact have two momentum scales given by $\sqrt{|c_1|}$ and $\sqrt{|c_2|}$. Accordingly, one can define $v_1 = \sqrt{|c_1|}/(2\mu_{12})$ and $v_2 = \sqrt{|c_2 - a|}/(2\mu_{23})$ for the velocities of the intermediate mesons.

From the previous analysis, three-point loop diagrams have two kinds of singularities: two-body threshold cusps and TSs. The two-body threshold singularities are encoded in the two velocities previously defined. When the TS, with its location implicitly defined via Eq. (45), is not in the considered kinematic region, the loop function of Eq. (44) can be expanded in a power series as

$$I(q) = \frac{\mathcal{N}}{\sqrt{a}} \left[\left(\frac{\pi}{2} - \frac{2\sqrt{ac_1}}{c_2 - c_1} \right) - \left(\frac{\pi}{2} - \frac{2\sqrt{ac_2}}{c_2 - c_1} \right) \right.$$
$$\left. + \mathcal{O}\left(\frac{(4ac_1)^{3/2}}{(c_2 - c_1)^3} \right) \right]$$
$$= \mathcal{N} \frac{2}{\sqrt{c_2} + \sqrt{c_1}} + \cdots. \qquad (51)$$

When the masses of all three intermediate particles are similar, $m_i \sim m$, the LO term in Eq. (51) may be written as

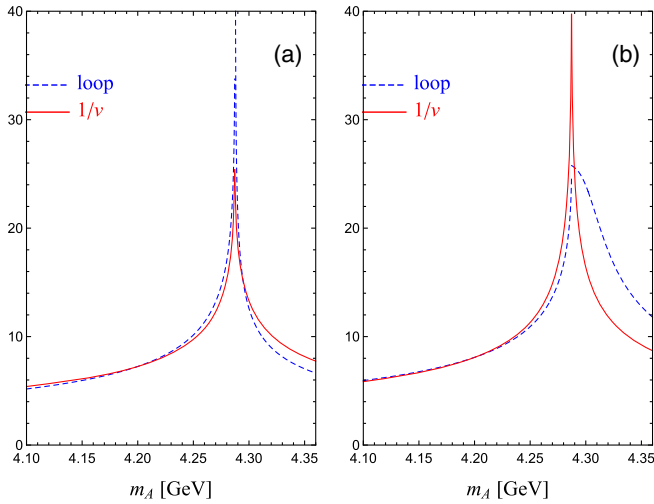FIG. 13.   A one-loop two-point self-energy diagram.

FIG. 12.   Comparison of the power counting rule for the scalar three-point loop integral $1/v$ with the numerical result evaluated using Eq. (43). The numerical result is normalized to $1/v$ at $m_A = 4.22$ GeV. The involved masses are given in Eq. (53), and the mass for the final heavy particle takes the value of (a) 3.886 and (b) 3.872 GeV.

$$I(q) \sim \frac{\mathcal{N}}{m} \frac{2}{v_1 + v_2}. \tag{52}$$

Thus the arithmetic mean of the two velocities characterizes the size of the triangle loop. It is therefore the relevant parameter to estimate the leading loop contribution for the transition of a heavy state into a light state and another heavy state.

The power counting in nonrelativistic velocities for a given loop diagram can be obtained by applying the following rules: The three-momentum of the intermediate nonrelativistic particles counts as $\mathcal{O}(v)$, the nonrelativistic energy counts as $\mathcal{O}(v^2)$, and each nonrelativistic propagator is of $\mathcal{O}(v^{-2})$. Thus, $I(q)$ scales as $\mathcal{O}(v^5/(v^2)^3) = \mathcal{O}(v^{-1})$. Comparing with Eq. (52), one sees that the velocity in the power counting should be understood as the average of v_1 and v_2 (Guo and Meißner, 2012b). In addition to the parts discussed, the amplitude for a given process can have factors of the external momentum q. To be general we do not count the external momentum q in powers of v, but keep it explicitly. This defines the power counting as detailed by Guo, Hanhart, and Meißner (2009c) and Guo *et al.* (2010, 2011). We denote this theory as NREFT$_{\mathrm{I}}$.

In order to demonstrate how the power counting rules work, we compare in Fig. 12 the values of $1/v$ with $v = (v_1 + v_2)/2$ and an explicit calculation of the loop function as given in Eq. (43). The curves are normalized at $m_A = 4.22$ GeV. The values used for the calculation are

$$m_1 = 2.420 \text{ GeV}, \quad m_2 = 1.867 \text{ GeV}, \quad m_3 = 2.009 \text{ GeV}. \tag{53}$$

For the external light particle we take $m_C = 0.140$ GeV for Fig. 12(a) and $m_C = 0$ for Fig. 12(b). In addition, we take two
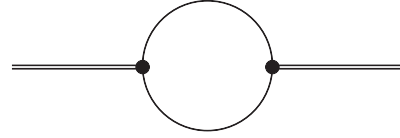
values for m_B, 3.886 and 3.872 GeV, and the results are shown as (a) and (b), respectively. Then (a) and (b) correspond to the loop integrals in the amplitudes for the $Y(4260) \to Z_c(3900)\pi$ and $Y(4260) \to X(3872)\gamma$, respectively, which will be discussed in Sec. VI.A. Using Eq. (45) or (46), we find that for $m_B = 3.886$ GeV there is a TS at $m_A = 4.288$ GeV, which is the reason for the sharp peak in the dashed line in Fig. 12(a). Note that in the plots the widths of the intermediate mesons were neglected. For $m_B = 3.872$ GeV, which is smaller than $m_2 + m_3$, and $m_C = 0$, the TS moves to the complex plane at $m_A = 4.301 - i0.018$ GeV with a clearly visible effect on the line shape; see the dashed line in Fig. 12(b). One sees from the figure that the simple power counting rule of Eq. (52) agrees remarkably well with the explicit calculation except for energies very close to the TS.

In addition to counting the loop integral as discussed, one also needs to take into account the vertices in order to obtain a proper estimate for a given loop amplitude. To illustrate the method let us start from the simplest two-point self-energy diagram shown in Fig. 13. We assume that the mass of the state is close to the threshold of the internal particles that can therefore be treated nonrelativistically. If the coupling is in an S wave, then the loop scales as $\mathcal{O}(v^5/(v^2)^2) = \mathcal{O}(v)$.[19] If the coupling is in a P wave, each vertex contributes an additional factor of v and the loop scales as $\mathcal{O}(v^3)$. Of course, the real part of the loop integral is divergent, and the resulting correction to the mass is scale dependent. However, since the scale dependence can be formally absorbed into the bare mass of the state this discussion is not of relevance here. Thus, we found that the effect of the two-hadron continuum on the self-energy of heavy quarkonia is parametrically suppressed, if the state is close to the threshold which implies a small value of v, and that this suppression increases for increasing orbital angular momentum of the two-hadron state.

Next we consider the one-loop diagram for the decay process $A \to BC$, with A and B heavy and C light, as depicted in Fig. 11. To be concrete, we assume that C couples to the intermediate states M_1 and M_3 in a P wave (such as the pion couples to the ground-state heavy mesons). This coupling structure leads to a factor of q (in the rest frame of A). The generalization to other situations is easy. The power counting rules for a few typical cases are then as follows:

(1) Both A and B couple to the intermediate states in an S wave. As a result the final state particles B and C must be in a P wave. Therefore Eq. (52) needs to be multiplied by q. Still, the $1/v$ enhancement factor quantifies the relative importance of the triangle diagram for the transition: the closer both A and B

---

[19]Here we focus only on the velocity scaling and neglect the geometric factor of $1/(4\pi)$.

to the corresponding thresholds, the more important the intermediate states. On top of this may come an additional enhancement driven, e.g., by large couplings characteristic for molecular states as derived in Sec. III.

(2) Either A or B couples to the intermediate states in an S wave with the other one in a P wave. In this case, because there is only one possible linearly independent external momentum for two-body decays, the internal momentum at the P-wave vertex must be turned into an external momentum. The amplitude scales as $\mathcal{O}(q^2/m^2 v)$. Since the decay should be in an S wave in this case, we introduced a factor $1/m^2$ to balance the dimension of the q^2 factor (Guo *et al.*, 2011) as in this case the loop contribution needs to be compared to a constant tree-level contribution.

(3) Both A and B couple to the intermediate states in a P wave. Each P-wave vertex contributes a factor of the internal momentum. In the power counting of NREFT$_\mathrm{I}$, the external momentum is kept explicitly. As a result, there are two possibilities for the scaling of the P-wave vertices: Each P-wave vertex scales either as mv or as the external momentum q. More insights can be obtained if we take a closer look at the relevant tensor loop integral:

$$I^{ij}(\boldsymbol{q}) = i \int \frac{d^4 l}{(2\pi)^4} l^i l^j \times [\text{integrand of } I(q)]. \quad (54)$$

In the rest frame of the initial particle, it can be decomposed into an S-wave part and a D-wave part as

$$I^{ij}(\boldsymbol{q}) = P_S^{ij} I_S(q) + P_D^{ij} I_D(q), \quad (55)$$

where

$$P_S^{ij} = \frac{\delta^{ij}}{\sqrt{3}}, \qquad P_D^{ij} = \frac{1}{\sqrt{6}}\left(3\frac{q^i q^j}{q^2} - \delta^{ij}\right), \quad (56)$$

are the S- and D-wave projectors, respectively, which satisfy $P_S^{ij} P_S^{ij} = 1$, $P_D^{ij} P_D^{ij} = 1$, and $P_S^{ij} P_D^{ij} = 0$. Then in the S-wave part $I_S(q)$, the internal momentum scales as $\mathcal{O}(v)$, and $I_S(q) \sim \mathcal{O}(v)$. In the D-wave part $I_D(q)$, the internal momentum turns external, and one gets $I_D(q) \sim \mathcal{O}(q^2/m^2 v)$, which would have the same scaling as $I_S(q)$ if $q/m \sim v$.[20] For the decay amplitude, the factor of q from the vertex coupling C to intermediate states needs to be taken into account additionally.

This nonrelativistic power counting scheme was proposed by Guo, Hanhart, and Meißner (2009c) to study the coupled-channel effects of charm-meson loops in charmonium transitions and studied in detail later (Guo *et al.*, 2011).

Applications to transitions between two heavy quarkonium states can be found in Guo *et al.* (2010), Guo, Hanhart, and Meißner (2010), Guo and Meißner (2012a, 2012b), Mehen and Yang (2012), and Guo, Meißner, and Shen (2014), and to transitions involving one or two XYZ states in Cleven *et al.* (2011a, 2013), Guo, Hanhart *et al.* (2013), Esposito, Guerrieri, and Pilloni (2015), Mehen (2015), Abreu and Lafayette Vasconcellos (2016), Huo and Chen (2016), Wu *et al.* (2016), and Y.-H. Chen *et al.* (2017). In particular, Cleven *et al.* (2013) demonstrated the implications of items (1) and (2). It was shown that, while the transitions of the Z_b states to $\Upsilon(nS)\pi$ potentially suffer from large higher order corrections, the transitions to $h_b(mP)\pi$ and $\chi_{bJ}(mP)\pi$ should be dominated by the triangle topology. The near-threshold cross section for $e^+ e^- \to D\bar{D}$ was studied by Chen and Zhao (2013) using NREFT as well.

It is clear that the power counting can be applied only to processes where the intermediate hadrons are nonrelativistic and especially close to their mass shells. Otherwise the loop diagrams receive contributions from large momenta and cannot be treated in a simple EFT including only the hadronic degrees of freedom of A, B, C, M_1, M_2, and M_3.

3. NREFT$_\mathrm{II}$ and XEFT

Because the $X(3872)$ is arguably the most important and interesting candidate for a hadronic molecule, here we discuss in some detail one NREFT designed specifically for studying the properties of the $X(3872)$. It is called XEFT and was proposed by Fleming *et al.* (2007) following the Kaplan-Savage-Wise approach to describe the nucleon-nucleon system (Kaplan, Savage, and Wise, 1998a, 1998b). It can be regarded as a special realization of NREFT$_\mathrm{II}$. Similar effective theories can be constructed for other possible hadronic molecules which are located very close to thresholds. For instance, in the framework of a similar theory, the $Z_b(10610)$ and $Z_b(10650)$ were studied by Mehen and Powell (2011, 2013) and the $Z_c(3900)$ by Wilbring, Hammer, and Meißner (2013).

The XEFT assumes the $X(3872)$ to be a hadronic molecule of $D^0\bar{D}^{*0} + $ c.c. The small binding energy (Patrignani *et al.*, 2016)

$$B_X = M_{D^0} + M_{D^{*0}} - M_X = 0.00 \pm 0.18 \text{ MeV} \quad (57)$$

implies that the long-distance part of the $X(3872)$ wave function is universal and is insensitive to the binding mechanism which takes place at a much shorter distance. The long-distance degrees of freedom are D^0, D^{*0}, $\bar{D}^0$, $\bar{D}^{*0}$, and π^0; all of them are treated nonrelativistically. For processes dominated by the long-distance scales such as the decays $X(3872) \to D^0\bar{D}^0\pi^0$ and $X(3872) \to D^0\bar{D}^0\gamma$ which can occur via the decay of the vector charm meson directly, the XEFT at LO can reproduce the results from the effective range theory which makes use of the universal two-body wave function of the $X(3872)$ at asymptotically long distances (Voloshin, 2004b, 2006)

$$\psi_X(r) \propto \frac{e^{-\gamma_0 r}}{r}, \quad (58)$$

---

[20]Noticing that $P_S^{ij} l^i l^j = l^2/\sqrt{3}$ and $P_D^{ij} l^i l^j = 2l^2 P_2(\cos\theta)/\sqrt{6}$ with $P_2(\cos\theta)$ the second Legendre polynomial, it can be shown that $I_S(q)$ is UV divergent while $I_D(q)$ is UV convergent (Albaladejo *et al.*, 2015; Shen *et al.*, 2016). The power counting of the D-wave part was not discussed by Guo *et al.* (2011).

where the $X(3872)$ is assumed to be below the $D^0\bar{D}^{*0}$ threshold, and $\gamma_0 = \sqrt{2\mu_0 B_X} \leq 20$ MeV with μ_0 the reduced mass of D^0 and $\bar{D}^{*0}$. Yet, it has the merit of being improvable order by order by including local operators and pion exchanges although unknown short-distance coefficients will be involved. For processes involving shorter-distance scales such as the decays of the $X(3872)$ into a charmonium and light particles, the XEFT can still be used by parametrizing the short-distance physics in terms of local operators employing factorization theorems and the operator product expansion (Braaten and Kusunoki, 2005b; Braaten and Lu, 2006). The XEFT can also be used even if the $X(3872)$ is a virtual state with a non-normalizable wave function (Hanhart *et al.*, 2007a) or a resonance above threshold.

The power counting and the next-to-leading order (NLO) corrections to the decay $X(3872) \to D^0\bar{D}^0\pi^0$ were studied by Fleming *et al.* (2007). The XEFT was also used to study the decays of the $X(3872)$ to the χ_{cJ} with one and two pions (Fleming and Mehen, 2008, 2012), the radiative transitions $X(3872) \to \psi(2S)\gamma$, $\psi(4040) \to X(3872)\gamma$ (Mehen and Springer, 2011), and $\psi(4160) \to X(3872)\gamma$ (Margaryan and Springer, 2013), the scattering of an ultrasoft pion (Braaten, Hammer, and Mehen, 2010) or D and D^* (Canham, Hammer, and Springer, 2009) off the $X(3872)$, and the quark mass dependence and finite-volume corrections of the $X(3872)$ binding energy (Jansen, Hammer, and Jia, 2014, 2015). The relation between the XEFT and the formalism of NREFT$_\mathrm{I}$ was clarified by Mehen (2015). As an extension of the XEFT in Alhakami and Birse (2015) a modified power counting was suggested to also take into account an expansion in the ratio between the pion mass and the charm-meson masses.

The need for such an expansion is removed, however, as soon as Galilean invariance is imposed on the interactions (Braaten, 2015).

In the following, we use the decay $X(3872) \to D^0\bar{D}^0\pi^0$ as an example to illustrate the power counting of the XEFT. The binding momentum $\gamma_0 \leq 20$ MeV sets the long-distance momentum scale in this theory. The typical momenta for the D^0 and D^{*0} are of the order of $p_D \sim p_{D^*} \sim \gamma_0$. The pion kinetic energy is less than 7 MeV, and thus the momentum for either an internal or external pion is also counted as $p_\pi \sim \gamma_0$. Furthermore, the pion exchange introduces another small scale $\mu = \sqrt{\Delta^2 - M_{\pi^0}^2} \simeq 44$ MeV, with $\Delta = M_{D^{*0}} - M_{D^0}$. Denoting all the small momentum scales by Q, we have

$$\{p_D, p_{D^*}, p_\pi, \mu, \gamma_0\} = \mathcal{O}(Q). \tag{59}$$

Thus, the measure for a one-loop integral is of $\mathcal{O}(Q^5)$, and each nonrelativistic propagator is of $\mathcal{O}(Q^{-2})$. All Feynman diagrams can then be assigned a power of Q.

The XEFT keeps as the degrees of freedom only those modes with a very low momentum $\sim \gamma_0$. The binding momentum for the D^+D^{*-} + c.c. channel at the $X(3872)$ mass is $\gamma_c \simeq 126$ MeV. It is treated as a hard scale, and the charged charm mesons are integrated out from the XEFT.

Denoting the field annihilating the D^0, $\bar{D}^0$, D^{*0}, and $\bar{D}^{*0}$ by D, $\bar{D}$, $\boldsymbol{D}$, and $\bar{\boldsymbol{D}}$, respectively, and taking the phase convention that $X(3872)$ is $(D^0\bar{D}^{*0} + \bar{D}D^{*0})/\sqrt{2}$, the relevant Lagrangian for the calculation up to the NLO is written as (Fleming *et al.*, 2007)

$$\mathcal{L}_{\mathrm{XEFT}} = \sum_{\boldsymbol{\phi}=\boldsymbol{D},\bar{\boldsymbol{D}}} \boldsymbol{\phi}^\dagger \left(i\partial_0 + \frac{\boldsymbol{\nabla}^2}{2M_{D^{*0}}} \right) \boldsymbol{\phi} + \sum_{\phi=D,\bar{D}} D^\dagger \left(i\partial_0 + \frac{\boldsymbol{\nabla}^2}{2M_{D^0}} \right) D + \pi^\dagger \left(i\partial_0 + \frac{\boldsymbol{\nabla}^2}{2M_{\pi^0}} + \delta \right) \pi$$
$$+ \left[\frac{g}{2F_\pi} \frac{1}{\sqrt{2M_{\pi^0}}} (D\boldsymbol{D}^\dagger \cdot \boldsymbol{\nabla}\pi + \bar{D}^\dagger \bar{\boldsymbol{D}} \cdot \boldsymbol{\nabla}\pi^\dagger) + \mathrm{H.c.} \right]$$
$$- \frac{C_0}{2} (\bar{\boldsymbol{D}}D + \boldsymbol{D}\bar{D})^\dagger \cdot (\bar{\boldsymbol{D}}D + \boldsymbol{D}\bar{D}) + \left[\frac{C_2}{16} (\bar{\boldsymbol{D}}D + \boldsymbol{D}\bar{D})^\dagger \cdot [\bar{\boldsymbol{D}}(\overset{\leftrightarrow}{\boldsymbol{\nabla}})^2 D + \boldsymbol{D}(\overset{\leftrightarrow}{\boldsymbol{\nabla}})^2 \bar{D}] + \mathrm{H.c.} \right]$$
$$+ \left[\frac{B_1}{\sqrt{2}} \frac{1}{\sqrt{2M_{\pi^0}}} (\bar{\boldsymbol{D}}D + \boldsymbol{D}\bar{D})^\dagger \cdot D\bar{D}\boldsymbol{\nabla}\pi + \mathrm{H.c.} \right]$$
$$+ \frac{C_\pi}{2M_{\pi^0}} (D^\dagger \pi^\dagger D\pi + \bar{D}^\dagger \pi^\dagger \bar{D}\pi) + C_{0D} D^\dagger \bar{D}^\dagger D\bar{D}, \tag{60}$$

where $\delta = \Delta - M_{\pi^0} \simeq 7$ MeV and $F_\pi = 92.2$ MeV is the pion decay constant. The first line contains the kinetic terms for the pseudoscalar and vector charm mesons as well as for the nonrelativistic pion, the second line is for the axial coupling of the pion to charm mesons with $g \simeq 0.6$ determined from the D^* width, the third line contains the LO and NLO contact interaction terms, and the fourth line contains the terms for a short-distance emission of a pion. The contact terms in the last line were not considered by Fleming *et al.* (2007), but also contribute to $X(3872) \to D^0\bar{D}^0\pi^0$ at NLO. In particular, the C_{0D} term may have a

significant impact on the line shapes as will become clear in the discussion to follow.

The Feynman diagrams relevant for the calculation of the $X(3872) \to D^0\bar{D}^0\pi^0$ decay width up to NLO are shown in Fig. 14. Figure 14(a) contributes at LO, Figs. 14(b) and 14(c) and Figs. 14(e) and 14(f) are the NLO diagrams calculated by Fleming *et al.* (2007), and Figs. 14(d) and 14(g) are two new diagrams from the new terms in the last line of the Lagrangian in Eq. (60). Here we discuss only the power counting for each diagram and the contributions missing in the original work (Fleming *et al.*, 2007), and refer to Fleming *et al.* (2007) for details of the calculation. One essential point of the XEFT is
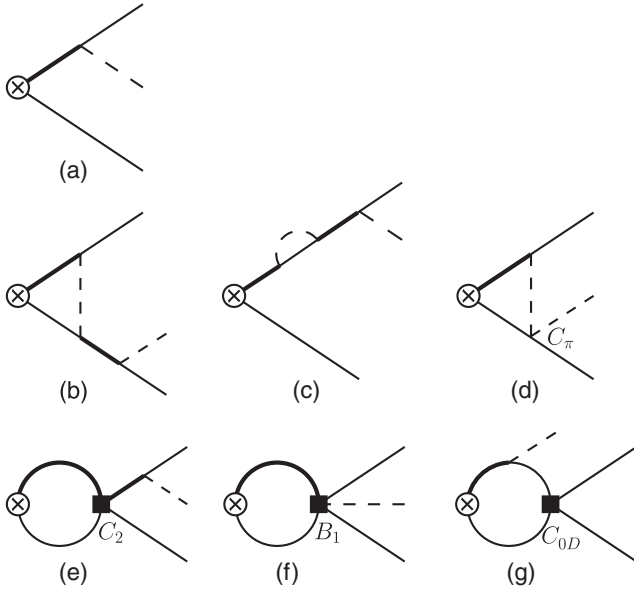
FIG. 14. (a) LO and (b)–(g) NLO diagrams for the calculation of the $X(3872) \to D^0 \bar{D}^0 \pi^0$ decay width. The circled crosses denote an insertion of the $X(3872)$, the thin and thick solid lines represent the pseudoscalar and vector charm mesons, respectively, and the dashed lines denote the pions.

that the pion exchange is treated perturbatively based on the observation that the two-pion exchange contribution is suppressed relative to the one-pion exchange by

$$\frac{g^2 \mu_0 \mu}{8\pi F_\pi^2} \simeq \frac{1}{20} - \frac{1}{10}. \tag{61}$$

Then the $X(3872)$ is generated through a resummation of the $D\bar{D}^*$ contact terms (the charge conjugated $\bar{D}D^*$ channel is always implied). The pole of the $X(3872)$ is at $E = -B_X$, and thus at LO

$$1 + C_0 \Sigma_0(-B_X) = 0, \tag{62}$$

where

$$\Sigma_0(E) = -\left(\frac{\Lambda_{\text{PDS}}}{2\pi}\right)^{4-D} \int \frac{d^{D-1}l}{(2\pi)^{D-1}} \frac{1}{E - l^2/(2\mu_0) + i\epsilon}$$
$$= \frac{\mu_0}{2\pi}(\Lambda_{\text{PDS}} - \sqrt{-2\mu_0 E - i\epsilon}) \tag{63}$$

is the two-point one-loop integral containing nonrelativistic D^0 and $\bar{D}^{*0}$ propagators in the power divergence subtraction (PDS) scheme (Kaplan, Savage, and Wise, 1998a, 1998b), where E is the energy defined relative to the threshold and Λ_{PDS} is the PDS scale. For Eq. (62) to be renormalization group invariant, C_0 needs to absorb the scale dependence of the loop integral:

$$C_0(\Lambda_{\text{PDS}}) = \frac{2\pi}{\mu_0(\gamma_0 - \Lambda_{\text{PDS}})}. \tag{64}$$

Keeping only momentum modes of order Q, the power counting for the loop integral is $\Sigma_0(E) = \mathcal{O}(Q^5/(Q^2)^2) = \mathcal{O}(Q)$.

One sees that the scale-independent part of C_0, $\bar{C}_0 = [\Lambda_{\text{PDS}} + 1/C_0(\Lambda_{\text{PDS}})]^{-1} = 2\pi/(\mu_0\gamma_0)$, indeed scales as Q^{-1}.

Now we consider the power counting of the decay amplitudes from the diagrams in Fig. 14. The decay rate can be obtained from these amplitudes properly taking into account the wave function renormalization Z (Fleming *et al.*, 2007) which accounts for the insertion of the $X(3872)$ interpolating field shown as circled crosses in Fig. 14. Note that for the calculation of the decay rate up to the NLO, one needs Z up to NLO (LO) for the LO (NLO) amplitude. The amplitude from Fig. 14(a) scales as $\mathcal{O}(Q/Q^2) = \mathcal{O}(Q^{-1})$ since there is one nonrelativistic propagator and one P-wave vertex which gives a factor of $p_\pi \sim Q$. Both one-loop diagrams [Figs. 14(b) and 14(c)] have four nonrelativistic propagators and three P-wave vertices, and thus scale as $\mathcal{O}(Q^0)$, 1 order higher than the LO diagram [Fig. 14(a)]. The coefficients C_2 and B_1 scale as Q^{-2} (Fleming *et al.*, 2007). Noticing that there are two derivatives in the C_2 term and one derivative in the B_1 term in the Lagrangian, the amplitudes from Figs. 14(e) and 14(f) should be counted as $\mathcal{O}(Q^0)$ as well.

Let us discuss Figs. 14(d) and 14(g) which were missing in the original calculation in Fleming *et al.* (2007). The C_π contact term can be matched to the chiral Lagrangian for the interaction between heavy and light mesons (Burdman and Donoghue, 1992; Wise, 1992; Yan *et al.*, 1992; Guo *et al.*, 2008). At LO of the chiral expansion the interaction between pions and pseudoscalar heavy mesons receives contributions from the Born term from the exchange of D^*, which constitutes a subdiagram to Figs. 14(b) and 14(c), and the Weinberg-Tomozawa term. It turns out that the amplitude for $D^0\pi^0 \to D^0\pi^0$ vanishes at LO. At NLO of the chiral expansion, there are several operators (Guo *et al.*, 2008; Guo, Hanhart, and Meißner, 2009b). In particular, it is easy to see that the h_0 and h_1 terms are proportional to the light quark mass or equivalently to M_π^2. The Feynman rule for the $D^0\pi^0 \to D^0\pi^0$ vertex from these two terms (using relativistic normalization for all the fields) is

$$i\mathcal{A}_{h_0,h_1} = i\frac{2}{3}(6h_0 + h_1)\frac{M_\pi^2}{F_\pi^2}. \tag{65}$$

The value of h_1 is fixed to be 0.42 from the mass splitting between the D_s and D mesons, and the $1/N_c$ suppressed parameter $h_0 \simeq 0.01$ from fitting to the lattice data for the pion mass dependence of charm-meson masses (L. Liu *et al.*, 2013). One sees $\mathcal{A}_{h_0,h_1} \simeq 0.65$. Hence, by matching to the chiral Lagrangian, C_π should scale as Q^0, which leads to the scaling of $\mathcal{O}(Q^0)$ for Fig. 14(d).

Figure 14(g) involves a short-distance contact interaction between D^0 and $\bar{D}^0$. If the vertex C_{0D} scales as Q^0, then diagram $(g) = \mathcal{O}(Q^0)$. However, the situation could be more complicated. From the HQSS analysis of the $X(3872)$ in Sec. III.D, the $X(3872)$ as a $D\bar{D}^*$ hadronic molecule should have three spin partners in the strict heavy quark limit; one of them has quantum numbers $J^{PC} = 0^{++}$ and couples to $D\bar{D}$ and $D^*\bar{D}^*$. Therefore, there is the possibility that the $D\bar{D}$ interaction needs to be resummed to generate a near-threshold pole. In this case, C_{0D} needs to be promoted to be $\mathcal{O}(Q^{-1})$,
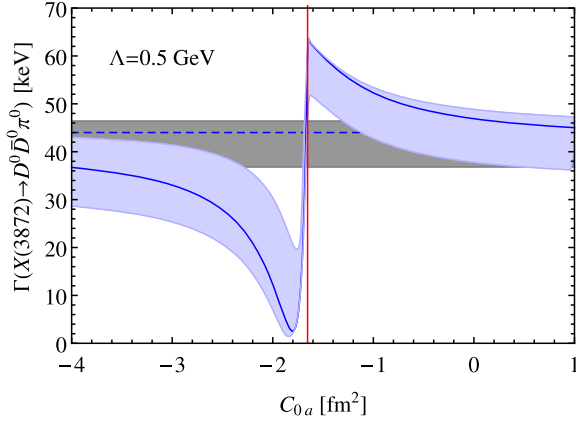
FIG. 15. The decay width of the $X(3872) \to D^0 \bar{D}^0 \pi^0$ taking into account the $D\bar{D}$ final state interaction in the framework of the Lippmann-Schwinger equation regularized by a Gaussian form factor. Here the cutoff in the Gaussian regulator is taken to be $\Lambda = 0.5$ GeV, and C_{0a} is the unknown isoscalar part of the $D\bar{D}$ contact term. The gray and blue bands correspond to the uncertainty bands without and with the $D\bar{D}$ final state interaction, respectively. The vertical line denotes the $D^0\bar{D}^0$ threshold. Adapted from Guo, Hidalgo-Duque *et al.*, 2014.

analogous to C_0. Then Fig. 14(g) appears at $\mathcal{O}(Q^{-1})$ making it a LO contribution. Clearly this can cause a large correction to the $X(3872) \to D^0\bar{D}^0\pi^0$ decay rate. This effect can be seen in Fig. 15, which is the result obtained by Guo, Hidalgo-Duque *et al.* (2014) using NREFT$_I$ in combination with the framework discussed in Sec. IV.B. The unknown parameter C_{0a} in the figure parametrizes the isoscalar part of $D^\dagger \bar{D}^\dagger D\bar{D}$ contact interaction [see Eq. (78)], playing a role similar to C_{0D} introduced in Eq. (60).

Since $X(3872) \to D^0\bar{D}^0\pi^0$ is an important process sensitive to the long-distance structure of the $X(3872)$, it would be interesting to revisit it considering the missing diagrams in XEFT. In particular, it was found that the nonanalytic corrections from the pion-exchange diagrams of Figs. 14(b) and 14(c) contribute only to ~1% of the decay rate (Fleming *et al.*, 2007). Whether this remains true after considering Fig. 14(d) remains to be seen.

It should be stressed that the role of nonperturbative pions on the $X(3872)$ properties has been studied in various papers (Baru *et al.*, 2011, 2013, 2016) which in many cases confirm the results of XEFT. However, also in these studies diagrams of the types shown in Figs. 14(d) and 14(g) were not included.

4. From NREFT$_I$ to XEFT

From the previous discussions, we see that all momentum scales much larger than $\gamma_0 \leq 20$ MeV have been integrated out from the XEFT. This is different from NREFT$_I$, where all nonrelativistic modes are kept as effective degrees of freedom including those with a momentum of the order of a few hundred of MeV. NREFT$_I$ when applied to the $X(3872)$ can be regarded as the high-energy theory for the XEFT. The short-distance operators in XEFT at the scale of a few hundred of MeV can be matched to NREFT$_I$. This has been discussed by Mehen (2015) in the context of calculations of the reactions $X(3872) \to \chi_{cJ}\pi^0$.

To show the relation between NREFT$_I$ and XEFT explicitly let us consider the case $c_2 \gg c_1$. The quantities c_2 and c_1 introduced in Eq. (42) define the locations of the two-body cuts of the triangle diagram. In the low-momentum region $l \sim \sqrt{c_1}$, the second factor in the integrand of Eq. (42) can be expanded in powers of l^2/c_2 and one gets

$$I(q) = \frac{4\mu_{12}\mu_{23}}{N_m c_2} \int^\Lambda \frac{d^3l}{(2\pi)^3} \frac{1}{l^2 + c_1 - i\epsilon} \left[1 + \mathcal{O}\left(\frac{c_1}{c_2}\right)\right]$$
$$\simeq \frac{\mu_{12}}{2\pi N_m [b_{23} + q^2/(2m_3)]} (\Lambda_{\text{PDS}} - \sqrt{c_1 - i\epsilon}). \quad (66)$$

The resulting momentum integral in the first line is divergent and needs to be regularized. The natural UV cutoff of the new effective theory is set by $\Lambda < \sqrt{c_2}$. We denote such a theory as NREFT$_{II}$. It reduces to the XEFT when applied to the $X(3872)$. In order to compare with the XEFT, in the second line of Eq. (66) we evaluate the integral in the PDS scheme which is equivalent to the sharp cutoff regularization by letting $\Lambda_{\text{PDS}} = 2\Lambda/\pi$ and dropping the terms of $\mathcal{O}(1/\Lambda)$. For a detailed comparison of dimensional versus cutoff regularization see Phillips, Beane, and Birse (1999).

For $m_1 = M_{D^{*0}}$, $m_2 = M_{D^0}$, $E_C = E_\pi$, and $m_A = M_X$, the second line of Eq.(66) reduces to

$$-\frac{1}{N_m(E_\pi + \Delta_H)} \frac{1}{C_0(\Lambda_{\text{PDS}})}, \quad (67)$$

where $\Delta_H = M_{D^0} + m_3 - M_X$, and the term $q^2/(2m_3)$ has been neglected. Terms of this form appear in the XEFT amplitudes for transitions between the $X(3872)$ and a charmonium with the emission of a light particle (Fleming and Mehen, 2008; Mehen and Springer, 2011; Fleming and Mehen, 2012; Margaryan and Springer, 2013).

The different power countings of XEFT and NREFT$_I$ have various implications that we now illustrate by two examples.

Since NREFT$_I$ keeps all nonrelativistic modes explicitly, the charged $D\bar{D}^*$ channel which has a momentum of $\gamma_c \simeq 126$ MeV needs to be kept as soft degrees of freedom. On the contrary, the XEFT keeps only the ultrasoft neutral charm mesons dynamically and the charged ones are integrated out. It was pointed out by Mehen (2015) that it is crucial to take into account the charged charm mesons for the calculation of the $X(3872) \to \chi_{cJ}\pi^0$ decay rate in NREFT$_I$ because their contribution cancels to a large extent the one from the neutral charm mesons as usual in isospin violating transitions (cf. the discussion in Sec. VI.A.3).[21] The situation for decays into an isoscalar pion pair $X(3872) \to \chi_{cJ}\pi\pi$ is different. We expect that the charged and neutral channels are still of similar order, but add up constructively.

Furthermore, in the XEFT calculation for $X(3872) \to \chi_{cJ}\pi^0$, there appears a new, reaction specific short-distance operator, labeled by $C_{\chi,0}$ in Fig. 16(c). To estimate its size it is matched onto two contributions in heavy meson chiral perturbation theory by Fleming and Mehen (2008, 2012).

---

[21]The role of the charged charm mesons for certain decays of the $X(3872)$ was already stressed by Gamermann and Oset (2009).
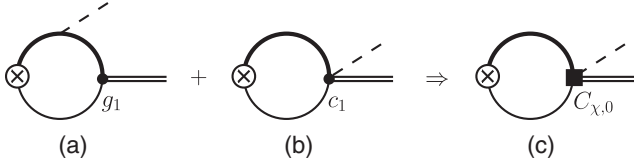
FIG. 16. Diagrams for calculating the decay rate for the process $X(3872) \to \chi_{c1}\pi^0$. The circled crosses denote an insertion of the $X(3872)$, the thin and thick solid lines represent the pseudoscalar and vector charm mesons, respectively, the dashed lines represent the pions, and the double lines correspond to the χ_{c1}.

Those are given by the exchange of a charm meson, which is proportional to the $\chi_{cJ}H\bar{H}$ coupling constant g_1, and a contact term accompanied by a low-energy constant c_1, shown in Figs. 16(a) and 16(b), respectively. The final result in XEFT then depends on the unknown ratio g_1/c_1. In NREFT$_{\rm I}$, however, the two contributions appear at different orders, since the amplitude from Fig. 16(b) is suppressed by v^2 compared with that from Fig. 16(a).

B. Formation of hadronic molecules

While so far the focus has been on transitions of molecular candidates, we now turn to their formation through two-hadron scattering. For illustration we focus in this section on the scattering of open-flavor heavy mesons off their anti-particles in a framework of NREFT similar to the EFT for nucleon-nucleon interactions (Epelbaum, Hammer, and Meißner, 2009). The example of the formation of $\Lambda(1405)$ from similar dynamics is discussed in Sec. VI.D. In this section we mainly discuss the method used by Nieves and Valderrama (2011, 2012), Valderrama (2012), Guo *et al.* (2013a, 2013b), and Hidalgo-Duque, Nieves, and Valderrama (2013). It is based on the Lippmann-Schwinger equation (LSE) regularized using a Gaussian vertex form factor. The coupled-channel LSE reads

$$T_{ij}(E; \mathbf{k}', \mathbf{k}) = V_{ij}(\mathbf{k}', \mathbf{k})$$
$$+ \sum_n \int \frac{d^3 l}{(2\pi)^3} \frac{V_{\rm in}(\mathbf{k}', \mathbf{l}) T_{nj}(E; \mathbf{l}, \mathbf{k})}{E - l^2/(2\mu_n) - \Delta_{n1} + i\epsilon}, \tag{68}$$

where μ_n is the reduced mass in the nth channel, E is the energy defined relative to the threshold of the first channel, and Δ_{n1} is the difference between the nth threshold and the first one. When the potential takes a separable form $V_{ij}(\mathbf{k}', \mathbf{k}) = \xi_i(\mathbf{k}') V_{ij} \varphi_j(\mathbf{k})$, where the V_{ij} are constants, Eq. (68) can be greatly simplified. In addition, for very near-threshold states one should expect a momentum expansion for the potential to converge fast and a dominance of S waves. Both the separability and the absence of higher partial waves will be spoiled as soon as the one-pion exchange is included on the potential level; this case will be discussed later in this section.

With a UV regulator such as of the Gaussian form (Epelbaum, Hammer, and Meißner, 2009),

$$V_{ij}(\mathbf{k}', \mathbf{k}) = e^{-k'^2/\Lambda^2} V_{ij} e^{-k^2/\Lambda^2}, \tag{69}$$

the LSE can be solved straightforwardly. If the T matrix has a near-threshold bound state pole, the effective coupling of this composite state to the constituents can be obtained by calculating the residue of the T-matrix element at the pole. For simplicity, we consider a single-channel problem with the LO contact term $V(\mathbf{k}', \mathbf{k}) = C_0 e^{-k'^2/\Lambda^2} e^{-k^2/\Lambda^2}$. The nonrelativistic T-matrix element for the scattering of the two hadrons is then given by

$$T_{\rm NR}(E) = [C_0^{-1} + \Sigma_{\rm NR}(E)]^{-1}, \tag{70}$$

where

$$\Sigma_{\rm NR}(E) = \frac{\mu}{2\pi}\left[\frac{\Lambda}{\sqrt{2\pi}} - \sqrt{-2\mu E - i\epsilon}\right] + \mathcal{O}(\Lambda^{-1}) \tag{71}$$

is the nonrelativistic two-point scalar loop function defined in Eq. (63) but evaluated with a Gaussian regulator. After renormalization by absorbing the cutoff dependence into C_0, we obtain

$$T_{\rm NR}(E) = \frac{2\pi/\mu}{\gamma - \sqrt{-2\mu E - i\epsilon}} + \mathcal{O}(\Lambda^{-1}). \tag{72}$$

The binding momentum γ was defined in Eq. (5). The effective coupling is obtained by taking the residue at the pole $E = -E_B$:

$$g_{\rm NR}^2 = \lim_{E \to -E_B} (E + E_B) T_{\rm NR}(E) = [\Sigma'_{\rm NR}(-E_B)]^{-1}$$
$$= \frac{2\pi\gamma}{\mu^2}. \tag{73}$$

It does not depend on C_0, and is scale independent up to terms suppressed by $1/\Lambda$. Multiplying $g_{\rm NR}^2$ by the factor $8m_1 m_2 M$ to get the relativistic normalization, we recover the expression for $g_{\rm eff}$ derived in Eq. (25) for $\lambda^2 = 0$. Thus we found that a potential of the kind given in Eq. (69) generates hadronic molecules. Deviations of this result behavior can be induced by momentum dependent interactions (or terms of order γ/Λ). This observation formed the basis for the generalization of the Weinberg compositeness criterion presented by Aceti and Oset (2012), Hyodo, Jido, and Hosaka (2012), Hyodo (2013a), and Sekihara, Hyodo, and Jido (2015).

To proceed we first need to say a few words about the scattering of heavy mesons. For infinitely heavy quarks the spin of the heavy quark decouples, and accordingly in a reaction not only the total angular momentum is conserved but also the spin of the heavy quark and thus the total angular momentum of the light quark system as well. Therefore, a heavy-light-quark system can be labeled by the total angular momentum of the light quark system j_ℓ. Accordingly the ground-state mesons D and D^* ($\bar{B}$ and $\bar{B}^*$) form a doublet with $j_\ell^P = 1/2^-$, where we deviate from the standard notation s_ℓ^P to remind the reader that the light quark part can be more complicated than just a single quark. Candidates of the next

doublets of excited states are $D_0^*(2400)^{22}$ and $D_1(2430)$ (the corresponding B mesons are still to be found), characterized by $j_\ell^P = 1/2^+$ and a width of about 300 MeV, and $D_1(2420)$ and $D_2^*(2460)$ [$\bar{B}_1(5721)$ and $\bar{B}_2^*(5747)$] with $j_\ell^P = 3/2^+$ and a width of about 30 MeV. Since the states with $j_\ell^P = 1/2^+$ are too broad to support hadronic molecules (Filin *et al.*, 2010; Guo and Meißner, 2011), in what follows we focus on the scattering of the ground-state mesons off their antiparticles as well as on that of the $j_\ell^P = 3/2^+$ mesons off the ground-state ones with one of them containing a heavy quark and the other a heavy antiquark.

We start with the former system. To be concrete, we take the charm mesons. In the particle basis, there are six S-wave meson pairs with given J^{PC} (Nieves and Valderrama, 2012):

$$0^{++}: \{D\bar{D}(^1S_0), D^*\bar{D}^*(^1S_0)\},$$
$$1^{+-}: \{D\bar{D}^*(^3S_1,-), D^*\bar{D}^*(^3S_1)\},$$
$$1^{++}: \{D\bar{D}^*(^3S_1,+)\},$$
$$2^{++}: \{D^*\bar{D}^*(^5S_2)\}, \tag{74}$$

where the individual partial waves are labeled as $^{2S+1}L_J$, with S, L, and J denoting the total spin, the angular momentum, and the total momentum of the two-meson system, respectively. We define the C-parity eigenstates as

$$D\bar{D}^*(\pm) = \frac{1}{\sqrt{2}}(D\bar{D}^* \pm D^*\bar{D}), \tag{75}$$

which comply with the convention[23] for the C-parity transformation $\hat{C}M = \bar{M}$. Because of HQSS, the interaction at LO is independent of the heavy quark spin and thus can be described by the matrix elements $\langle j'_{1\ell}, j'_{2\ell}, j_\ell | \hat{\mathcal{H}}_I | j_{1\ell}, j_{2\ell}, j_\ell \rangle$ where the light-quark systems get coupled to a total light-quark angular momentum of the two-meson system j_ℓ. Thus, for the systems under consideration, we have two independent terms for each isospin ($I = 0$ or 1): $\langle 1/2, 1/2, 0 | \hat{\mathcal{H}}_I | 1/2, 1/2, 0 \rangle$ and $\langle 1/2, 1/2, 1 | \hat{\mathcal{H}}_I | 1/2, 1/2, 1 \rangle$. This simple observation leads to the conclusion that in the strict heavy-quark limit the six pairs in Eq. (74) are grouped into two multiplets with $j_\ell = 0$ and 1, respectively. In the heavy-quark limit, it is convenient to use a basis of states characterized via $j_\ell^{PC} \otimes s_{c\bar{c}}^{PC}$, where $s_{c\bar{c}}$ refers to the total spin of the c and $\bar{c}$ pair. For the case of S-wave interactions only, both j_ℓ^{PC} and $s_{c\bar{c}}^{PC}$ can only be in 0^{-+} or 1^{--}. Therefore, the spin multiplet with $j_\ell = 0$ contains two states with quantum numbers:

$$0_\ell^{-+} \otimes 0_{c\bar{c}}^{-+} = 0^{++}, \qquad 0_\ell^{-+} \otimes 1_{c\bar{c}}^{--} = 1^{+-}, \tag{76}$$

---

[22]The $D\pi S$-wave resonant structure is probably more complicated than a single broad resonance, as demonstrated by a two-pole structure in Albaladejo, Fernandez-Soler *et al.* (2017).

[23]Note that a different convention for the C-parity operator was used by Nieves and Valderrama (2012). As a consequence, the off-diagonal transitions of $V_{\rm LO}^{(0^{++})}$ in Nieves and Valderrama (2012) have a different sign as compared to Eq. (78); see also Sec. VI.A in Guo, Hanhart *et al.* (2016) for further details of our convention.

and the spin multiplet for $j_\ell = 1$ has the following four states:

$$1_\ell^{--} \otimes 0_{c\bar{c}}^{-+} = 1^{+-}, \qquad 1_\ell^{--} \otimes 1_{c\bar{c}}^{--} = 0^{++} \oplus 1^{++} \oplus 2^{++}. \tag{77}$$

It becomes clear that if the 1^{++} state $X(3872)$ is a $D\bar{D}^*$ molecule, then it is in the multiplet with $j_\ell = 1$ (Voloshin, 2004a), and has three spin partners with $J^{PC} = 0^{++}, 2^{++}$, and 1^{+-} in the strict heavy quark limit as pointed out by Hidalgo-Duque *et al.* (2013) and Baru *et al.* (2016). Based on an analogous reasoning it was suggested already earlier that $Z_b(10610)$ and $Z_b(10650)$ might have four more isovector partners $W_{b0}^{(\prime)}$, W_{b1}, and W_{b2} (Bondar *et al.*, 2011; Mehen and Powell, 2011; Voloshin, 2011). A detailed and quantitative analysis of these W_{bJ} states can be found in Baru *et al.* (2017).

It is worthwhile to note that the two 1^{+-} states are in different multiplets with $j_\ell = 0$ and 1, respectively, and thus cannot be related to each other via HQSS. However, the isovectors $Z_b(10610)$ and $Z_b(10650)$ are located with similar distances to the $B\bar{B}^*$ and $B^*\bar{B}^*$ thresholds, respectively. Such an approximate degeneracy suggests that the isovector interactions in the $j_\ell = 0$ and 1 sectors are approximately the same, and the off-diagonal transition strength in the isovector channel between the two meson pairs with $J^{PC} = 1^{+-}$ in Eq. (74) approximately vanishes. A fit to the Belle data of the Z_b line shapes with HQSS constraints implemented also leads to nearly vanishing channel coupling (Guo, Hanhart *et al.*, 2016). This points toward an additional "light quark spin symmetry" as proposed by Voloshin (2016b). While a deeper understanding for such a phenomenon is still missing, it seems to be realized in the charm sector as well for the charged $Z_c(3900)$ (Ablikim *et al.*, 2013a; Z. Q. Liu *et al.*, 2013) and $Z_c(4020)$ (Ablikim *et al.*, 2013b) observed by the BESIII and Belle Collaborations. Valderrama (2012) argued that channel couplings are suppressed while Baru *et al.* (2016) claimed they were important to keep a well-defined spin symmetry limit. We come back to this controversy later in this section.

When the physical nondegenerate masses for the heavy mesons are used, one needs to switch to the basis in terms of physical states in Eq. (74). In this basis and for a given set of quantum numbers $\{JPC\}$, the LO EFT potentials $V_{\rm LO}^{(JPC)}$, which respect HQSS, read (AlFiky, Gabbiani, and Petrov, 2006; Nieves and Valderrama, 2012; Valderrama, 2012)

$$V_{\rm LO}^{(0^{++})} = \begin{pmatrix} C_{0a} & -\sqrt{3}C_{0b} \\ -\sqrt{3}C_{0b} & C_{0a} - 2C_{0b} \end{pmatrix}, \tag{78}$$

$$V_{\rm LO}^{(1^{+-})} = \begin{pmatrix} C_{0a} - C_{0b} & 2C_{0b} \\ 2C_{0b} & C_{0a} - C_{0b} \end{pmatrix}, \tag{79}$$

$$V_{\rm LO}^{(1^{++})} = C_{0a} + C_{0b}, \tag{80}$$

$$V_{\rm LO}^{(2^{++})} = C_{0a} + C_{0b}, \tag{81}$$

where C_{0a} and C_{0b} are two independent low-energy constants. Thus, since in the spin symmetry limit D and D^* are degenerate, implying that $D\bar{D}^*$ and $D^*\bar{D}^*$ loops are equal,

TABLE V. Predictions of the partners of the $X(3872)$ for $\Lambda = 0.5$ GeV in Guo *et al.* (2013a).

J^{PC}	States	Thresholds (MeV)	Masses (MeV)
1^{++}	$\frac{1}{\sqrt{2}}(D\bar{D}^* + D^*\bar{D})$	3 875.87	3 871.68 (input)
2^{++}	$D^*\bar{D}^*$	4 017.3	4012^{+4}_{-5}
1^{++}	$\frac{1}{\sqrt{2}}(B\bar{B}^* + B^*\bar{B})$	10 604.4	$10\,580^{+9}_{-8}$
2^{++}	$B^*\bar{B}^*$	10 650.2	$10\,626^{+8}_{-9}$
2^+	D^*B^*	7 333.7	7322^{+6}_{-7}

the equality of the potentials in the 1^{++} and 2^{++} channels immediately predicts equal binding energies for the two states in this limit.

Once HQSS violation is introduced into the system by the use of the physical masses, the two-multiplet pattern gets changed; however, the close connection between the 1^{++} and 2^{++} states persists. An inclusion of the one-pion exchange necessitates an extension of the basis, since now also D waves need to be included. In fact, HQSS is preserved only if all allowed D waves are kept in the system, even if the masses of the open-flavor states are still kept degenerate (Baru *et al.*, 2016). The probably most striking effect of the D waves, once the $D^* - D$ mass difference is included, is that now transitions of the 2^{++} $D^*\bar{D}^*$ S-wave state to the $D\bar{D}$ and $D\bar{D}^*$ D wave become possible. It allows for a width of this state of up to several tens of MeV (Albaladejo *et al.*, 2015; Baru *et al.*, 2016), which might be accompanied by a sizable shift in mass. In addition, spin symmetry relations might get modified via the coupling of the molecular states with regular charmonia as discussed recently (Cincioglu *et al.*, 2016).

For near-threshold states it is natural to assume that the contact terms are independent of the heavy quark mass—phenomenologically they can be viewed as parametrizing the exchange of light meson resonances. Then one can also predict the heavy-quark flavor partners of the $X(3872)$. The heavy-quark spin and flavor partners of the $X(3872)$ predicted by Guo *et al.* (2013a) with $\Lambda = 0.5$ GeV are listed in Table V.

The $Z_b(10610)$ can be related to the $Z_b(10650)$ when the off-diagonal interaction is neglected. Their hidden-charm partners are found to be virtual states in this formalism (Guo *et al.*, 2013a), which may correspond to the $Z_c(3900)$ and $Z_c(4020)$. In fact, it was shown by Albaladejo, Guo *et al.* (2016) that the BESIII data for the $Z_c(3900)$ in both the $J/\psi\pi$ (Ablikim *et al.*, 2013a) and $D\bar{D}^*$ (Ablikim *et al.*, 2015a) modes can be well fitted with either a resonance above the $D\bar{D}^*$ threshold or a virtual state below.

The number of the LO contact terms is larger for the interaction between a pair of $j_\ell = 1/2$ and $3/2$ heavy and antiheavy mesons. For each isospin, 0 or 1, in the heavy-quark limit there are four independent interactions denoted as $\langle j_{1\ell}, j_{2\ell}, j_\ell | \hat{\mathcal{H}}_I | j'_{1\ell}, j'_{2\ell}, j_\ell \rangle$, where now j_ℓ can take values 1 or 2:

$$F^d_{Ij_\ell} \equiv \langle \tfrac{1}{2}, \tfrac{3}{2}, j_\ell | \hat{\mathcal{H}}_I | \tfrac{1}{2}, \tfrac{3}{2}, j_\ell \rangle,$$
$$F^c_{Ij_\ell} \equiv \langle \tfrac{1}{2}, \tfrac{3}{2}, j_\ell | \hat{\mathcal{H}}_I | \tfrac{3}{2}, \tfrac{1}{2}, j_\ell \rangle. \tag{82}$$

The relevant combinations of these constants for a given heavy-meson pair can be worked out by changing the basis by

TABLE VI. The diagonal contact terms for the S-wave interaction between a pair of $j^P_\ell = 1/2^-$ and $3/2^+$ heavy and antiheavy mesons.

J^{PC}	Meson pairs	Contact terms
1^{--}	$\frac{1}{\sqrt{2}}(D\bar{D}_1 - D_1\bar{D})$	$\frac{1}{8}(-F^c_{I1} - 5F^c_{I2} + 3F^d_{I1} + 5F^d_{I2})$
	$\frac{1}{\sqrt{2}}(D^*\bar{D}_1 - D_1\bar{D}^*)$	$\frac{1}{16}[5(F^c_{I2} + F^d_{I2}) - 7F^c_{I1} + 11F^d_{I1}]$
	$\frac{1}{\sqrt{2}}(D^*\bar{D}_2 - D_2\bar{D}^*)$	$\frac{1}{16}(-5F^c_{I1} - F^c_{I2} + 15F^d_{I1} + F^d_{I2})$
0^{--}	$\frac{1}{\sqrt{2}}(D^*\bar{D}_1 - D_1\bar{D}^*)$	$F^c_{I1} + F^d_{I1}$
2^{--}	$\frac{1}{\sqrt{2}}(D\bar{D}_2 - D_2\bar{D})$	$\frac{1}{8}(3F^c_{I1} - F^c_{I2} + 3F^d_{I1} + 5F^d_{I2})$
	$\frac{1}{\sqrt{2}}(D^*\bar{D}_1 - D_1\bar{D}^*)$	$\frac{1}{16}(F^c_{I1} - 3F^c_{I2} + F^d_{I1} + 15F^d_{I2})$
	$\frac{1}{\sqrt{2}}(D^*\bar{D}_2 - D_2\bar{D}^*)$	$\frac{1}{16}(-9F^c_{I1} - 5F^c_{I2} + 9F^d_{I1} + 7F^d_{I2})$
3^{--}	$\frac{1}{\sqrt{2}}(D^*\bar{D}_2 - D_2\bar{D}^*)$	$F^d_{I2} - F^c_{I2}$
0^{-+}	$\frac{1}{\sqrt{2}}(D^*\bar{D}_1 + D_1\bar{D}^*)$	$F^d_{I1} - F^c_{I1}$
1^{-+}	$\frac{1}{\sqrt{2}}(D\bar{D}_1 + D_1\bar{D})$	$\frac{1}{8}[5(F^c_{I2} + F^d_{I2}) + F^c_{I1} + 3F^d_{I1}]$
	$\frac{1}{\sqrt{2}}(D^*\bar{D}_1 + D_1\bar{D}^*)$	$\frac{1}{16}(7F^c_{I1} - 5F^c_{I2} + 11F^d_{I1} + 5F^d_{I2})$
	$\frac{1}{\sqrt{2}}(D^*\bar{D}_2 + D_2\bar{D}^*)$	$\frac{1}{16}(5F^c_{I1} + F^c_{I2} + 15F^d_{I1} + F^d_{I2})$
2^{-+}	$\frac{1}{\sqrt{2}}(D\bar{D}_2 + D_2\bar{D})$	$\frac{1}{8}(-3F^c_{I1} + F^c_{I2} + 3F^d_{I1} + 5F^d_{I2})$
	$\frac{1}{\sqrt{2}}(D^*\bar{D}_1 + D_1\bar{D}^*)$	$\frac{1}{16}[3(F^c_{I2} + 5F^d_{I2}) - F^c_{I1} + F^d_{I1}]$
	$\frac{1}{\sqrt{2}}(D^*\bar{D}_2 + D_2\bar{D}^*)$	$\frac{1}{16}(9F^c_{I1} + 5F^c_{I2} + 9F^d_{I1} + 7F^d_{I2})$
3^{-+}	$\frac{1}{\sqrt{2}}(D^*\bar{D}_2 + D_2\bar{D}^*)$	$F^c_{I2} + F^d_{I2}$

means of a unitary transformation (Ohkoda *et al.*, 2012a; Xiao, Nieves, and Oset, 2013):

$$|s_{1c}, j_{1\ell}, j_1; s_{2c}, j_{2\ell}, j_2; J\rangle$$
$$= \sum_{s_{c\bar{c}}, j_\ell} \sqrt{(2j_1 + 1)(2j_2 + 1)(2s_{c\bar{c}} + 1)(2j_\ell + 1)}$$
$$\times \begin{Bmatrix} s_{1c} & s_{2c} & s_{c\bar{c}} \\ j_{1\ell} & j_{2\ell} & j_\ell \\ j_1 & j_2 & J \end{Bmatrix} |s_{1c}, s_{2c}, s_{c\bar{c}}; j_{1\ell}, j_{2\ell}, j_\ell; J\rangle, \tag{83}$$

where j_1 and j_2 are the spins of the two heavy mesons, J is the total angular momentum of the whole system, and s_{1c} and s_{2c} are the spins of the heavy quark. Noticing that the total spin of the heavy quark and antiquark $s_{c\bar{c}}$ is conserved in the heavy-quark limit, and combining the meson pairs into eigenstates of C parity, one can obtain the contact terms for the S-wave interaction between a pair of $j_\ell = 1/2$ and $3/2$ heavy and antiheavy mesons. The diagonal ones are listed in Table VI. One sees that the linear combinations are different for all channels, and it is not as easy as in the case of $X(3872)$ to predict spin partners for the $Y(4260)$ based on the assumption that it is predominantly a $D_1\bar{D}$ state. The possibility of S-wave hadronic molecules with exotic quantum numbers 1^{-+} was discussed by Q. Wang (2014).

However, one nontrivial prediction for the spectrum of molecular states in the heavy quarkonium spectrum becomes apparent immediately from the previous discussion: Since the most bound states appear in S waves the lightest negative parity vector state can be formed only from $j^P_\ell = 1/2^-$ and $3/2^+$ heavy and antiheavy mesons.

Therefore the mass difference of $X(3872)$ as a bound state of two ground-state $j_\ell^P = 1^-/2$ mesons (D and D^*) and the lightest exotic vector state $Y(4260)$ (388 MeV) should be of the order of the mass difference of the lightest $3/2^+$ state and the D^* (410 MeV). Clearly this prediction is nicely realized in nature. Note that from this reasoning it also follows that if the $Y(4008)$ indeed were to exist it could not be a hadronic molecule. In this context it is interesting to note that the most resent data from BESIII on $e^+ e^- \to J/\psi \pi\pi$ (Ablikim *et al.*, 2017c) do not seem to show evidence for the $Y(4008)$; cf. Fig. 5.

C. Impact of hadron loops on regular quarkonia

In the previous sections we argued that meson loops play a prominent role in both the formation and the decays of hadronic molecules. One may wonder if they also have an impact on the properties of regular charmonia. In this section we demonstrate that certain processes for regular hadrons, largely well described by the quark model, can also be influenced by significant meson-loop effects, since reaction rates can receive an enhancement due to the nearly on-shell intermediate heavy mesons. The origin of this mechanism is that for most heavy quarkonium transitions $M_{Q\bar{Q}} - 2M_{Q\bar{q}} \ll M_{Q\bar{q}}$, where $M_{Q\bar{Q}}$ and $M_{Q\bar{q}}$ are the masses of the heavy quarkonium and an open-flavor heavy meson, respectively. As a result, the intermediate heavy mesons are nonrelativistic with a small velocity

$$v \sim \sqrt{|M_{Q\bar{Q}} - 2m_{Q\bar{q}}|/m_{Q\bar{q}}} \ll 1, \quad (84)$$

and the meson loops in the transitions can be investigated using NREFT$_\text{I}$. We highlight this effect on two examples in what follows.[24]

We start with the hindered $M1$ transitions between two P-wave heavy quarkonia with different radial excitations, such as the $h_c(2P) \to \gamma\chi_{cJ}(1P)$. Guo and Meißner (2012a) and Guo, Meißner, and Yang (2016) proposed that such transitions are very sensitive to meson-loop effects, and the pertinent partial widths provide a way to extract the coupling constants between the P-wave heavy quarkonia and heavy open-flavor mesons. In quark models the amplitude for such a transition is

---

[24]The effects of meson loops in heavy quarkonium spectrum have been investigated by Eichten *et al.* (1978, 1980), Ono and Törnqvist (1984), Kalashnikova (2005), Eichten, Lane, and Quigg (2006), Pennington and Wilson (2007), Barnes and Swanson (2008), Li, Meng, and Chao (2009), Danilkin and Simonov (2010a, 2010b), Ortega *et al.* (2010), Bali, Collins, and Ehmann (2011), Liu and Ding (2012), Ferretti, Galatà, and Santopinto (2013, 2014), Ferretti and Santopinto (2014), Zhou and Xiao (2014, 2017), Du, Meißner, and Wang (2016), Hammer, Hanhart, and Nefediev (2016), and Lu, Anwar, and Zou (2016, 2017), and in heavy quarkonium transitions by Ono *et al.* (1985), Lipkin and Tuan (1988), Moxhay (1989), Zhou and Kuang (1991), Li and Zhao (2008, 2011), Meng and Chao (2008a, 2008b), Liu, Zhang, and Li (2009), Zhang, Li, and Zhao (2009), Zhang and Zhao (2010), Wang, Liu, and Zhao (2011), Z.-k. Guo *et al.* (2012), Wang, Li, and Zhao (2012), Li, Liu *et al.* (2013), and Cao *et al.* (2016).
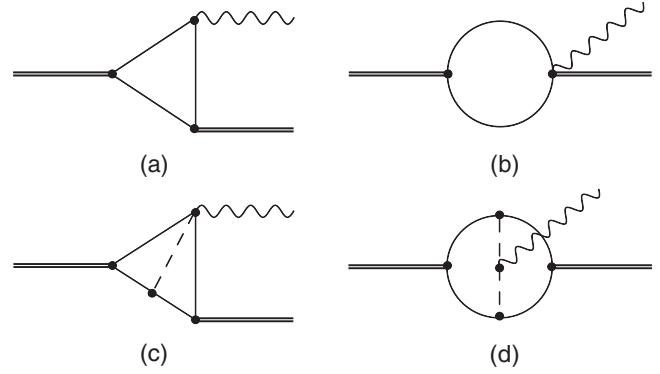
FIG. 17. Feynman diagrams for the coupled-channel effects for the hindered $M1$ transitions between heavy quarkonia. The one-loop contributions are given by (a) and (b). (c) and (d) are two typical two-loop diagrams. The double, solid, wavy, and dashed lines represent heavy quarkonia, heavy mesons, photons, and pions, respectively. Adapted from Guo and Meißner, 2012a.

proportional to the overlap of the wave functions of the initial and final heavy quarkonia, which is small and quite model dependent due to the different radial excitations—this is why they are called "hindered." This suppression is avoided in the coupled-channel mechanism of heavy-meson loops. In this mechanism, the initial and final P-wave heavy quarkonia couple to the ground-state pseudoscalar and vector heavy mesons in an S wave. A few diagrams contributing to this mechanism are shown in Fig. 17. In Fig. 17(a), the photon is emitted via its magnetic coupling to intermediate heavy mesons. In Fig. 17(b), since the S-wave vertices do not have any derivative at LO, the photon couples in a gauge invariant way to one of the vertices in the two-point loop diagram. Figures 17(c) and 17(d) are two typical two-loop diagrams. From the power counting rules discussed in Sec. IV.A.2, Fig. 17(a) provides the leading contribution, while Fig. 17(b) is of higher order in the velocity counting because there is one less nonrelativistic propagator. Their amplitudes scale as

$$\mathcal{A}_{(a)} \sim \frac{E_\gamma}{m_Q v}, \qquad \mathcal{A}_{(b)} \sim \frac{E_\gamma v}{m_Q}, \quad (85)$$

respectively, where E_γ is the photon energy, and the dependence on the coupling constants is dropped. The $1/m_Q$ suppression comes from the fact that the polarization of a heavy (anti)quark needs to be flipped in the $M1$ transitions. For the two-loop diagram in Fig. 17(c), the amplitude scales as

$$\mathcal{A}_{(c)} \sim \frac{(v^5)^2}{(v^2)^5} \frac{g^2}{(4\pi)^2 F_\pi^2} \frac{E_\gamma}{m_Q} M_H^2 = \frac{E_\gamma}{m_Q} \left(\frac{g M_H}{\Lambda_\chi} \right)^2, \quad (86)$$

where the factor $1/(4\pi)^2$ appears because there is one more loop and the hadronic scale $\Lambda_\chi = 4\pi F_\pi \sim 1$ GeV was introduced as the hard scale for the chiral expansion. The factor of M_H^2 was introduced to match dimensions with those of Eqs. (85). Figure 17(d) has the same scaling as Fig. 17(c). Since the axial coupling constant $g \simeq 0.6$ for the charm case as determined from the width of $D^* \to D\pi$, and about 0.5 for the bottom (Flynn *et al.*, 2016), one has $g M_D/\Lambda_\chi \lesssim 1$ and

$gM_B/\Lambda_\chi \simeq 2$. The value for v defined as $(v_1 + v_2)/2$ is about 0.4 for the transitions from the $2P$ to $1P$ charmonium states (Guo and Meißner, 2012a), and ranges from 0.3 to 0.2 for the transitions between $1P$, $2P$, and $3P$ bottomonia (Guo, Meißner, and Yang, 2016). Hence, the two-loop diagrams are suppressed in the charm sector, while they are of the same order as Fig. 17(a) for the bottom sector. Therefore, one can make predictions for the charmonium transitions by calculating the loops corresponding to Fig. 17(a). The results depend on a product of two unknown coupling constants of the $1P$ and $2P$ charmonia to the charm mesons. Taking model values for them, the decay width of the $\chi_{c2}(2P) \rightarrow \gamma h_c(1P)$ is of $\mathcal{O}(100 \text{ keV})$, 2 orders of magnitude larger than the quark model prediction, 1.3 keV (Barnes, Godfrey, and Swanson, 2005). Although quantitative predictions cannot be made for the bottomonium transitions, it is expected that once such transitions would be observed they must be due to coupled-channel effects as the partial widths were predicted to be in the range from a sub-eV to an eV level in a quark model calculation that does not include meson-loop effects (Godfrey and Moats, 2015). Guo and Meißner (2012a) and Guo, Meißner, and Yang (2016) suggested that the coupled-channel effects can be checked by comparing results from both fully dynamical and quenched lattice QCD which has and does not have coupled-channel effects, respectively. Recent developments in lattice QCD calculations of radiative decays (Dudek, Edwards, and Richards, 2006; Dudek, Edwards, and Thomas, 2009; Meyer, 2011; Agadjanov *et al.*, 2014; Feng *et al.*, 2015; Owen *et al.*, 2015; Shultz, Dudek, and Edwards, 2015; Briceño *et al.*, 2016; Leskovec *et al.*, 2016) should be helpful in illuminating this issue.

There are other heavy quarkonium transitions driven mainly by the coupled-channel effects. A detailed study on the transitions between two charmonia (S and P waves) with the emission of a pion or eta can be found in Guo *et al.* (2011). It was found that whether the coupled-channel effects play a sizable role depends on the process. This is a result of the power counting analysis; see the itemized discussion in Sec. IV.A.2. In particular, the single-pion or eta transitions between two S-wave and P-wave charmonia receive important contributions from charm-meson loops. Therefore, the long-standing suggestion that the $\psi' \rightarrow J/\psi \, \eta/\pi^0$ transitions can be used to extract the light quark mass ratio (Ioffe, 1979) needs to be reexamined. In fact, if we assume that the triangle charm meson-loop diagrams saturate the transitions, the resulting prediction of $\mathcal{B}(\psi' \rightarrow J/\psi\pi^0)/\mathcal{B}(\psi' \rightarrow J/\psi\eta)$ is consistent with the experimental data. These transitions were revisited considering both the loop and tree diagrams in Mehen and Yang (2012). Again based on the same power counting rules it was argued that the transitions $\Upsilon(4S) \rightarrow h_b\pi^0/\eta$ have only a small pollution from the bottom-meson loops and are dominated by a short-distance contribution proportional to the light quark mass difference (Guo, Hanhart, and Meißner, 2010). They could be used for the extraction of the light quark mass ratio. Furthermore, the prediction made before the discovery of the $h_b(1P)$ on the branching fraction of the order of 10^{-3} for the decay $\Upsilon(4S) \rightarrow h_b\eta$ was verified by the Belle measurement $(2.18 \pm 0.11 \pm 0.18) \times 10^{-3}$ (Tamponi *et al.*, 2015).

Parameter-free predictions can be made for the ratios of partial widths of decays dominated by the coupled-channel effects of heavy mesons in the same spin multiplet, since all the coupling constants will get canceled in the ratios. Such predictions on the hindered $M1$ transitions between P-wave heavy quarkonia can be found in Guo and Meißner (2012a) and Guo, Meißner, and Yang (2016).

Guo and Meißner (2012b) pointed out that coupled-channel effects can even introduce sizable and nonanalytic pion mass dependence in heavy quarkonium systems which couple to open-flavor heavy-meson pairs in an S wave.

To summarize this section, we stress that whether meson-loop effects are important for the properties of quarkonia or not depends not only on the proximity to the relevant threshold, it is also depends on the particular transition studied.

V. HADRONIC MOLECULES IN LATTICE QCD

Lattice QCD is, in principle, the tool to calculate the spectrum of QCD from first principles. There has been remarkable progress in the last years in this field (Baron *et al.*, 2010; Dürr *et al.*, 2008; Liu *et al.*, 2012; Edwards *et al.*, 2011; Liu, 2017). Still, the extraction of the properties of resonances and, in particular, of hadronic molecules from finite-volume calculations poses severe challenges. When QCD is put on a Euclidean spacetime lattice with a finite spacetime volume, asymptotic states cannot be defined and right-hand cuts are replaced by poles, thus preventing a direct calculation of scattering and resonance properties. This obstacle was overcome by Lüscher a long time ago. He derived a relation between the energy shift in the finite volume and the scattering phase shift in the continuum (Lüscher, 1986, 1991); see also Wiese (1989) and DeGrand (1991). This approach has become known and used as Lüscher's method. More precisely, in order to determine the mass and width from the measured spectrum, one first extracts the scattering phase shift by using the Lüscher equation. In the next step, using some parametrization for the K matrix (e.g., the effective range expansion), a continuation into the complex energy plane is performed. As noted in Sec. III.A, resonances correspond to poles of the scattering T matrix on the second Riemann sheet, and the real and imaginary parts of the pole position define the mass and the width of a resonance. An example is given by the ρ meson that has been considered using Lüscher's method; see, e.g., Aoki *et al.* (2011), Feng, Jansen, and Renner (2011), Lang *et al.* (2011), and Dudek, Edwards, and Thomas (2013). In these papers it was shown that, even for such realistic calculations of a well-isolated resonance, the inclusion of hadron-hadron-type interpolating operators is mandatory, and it is simply not sufficient to represent the decaying resonance by properly chosen quark bilinears (for mesons). For the discussion of hadronic molecules (or most other hadron resonances), this method needs to be extended in various directions, such as considering higher partial waves and spins (Bernard *et al.*, 2008; König, Lee, and Hammer, 2011, 2012; Luu and Savage, 2011; Göckeler *et al.*, 2012; Briceño and Davoudi, 2013a), moving frames (Rummukainen and Gottlieb, 1995; Bour *et al.*, 2011; Davoudi and Savage, 2011; Fu, 2012; Göckeler *et al.*, 2012;

Leskovec and Prelovsek, 2012), multichannel scattering (Liu, Feng, and He, 2006; Lage, Meißner, and Rusetsky, 2009; Bernard *et al.*, 2011; Döring, Haidenbauer *et al.*, 2011; P. Guo *et al.*, 2013; N. Li and Liu, 2013), including the use of unitarized chiral perturbation theory (and related methods) (Döring, Meißner *et al.*, 2011; Albaladejo *et al.*, 2012; Döring and Meißner, 2012; Martínez Torres *et al.*, 2012; J.-J. Wu *et al.*, 2014; Hu *et al.*, 2016), and three-particle final states (Kreuzer and Hammer, 2011; Polejaeva and Rusetsky, 2012; Briceño and Davoudi, 2013b; Hansen and Sharpe, 2014, 2015, 2016a, 2016b, 2017; Meißner, Ríos, and Rusetsky, 2015; Guo and Gasparian, 2017).

Here we do not attempt to review the lattice QCD approach to the hadron spectrum in any detail but just focus on what is relevant for the investigation of possible hadronic molecules. In Sec. V.A we summarize the Lüscher method and its extension to the multichannel space, followed by a discussion of the compositeness criterion in a finite volume; see Sec. V.C. In Sec. V.B, we discuss how the quark mass dependence of certain observables can be used to differentiate hadronic molecules from more compact multiquark states and in Sec. V.D we summarize pertinent lattice QCD calculations for the possible molecular states containing charm quarks. A final section is devoted to certain states made of light quarks only.

A. Resonances in a finite volume

The essence of the Lüscher approach can be understood in a simple nonrelativistic model for the scattering of identical, spinless particles of mass m in $1+1$ dimensions. In the c.m. frame, the relative momentum is quantized according to $p = (2\pi/L)n$, with L the spatial lattice extension and n an integer. In the case of no interactions between these particles, the energy of the two-particle system is simply given by $E = 2m + p^2/m$, which means that the free energy level n scales as n^2/L^2 with the volume and thus levels with different n do not intersect. In the presence of interactions, this behavior is modified. Let us assume that this interaction leads to a narrow resonance at $\sqrt{s_R} = E_R - i\Gamma_R/2$, that is $\Gamma_R \ll E_R$. In the infinite-volume limit, this interaction leads to a phase shift $\delta(p)$ in the asymptotic wave function. Furthermore, in the presence of a resonance, the phase shift will change by π [known as Levinson's theorem (Levinson, 1949)]. In a finite volume, this behavior translates into the boundary condition

$$pL + 2\delta(p) = 2\pi m, \qquad m \in \mathbb{Z}. \tag{87}$$

This condition provides the link between the volume dependence of the energy levels in the interacting system and the continuum phase shift. If one follows an energy level inward from the asymptotic region to smaller lattice sizes, in the vicinity of a resonance, this boundary condition causes a visible distortion, the so-called *avoided level crossing*; cf. Fig. 18. The plateau, where the energy of the two-particle system is almost volume independent, corresponds to the real part of the pole E_R. The imaginary part of the pole is given by the slope according to $d\delta(p)/dE|_{E_R} = 2/\Gamma_R$. Clearly, this method can work only when certain conditions are fulfilled.
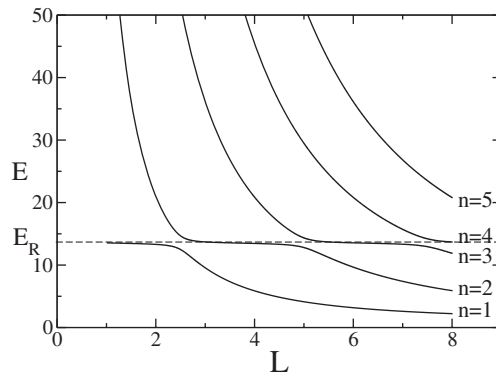
FIG. 18. Energy levels of an interacting two-particle system. In the case of a resonance in this system, the energy levels exhibit the avoided level crossing (plateau) that allows one to read off the resonance energy E_R directly.

First, the method as described here is restricted to the elastic two-particle case. Second, one has to make sure that the interaction range of the particles is much smaller than the size of the box to make the notion of asymptotic states possible. Third, to suppress polarization effects that arise from the interactions of the lightest particles in the theory with each other around the torus, one has to choose L such that $1/m \ll L$.

We now consider the extension of the Lüscher method to the multichannel case, as most hadronic molecules are located close to a two-particle threshold or between two close-by thresholds. To achieve this extension, an appropriate tool is a particular version of an NREFT, because up to the energies where multiparticle inelastic states become significant, such a framework is completely equivalent to the relativistic field theory, provided the couplings in the nonrelativistic framework are determined from matching to the relativistic S-matrix elements; for details and further references, see Colangelo *et al.* (2006), Bernard *et al.*, (2008), and Gasser, Kubis, and Rusetsky (2011). For the one-channel case, Beane *et al.* (2005) already showed that using such an NREFT one obtains a simple and transparent proof of Lüscher's formula.

To keep the presentation simple, we first consider a two-channel LSE in NREFT in the infinite volume. Let us consider antikaon-nucleon scattering in the region of the $\Lambda(1405)$ resonance $\bar{K}N \to \bar{K}N, \Sigma\pi$. The channel number 1 refers to $\bar{K}N$ and 2 to $\Sigma\pi$ with total isospin $I = 0$. The resonance $\Lambda(1405)$ is located between two thresholds, on the second Riemann sheet, close to the real axis. The two thresholds are given by $s_t = (m_N + M_K)^2$ and $s'_t = (m_\Sigma + M_\pi)^2$. We work in the isospin limit and neglect the fact that there are really two poles; see Oller and Meißner (2001) and Jido *et al.* (2003) and Sec. VI.D.[25] For energies above the $\bar{K}N$ threshold, $s > (m_N + M_K)^2$, the coupled-channel LSE for the T-matrix elements $T_{ij}(s)$ in dimensionally regularized NREFT reads (we consider only S waves here)

---

[25]Note that in this two-channel formulation one only has one pole corresponding to one $\Lambda(1405)$. To deal with the two-pole scenario requires the inclusion of more channels and explicit isospin breaking.

$$T_{11} = H_{11} + H_{11} iq_1 T_{11} + H_{12} iq_2 T_{21},$$
$$T_{21} = H_{21} + H_{21} iq_1 T_{11} + H_{22} iq_2 T_{21}, \qquad (88)$$

where $q_1 = \lambda^{1/2}(s, m_N^2, M_K^2)/(2\sqrt{s})$, $q_2 = \lambda^{1/2}(s, m_\Sigma^2, M_\pi^2)/(2\sqrt{s})$, and $\lambda(x, y, z) = x^2 + y^2 + z^2 - 2xy - 2yz - 2zx$ is the Källén function. Furthermore, $H_{ij}(s)$ denotes the driving potential in the corresponding channel, i.e., the matrix element of the interaction Hamiltonian between the free two-particle states. Continuation of the c.m. momentum q_1 below threshold $(m_\Sigma + M_\pi)^2 < s < (m_N + M_K)^2$ is obtained via

$$iq_1 \rightarrow -\kappa_1 = -\frac{[-\lambda(s, M_K^2, m_N^2)]^{1/2}}{2\sqrt{s}}. \qquad (89)$$

The resonance corresponds to a pole on the second Riemann sheet in the complex s plane. Its position is given by the solution of the secular equation

$$\Delta(s) = 1 + \kappa_1^R H_{11} - \kappa_2^R H_{22} - \kappa_1^R \kappa_2^R (H_{11} H_{22} - H_{12}^2) \qquad (90)$$

with $\kappa_1^R = -[-\lambda(s_R, m_N^2, M_K^2)]^{1/2}/(2\sqrt{s_R})$ and $\kappa_2^R = [-\lambda(s_R, m_\Sigma^2, M_\pi^2)^{1/2}]/(2\sqrt{s_R})$. The energy and width of the resonance are then given by $\sqrt{s_R} = E_R - i\Gamma_R/2$.

Consider next the same problem in a finite volume. Only discrete values of the three-momentum are allowed, given by $\boldsymbol{k} = (2\pi/L)\boldsymbol{n}$, with $\boldsymbol{n}$ a triplet of integer numbers. Thus, we replace the three-momentum integration in the loops by a discrete sum (Bernard *et al.*, 2008). The rotational symmetry is broken to a cubic symmetry, so mixing of different partial waves occurs. Here, however, we consider only S waves, neglecting the small mixing to higher partial waves. If necessary, the mixing can be easily included at a later stage (Bernard *et al.*, 2008; Döring *et al.*, 2012). The finite-volume version of the LSE Eq. (88) then takes the form

$$T_{11} = H_{11} - \frac{2Z_{00}(1; k_1^2)}{\sqrt{\pi}L} H_{11} T_{11} - \frac{2Z_{00}(1; k_2^2)}{\sqrt{\pi}L} H_{12} T_{21},$$
$$T_{21} = H_{21} - \frac{2Z_{00}(1; k_1^2)}{\sqrt{\pi}L} H_{21} T_{11} - \frac{2Z_{00}(1; k_2^2)}{\sqrt{\pi}L} H_{22} T_{21},$$
$$\qquad (91)$$

with

$$k_{1/2}^2 = \left(\frac{L}{2\pi}\right)^2 \frac{\lambda(s, M_{K/\pi}^2, m_{N/\Sigma}^2)}{4s},$$
$$Z_{00}(1; k^2) = \frac{1}{\sqrt{4\pi}} \lim_{r \to 1} \sum_{\boldsymbol{n} \in \mathbb{R}^3} \frac{1}{(\boldsymbol{n}^2 - k^2)^r}. \qquad (92)$$

Here we neglected the terms that vanish exponentially at large L. The secular equation that determines the spectrum can be brought into the form

$$1 - \frac{2}{\sqrt{\pi}L} Z_{00}(1; k_2^2) F(s, L) = 0,$$
$$F(s, L) = \left[H_{22} - \frac{2Z_{00}(1; k_1^2)}{\sqrt{\pi}L} (H_{11} H_{22} - H_{12}^2) \right]$$
$$\times \left[1 - \frac{2Z_{00}(1; k_1^2)}{\sqrt{\pi}L} H_{11} \right]^{-1}. \qquad (93)$$

This can be rewritten as

$$\delta(s, L) = -\phi(k_2) + n\pi, \qquad n = 0, 1, 2, \ldots,$$
$$\phi(k_2) = -\arctan \frac{\pi^{3/2} k_2}{Z_{00}(1; k_2^2)}, \qquad (94)$$

with

$$\tan \delta(s, L) = q_2(s) F(s, L). \qquad (95)$$

$\delta(s, L)$ is called the *pseudophase*. The dependence of the pseudophase on s and L is very different from that of the usual scattering phase. Namely, the elastic phase extracted from the lattice data by using Lüscher's formula is independent of the volume modulo terms that exponentially vanish at a large L. Further, the energies where the phase passes through $\pi/2$ lie close to the real resonance locations. In contrast with this, the pseudophase contains the function $Z_{00}(1; k_1^2)$, which does not vanish exponentially at a large L and a positive k_1^2. Moreover, the tangent of the pseudophase contains a tower of poles at the energies given by the roots of the equation $1 - (2/\pi L) Z_{00}(1; k_1^2) H_{11} = 0$. On the other hand, in the infinite volume this equation reduces to $1 + \kappa_1^R H_{11} = 0$ [cf. with Eq. (90)], which has only one root below threshold very close to the position of the $\Lambda(1405)$. Other roots in a finite volume stem from oscillations of $Z_{00}(1, k_1^2)$ between $-\infty$ and $+\infty$ when the variable k_1^2 varies along the positive semiaxis. Their locations depend on H_{11} and thus contain information of the infinite-volume interaction. This is an effect of discrete energy levels in the "shielded" channel, which is the channel with the lower threshold in the coupled-channel system. The pseudophase depends on the three real functions H_{11}, H_{12}, and H_{22}. Based on synthetic data Lage, Meißner, and Rusetsky (2009) showed that a measurement of the lowest two eigenvalues at energies between 1.4 and 1.5 GeV allows one to reconstruct the pseudophase and to extract in principle the pole position. It was further pointed out in that work that two-particle thresholds also lead to an avoided level crossing, so the extraction of the resonance properties from the corresponding plateaus in the energy dependence of certain levels is no longer possible. In the case of real data, taking into account the uncertainties of each measurements, one has to measure more levels on a finer energy grid. To obtain a sufficient amount of data in a given volume, twisting and asymmetric boxes can also be helpful. First such calculations have become available recently and will be discussed next.

An alternative formulation that allows the use of fully relativistic two-particle propagators and can easily be matched to the representation of a given scattering amplitude based on unitarized chiral perturbation theory (UCHPT) was worked

out by Döring, Meißner *et al.* (2011). The method is based on the observation that in coupled-channel UCHPT certain resonances are dynamically generated, e.g., the light scalar mesons in the coupled $\pi\pi/\bar{K}K$ system. The basic idea is to consider this approach in a finite volume to produce the volume-dependent discrete energy spectrum. Reversing the argument, one is then able to fit the parameters of the chiral potential to the measured energy spectrum on the lattice and, in the next step, determine the resonance locations by solving the scattering equations in the infinite volume. By construction, this method fulfills the constraints from chiral symmetry such as the appearance of Adler zeros at certain unphysical points. For recent developments using a relativistic framework, see Briceño *et al.* (2015) and Briceño and Hansen (2015, 2016).

B. Quark mass dependence

To reduce numerical noise as well as to speed up algorithms, lattice calculations are often performed at unphysical values of the light quark masses. While this at first sight may appear as a disadvantage, it is indeed a virtue as it enables a new handle on investigating the structure of certain states. However, in the case of multiple coupled channels, one also has to be aware that thresholds and poles can move very strongly as a function of the quark masses. This intricate interplay between *S*-wave thresholds and resonances needs to be accounted for when one tries to extract the resonance properties.

To address the first issue, we specifically consider the charm-strange mesons $D_{s0}^*(2317)$ and $D_{s1}(2460)$. Cleven *et al.* (2011b) showed that, in the molecular picture describing these as DK and D^*K bound states, a particular pion and kaon mass dependence arises. Consider first the dependence on the light quark masses that can be mapped onto the pion mass dependence utilizing the Gell-Mann–Oakes–Renner relation (Gell-Mann, Oakes, and Renner, 1968), $M_{\pi^\pm}^2 = B(m_u + m_d)$ that naturally arises in QCD as the leading term in the chiral expansion of the Goldstone boson mass. Here B is related to the vacuum expectation value of the quark condensate. In fact, this relation is fulfilled to better than 94% in QCD (Colangelo, Gasser, and Leutwyler, 2001). Cleven *et al.* (2011b) showed that the pion mass dependence of such a molecular state is much more pronounced than for a simple $c\bar{s}$ state. Even more telling and unique is, however, the kaon mass dependence. For that, consider the M_K dependence of the mass of a bound state of a kaon and some other hadron. The mass of such a kaonic bound state is given by

$$M = M_K + M_h - E_B, \tag{96}$$

where M_h is the mass of the other hadron, and E_B denotes the binding energy. Although both M_h and E_B have some kaon mass dependence, it is expected to be a lot weaker than that of the kaon itself. Thus, the important implication of this simple formula is that the leading kaon mass dependence of a kaon-hadron bound state is linear, and the slope is unity. The only exception to this argument is if the other hadron is also a kaon or antikaon. In this case, the leading kaon mass dependence is still linear but with the slope being changed to 2. Hence, as for

the DK and D^*K bound states, one expects that their masses are linear in the kaon mass, and the slope is approximately 1. This expectation is borne out by the explicit calculations performed by Cleven *et al.* (2011b). Early lattice QCD attempts to investigate this peculiar kaon mass dependence have led to inconclusive results (McNeile, 2011). Other papers that discuss methods to analyze the structure of states based on their quark mass dependence or the behavior at large number of colors are Peláez and Ríos (2006, 2010), Hanhart, Peláez, and Ríos (2008), Bernard *et al.* (2011), Guo and Oller (2011), Nebreda, Peláez, and Ríos (2011), Albaladejo and Oller (2012), and Guo, Meißner, and Yao (2015).

The second issue we want to address is the intricate interplay of *S*-wave thresholds and resonance pole positions with varying quark masses, as detailed by Döring, Mai, and Meißner (2013). In that paper, pion-nucleon scattering in the $J^P = 1/2^-$ sector in the finite volume and at varying quark masses based on UCHPT was studied. In the infinite volume, both $N(1535)$ and $N(1650)$ are dynamically generated from the coupled-channel dynamics of the isospin $I = 1/2$ and strangeness $S = 0$ $\pi N, \eta N, K\Lambda$, and $K\Sigma$ system. Having fixed the corresponding LECs in the infinite volume, one can straightforwardly calculate the spectrum in the finite volume provided one knows the octet Goldstone boson masses, the masses of the ground-state octet baryons, and the meson decay constants. Such sets of data at different quark masses are given by the ETMC and QCDSF Collaborations. ETMC provides masses and decay constants for $M_\pi = 269$ MeV and the kaon mass close to its physical value (Alexandrou *et al.*, 2009; Ottnad *et al.*, 2012). Quite differently, the QCDSF Collaboration (Bietenholz *et al.*, 2011) obtains the baryon and meson masses from an alternative approach to tune the quark masses. Most importantly, while the lattice size and spacing are comparable to those of the ETMC, the strange quark mass differs significantly from the physical value. The latter results in a different ordering of the masses of the ground-state octet mesons and, consequently, in a different ordering of meson-baryon thresholds. For the ETMC parameters, all thresholds are moved to higher energies. The cusp at the ηN threshold has become more pronounced, but no clear resonance shapes are visible. Indeed, going to the complex plane, one finds that the poles are hidden in the Riemann sheets which are not directly connected to the physical one by crossing the cut at the energies corresponding to the real parts of the poles. Using the QCDSF parameters, the situation is very different. In contrast to the ETMC case, a clear resonance signal is visible below the $K\Lambda$ threshold, that is the first inelastic channel in this parameter setup. Indeed, one finds a pole on the corresponding Riemann sheet. Unlike in the ETMC case, it is not hidden behind a threshold. Between the $K\Lambda$ and the $K\Sigma$ threshold, there is only a hidden pole. The $K\Sigma$ and ηN thresholds are almost degenerate, and on sheets corresponding to these higher-lying thresholds one finds only hidden poles. For more details, see Döring, Mai, and Meißner (2013). In that paper, strategies to overcome such types of difficulties are also discussed.

It is worthwhile to mention that the composition of a hadron in general may vary when changing the quark masses. However, as long as the quark masses are not very different

from the physical values, the quark mass dependence is rather suggestive toward revealing the internal structure as different structures should result in different quark mass dependence.

C. Measuring compositeness on lattice

As discussed in Sec. III.B.1, the Weinberg compositeness criterion offers a possibility to disentangle compact bound states from loosely bound hadronic molecules. By measuring the low-energy scattering observables in lattice using the Lüscher formalism discussed before, one can extract the compositeness by using Eqs. (18). For related work, see, e.g., Suganuma *et al.* (2007), Martínez Torres *et al.* (2012), Albaladejo *et al.* (2013), and Ozaki and Sasaki (2013). Agadjanov *et al.* (2015) pointed out that the use of partially twisted boundary conditions is easier than studying the volume dependence in lattice for measuring the compositeness. The basic object in that work is the scattering amplitude in the finite volume, which can be obtained from the corresponding loop function $\tilde{G}_L^\theta(s) = G(s) + \Delta G_L^\theta(s)$ (Döring, Meißner *et al.*, 2011), where ΔG_L^θ can be related to the modified Lüscher function Z_{00}^θ via

$$\Delta G_L^\theta(s) = \frac{1}{8\pi\sqrt{s}}\left(ik - \frac{2}{\sqrt{\pi}L}Z_{00}^\theta(1,\hat{k}^2)\right) + \cdots, \quad (97)$$

with $\hat{k} = kL/(2\pi)$ and the ellipsis denotes terms that are exponentially suppressed with the lattice size L (Döring, Meißner *et al.*, 2011). Here, in case of twisted boundary conditions, the momenta also depend on the twist angle $\boldsymbol{\theta}$ according to $\boldsymbol{q}_n = (2\pi/L)\boldsymbol{n} + (\boldsymbol{\theta}/L), 0 \leq \theta_i < 2\pi$. In case of a bound state with mass M in the infinite volume, the scattering amplitude should have a pole at $s = M^2$, with the corresponding binding momentum $k_B \equiv i\kappa, \kappa > 0$, given by

$$\psi(k_B^2) + \kappa = -8\pi M[V^{-1}(M^2) - G(M^2)] = 0, \quad (98)$$

with $\psi(k^2)$ the analytic continuation of $k\cot\delta(k)$ for arbitrary complex values of k^2. From this, it is straightforward to evaluate the pole position shift,

$$\kappa_L - \kappa = \frac{1}{1 - 2\kappa\psi'(k_B^2)}[-8\pi M_L \Delta G_L^\theta(M_L^2) + \psi'(k_B^2)(\kappa_L - \kappa)^2],$$
$$(99)$$

where the prime denotes differentiation with respect to k^2. Equation (99) gives the bound state pole position κ_L (and thus the finite-volume mass M_L) as a function of the infinite-volume parameters g^2 and κ. Having determined these parameters from the bound state levels κ_L, one is then able to determine the wave function renormalization constant Z in the infinite volume. Agadjanov *et al.* (2015) scrutinized this procedure using synthetic lattice data for a simple toy model and a molecular model for the charm scalar meson $D_{s0}^*(2317)$. An important finding of this work is that the extraction of Z is facilitated by using twisted boundary conditions, measuring the dependence of the spectrum on the twist angle. Also, the limitations of this approach are discussed in detail. It remains

to be seen how useful this method is for real lattice data. For related papers, also making use of twisted boundary conditions to explore the nature of states, see, e.g., Ozaki and Sasaki (2013), Briceño *et al.* (2014), and Körber and Luu (2016). A different approach to quantify compositeness in a finite volume was recently given by Tsuchida and Hyodo (2017). Using this method, the $\bar{K}N$ component of the $\Lambda(1405)$ was found to be 58%, and the $\Sigma\pi$ and other components also contribute to its structure. This is interpreted as a reflection of the two-pole scenario of the $\Lambda(1405)$.

D. Lattice QCD results on the charm-strange mesons and *XYZ* states

There have been quite a few studies of the charm-strange mesons and some of the *XYZ* states in lattice QCD. However, there are few conclusive results at present, so we expect that this section will be the most quickly outdated.

Let us consider first the charm-strange mesons. A pioneering lattice study of the low-energy interaction between a light pseudoscalar meson and a charmed pseudoscalar meson was presented by L. Liu *et al.* (2013). The scattering lengths of the five channels $D\bar{K}(I=0)$, $D\bar{K}(I=1)$, $D_s K$, $D\pi(I=3/2)$, and $D_s\pi$ were calculated based on four ensembles with pion masses of 301, 364, 511, and 617 MeV. These channels are free of contributions from disconnected diagrams. SU(3) UCHPT as developed by Guo, Hanhart, and Meißner (2009b) was used to perform the chiral extrapolation. The LECs of the chiral Lagrangian were determined from a fit to the lattice results. With the same set of LECs and the masses of the involved mesons set to their physical values, predictions for the other channels including $DK(I=0)$, $DK(I=1)$, $D\pi(I=1/2)$, and $D_s\bar{K}$ were made. In particular, it was found that the attractive interaction in the $DK(I=0)$ channel is strong enough so that a pole is generated in the unitarized scattering amplitude. Within 1σ uncertainties of the parameters, the pole is at 2315^{+18}_{-28} MeV, and it is always below the DK threshold. From calculating the wave function normalization constant, it was found that this pole is mainly an *S*-wave DK bound state [the pertinent scattering length being close to -1 fm as predicted by Guo, Hanhart, and Meißner (2009b) for such a molecular state using Eq. (18)]. Further, a much sharper prediction of the isospin breaking decay width of $D_{s0}^*(2317) \to D_s\pi$ could be given

$$\Gamma(D_{s0}^*(2317) \to D_s\pi) = 133 \pm 22 \text{ keV}, \quad (100)$$

to be contrasted with the molecular prediction without lattice data, $\Gamma(D_{s0}^*(2317) \to D_s\pi) = 180 \pm 110$ keV (Guo *et al.*, 2008), and typical quark model predictions for a $c\bar{s}$ charm scalar meson of the order of 10 keV (Godfrey, 2003; Faessler *et al.*, 2007). For a similar study using a covariant UCHPT instead of the heavy-baryon formalism, see Altenbuchinger, Geng, and Weise (2014).

A systematic study of the charm scalar and axial mesons at lighter pion masses ($M_\pi = 156$ and 266 MeV) was performed by Mohler *et al.* (2013), Mohler, Prelovsek, and Woloshyn (2013), and Lang *et al.* (2014). These data were later reanalyzed with the help of finite-volume UCHPT (Martínez Torres *et al.*, 2015). Most notably, the DK

scattering with $J^P = 0^+$ was investigated by Mohler *et al.* (2013) using DK as well as $c\bar{s}$ interpolating fields. Clear evidence of a bound state below the DK threshold was found and the corresponding scattering length was $a_0 = -1.33(20)$ fm, consistent with the molecular scenario. Martínez Torres *et al.* (2015) found a 70% DK (D^*K) component in the $D_{s0}^*(2317)$ [$D_{s1}(2460)$] state.

The most systematic study in the coupled-channel $D\pi$, $D\eta$, and $D_s\bar{K}$ system with isospin $1/2$ and $3/2$ was reported by Moir *et al.* (2016). Using a large basis of quark-antiquark and meson-meson basis states, the finite-volume energy spectrum could be calculated to high precision, allowing for the extraction of the scattering amplitudes in the S, P, and D waves. With the help of the coupled-channel Lüscher formalism and various parametrizations of the T matrix, three poles were found in the complex plane: a $J^P = 0^+$ near-threshold bound state, $M_S = 2275.9 \pm 0.9$ MeV, with a large coupling to $D\pi$, a deeply bound $J^P = 1^-$ state, $M_P = 2009 \pm 2$ MeV, and evidence for a $J^P = 2^+$ narrow resonance coupled predominantly to $D\pi$, $M_D = 2527 \pm 3$ MeV. An interesting observation was made by Albaladejo, Fernandez-Soler *et al.* (2017). Using UCHPT, it was shown that there are in fact two ($I = 1/2, J^P = 0^+$) poles in the region of the $D_0^*(2400)$ in the coupled-channel $D\pi$, $D\eta$, and $D_s\bar{K}$ scattering amplitudes. They couple differently to the involved channels and thus should be understood as two states. Having all the parameters fixed from earlier studies in L. Liu *et al.* (2013), the energy levels for the coupled-channel system in a finite volume were predicted. These agree remarkably well with the lattice QCD results by Moir *et al.* (2016). The intricate interplay of close-by thresholds and resonance poles already pointed out by Döring, Mai, and Meißner (2013) was also found, and it was stressed that more high-statistics data are needed to better determine the higher mass pole.

We now turn to the *XYZ* states. Consider first the $X(3872)$. There have been a number of studies using diquark-diquark or tetraquark interpolating fields over the years, but none of these has been conclusive (Chiu and Hsieh, 2007; Yang *et al.*, 2013). Evidence for a bound state with $J^{PC} = 1^{++}$ 11 ± 7 MeV below the $D\bar{D}^*$ threshold was reported by Prelovsek and Leskovec (2013a). This establishes a candidate for the $X(3872)$ in addition to the nearby scattering states $D\bar{D}^*$ and $J/\psi\rho$. This computation was performed at $M_\pi = 266$ MeV but in a small volume $L \simeq 2$ fm. This finding was validated using the highly improved staggered quark action (Lee *et al.*, 2014). Finally, a refined study also allowing for the mixing of tetraquark interpolators with $\bar{c}c$ components was presented by Padmanath, Lang, and Prelovsek (2015). A candidate for the $X(3872)$ with $I = 0$ was observed very close to the experimental state only if both $\bar{c}c$ and $D\bar{D}^*$ interpolators are included. However, the candidate is not found if diquark-antidiquark and $D\bar{D}^*$ are used in the absence of $\bar{c}c$. Garzon *et al.* (2014), Jansen, Hammer, and Jia (2014, 2015), and Baru *et al.* (2015a) worked out strategies for extracting the properties of the $X(3872)$ from finite-volume data (at unphysical quark masses).

Consider next the $Z_c(3900)$. Various lattice calculations have been performed, which, however, did not lead to conclusive results (Prelovsek and Leskovec, 2013b; Chen *et al.*, 2014; Prelovsek *et al.*, 2015; Ikeda *et al.*, 2016). For example, in recent work Ikeda *et al.* (2016) argued that this state is most probably a threshold cusp. Also, a systematic analysis of most of these data using a finite-volume version of the framework in Albaladejo, Guo *et al.* (2016) did not allow for a definite conclusion on the nature of the $Z_c(3900)$ (Albaladejo, Fernandez-Soler, and Nieves, 2016).

The Chinese Lattice QCD Collaboration also studied $D^*\bar{D}_1$ (Meng *et al.*, 2009; T. Chen *et al.*, 2016) and $D^*\bar{D}$ scattering (Y. Chen *et al.*, 2015) with the aim of investigating the structure of $Z_c(4430)$ and $Z_c(4025)$, respectively. These studies were mostly exploratory and no definite statements could be drawn.

E. Lattice QCD results on hadrons built from light quarks

Here we summarize some recent results on hadrons made entirely of light u, d, and s quarks, more precisely, the scalar mesons $f_0(500)$ and $a_0(980)$ as well as $\Lambda(1405)$.

The first determination of the energy dependence of the isoscalar $\pi\pi$ elastic scattering phase shift and the extraction of the $f_0(500)$ based on dynamical QCD using the methods previously described was given by the Hadron Spectrum Collaboration in Briceño *et al.* (2017). From the volume dependence of the spectrum the S-wave phase shift up to the $K\bar{K}$ threshold could be extracted. The calculations were performed at pion masses of 236 and 391 MeV. The resulting amplitudes are described in terms of a scalar meson which evolves from a bound state below the $\pi\pi$ threshold at the heavier quark mass to a broad resonance at the lighter quark mass. This is in line with the prediction of Hanhart, Peláez, and Ríos (2008) based on UCHPT to one loop. Earlier, the same collaboration had analyzed the coupled-channel $\pi\eta$, $K\bar{K}$, and $\pi\eta'$ system with isospin $I = 1$ and extracted properties of the $a_0(980)$ meson (Dudek, Edwards, and Wilson, 2016). The model-independent lattice data on energy levels were reanalyzed using UCHPT by Döring, Hu, and Mai (2016) and Guo *et al.* (2017). In particular, Guo *et al.* (2017) pointed out some ambiguities in the $I = 1$ solution.

There have been quite a few studies of the $\Lambda(1405)$ as a simple three-quark baryon state by various lattice collaborations. In view of the intricacies of the coupled-channel K^-p scattering discussed earlier, we will not further consider these as coupled-channel effects must be considered. An exception is the analysis of Hall *et al.* (2015) based on the PCAS-CS ensembles (Aoki *et al.*, 2009) with three-quark sources allowing for scalar and vector diquark configurations that lead to the vanishing of the strange magnetic form factor of $\Lambda(1405)$ at the physical pion mass. It is argued that this can happen only if $\Lambda(1405)$ is mostly an antikaon-nucleon molecule. This is further validated by applying a finite-volume Hamiltonian approach to the measured energy levels (J.-J. Wu *et al.*, 2014). This lattice QCD result appears to be at odds with the accepted two-pole scenario. However, as pointed out in the UCHPT analysis of Molina and Döring (2016), these results exhibit some shortcomings. It is argued in that work that what is really discussed in Hall *et al.* (2015) is the heavier of the

two poles. In particular, the complete absence of the $\pi\Sigma$ threshold in these data is discussed, as this threshold would couple stronger to the lighter pole. This effect is presumably due to the neglect of the baryon-meson interpolating fields in Hall *et al.* (2015). The required operators are also specified in Molina and Döring (2016). It will be interesting to see lattice QCD calculations including all the relevant channels and required interpolating fields. We also point out that better methods to calculate the matrix elements of unstable states have been given by Bernard *et al.* (2012) and Briceño and Hansen (2016).

VI. PHENOMENOLOGICAL MANIFESTATIONS OF HADRONIC MOLECULES

A large number of theoretical studies on the recently discovered exotic candidates focus on the computation of masses (Brambilla *et al.*, 2014; Chen, Chen *et al.*, 2016; Esposito, Pilloni, and Polosa, 2017; Lebed, Mitchell, and Swanson, 2017). However, from the discussions in Secs. III and IV, it is clear that the internal structure and especially the molecular nature of a physical state manifest themselves predominantly in some properly identified dynamical production and decay processes. For near-threshold hadronic molecules, the pertinent observables are provided by a set of low-energy quantities: the scattering length and effective range for the constituent-hadron system or, equivalently, the effective coupling of the hadronic molecular candidate to its constituents, since these quantities are heavily intertwined as demonstrated in Sec. III. As discussed in detail there, the probability to find the two-hadron component in the physical state $(1 - \lambda^2)$ can be extracted directly from these quantities. However, due to the presence of various energy scales driven by different physics aspects, not all production and decay processes are sensitive to the effective coupling as will be discussed with various examples mainly on the XYZ states in this section. In addition, the implications of heavy quark spin and flavor symmetries on the spectrum of hadronic molecules as well as the interplay between hadronic molecules and nearby triangle singularities are presented.

A. Long-distance production and decay mechanisms

As in Sec. III, we denote the wave function of a hadronic molecule candidate as Ψ. In order to allow for a quantitatively controlled analysis, the state must be located close to the relevant two-body threshold of h_1 and h_2. Then the long-distance momentum scale is given by $\gamma = \sqrt{2\mu E_B}$; cf. Eq. (5) with $\gamma \ll \beta$, where β is the inverse of the range of forces. We define two classes of production and decay processes, namely,

- long-distance processes, in which the momenta of all particles in the c.m. frame of $h_1 h_2$ are of $\mathcal{O}(\gamma)$;
- short-distance processes, which involve particles with a momentum $\gtrsim \beta$ in the c.m. frame of $h_1 h_2$.

It is shown in this section that only the former are sensitive to the molecular component of the state investigated. The complications in the latter will be discussed in the next section.

1. Decays into the constituents and transitions between molecular states

The long-distance processes involving hadronic molecules can be computed using the EFT machinery introduced in Sec. IV. When only the degrees of freedom with momenta of $\mathcal{O}(\gamma)$ are kept, the EFT is XEFT or, more generally, NREFT$_{\mathrm{II}}$. When all particle energies are much smaller than $\beta^2/(2\mu)$ in the $h_1 h_2$ c.m. frame, the amplitudes involving pure molecular states for the pertinent processes are at LO determined by the scattering length universality (Braaten and Hammer, 2006). Decay amplitudes are then proportional to the effective coupling g_{eff} defined in Eq. (26) which can also be expressed in terms of the scattering length. Clearly such an approach cannot be simply applied to predominantly compact states since then g_{eff} becomes small and short-distance mechanisms become more important than hadronic loops.

For instance, as soon as the $X(3872)$ is treated as a $D\bar{D}^*$ molecule, the most important long-distance processes are its decays into $D^0\bar{D}^{*0} \to D^0[\bar{D}^0\pi^0/\bar{D}^0\gamma]$, discussed in Sec. IV.A.4. The decay rates and the momentum distributions of the final states serve as a good probe for the structure of $X(3872)$ (Voloshin, 2004b).[26] Higher order corrections can be calculated using NREFT$_{\mathrm{I}}$ detailed in Sec. IV.A.2. For the $Y(4260)$, the most important process for the detection of its $D_1\bar{D}$ component would be the decay into $D_1\bar{D} \to [D^*\pi/D^*\gamma]\bar{D}$ (Cleven, Wang *et al.*, 2014; Qin, Xue, and Zhao, 2016).

It may happen that two of the particles in the final states in the mentioned three-body decays form another hadronic molecule in the final state. The transition of a shallow bound state into a light particle and another shallow bound state receives two enhancements: large coupling constants for the vertices involving the molecular states and the $1/v \simeq 2/(v_1 + v_2)$ factor as shown in Sec. IV.A.2, where v_1 and v_2 denote the relative velocities of the heavy mesons before and after the emission of the light particle [see Fig. 11 and Eq. (52)].

The possibility of a near-threshold pole in the $D\bar{D}$ final state interaction and its possible influence on the $X(3872) \to D^0\bar{D}^0\pi^0$ transition was studied by Guo, Hidalgo-Duque *et al.* (2014); cf. Fig. 15. Note that experimental information on this distribution does not yet exist.[27] However, the interplay of hadronic molecules in the final and initial states might well have been observed already as detailed in the remaining parts of this section.

The $D_1(2420)\bar{D}$ threshold in the $J^{PC} = 1^{--}$ channel is the closest S-wave open-charm threshold that the $Y(4260)$ can couple to. It is at the same time the lowest S-wave open-charm threshold with vector quantum numbers, which provides a natural explanation why the first (established) exotic vector

---

[26]These decays were also discussed by Swanson (2004b), Voloshin (2006), Fleming *et al.* (2007), Meng and Chao (2007), Braaten and Stapleton (2010), Liang, Molina, and Oset (2010), Baru *et al.* (2011), Guo, Hidalgo-Duque *et al.* (2014), and Polosa (2015).

[27]A few calculations based on phenomenological models suggested the possible existence of a $D\bar{D}$ bound state (Wong, 2004; Zhang *et al.*, 2006; Fernández-Caramés, Valcarce, and Vijande, 2009; Zhang and Huang, 2009; Liu *et al.*, 2010; Li *et al.*, 2012).
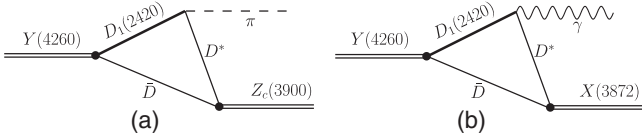
FIG. 19. Schematic diagrams for the decays of the $Y(4260)$ to $Z_c(3900)\pi$ and to $X(3872)\gamma$ assuming that $D_1\bar{D}$ − c.c. dominates the dynamics. The diagrams from the charge conjugated channel are not shown.

state is significantly heavier than the $X(3872)$. Assuming that $Y(4260)$ is a $D_1\bar{D}$ molecule and $X(3872)$ and $Z_c(3900)$ are $D^*\bar{D}$ molecules with $J^{PC} = 1^{++}$ and 1^{+-}, respectively, the decays of $Y(4260)$ into $Z_c\pi$ and $X(3872)\gamma$ will occur through the mechanisms shown in Figs. 19(a) and 19(b), where the type of the light particle accompanying the hadronic molecular state is controlled by the positive and negative C parities of the π^0 and photon, respectively. Since $v \lesssim 0.1$ for both transitions, $1/v$ indeed provides a large factor, shown as the solid lines in Fig. 12. Therefore, a copious production of $Z_c(3900)$ from $Y(4260) \to Z_c(3900)\pi$ transitions as observed at both BESIII and Belle (Ablikim *et al.*, 2013a; Z. Q. Liu *et al.*, 2013) appears naturally within this dynamical picture (Wang, Hanhart, and Zhao, 2013a). In addition, if this explanation is indeed correct, the $X(3872)$ must also be necessarily produced with a large rate for the production in $Y(4260)$ radiative decays (Guo, Hanhart *et al.*, 2013). Indeed, assuming that the $Y(4260)$ and $X(3872)$ are pure bound states of $D_1\bar{D}$ and $D^0\bar{D}^{*0}$,[28] respectively, one can get the coupling strengths using the relation in Eq. (24) with $\lambda^2 = Z = 0$:

$$|g_{NR,X}| = (0.20 \pm 0.20 \pm 0.03) \text{ GeV}^{-1/2},$$
$$|g_{NR,Y}| = (1.26 \pm 0.09 \pm 0.66) \text{ GeV}^{-1/2}, \quad (101)$$

where we have taken the $X(3872)$ binding energy to be 90 ± 90 keV, the first errors are from the uncertainties of the binding energies, and the second ones are from the approximation of Eq. (24) due to neglecting terms suppressed by γ/β. Here the inverse of the range of forces is conservatively estimated by $\beta \sim \sqrt{2\mu\Delta_{th}}$, with Δ_{th} the difference between the threshold of the components and the next close one, which is $M_{D^{*+}} + M_{D^+} - M_{D^{*0}} - M_{D^0}$ for the $X(3872)$ and $M_{D_1} + M_{D^*} - M_{D_1} - M_D$ for the $Y(4260)$, respectively. The partial width for the $Y(4260) \to X(3872)\gamma$ in NREFT$_I$ can reach a few tens of keV depending on the exact value of the $X(3872)$ binding energy (Guo, Hanhart *et al.*, 2013). The predicted copious production of the $X(3872)$ in the $Y(4260)$ radiative decays was later confirmed by BESIII (Ablikim *et al.*, 2014d).

It is worthwhile to mention that if the c.m. energy of the e^+e^- collisions is very close to the $D_1(2420)\bar{D}$ threshold at around 4.29 GeV,[29] the production of the $Z_c(3900)$ and $X(3872)$ via the mechanism under consideration gets even more enhanced since the kinematical condition for the TS discussed in Sec. IV.A.1 is then (nearly) satisfied. However, the resulting enhancement is balanced by the fact that the energy is away from the peak of the $Y(4260)$ spectral function.

It should be mentioned that some experimental observations consistent with hadronic molecules are also claimed to be consistent with other models. For instance, treating both the $X(3872)$ and $Y(4260)$ as tetraquarks also leads to a sizable width for the radiative decay $Y(4260) \to X(3872)\gamma$ (Chen, Maiani *et al.*, 2015). However, large transitions to the constituents of the hadronic molecules appear to be unique signatures for the molecular states. In addition, their importance leaves visible imprints in the line shapes of states such as the $Y(4260)$ (Cleven, Wang *et al.*, 2014; Qin, Xue, and Zhao, 2016).

2. More on line shapes

The line shape of a hadronic molecule near its constituent threshold reflects a long-distance phenomenon and can be used as a criterion for establishing their nature. The energy dependence of a hadronic molecule production line shape generally does not appear to be trivial.

The data available at present for the line shapes of $X(3872)$ appear to be insufficient for a unique conclusion about the pole locations of the state. For example, a simultaneous fit of the line shape of the $X(3872)$ in the $J/\psi\pi\pi$ and the $D^{*0}\bar{D}^0$ invariant mass distributions employing a generalized Flatté parametrization (Hanhart *et al.*, 2007a) revealed that $X(3872)$ is a virtual state. However, as soon as an explicit quarkonium pole is included in the analysis, Kalashnikova and Nefediev (2009), Zhang, Meng, and Zheng (2009), and Meng *et al.* (2015) found that $X(3872)$ is the 2^3P_1 charmonium with a large coupling to the $D^0\bar{D}^{*0}$ channel; in light of the discussion of Sec. III.B one needs to conclude that also in this case the $X(3872)$ has a sizable molecular admixture. It should also be stressed that in Hanhart *et al.* (2007a) the width of the D^* was omitted, which might distort the line shapes (cf. Sec. III.C) as was pointed out by Braaten and Lu (2007) and Braaten and Stapleton (2010). According to these analyses, once this effect is included, the fit favors a bound state solution. Another study based on an improved Flatté formula (Artoisenet, Braaten, and Kang, 2010) notices that the current data can accept $X(3872)$ as both a $D^0\bar{D}^{*0}$ hadronic molecule or the fine-tuned 2^3P_1 charmonium coupled with the $D^0\bar{D}^{*0}$ channel. Also the more recent analysis of Kang and Oller (2017) finds solutions with either a bound state pole or virtual states. Thus, to further

---

[28] It was emphasized in Sec. IV.A.4 that the charged charm mesons need to be taken into account for the $X(3872)$ in the framework of NREFT$_I$ since they are below the hard scale and should be treated explicitly. The reason for neglecting them here is that the rate for the $D_1^0 \to D^{*0}\gamma$ is at least 1 order of magnitude larger than that for the $D_1^+ \to D^{*+}\gamma$ from nonrelativistic quark model calculations (Fayya-zuddin, and Mobarek, 1994; Close and Swanson, 2005; Godfrey, 2005).

[29] The production of an S-wave pair of $D_1(2420)$ and $\bar{D}$, which are $j_\ell^P = 3/2^+$ and $j_\ell = 1/2^-$ states, respectively, breaks HQSS (Li and Voloshin, 2013). This point was in fact already noticed in the classical papers of the Cornell model; see Table VI in Eichten *et al.* (1978) and Table VIII in Eichten *et al.* (1980). However, in the energy region about 4.2 GeV HQSS breaking can be sizable (Wang *et al.*, 2014).

investigate the nature of $X(3872)$ a high-resolution scan of its line shapes, especially within a few MeV of the $D^0 \bar{D}^{*0}$ threshold, is necessary.

A study of the line shapes of the two Z_b states in $h_b(1P, 2P)\pi$ channels has been presented by Cleven *et al.* (2011a) based on the NREFT$_I$ framework discussed in Sec. IV. By fitting to the $h_b(1P, 2P)\pi$ invariant mass distribution, it was found that the current data are consistent with the two Z_b states being $B\bar{B}^*$ and $B^*\bar{B}^*$ bound states, respectively. Their line shapes in the elastic channels are also studied in the XEFT and NREFT$_{II}$ (see Sec. IV.A.3) framework with the HQSS breaking operator included explicitly in Mehen and Powell (2013) where, however, no pole locations were extracted. The line shapes of the two Z_b states were investigated in both elastic and inelastic channels in Hanhart *et al.* (2015) and Guo, Hanhart *et al.* (2016) based on separable interactions; see Fig. 2. An explicit calculation revealed that the line shapes get distorted very little when a nonseparable interaction is included, such as the one-pion-exchange potential. Similar studies of the $Z_c(3900)$ line shape in both $J/\psi\pi$ and $D\bar{D}^*$ can be found in Zhou and Xiao (2015), Albaladejo, Guo *et al.* (2016), and Pilloni *et al.* (2017). Based on these results one needs to state that the data currently available for the $Z_c(3900)$ are also insufficient to pin down the pole locations.

The situation in which it is not easy to extract the pole locations is partly because the observed peaks for the $X(3872)$, $Z_c(3900)$, and Z_b states are too close to the thresholds. Being tens of MeV below the $D_1\bar{D}$ threshold, which, however, also means a larger uncertainty, the $Y(4260)$ situation is different. One clearly sees a nontrivial structure around the $D_1\bar{D}$ threshold in the $Y(4260)$ line shape in the $J/\psi\pi\pi$ invariant mass distribution; cf. Fig. 5. It indicates that the coupling to the $D_1\bar{D}$ plays an essential role in understanding the $Y(4260)$ in line with the analysis in Sec. III.C. Correspondingly the molecular picture predicts a highly nontrivial energy dependence for $e^+e^- \to D_1\bar{D} \to [D^*\pi]D$ (Cleven, Wang *et al.*, 2014); cf. the middle panel in Fig. 6 that awaits experimental confirmation at BESIII.

3. Enhanced isospin violations in molecular transitions

As argued in Sec. III.B for molecular states the coupling of the pole to the continuum channel that forms the state is large. As a consequence of this loop effects get important that can lead to very much enhanced isospin violations if the molecular state is close to the relevant threshold. To be concrete we start with a detailed discussion of the implications of this observation for the f_0–a_0 mixing, first discussed by Achasov, Devyanin, and Shestakov (1979). If both the isoscalar $f_0(980)$ and the isovector $a_0(980)$ were $\bar{K}K$ molecular states, the leading mixing effect of the two scalar mesons would be the difference of the loop functions of charged and neutral kaons as depicted in Fig. 20 (in isospin conserving transitions the sum enters). In the near-threshold regime we approximate the loops by their leading energy dependence provided by the respective unitarity cuts:
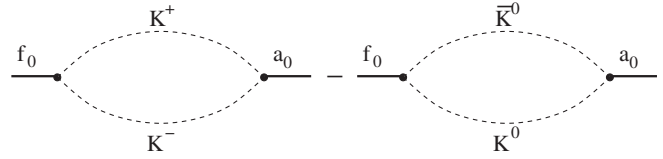

FIG. 20. Graphical illustration of the leading contribution to the $f_0 - a_0$ mixing matrix element.

$$\langle f_0|T|a_0\rangle = ig_{f_0 K\bar{K}} g_{a_0 K\bar{K}} \sqrt{s}(p_{K^0} - p_{K^+})$$
$$+ \mathcal{O}(p_{K^0}^2 - p_{K^+}^2), \tag{102}$$

where p_K denotes the modulus of the relative momentum of the kaon pair. Obviously, this leading contribution model independently provides a measure of the product of the effective couplings of a_0 and f_0 to the kaons and therefore, as discussed in Sec. III.B.1, to the molecular admixture of both states. In the isospin limit the loops cancel exactly. However, as soon as the masses of the two-hadron states are different due to isospin violations ($M_{K^0} - M_{K^+} = 4$ MeV), there appears an offset in the thresholds and the mentioned cancellation is no longer complete. This results in a transition between different isospins with all its strength located in between the two thresholds. Hanhart, Kubis, and Peláez (2007) and Wu, Zhao, and Zou (2007) predicted that this very peculiar effect should show up prominently in the transition $J/\psi \to \phi\pi^0\eta$, if both $f_0(980)$ and $a_0(980)$ are $K\bar{K}$ molecular states, since only then the coupling of the states to the $K\bar{K}$ is sufficiently strong for the effect to be observable. A few years later the predicted very narrow signal was measured at BESIII (Ablikim *et al.*, 2011) providing strong evidence for a prominent molecular admixture in these light scalar mesons.

Another prominent example where a molecular nature of a near-threshold state leads to a natural explanation of a large isospin violation is the equal decay rate of the $X(3872)$ to the isoscalar $\pi\pi\pi J/\psi$ and the isovector $\pi\pi J/\psi$ channels, where in both cases the few-pion systems carry vector quantum numbers and thus may be viewed as coming from the decay of an ω and a ρ^0 meson, respectively. The argument goes as follows: The mass of the $X(3872)$ is located 7 MeV below the nominal $\omega J/\psi$ threshold, but 5 MeV above the nominal $\rho^0 J/\psi$ threshold. In addition, the width of the ω is only 8 MeV such that the decay of the $X(3872)$ into the $\rho^0 J/\psi$ channel is strongly favored kinematically. Therefore, the $X(3872)$ cannot have a significant isovector component in its wave function since otherwise it would significantly more often decay into the $\rho^0 J/\psi$ than into the $\omega J/\psi$ channel. However, a calculation for an isoscalar $X(3872)$ that predominantly decays via $D^*\bar{D}$ loops naturally gives the experimental branching ratios for the pion J/ψ channels simply because the close proximity of the mass of the X to the neutral $D^*\bar{D}$ threshold automatically produces an enhanced isospin violation in the necessary strength, if the $X(3872)$ is a $D^*\bar{D}$ molecule, since only then the coupling to continuum is strong enough (Gamermann and Oset, 2009). An isoscalar nature of the $X(3872)$ is also required from a study of other possible decay channels

(Mehen, 2015), and its effective couplings to the charged and neutral channels are basically the same (Hidalgo-Duque, Nieves, and Valderrama, 2013; Guo, Hidalgo-Duque *et al.*, 2014).

As the last example in this context we mention the hadronic width of the isoscalar $D_{s0}^*(2317)$. This state is located below the DK threshold and as such can decay strongly only via isospin violation into the isovector $D_s\pi$ channel. The two most prominent decay mechanisms of $D_{s0}^*(2317)$ are an isospin conserving transition into $D_s\eta$, followed by the isospin violating $\pi\eta$ mixing amplitude, and the isospin violating difference between a D^0K^+ and a D^+K^0 loop [subleading contributions to this transition were studied by Guo *et al.* (2008)]. The former mechanism should be present regardless of the nature of the state, which typically leads to widths of the order of 10 keV (Colangelo and De Fazio, 2003). The latter mechanism, however, is large if indeed the $D_{s0}^*(2317)$ were a DK molecule. In fact typical calculations for molecular states give a width of the order of 100 keV (Faessler *et al.*, 2007; Lutz and Soyeur, 2008; L. Liu *et al.*, 2013); for more details see Sec. V.D. Thus, if this admittedly small width could be measured, e.g., at $\bar{\text{P}}$ANDA, its value would provide direct experimental access to the nature of $D_{s0}^*(2317)$.

4. Enhanced production of hadronic molecules and conventional hadrons due to triangle singularities

From the analysis in Sec. IV.A.1, we see that the TS on the physical boundary is always located close to the threshold of the intermediate particles. Furthermore, its effect is most pronounced if the two intermediate particles are in an S wave, since otherwise the centrifugal barrier suppresses small momenta. Hadronic molecules are located naturally near thresholds as well, and in all cases considered couple in S wave to its constituents. Therefore, in the course of this review there are two important aspects of TS that need to be discussed: On the one hand, a TS may lead to a pronounced structure in experimental observables that could be mistaken as a state; on the other hand, a TS can enhance the production of a hadronic molecule in a given reaction. Note also that the production of the conventional hadrons can be strongly enhanced by a TS within small energy regions. This is accompanied by a significant distortion of the line shapes since the location of the TS depends on the invariant masses of the external states. For example, the signal in the $\eta\pi\pi$ channel interpreted as $\eta(1405)$ and the signal in the $K\bar{K}\pi$ interpreted as $\eta(1475)$ could find their origin in a single pole accompanied by a TS (Wu *et al.*, 2012, 2013). We note that although P-wave couplings are present in the triangle loop for the $\eta(1405/1475)$ decays, the perfect satisfaction of the TS condition, Eq. (46), causes detectable effects in these decays.

Since the $K\bar{K}^*$ system can contribute to both $I = 0$ and 1 channels with $J^{PC} = 1^{++}$ and 1^{+-}, one expects that the TS may cause enhancements also in these channels. In the following we list those possible enhancements and their quantum numbers which can be searched for in experiment:

$$f_1(1420), 0^+, 1^{++}: \quad \frac{1}{\sqrt{2}}(K^*\bar{K} - K\bar{K}^*)$$
$$\to K\bar{K}\pi, \eta\pi\pi, [3\pi],$$

$$a_1(1420), 1^-, 1^{++}: \quad \frac{1}{\sqrt{2}}(K^*\bar{K} - K\bar{K}^*)$$
$$\to K\bar{K}\pi, 3\pi, [\eta\pi\pi],$$

$$\tilde{h}_1(1420), 0^-, 1^{+-}: \quad \frac{1}{\sqrt{2}}(K^*\bar{K} + K\bar{K}^*)$$
$$\to \rho\pi, \omega\eta, (\phi\eta), [\omega\pi], [\rho\pi], [\phi\pi],$$

$$\tilde{b}_1(1420), 1^+, 1^{+-}: \quad \frac{1}{\sqrt{2}}(K^*\bar{K} + K\bar{K}^*)$$
$$\to \phi\pi, \omega\pi, \rho\eta, [\rho\pi], [\omega\eta], \qquad (103)$$

where $\tilde{h}_1(1420)$ and $\tilde{b}_1(1420)$ refer to the TSs whether or not there exist resonances around. Note that the $f_1(1420)$ needs to be taken into account for the angular distribution in the $J/\psi \to \gamma 3\pi$ process (Ablikim *et al.*, 2012), and a detailed partial-wave analysis suggests the presence of the $f_1(1420)$ resonance together with a TS mechanism (Wu *et al.*, 2013), while Debastiani, Aceti *et al.* (2017) argued that the $f_1(1420)$ is the manifestation of the $f_1(1285)$ at higher energies due to the TS. The $a_1(1420)$ was reported by the COMPASS Collaboration in $\pi^- p \to \pi^-\pi^-\pi^+ p$ and $\pi^-\pi^0\pi^0 p$ (Adolph *et al.*, 2015) and can be well explained by the TS mechanism (Mikhasenko, Ketzer, and Sarantsev, 2015; Liu, Oka, and Zhao, 2016). The decay channels in the square brackets are G-parity violating and those in the round brackets are limited by the phase space. One notices that there are states observed in the relevant mass regions, namely, $a_1(1260)$, $f_1(1285)$, $h_1(1170)$, and $b_1(1235)$ (Patrignani *et al.*, 2016). Although most of these states have masses outside of the TS favored mass region, i.e., 1.385–1.442 GeV (Liu, Oka, and Zhao, 2016), the $h_1(1380)$ is located at the edge of the TS kinematics and some detectable effects could be expected (Guo, Hanhart *et al.*, 2013; Ablikim *et al.*, 2014d). Note that when there is a TS in action, the peak position for a resonance could be shifted toward its location. Some structures around thresholds of a pair of other light hadrons were also suggested to be due to a TS, for instance, the $f_2(1810)$ around the $K^*\bar{K}^*$ threshold (Xie, Geng, and Oset, 2017) and the $\phi(2170)$ around the $N\bar{\Delta}$ threshold (Lorenz, Hammer, and Meißner, 2015).

In the heavy quarkonium sector, the most famous example for an enhanced production rate via the TS is the observation of the $Z_c(3900)$ at the mass region of $Y(4260)$ (Liu and Li, 2013; Wang, Hanhart, and Zhao, 2013a, 2013b; Szczepaniak, 2015; Gong, Pang *et al.*, 2016; Pilloni *et al.*, 2017). In addition, the sensitivity of the TS to the kinematics of the reaction might well be the reason why the $Z_c(4020)$ is not seen in the same decay (Wang, Hanhart, and Zhao, 2013a, 2013b). As discussed in Sec. VI.A, the same mechanism also enhances the transition $Y(4260) \to \gamma X(3872)$ (Guo, Hanhart *et al.*, 2013) and suggests that the rate for $e^+e^- \to \gamma X_2$, which can be used to search for the spin-2 partner of the $X(3872)$, X_2 (see Sec. IV.B), gets most enhanced if the e^+e^- collision

TABLE VII. The triangle loops $[M_1 M_2 M_3]$ corresponding to Fig. 11 which have shown large impact on the production of hadronic molecules and conventional hadrons in experiment are listed in the first column. The second column is the measured process with the final states in parentheses. The check marks in the last column indicate that the triangle singularity of the corresponding process locates in the physical region, i.e., satisfying Eq. (46). Although the singularity of the process without a check mark is not located in the physical region, since it is not far away, it can still enhance the corresponding production rate significantly.

$[M_1 M_2 M_3]$	$A \to BC(\to$ final states)	Eq. (46)
$[K^* KK]$	$\eta(1405/1475) \to a_0(980)\pi(\to 3\pi)$ (Wu *et al.*, 2012, 2013)	✓
	$a_1(1420) \to f_0(980)\pi(\to \eta\pi\pi)$ (Mikhasenko, Ketzer, and Sarantsev, 2015; Liu, Oka, and Zhao, 2016)	✓
$[D_1 DD^*]$	$Y(4260) \to X(3872)\gamma$ (Guo, Hanhart *et al.*, 2013)	
	$Y(4260) \to Z_c(3900)\pi$ (Wang, Hanhart, and Zhao, 2013a, 2013b; Szczepaniak, 2015; Gong, Pang *et al.*, 2016)	
$[\Lambda(1890)\chi_{c1}p]$	$\Lambda_b \to P_c(4450)K$ (Guo *et al.*, 2015; Bayar *et al.*, 2016; Liu, Wang, and Zhao, 2016)	✓
$[D_{s3}(2860)\Lambda_c(2595)D]$	$\Lambda_b \to P_c(4450)K$ (Liu, Wang, and Zhao, 2016)	

energy is between 4.4 and 4.5 GeV (Guo, Meißner, and Yang, 2015).[30] A candidate for the analog of $Y(4260)$ in the bottomonium sector is $\Upsilon(11020)$, since it is located close to the $B_1\bar{B}$ threshold (Wang, Hanhart, and Zhao, 2013b; Bondar and Voloshin, 2016). Here the TS could affect both the $Z_b(10610)$ and $Z_b(10650)$ (Wang, Hanhart, and Zhao, 2013b), although at the mass of $\Upsilon(11020)$ the production of the lower Z_b state is more favored since the corresponding TS is closer (Bondar and Voloshin, 2016). Based on the current statistics in Belle (Bondar and Voloshin, 2016), it is difficult to judge whether there is one peak or two peaks present in Fig. 3. Pakhlov and Uglov (2015) and Uglov and Pakhlov (2016) claimed the structure identified as the charged exotic $Z_c(4430)$ observed in the $\pi\psi'$ final states by Belle (Mizuk *et al.*, 2009; Chilikin *et al.*, 2013) and LHCb (Aaij *et al.*, 2015a) was not to be connected to a pole but to owe its existence to the presence of a TS.

Suggestions to search for resonancelike structures due to the TS in the heavy meson and heavy quarkonium mass regions can be found in Liu (2014), Liu and Oka (2016a), Liu, Oka, and Zhao (2016), and Liu and Meißner (2017). In particular, the recent BESIII results on the $\pi^{\pm}\psi'$ invariant mass distributions for the $e^+ e^- \to \pi^+ \pi^- \psi'$ process at different c.m. energies seem in line with the predictions made by Liu (2014). Some of the strongly favored triangle loops are listed in Table VII.

The $P_c(4450)$ structure observed by LHCb (Aaij *et al.*, 2015b) in Λ_b decays, no matter what its nature is, also contains a TS contribution, as long as it strongly couples in an S wave (Bayar *et al.*, 2016) to either $\chi_{c1}p$ (Guo *et al.*, 2015, 2016; Meißner and Oller, 2015; Liu, Wang, and Zhao, 2016) or $\Lambda_c(2595)\bar{D}$ (Liu, Wang, and Zhao, 2016). Recent discussions on the role of TSs in the light baryonic sector can be found in Debastiani, Sakai, and Oset (2017), Roca and Oset (2017), Samart, Liang, and Oset (2017), and Wang *et al.* (2017).

It is worthwhile to emphasize that once the kinematics for a process (nearly) satisfies the TS condition given in Eq. (46),

the enhancement in reaction rates due to a TS contribution is always there and can produce a narrow peak once the relevant coupling is in an S wave (Bayar *et al.*, 2016). The only question is whether it is strong enough to produce the observed or an observable structure. Complications due to the interference between the TS and a tree-level contribution are discussed by Schmid (1967) and Goebel, Tuan, and Simmons (1983) in the single-channel case, and in Anisovich and Anisovich (1995) and Szczepaniak (2016) for coupled channels. The key to distinguishing whether a structure is solely due to a TS or originates from a genuine resonance is the sensitivity of the TS on kinematics: If in reactions with different kinematics the same structure is observed, it most likely reflects the existence of a pole (resonance).

B. Short-distance production and decay mechanisms

In Sec. VI.A we discussed both decay and production mechanisms sensitive to the long-range parts of the wave function of a state and therefore sensitive to its molecular nature. Here we demonstrate that there are also decays and production reactions that do not allow one to extract the molecular component of a given state. We start with an example of the former to then switch to the latter.

It was claimed long ago (Swanson, 2004a) that the ratio

$$\frac{\mathcal{B}(X(3872) \to \gamma\psi')}{\mathcal{B}(X(3872) \to \gamma J/\psi)},$$

with the measured value given in Eq. (3) is very sensitive to the molecular component of the $X(3872)$ wave function. In particular, using vector meson dominance and a quark model, Swanson (2004a) predicted it to be about 4×10^{-3} if the $X(3872)$ is a hadronic molecule with a dominant $D^0 \bar{D}^{*0}$ component plus a small admixture of the $\rho J/\psi$ and $\omega J/\psi$. However, as demonstrated by Guo, Hanhart, Kalashnikova *et al.* (2015), when radiative decays of $X(3872)$ are calculated using $\mathrm{NREFT_I}$ (see Sec. IV.A.2) field theoretic consistency calls for the inclusion of a counter term at LO. In other words, the transitions are controlled by short-distance instead of long-distance dynamics and therefore do not allow one to extract any information on the molecular component of the $X(3872)$ wave function.

---

[30]This suggestion is based on the assumption that the X_2 mass is very close to the $D^*\bar{D}^*$ threshold. If its mass is tens of MeV below the threshold as suggested by Baru *et al.* (2016), then the TS would be farther away from the physical boundary and the production would get less enhanced.

There have also been many claims that production rates of multiquark states in high-energy collisions are sensitive to a molecular admixture of those states. The production of the $X(3872)$ at hadron colliders was debated by Bignamini *et al.* (2009, 2010), Artoisenet and Braaten (2010, 2011), Butenschoen, He, and Kniehl (2013), Esposito *et al.* (2013), and Meng, Han, and Chao (2017), and that of the spin and flavor partners of the $X(3872)$ was discussed by Bignamini *et al.* (2010), Guo, Meißner, and Wang (2014), and Guo *et al.* (2014b). For the production of the $X(3872)$ in B decays, see Braaten, Kusunoki, and Nussinov (2004), Braaten and Kusunoki (2005a), Fan *et al.* (2012), Meng, Gao, and Chao (2013), and Meng, Han, and Chao (2017). The production of the $X(3872)$ in heavy ion collisions was discussed by Cho and Lee (2013) and Martínez Torres *et al.* (2014) and by the ExHIC Collaboration including other hadronic molecular candidates (Cho *et al.*, 2011a, 2011b; Cho, Song, and Lee, 2015). Larionov, Strikman, and Bleicher (2015) proposed that the hadronic molecular component of the $X(3872)$ could be extracted from its production in antiproton-nucleus collisions. Prompt productions of diquark-antidiquark tetraquarks at the LHC were studied by Guerrieri *et al.* (2014). Here we discuss to what extent high-energy reactions can be used to disentangle the structure of a near-threshold state.

The underlying physics for the short-distance production and decay processes of a shallow hadronic molecule is characterized by vastly different scales. This allows for a derivation of factorization formulas for the corresponding amplitudes (Braaten, Kusunoki, and Nussinov, 2004; Braaten and Kusunoki, 2005a, 2005b; Braaten and Lu, 2006).

We illustrate the production of a h_1h_2 pair and a near-threshold state with wave function Ψ in Fig. 21, where Γ denotes a short-distance source. The pair of h_1 and h_2 can be directly produced at short distances shown as Fig. 21(a), and through rescattering shown as Fig. 21(b). If the rescattering strength were weak, the production would be well approximated by only the Γ term. There would also be no drastic energy dependence in the near-threshold region, and the strength of the S-wave cusp exactly at the threshold would not be strong enough to produce a narrow peak (Guo, Hanhart, Wang, and Zhao, 2015). However, if the rescattering is strongly attractive, the amplitude T possesses a pole, which we assume to be located close to the threshold with a small binding energy E_B. Then one gets for the production amplitude of a given decay channel j of the state of interest:

$$
\mathcal{M}_j(\boldsymbol{k}; E) = \Gamma_j^\Lambda(\boldsymbol{k}; E)
$$
$$
+ \sum_i \int_\Lambda \frac{d^3 q}{(2\pi)^3} \Gamma_i^\Lambda(\boldsymbol{q}; E) G_i(\boldsymbol{q}; E) T_{ij}(\boldsymbol{q}, \boldsymbol{k}; E),
$$

$$(104)$$

where G_i (Γ_i^Λ) is the propagator (short-distance production amplitude) for the ith intermediate channel and Λ denotes the cutoff of the integral. In principle all dynamical degrees of freedom below the energy scale Λ should be accounted for. The short-distance contribution Γ_i^Λ also serves to absorb the Λ dependence, and as a result $\mathcal{M}$ is Λ independent.
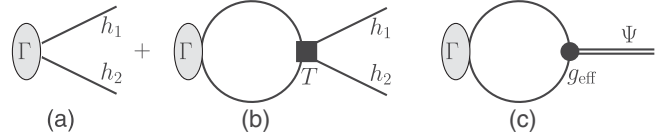

FIG. 21. (a), (b) Production of a pair of hadrons and the (c) hadronic molecule formed by them from a source Γ. Here the shaded areas, the solid lines, and the double line denote the source, the constituent hadrons, and the hadronic molecule, respectively.

Let us consider the kinematic situation in which the c.m. momentum of h_1 and h_2 is very small, $\sim\gamma$, and Λ is much larger than $\gamma^2/(2\mu)$ but still small enough to prevent other channels from being dynamical. In this case, the intermediate state for Fig. 21(b) is h_1h_2. The LO term of the momentum expansion of Γ^Λ is simply a constant. The nonrelativistic two-body propagator is $G(\boldsymbol{q}; E) = [E - \boldsymbol{q}^2/(2\mu) + i\epsilon]^{-1}$, and the T matrix is given by Eq. (70). Thus, one obtains

$$
\mathcal{M}(\boldsymbol{k}; E) = \Gamma^\Lambda \left[1 + \frac{\Lambda/\sqrt{2\pi} - \sqrt{-2\mu E} + \mathcal{O}(\Lambda^{-1})}{\gamma - \sqrt{-2\mu E}} \right]. \quad (105)
$$

If $\Gamma^\Lambda \propto \Lambda^{-1}$, the LO Λ dependence will be absorbed (Braaten and Kusunoki, 2005a), and the factorization formula (Braaten, Kusunoki, and Nussinov, 2004; Braaten and Kusunoki, 2005a, 2005b) for the production of the low-momentum h_1h_2 pair follows:

$$
\mathcal{M}(\boldsymbol{k}; E) = \frac{\Gamma\mu}{(2\pi)^{3/2}} T_{\mathrm{NR}}(E) + \mathcal{O}(\Lambda^{-1}), \quad (106)
$$

where $\Gamma \equiv \Gamma^\Lambda\Lambda$ is the short-distance part, and the long-distance part $T_{\mathrm{NR}}(E) = (2\pi/\mu)(\gamma - \sqrt{-2\mu E})^{-1}$ is provided by the scattering T matrix. From the derivation in Braaten and Lu (2006), it becomes clear that the short-distance part is the Wilson coefficient of the operator production expansion in the EFT. A similar factorization formula was derived by Guo *et al.* (2014a) with the help of chiral symmetry for high-energy productions of kaonic bound states predicted by Guo and Meißner (2011).

The amplitude for the production of the near-threshold state is obtained from Eq. (106) by replacing $T_{\mathrm{NR}}(E)$ by the square root of its residue g_{NR}^2 given in Eq. (73) and multiplying the factor $1/\sqrt{2\mu}$ to account for the difference in normalization factors

$$
\mathcal{M}_\Psi = \frac{\Gamma\sqrt{\mu}}{4(\pi)^{3/2}} g_{\mathrm{NR}} + \mathcal{O}(\Lambda^{-1}). \quad (107)
$$

Hence, the production rate $\propto g_{\mathrm{NR}}^2 \propto \sqrt{E_B}$ [cf. Eq. (25)] seems suppressed for very loosely bound states, which is consistent with the common intuition (Braaten, Kusunoki, and Nussinov, 2004; Artoisenet and Braaten, 2010). In particular, one expects a suppression of a loosely bound state in high-energy reactions. The factorization as explained is the foundation for the proposal to extract the short-distance production mechanism of $X(3872)$ in B_c semileptonic and hadronic decays (Wang and Zhao, 2016).

Note that it is a straightforward consequence of Eq. (107) that in ratios of short-distance production rates for two hadronic molecules related to each other through some symmetry the long-distance part containing the information of the structure of the states cancels, and the remaining part solely reflects the difference in the short-distance dynamics and phase space. It could be misleading if such ratios are taken as evidence in support of or against the dominantly composite nature of given states.

All the derivations of the factorization formula are based on the LO NREFT$_{\rm II}$ so far, which allows self-consistently only the possibility that Ψ is a composite system of h_1 and h_2; see the discussion after Eq. (73). If we go to higher orders, momentum-dependent terms need to be kept in the potential as well as the short-distance production amplitude. The probability of Ψ to be a $h_1 h_2$ composite system would be $1 - \lambda^2 < 1$, and thus one would also need to introduce a contact production term for Ψ. These new terms parametrize the short-distance physics though a detailed dynamics which depends on the more fundamental theory that cannot be specified within the EFT. Such contributions could be interpreted as a short-distance core of the physical wave function Ψ. The factorization and the related renormalization at higher orders for the near-threshold production of $h_1 h_2$ and Ψ in short-distance processes remain to be worked out.

The long-distance contribution in Eqs. (106) and (107) is calculable in NREFT, and the short-distance contribution is subject to the more fundamental theories which are QCD and/or electroweak theory. For inclusive high-energy hadron collisions, one is not able to calculate the short-distance contribution model independently [for estimates using Monte Carlo event generators, see Bignamini *et al.* (2009, 2010), Artoisenet and Braaten (2010, 2011), Esposito *et al.* (2013), Guo *et al.* (2014a, 2014b), and Guo, Meißner, and Wang (2014)], and thus only the order of magnitude of the production cross sections can be estimated. For the production of hadronic molecules in heavy-meson decays such as B decays, again one normally is able only to get an order-of-magnitude estimate at best due to the nonperturbative nature of QCD which dominates the hadronic effects in the short-distance part. The production rate of the $X(3872)$ in B decays was estimated in Braaten, Kusunoki, and Nussinov (2004) and Braaten and Kusunoki (2005a). In particular, Braaten and Kusunoki (2005a) predicted that the branching fraction of $B^0 \to X(3872)K^0$ should be much smaller than that of $B^+ \to X(3872)K^+$ assuming that the $X(3872)$ is a $D^0\bar{D}^{*0}$ hadronic molecule. The prediction seems to be in contradiction with the later measurements (Patrignani *et al.*, 2016) summarized in Sec. II giving a ratio of around 0.5; cf. Eq. (4). However, as mentioned the $X(3872)$ is to a good approximation an isoscalar state. Its couplings to the neutral $D^0\bar{D}^{*0}$ and the charged D^+D^{*-} channels are almost the same even if the isospin breaking is taken into account (Gamermann and Oset, 2009; Guo, Hidalgo-Duque *et al.*, 2014). Therefore Eq. (107) needs to be generalized to coupled channels. In particular, the production of Ψ gets modified to

$$\mathcal{M}_\Psi = \frac{1}{4(\pi)^{3/2}} \sum_i \Gamma_i \sqrt{\mu_i} g_{\mathrm{NR},i} + \mathcal{O}(\Lambda^{-1}), \qquad (108)$$

where the summation runs over all possible intermediate channels below the cutoff Λ. Notably, $g_{\mathrm{NR},i}$ denotes the coupling of the Ψ state to the ith channel. As a result, the $X(3872)$ production rates in neutral and charged B decays should be similar. This may also be understood as the short-distance parts in Braaten and Kusunoki (2005a) should include the charged channel and were not properly estimated.

We now turn to the discussion of production rates of shallow bound states such as $X(3872)$ at hadron colliders. It was claimed that the cross section for the inclusive $X(3872)$ production at high p_T at the Fermilab Tevatron in $\bar{p}p$ collisions is too large to be consistent with the interpretation of $X(3872)$ as a $D^0\bar{D}^{*0}$ molecule (Bignamini *et al.*, 2009). The reasoning was based on the following estimate for an upper bound of the cross section:

$$
\begin{aligned}
\sigma(\bar{p}p \to X) &\sim \left| \int d^3\mathbf{k} \langle X|D^0\bar{D}^{*0}(\mathbf{k})\rangle \langle D^0\bar{D}^{*0}(\mathbf{k})|\bar{p}p\rangle \right|^2 \\
&\simeq \left| \int_\mathcal{R} d^3\mathbf{k} \langle X|D^0\bar{D}^{*0}(\mathbf{k})\rangle \langle D^0\bar{D}^{*0}(\mathbf{k})|\bar{p}p\rangle \right|^2 \\
&\leq \int_\mathcal{R} d^3\mathbf{k} |\Psi(\mathbf{k})|^2 \int_\mathcal{R} d^3\mathbf{k} |\langle D^0\bar{D}^{*0}(\mathbf{k})|\bar{p}p\rangle|^2 \\
&\leq \int_\mathcal{R} d^3\mathbf{k} |\langle D^0\bar{D}^{*0}(\mathbf{k})|\bar{p}p\rangle|^2 \\
&\sim \sigma(\bar{p}p \to X)^{\mathrm{max}},
\end{aligned}
\qquad (109)
$$

where $\mathcal{R}$ means that the momentum integration receives support only up to some characteristic scale $\mathcal{R}$. The upper bound previously quoted depends drastically on the value of $\mathcal{R}$. A value of $\mathcal{R} = 35$ MeV $\simeq \gamma$, the binding momentum of the $X(3872)$, was chosen by Bignamini *et al.* (2009). The so-estimated upper bound of 0.071 nb is orders of magnitude smaller than the Fermilab Tevatron result of 37 to 115 nb.

However, for the derivation in Eq. (109) to be valid $\mathcal{R}$ must be large enough that the wave function of the bound state gets largely probed for otherwise the symbol between the first and the second integral needs to be changed from $\simeq$ to $\gg$ and the whole line of reasoning gets spoiled. But this requirement calls for values of $\mathcal{R}$ much larger than the binding momentum. To demonstrate this claim we switch to the deuteron wave function. Figure 22 shows the averaged deuteron wave function calculated from $\bar{\Psi}_\Lambda(\mathcal{R}) = \int_\mathcal{R} d^3\mathbf{k} \Psi_\Lambda(\mathbf{k})$, where the subindex Λ indicates that a regulator needs to be specified to get a well-defined wave function [for more details, see Nogga and Hanhart (2006)]. The right panel in the figure is a zoom in linear scale to the relevant $\mathcal{R}$ range. From the figure, it is clear that $\bar{\Psi}_\Lambda(\mathcal{R})$ is far from being saturated for $\mathcal{R} \simeq 45$ MeV which is the deuteron binding momentum. One needs to take $\mathcal{R} \sim 2M_\pi \sim 300$ MeV, the order of the inverse range of forces as pointed out by Artoisenet and Braaten (2010, 2011) based on rescattering arguments, to get a reasonable estimate so that the second line in Eq. (109) can be a good approximation of the first line. With such a large support $\mathcal{R}$, the upper bound becomes consistent with the Fermilab Tevatron measurement (Bignamini *et al.*, 2009; Artoisenet and Braaten, 2010, 2011). In addition, as discussed in the case of the B decays, the charged channels need to be considered as well.
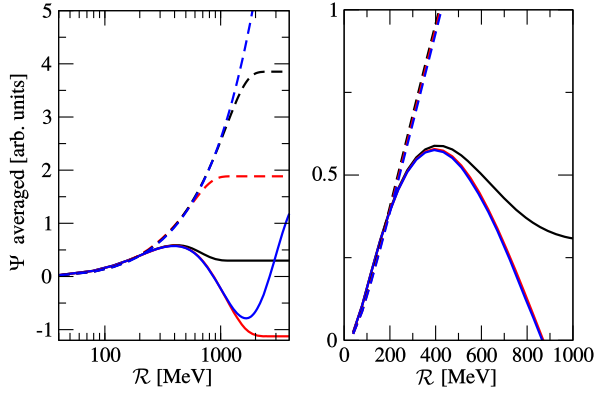
FIG. 22. Averaged deuteron wave functions for various cutoff values: $\Lambda = 0.8$, 1.5, and 4 GeV shown as black, red, and blue curves, respectively. The solid (dashed) lines show the result for the wave functions with (without) one-pion exchange. From Albaladejo, Guo *et al.*, 2017.

In fact, with the factorization derived, it was suggested that one can estimate the cross section by combining the use of Monte Carlo event generators, such as PYTHIA (Sjostrand, Mrenna, and Skands, 2008) and HERWIG (Bahr *et al.*, 2008), and EFT to get the short-distance and long-distance contributions, respectively (Artoisenet and Braaten, 2010, 2011; Guo *et al.*, 2014b). In Table VIII, we show the estimates obtained by Albaladejo, Guo *et al.* (2017). Indeed, if a small cutoff is used, $\Lambda = 0.1$ GeV, and only the neutral charmed mesons are considered by using (Guo *et al.*, 2014a, 2014b)

$$\sigma(pp/\bar{p} \to X) \approx C 2\pi^2 \left| \int \frac{d^3\boldsymbol{k}}{(2\pi)^3} \Psi_X(\boldsymbol{k}) \right|^2 = C 2\pi^2 |g_{\mathrm{NR},X} \Sigma_{\mathrm{NR}}(-E_B)|^2, \quad (110)$$

the obtained cross sections are orders of magnitude smaller than the data, in line with the observation in Bignamini *et al.* (2009). Here $C = (d\sigma[D^0\bar{D}^{*0}]/dk)/k^2$, playing the role of $|\Gamma^\Lambda|^2$ in Eq. (105), is a constant determined from fitting to the differential cross section of the direct production of the charmed-meson pair from PYTHIA and HERWIG, $\Psi_X(\boldsymbol{k})$ is the momentum space wave function of the $X(3872)$, $g_{\mathrm{NR},X}$ is the coupling of the $X(3872)$ to $D^0\bar{D}^{*0}$, and $\Sigma_{\mathrm{NR}}(-E_B)$ is the loop function in Eq. (71) but keeping the full Λ dependence from the Gaussian regulator. However, when a larger cutoff in the range of [0.5, 1.0] GeV is used, the cross sections become consistent with both the CDF and CMS measurements. One important point is that the charged $D^+D^{*-} + $ c.c. channel needs to be taken into account for this case as discussed. This is because the binding momentum for the charged channel $\gamma_\pm \simeq 126$ MeV is well below the cutoff so that the charged charmed mesons should also play a dynamical role.

Finally, in Esposito, Guerrieri, Maiani *et al.* (2015), the cross sections for the production of light (hyper)nuclei at small p_T at ALICE (Adam *et al.*, 2016) were extrapolated to large p_T, and it was found that they are much smaller than the $X(3872)$ production at large p_T at CMS (Chatrchyan *et al.*, 2013a). Since light (hyper)nuclei are loosely bound states of baryons, they concluded that loosely bound states are hardly

TABLE VIII. Integrated cross sections (in units of nb) reported by Albaladejo, Guo *et al.* (2017) for the inclusive $pp/\bar{p} \to X(3872)$ processes in comparison with the CDF (Bauer, 2005) and CMS (Chatrchyan *et al.*, 2013a) data converted into cross sections (Guo *et al.*, 2014b). The ranges of the results cover those obtained using both PYTHIA and HERWIG. Here we have converted the experimental data into cross sections (Guo *et al.*, 2014b).

$\sigma(pp/\bar{p} \to X)$	$\Lambda = 0.1$ GeV	$\Lambda = [0.5, 1]$ GeV	Experiment
Tevatron	0.05–0.07	5–29	37–115
LHC 7	0.04–0.12	4–55	13–39

produced at high p_T, and therefore disfavored the hadronic molecular interpretation of the $X(3872)$. However, although the long-distance contributions for these productions can be managed in the EFT or universality framework, the short-distance contribution for the $X(3872)$ is completely different from that for light nuclei. This leads to a different energy dependence of the cross sections for light nuclei and the $X(3872)$, and makes such a direct comparison questionable. One essential difference is as follows: At short distances, the $X(3872)$ can be produced through $c\bar{c}$ or $u\bar{u}(d\bar{d})$, which hadronizes into a pair of charmed mesons at larger distances, while the minimal quark number in the light nuclei is always $3N$, with N the number of baryons, giving rise to a suppression. Therefore, it is natural that the $X(3872)$ production cross section at very high p_T is orders of magnitude larger than that of light nuclei. This point also leads to the critique (Guo, Meißner, and Wang, 2017),[31] which was appreciated by Voloshin (2016a), against the use of constituent counting rules in hard exclusive processes as a way to identifying mulqituark states with a hidden-flavor $q\bar{q}$ pair (Kawamura, Kumano, and Sekihara, 2013; Kawamura and Kumano, 2014; Brodsky and Lebed, 2015; Chang, Kumano, and Sekihara, 2016).

To summarize, the production and decay processes with a large energy release involve both long- and short-distance scales. Only the long-distance part is sensitive to the low-energy quantities, thus to the hadronic molecular structure, and can be dealt with in the EFT framework. On the contrary, high-energy production rates depend crucially on what happens at short distances, which is often unknown although in principle could be extracted from other reactions depending on the same short-distance physics. However, despite the fact that it is hard to calculate the integrated production rates, the differential invariant mass distributions around the near-threshold states provide a direct access to their line shapes and precise, high-resolution data on those are urgently called for. This was discussed in general in Sec. III.C and also in Sec. VI.A.2.

C. Implications of heavy quark spin and flavor symmetries

It turns out that HQSS, and especially its breaking, is also an important diagnostic tool when it comes to understanding the structure of certain states (Cleven *et al.*, 2015). The most straightforward example to illustrate this point is the spin

---

[31]For a response, see Brodsky, Lebed, and Lyubovitskij (2017).

TABLE IX.   Possible spin and flavor partners of heavy-flavor hadronic molecules. For the experimentally established states, the masses and decay modes are from Patrignani *et al.* (2016). The predicted partners are denoted by question marks. The predictions from Guo *et al.* (2013a) are those computed with a 0.5 GeV cutoff, and the result from Baru *et al.* (2016) is from the results with the cutoff limited between 0.8 and 1.0 GeV.

$J^{P(C)}$	State	Main component	Mass (MeV)	(Expected) main decay mode(s)
0^+	$D_{s0}^*(2317)$	DK	2317.7 ± 0.6	$D_s^+ \pi^0$
1^+	$D_{s1}(2460)$	D^*K	2459.5 ± 0.6	$D_s^{*+}\pi^0, D_s^{(*)+}\gamma$
0^+	$B_{s0}^*(?)$	$B\bar{K}$	5730 ± 16	$B_s^{*0}\gamma, B_s^0\pi^0$
1^+	$B_{s1}(?)$	$B^*\bar{K}$	5776 ± 16	$B_s^{(*)0}\gamma, B_s^{*0}\pi^0$
1^-	$D_{s1}^*(2860)$	$D_1(2420)K$	2859 ± 27	DK, D^*K
2^-	$D_{s2}^*(?)$	$D_2(2460)K$	2910 ± 9 (Guo and Meißner, 2011)	$D^*K, D_s^*\eta$
1^-	$B_{s1}^*(?)$	$B_1(5720)\bar{K}$	6151 ± 33 (Guo and Meißner, 2011)	$B^{(*)}\bar{K}, B_s^{(*)}\eta$
2^-	$B_{s2}^*(?)$	$B_2(5747)\bar{K}$	6169 ± 33 (Guo and Meißner, 2011)	$B^*\bar{K}, B_s^*\eta$
1^{++}	$X(3872)$	$D\bar{D}^*$	3871.69 ± 0.17	$D^0\bar{D}^0\pi^0, J/\psi\pi\pi, J/\psi\pi\pi\pi$
2^{++}	$X_2(?)$	$D^*\bar{D}^*$	4012_{-5}^{+4} (Guo *et al.*, 2013a) 3980 ± 20 (Baru *et al.*, 2016)	$D\bar{D}^{(*)}, J/\psi\omega$
1^{++}	$X_b(?)$	$B\bar{B}^*$	10580_{-8}^{+9} (Guo *et al.*, 2013a)	$\Upsilon(nS)\omega, \chi_{bJ}\pi\pi$
2^{++}	$X_{b2}(?)$	$B^*\bar{B}^*$	10626_{-9}^{+8} (Guo *et al.*, 2013a)	$B\bar{B}^{(*)}, \Upsilon(nS)\omega, \chi_{bJ}\pi\pi$
2^+	$X_{bc}(?)$	D^*B^*	7322_{-7}^{+6} (Guo *et al.*, 2013a)	DB, DB^*, D^*B

doublet made of $D_{s0}^*(2317)$ and $D_{s1}(2460)$. On the one hand, both are not only significantly lighter than the prediction of the quark model as reported by Di Pierro and Eichten (2001), also their spin splitting differs. On the other hand, the mass difference of the two states agrees exactly with the mass difference between the D and the D^*, which would be a natural result if $D_{s0}(2317)$ and $D_{s1}^*(2460)$ were DK and D^*K molecular states, respectively, since at LO in the heavy quark expansion the DK interaction agrees to the D^*K interaction (Kolomeitsev and Lutz, 2004). In complete analogy Guo, Hanhart, and Meißner (2009a) argued that, if indeed the $J^{PC} = 1^{--}$ state $Y(4660)$ were a bound system of ψ' and $f_0(980)$ as conjectured by Guo, Hanhart, and Meißner (2008), there should exist a $J^{PC} = 0^{-+}$ state which is a $\eta_c' f_0(980)$ bound system. The mass difference of the latter state to the $\eta_c' f_0(980)$ should agree to that of $Y(4660)$ to the $\psi' f_0(980)$ threshold,[32] and it was even possible to estimate the decay width of the state as well as a most suitable discovery channel. For more discussion on the implications of HQSS for the spectrum of exotic states see Cleven *et al.* (2015), where also predictions from other approaches are contrasted to those of the molecular picture.

More predictions can be made for heavy-flavor hadronic molecules by using heavy quark flavor symmetry. The LO predictions are rather straightforward if there is only a single heavy quark in the system. For instance, one would expect the $D_{s0}^*(2317)$ as a DK bound state to have a bottom partner, a $\bar{B}K$ bound state, with almost the same binding energy. This prediction together with the one for the bottom partner of the $D_{s1}(2460)$ is given in the fourth and fifth rows in Table IX, where the error of 16 MeV accounts for the use of heavy quark flavor symmetry and is estimated as $2(M_D + M_K - M_{D_{s0}^*(2317)}) \times \Lambda_{QCD}(m_c^{-1} - m_b^{-1})$. Such simple predictions are in remarkable agreement with the lattice results of the

lowest-lying 0^+ and 1^+ bottom-strange mesons: $5711 \pm 13 \pm 19$ MeV for the B_{s0}^* and $5750 \pm 17 \pm 19$ MeV for the B_{s1} (Lang *et al.*, 2015). This agreement may be regarded as further support of the hadronic molecular nature of the $D_{s0}^*(2317)$ and $D_{s1}(2460)$ states. For more complicated predictions of these two states using various versions of UCHPT, see Kolomeitsev and Lutz (2004), Guo, Shen *et al.* (2006), Guo, Shen, and Chiang (2007), Cleven *et al.* (2011b), Altenbuchinger, Geng, and Weise (2014), Cleven, Grießhammer *et al.* (2014), and Torres-Rincon, Tolos, and Romanets (2014).

A more detailed discussion of spin symmetry partners of hadronic molecules formed by a pair of S-wave heavy mesons can be found in Sec. IV.B. Some of the spectroscopic consequences of HQSS and heavy quark flavor symmetry for hadronic molecules are listed in Table IX.

D. Baryon candidates for hadronic molecules

For a discussion of and references for charmed baryons and the P_c pentaquark structures as possible hadronic molecules see Sec. II. The closing part of this section will be used to describe the most recent developments about the $\Lambda(1405)$ which basically settled the debate on the nature of this famous state. What is described next is yet another example of how the interplay of high quality data and systematic theoretical investigations allows one to identify the nature of certain states.

As already stressed in Sec. II.D.1, there are good reasons to classify the $\Lambda(1405)$ as an exotic particle, since it does not at all fit into the pattern of the otherwise in this mass range quite successful quark models.

Using information on $\bar{K}N$ scattering the existence of the $\Lambda(1405)$ was predicted by Dalitz and Tuan (1959, 1960) before its observation. Already this study highlights the importance of the $\bar{K}N$ dynamics for the $\Lambda(1405)$. In most modern investigations it appears as a dynamically generated state through coupled-channel effects among all the ten isospin channels (K^-p, $\bar{K}^0n$, $\pi^0\Lambda$, $\pi^0\Sigma^0$, $\pi^+\Sigma^-$, $\pi^-\Sigma^+$, $\eta\Lambda$,

---

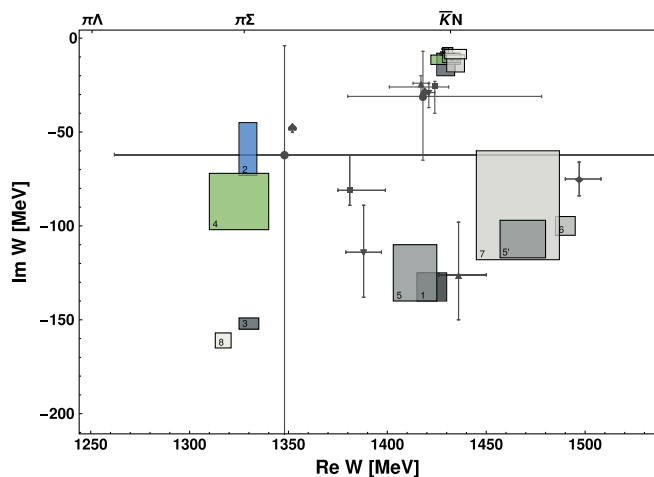[32]This prediction receives support from a calculation using QCD sum rules (Wang and Zhang, 2010a).

FIG. 23. Positions of the two poles of the $\Lambda(1405)$ in the complex plane. Filled circles: Borasoy, Meißner, and Nißler (2006), filled squares: Ikeda, Hyodo, and Weise (2012), triangles: Guo and Oller (2013), boxes: Mai and Meißner (2015), and spades: Roca and Oset (2013). The labels and colors are described in the text. Figure courtesy of Maxim Mai.

$\eta\Sigma^0$, $K^+\Xi^-$, and $K^0\Xi^0$) or some of them, in other words, a hadronic molecule. This coupled-channel problem has been studied by solving the LSE or Bethe-Salpeter equation with interaction kernels derived from chiral perturbation theory within a given accuracy. This procedure was first proposed by Kaiser, Siegel, and Weise (1995) and further refined by Oller and Meißner (2001) and various follow-ups. The major finding of Oller and Meißner (2001) was the fact that there are indeed two poles, one stronger coupled to the $\bar{K}N$ channel and the other to $\Sigma\pi$, which should thus be understood as two distinct states. Both poles are located at the second Riemann sheet and have shadow poles in the third one (Oller and Meißner, 2001). This two-pole scenario can be understood by considering the SU(3) limit and its subsequent breaking (Jido *et al.*, 2003). Presently, various groups performed calculations to the NLO accuracy (Ikeda, Hyodo, and Weise, 2012; Guo and Oller, 2013; Mai and Meißner, 2013); see also the recent comparison of all these works in Cieplý *et al.* (2016) and the minireview by the PDG (Patrignani *et al.*, 2016). Including the photoproduction data on $\gamma p \to K^+\Sigma\pi$ from CLAS (Moriya *et al.*, 2013), one finds that the heavier of the poles is fairly well pinned down, while the lighter one still shows some sizable spread in its mass and width (Mai and Meißner, 2015). All this is captured in Fig. 23. Fitting only the scattering and threshold ratio data with the NLO kernel, one finds two poles, but with very limited precision (Borasoy, Meißner, and Nißler, 2006). Adding the precise kaonic hydrogen data, the situation changes markedly, as shown by the different solutions found by various groups (Ikeda, Hyodo, and Weise, 2012; Guo and Oller, 2013; Mai and Meißner, 2013). Still, as first pointed out by Mai and Meißner (2015), even with these data there is a multitude of solutions with almost equal χ^2, as depicted by the boxes labeled 1, ..., 8 in Fig. 23. However, the photoproduction data severely constrain this space of solutions. From the eight solutions only two survive, the blue (solution 2) and the green (solution 4) boxes in the figure from Mai and Meißner

(2015) as well as the modified LO solution depicted by the spades from Roca and Oset (2013). This again is an example that only through an interplay of various reactions one is able to pin down the precise structure of hadronic molecules (or other hadronic resonances). Clearly, more data on $\pi\Sigma$ mass distributions are needed to further sharpen these conclusions (Ohnishi *et al.*, 2016).

VII. SUMMARY AND OUTLOOK

In this review, we discussed the experimental indications for and the theoretical approaches to hadronic molecules, which are a particular manifestation of nonconventional states in the spectrum of QCD. The observation that these multi-hadron bound states appear close to or in between two-particle thresholds allows one to write down nonrelativistic effective field theories. This gives a systematic access to the production, decay processes, and other reactions involving hadronic molecules. In the last decade or so, through precise measurements of the spectrum of QCD involving charm and bottom quarks, more and more potential hadronic molecules have been observed. We have shown how explicit calculations of various decay modes can be used to test this scenario. This is the only way to eventually disentangle hadronic molecules from other multiquark states such as tetraquarks. More detailed and accurate measurements are therefore called for, complemented by first-principle lattice QCD calculations with parameters close to the physical point and accounting for the involved coupled-channel dynamics related. More than 60 years after Weinberg's groundbreaking work on the question whether the deuteron is an elementary particle, we are now in the position to identify many more of such loosely bound states in the spectrum of QCD and to obtain a deeper understanding of the mechanism underlying the appearance and binding of hadronic molecules.

ACKNOWLEDGMENTS

REFERENCES

Aaij, R., *et al.* (LHCb Collaboration), 2012, Eur. Phys. J. C **72**, 1972.
Aaij, R., *et al.* (LHCb Collaboration), 2013, Phys. Rev. Lett. **110**, 222001.
Aaij, R., *et al.* (LHCb Collaboration), 2014a, Nucl. Phys. B **886**, 665.

Aaij, R., *et al.* (LHCb Collaboration), 2014b, Phys. Rev. Lett. **113**, 162001.

Aaij, R., *et al.* (LHCb Collaboration), 2015a, Phys. Rev. D **92**, 112009.

Aaij, R., *et al.* (LHCb Collaboration), 2015b, Phys. Rev. Lett. **115**, 072001.

Aaij, R., *et al.* (LHCb Collaboration), 2015c, Phys. Rev. D **92**, 011102.

Aaij, R., *et al.* (LHCb Collaboration), 2016a, Phys. Rev. Lett. **117**, 082003; **118**, 119901(E) (2017).

Aaij, R., *et al.* (LHCb Collaboration), 2016b, Phys. Rev. Lett. **117**, 152003; **118**, 109904(E) (2017).

Aaij, R., *et al.* (LHCb Collaboration), **2016**c, J. High Energy Phys. 05, 132.

Aaij, R., *et al.* (LHCb Collaboration), 2016d, Chin. Phys. C **40**, 011001.

Aaij, R., *et al.* (LHCb Collaboration), 2017a, Phys. Rev. D **95**, 012002.

Aaij, R., *et al.* (LHCb Collaboration), 2017b, Phys. Rev. Lett. **118**, 022003.

Aaij, R., *et al.* (LHCb Collaboration), 2017c, Phys. Rev. Lett. **119**, 062001.

Aaij, R., *et al.* (LHCb Collaboration), **2017**d, J. High Energy Phys. 05, 030.

Aaltonen, T., *et al.* (CDF Collaboration), 2009, Phys. Rev. Lett. **103**, 152001.

Abazov, V. M., *et al.* (D0 Collaboration), 2004, Phys. Rev. Lett. **93**, 162002.

Abazov, V. M., *et al.* (D0 Collaboration), 2016, Phys. Rev. Lett. **117**, 022003.

Abdesselam, A., *et al.* (Belle Collaboration), 2016, Phys. Rev. Lett. **117**, 142001.

Abe, K., *et al.* (Belle Collaboration), 2005, in "Lepton and photon interactions at high energies," Proceedings, 22nd International Symposium, LP 2005, arXiv:hep-ex/0505037.

Ablikim, M., *et al.* (BESIII Collaboration), 2011, Phys. Rev. D **83**, 032003.

Ablikim, M., *et al.* (BESIII Collaboration), 2012, Phys. Rev. Lett. **108**, 182001.

Ablikim, M., *et al.* (BESIII Collaboration), 2013a, Phys. Rev. Lett. **110**, 252001.

Ablikim, M., *et al.* (BESIII Collaboration), 2013b, Phys. Rev. Lett. **111**, 242001.

Ablikim, M., *et al.* (BESIII Collaboration), 2014a, Phys. Rev. Lett. **112**, 132001.

Ablikim, M., *et al.* (BESIII Collaboration), 2014b, Phys. Rev. Lett. **112**, 022001.

Ablikim, M., *et al.* (BESIII Collaboration), 2014c, Phys. Rev. Lett. **113**, 212002.

Ablikim, M., *et al.* (BESIII Collaboration), 2014d, Phys. Rev. Lett. **112**, 092001.

Ablikim, M., *et al.* (BESIII Collaboration), 2015a, Phys. Rev. D **92**, 092006.

Ablikim, M., *et al.* (BESIII Collaboration), 2015b, Phys. Rev. D **91**, 112005.

Ablikim, M., *et al.* (BESIII Collaboration), 2015c, Phys. Rev. Lett. **115**, 182002.

Ablikim, M., *et al.* (BESIII Collaboration), 2015d, Phys. Rev. Lett. **115**, 222002.

Ablikim, M., *et al.* (BESIII Collaboration), 2015e, Phys. Rev. Lett. **115**, 112003.

Ablikim, M., *et al.* (BESIII Collaboration), 2015f, Phys. Rev. Lett. **114**, 092003.

Ablikim, M., *et al.* (BESIII Collaboration), 2016a, Phys. Rev. D **93**, 011102.

Ablikim, M., *et al.* (BESIII Collaboration), 2016b, Phys. Rev. D **94**, 032009.

Ablikim, M., *et al.*, 2017a, Phys. Rev. D **96**, 032004.

Ablikim, M., *et al.* (BESIII Collaboration), 2017b, Phys. Rev. Lett. **118**, 092002.

Ablikim, M., *et al.* (BESIII Collaboration), 2017c, Phys. Rev. Lett. **118**, 092001.

Abreu, L. M., and A. Lafayette Vasconcellos, 2016, Phys. Rev. D **94**, 096009.

Abulencia, A., *et al.* (CDF Collaboration), 2006, Phys. Rev. Lett. **96**, 102002.

Abulencia, A., *et al.* (CDF Collaboration), 2007, Phys. Rev. Lett. **98**, 132002.

Aceti, F., L. R. Dai, and E. Oset, 2016, Phys. Rev. D **94**, 096015.

Aceti, F., W. H. Liang, E. Oset, J. J. Wu, and B. S. Zou, 2012, Phys. Rev. D **86**, 114007.

Aceti, F., and E. Oset, 2012, Phys. Rev. D **86**, 014012.

Achasov, N. N., S. A. Devyanin, and G. N. Shestakov, 1979, Phys. Lett. B **88**, 367.

Acosta, D., *et al.* (CDF Collaboration), 2004, Phys. Rev. Lett. **93**, 072001.

Adam, J., *et al.* (ALICE Collaboration), 2016, Phys. Rev. C **93**, 024917.

Adolph, C., *et al.* (COMPASS Collaboration), 2015, Phys. Rev. Lett. **115**, 082001.

Agadjanov, A., V. Bernard, U.-G. Meißner, and A. Rusetsky, 2014, Nucl. Phys. B **886**, 1199.

Agadjanov, D., F.-K. Guo, G. Ríos, and A. Rusetsky, **2015**, J. High Energy Phys. 01, 118.

Agakishiev, G., *et al.* (HADES Collaboration), 2013, Phys. Rev. C **87**, 025201.

Aitchison, I. J. R., 2015, arXiv:1507.02697.

Albaladejo, M., J. A. Oller, E. Oset, G. Ríos, and L. Roca, **2012**, J. High Energy Phys. 08, 071.

Albaladejo, M., P. Fernandez-Soler, F.-K. Guo, and J. Nieves, 2017, Phys. Lett. B **767**, 465.

Albaladejo, M., P. Fernandez-Soler, and J. Nieves, 2016, Eur. Phys. J. C **76**, 573.

Albaladejo, M., F.-K. Guo, C. Hanhart, C. Hidalgo-Duque, U.-G. Meißner, J. Nieves, A. Nogga, and Z. Yang, 2017, Chin. Phys. C **41**, 121001.

Albaladejo, M., F.-K. Guo, C. Hidalgo-Duque, and J. Nieves, 2016, Phys. Lett. B **755**, 337.

Albaladejo, M., F.-K. Guo, C. Hidalgo-Duque, J. Nieves, and M. P. Valderrama, 2015, Eur. Phys. J. C **75**, 547.

Albaladejo, M., C. Hidalgo-Duque, J. Nieves, and E. Oset, 2013, Phys. Rev. D **88**, 014510.

Albaladejo, M., D. Jido, J. Nieves, and E. Oset, 2016, Eur. Phys. J. C **76**, 300.

Albaladejo, M., and J. A. Oller, 2012, Phys. Rev. D **86**, 034003.

Alexandrou, C., R. Baron, J. Carbonell, V. Drach, P. Guichon, K. Jansen, T. Korzec, and O. Pene (ETM Collaboration), 2009, Phys. Rev. D **80**, 114503.

AlFiky, M. T., F. Gabbiani, and A. A. Petrov, 2006, Phys. Lett. B **640**, 238.

Alhakami, M. H., and M. C. Birse, 2015, Phys. Rev. D **91**, 054019.

Alston, M. H., L. W. Alvarez, P. Eberhard, M. L. Good, W. Graziano, H. K. Ticho, and S. G. Wojcicki, 1961, Phys. Rev. Lett. **6**, 698.

Altenbuchinger, M., L. S. Geng, and W. Weise, 2014, Phys. Rev. D **89**, 014026.

Anisovich, A. V., and V. V. Anisovich, 1995, Phys. Lett. B **345**, 321.

Anisovich, V. V., D. V. Bugg, A. V. Sarantsev, and B. S. Zou, 1995, Phys. Rev. D **51**, R4619.

Aoki, S., *et al.* (PACS-CS Collaboration), 2009, Phys. Rev. D **79**, 034503.

Aoki, S., *et al.* (CS Collaboration), 2011, Phys. Rev. D **84**, 094505.

Artoisenet, P., and E. Braaten, 2010, Phys. Rev. D **81**, 114018.

Artoisenet, P., and E. Braaten, 2011, Phys. Rev. D **83**, 014019.

Artoisenet, P., E. Braaten, and D. Kang, 2010, Phys. Rev. D **82**, 014013.

Au, K. L., D. Morgan, and M. R. Pennington, 1987, Phys. Rev. D **35**, 1633.

Aubert, B., *et al.* (*BABAR* Collaboration), 2003, Phys. Rev. Lett. **90**, 242001.

Aubert, B., *et al.* (*BABAR* Collaboration), 2005a, Phys. Rev. Lett. **95**, 142001.

Aubert, B., *et al.* (*BABAR* Collaboration), 2005b, Phys. Rev. D **71**, 031501.

Aubert, B., *et al.* (*BABAR* Collaboration), 2005c, Phys. Rev. D **71**, 071103.

Aubert, B., *et al.* (*BABAR* Collaboration), 2006a, Phys. Rev. Lett. **97**, 222001.

Aubert, B., *et al.* (*BABAR* Collaboration), 2006b, Phys. Rev. D **74**, 071101.

Aubert, B., *et al.* (*BABAR* Collaboration), 2006c, Phys. Rev. D **73**, 011101.

Aubert, B., *et al.* (*BABAR* Collaboration), 2007, Phys. Rev. Lett. **98**, 212001.

Aubert, B., *et al.* (*BABAR* Collaboration), 2008, Phys. Rev. D **77**, 111101.

Aushev, T., *et al.* (Belle Collaboration), 2010, Phys. Rev. D **81**, 031103.

Azizi, K., Y. Sarac, and H. Sundu, 2017, Phys. Rev. D **95**, 094016.

Bahr, M., *et al.*, 2008, Eur. Phys. J. C **58**, 639.

Bali, G. S., S. Collins, and C. Ehmann, 2011, Phys. Rev. D **84**, 094506.

Barnes, T., F. E. Close, and H. J. Lipkin, 2003, Phys. Rev. D **68**, 054006.

Barnes, T., F. E. Close, and E. S. Swanson, 1995, Phys. Rev. D **52**, 5242.

Barnes, T., S. Godfrey, and E. S. Swanson, 2005, Phys. Rev. D **72**, 054026.

Barnes, T., and E. S. Swanson, 2008, Phys. Rev. C **77**, 055206.

Baron, R., *et al.*, 2010, J. High Energy Phys. 06, 111.

Baru, V., E. Epelbaum, A. A. Filin, J. Gegelia, and A. V. Nefediev, 2015a, Phys. Rev. D **92**, 114016.

Baru, V., E. Epelbaum, A. A. Filin, F.-K. Guo, H.-W. Hammer, C. Hanhart, U.-G. Meißner, and A. V. Nefediev, 2015b, Phys. Rev. D **91**, 034002.

Baru, V., E. Epelbaum, A. A. Filin, C. Hanhart, U.-G. Meißner, and A. V. Nefediev, 2013, Phys. Lett. B **726**, 537.

Baru, V., E. Epelbaum, A. A. Filin, C. Hanhart, U.-G. Meißner, and A. V. Nefediev, 2016, Phys. Lett. B **763**, 20.

Baru, V., E. Epelbaum, A. A. Filin, C. Hanhart, and A. V. Nefediev, 2017, J. High Energy Phys. 06, 158.

Baru, V., A. A. Filin, C. Hanhart, Y. S. Kalashnikova, A. E. Kudryavtsev, and A. V. Nefediev, 2011, Phys. Rev. D **84**, 074029.

Baru, V., J. Haidenbauer, C. Hanhart, Y. Kalashnikova, and A. E. Kudryavtsev, 2004, Phys. Lett. B **586**, 53.

Baru, V., J. Haidenbauer, C. Hanhart, A. E. Kudryavtsev, and U.-G. Meißner, 2005, Eur. Phys. J. A **23**, 523.

Baru, V., C. Hanhart, Y. S. Kalashnikova, A. E. Kudryavtsev, and A. V. Nefediev, 2010, Eur. Phys. J. A **44**, 93.

Bauer, G., *et al.* (CDF Collaboration), 2005, Int. J. Mod. Phys. A **20**, 3765.

Bayar, M., F. Aceti, F.-K. Guo, and E. Oset, 2016, Phys. Rev. D **94**, 074039.

Bazzi, M., *et al.* (SIDDHARTA Collaboration), 2011, Phys. Lett. B **704**, 113.

Bazzi, M., *et al.*, 2012, Nucl. Phys. A **881**, 88.

Beane, S. R., P. F. Bedaque, A. Parreno, and M. J. Savage, 2005, Nucl. Phys. A **747**, 55.

Beane, S. R., E. Chang, S. D. Cohen, W. Detmold, H. W. Lin, T. C. Luu, K. Orginos, A. Parreno, M. J. Savage, and A. Walker-Loud (NPLQCD Collaboration), 2013, Phys. Rev. D **87**, 034506.

Berkowitz, E., T. Kurth, A. Nicholson, B. Joo, E. Rinaldi, M. Strother, P. M. Vranas, and A. Walker-Loud, 2017, Phys. Lett. B **765**, 285.

Bernard, V., D. Hoja, U.-G. Meißner, and A. Rusetsky, **2012**, J. High Energy Phys. 09, 023.

Bernard, V., M. Lage, U.-G. Meißner, and A. Rusetsky, 2008, J. High Energy Phys. 08, 024.

Bernard, V., M. Lage, U.-G. Meißner, and A. Rusetsky, 2011, J. High Energy Phys. 01, 019.

Besson, D., *et al.* (CLEO Collaboration), 2003, Phys. Rev. D **68**, 032002; **75**, 119908(E) (2007).

Bhardwaj, V., *et al.* (Belle Collaboration), 2011, Phys. Rev. Lett. **107**, 091803.

Bietenholz, W., *et al.*, 2011, Phys. Rev. D **84**, 054509.

Bignamini, C., B. Grinstein, F. Piccinini, A. D. Polosa, V. Riquer, and C. Sabelli, 2010, Phys. Lett. B **684**, 228.

Bignamini, C., B. Grinstein, F. Piccinini, A. D. Polosa, and C. Sabelli, 2009, Phys. Rev. Lett. **103**, 162001.

Blechman, A. E., A. F. Falk, D. Pirjol, and J. M. Yelton, 2003, Phys. Rev. D **67**, 074033.

Bondar, A., *et al.* (Belle Collaboration), 2012, Phys. Rev. Lett. **108**, 122001.

Bondar, A. E., A. Garmash, A. I. Milstein, R. Mizuk, and M. B. Voloshin, 2011, Phys. Rev. D **84**, 054010.

Bondar, A. E., R. V. Mizuk, and M. B. Voloshin, 2017, Mod. Phys. Lett. A **32**, 1750025.

Bondar, A. E., and M. B. Voloshin, 2016, Phys. Rev. D **93**, 094008.

Borasoy, B., U.-G. Meißner, and R. Nißler, 2006, Phys. Rev. C **74**, 055201.

Bour, S., S. Koenig, D. Lee, H.-W. Hammer, and U.-G. Meißner, 2011, Phys. Rev. D **84**, 091503.

Braaten, E., 2015, Phys. Rev. D **91**, 114007.

Braaten, E., and H.-W. Hammer, 2006, Phys. Rep. **428**, 259.

Braaten, E., H.-W. Hammer, and T. Mehen, 2010, Phys. Rev. D **82**, 034018.

Braaten, E., and M. Kusunoki, 2005a, Phys. Rev. D **71**, 074005.

Braaten, E., and M. Kusunoki, 2005b, Phys. Rev. D **72**, 014012.

Braaten, E., M. Kusunoki, and S. Nussinov, 2004, Phys. Rev. Lett. **93**, 162001.

Braaten, E., and M. Lu, 2006, Phys. Rev. D **74**, 054020.

Braaten, E., and M. Lu, 2007, Phys. Rev. D **76**, 094028.

Braaten, E., and J. Stapleton, 2010, Phys. Rev. D **81**, 014019.

Brambilla, N., *et al.*, 2011, Eur. Phys. J. C **71**, 1534.

Brambilla, N., *et al.*, 2014, Eur. Phys. J. C **74**, 2981.

Briceño, R. A., and Z. Davoudi, 2013a, Phys. Rev. D **88**, 094507.

Briceño, R. A., and Z. Davoudi, 2013b, Phys. Rev. D **87**, 094507.

Briceño, R. A., Z. Davoudi, T. C. Luu, and M. J. Savage, 2014, Phys. Rev. D **89**, 074509.

Briceño, R. A., J. J. Dudek, R. G. Edwards, C. J. Shultz, C. E. Thomas, and D. J. Wilson, 2015, Phys. Rev. Lett. **115**, 242001.

Briceño, R. A., J. J. Dudek, R. G. Edwards, C. J. Shultz, C. E. Thomas, and D. J. Wilson, 2016, Phys. Rev. D **93**, 114508.

Briceño, R. A., J. J. Dudek, R. G. Edwards, and D. J. Wilson, 2017, Phys. Rev. Lett. **118**, 022002.

Briceño, R. A., and M. T. Hansen, 2015, Phys. Rev. D **92**, 074509.

Briceño, R. A., and M. T. Hansen, 2016, Phys. Rev. D **94**, 013008.

Brodsky, S. J., and R. F. Lebed, 2015, Phys. Rev. D **91**, 114025.

Brodsky, S. J., R. F. Lebed, and V. E. Lyubovitskij, 2017, Phys. Lett. B **764**, 174.

Bronzan, J. B., 1964, Phys. Rev. **134**, B687.

Bruns, P. C., M. Mai, and U.-G. Meißner, 2011, Phys. Lett. B **697**, 254.

Bugg, D. V., 2004, Phys. Lett. B **598**, 8.

Bugg, D. V., 2011, Europhys. Lett. **96**, 11002.

Burdman, G., and J. F. Donoghue, 1992, Phys. Lett. B **280**, 287.

Burns, T. J., and E. S. Swanson, 2016, Phys. Lett. B **760**, 627.

Butenschoen, M., Z.-G. He, and B. A. Kniehl, 2013, Phys. Rev. D **88**, 011501.

Canham, D. L., H.-W. Hammer, and R. P. Springer, 2009, Phys. Rev. D **80**, 014009.

Cao, Z., M. Cleven, Q. Wang, and Q. Zhao, 2016, Eur. Phys. J. C **76**, 601.

Chang, T. S., 1983, written in 1965, *Introduction to Dispersion Relation, Vol. II* (in Chinese) (Science Press, Beijing).

Chang, W.-C., S. Kumano, and T. Sekihara, 2016, Phys. Rev. D **93**, 034006.

Chatrchyan, S., *et al.* (CMS Collaboration), **2013**a, J. High Energy Phys. 04, 154.

Chatrchyan, S., *et al.* (CMS Collaboration), 2013b, Phys. Lett. B **727**, 57.

Chen, B., X. Liu, and A. Zhang, 2017, Phys. Rev. D **95**, 074022.

Chen, B., K.-W. Wei, X. Liu, and T. Matsuki, 2017, Eur. Phys. J. C **77**, 154.

Chen, D.-Y., and X. Liu, 2011, Phys. Rev. D **84**, 094003.

Chen, D.-Y., X. Liu, and T. Matsuki, 2013, Phys. Rev. D **88**, 036008.

Chen, G.-Y., W.-S. Huo, and Q. Zhao, 2015, Chin. Phys. C **39**, 093101.

Chen, G.-Y., and Q. Zhao, 2013, Phys. Lett. B **718**, 1369.

Chen, H.-X., W. Chen, X. Liu, Y.-R. Liu, and S.-L. Zhu, 2017, Rep. Prog. Phys. **80**, 076201.

Chen, H.-X., W. Chen, X. Liu, T. G. Steele, and S.-L. Zhu, 2015, Phys. Rev. Lett. **115**, 172001.

Chen, H.-X., W. Chen, X. Liu, and S.-L. Zhu, 2016, Phys. Rep. **639**, 1.

Chen, H.-X., E.-L. Cui, W. Chen, X. Liu, T. G. Steele, and S.-L. Zhu, 2016, Eur. Phys. J. C **76**, 572.

Chen, H.-X., L. Maiani, A. D. Polosa, and V. Riquer, 2015, Eur. Phys. J. C **75**, 550.

Chen, H.-X., Q. Mao, A. Hosaka, X. Liu, and S.-L. Zhu, 2016, Phys. Rev. D **94**, 114016.

Chen, R., X. Liu, X.-Q. Li, and S.-L. Zhu, 2015, Phys. Rev. Lett. **115**, 132002.

Chen, R., X. Liu, and S.-L. Zhu, 2016, Nucl. Phys. A **954**, 406.

Chen, T., *et al.* (CLQCD Collaboration), 2016e, Phys. Rev. D **93**, 114501.

Chen, W., T. G. Steele, H.-X. Chen, and S.-L. Zhu, 2015, Phys. Rev. D **92**, 054002.

Chen, Y., *et al.*, 2014, Phys. Rev. D **89**, 094506.

Chen, Y., *et al.* (CLQCD Collaboration), 2015, Phys. Rev. D **92**, 054507.

Chen, Y.-H., M. Cleven, J. T. Daub, F.-K. Guo, C. Hanhart, B. Kubis, U.-G. Meißner, and B.-S. Zou, 2017, Phys. Rev. D **95**, 034022.

Chen, Y.-H., J. T. Daub, F.-K. Guo, B. Kubis, U.-G. Meißner, and B.-S. Zou, 2016, Phys. Rev. D **93**, 034030.

Cheng, C., J.-J. Xie, and X. Cao, 2016, Commun. Theor. Phys. **66**, 675.

Cheng, H.-Y., and C.-K. Chua, 2007, Phys. Rev. D **75**, 014006.

Cheng, H.-Y., and C.-K. Chua, 2015, Phys. Rev. D **92**, 074014.

Chilikin, K., *et al.* (Belle Collaboration), 2013, Phys. Rev. D **88**, 074026.

Chiu, T.-W., and T.-H. Hsieh (TWQCD Collaboration), 2007, Phys. Lett. B **646**, 95.

Cho, S., and S. H. Lee, 2013, Phys. Rev. C **88**, 054901.

Cho, S., T. Song, and S. H. Lee, 2015, arXiv:1511.08019.

Cho, S., *et al.* (ExHIC Collaboration), 2011a, Phys. Rev. Lett. **106**, 212001.

Cho, S., *et al.* (ExHIC Collaboration), 2011b, Phys. Rev. C **84**, 064910.

Choi, S. K., *et al.* (Belle Collaboration), 2003, Phys. Rev. Lett. **91**, 262001.

Choi, S. K., *et al.* (Belle Collaboration), 2015, Phys. Rev. D **91**, 092011; **92**, 039905(E) (2015).

Ciborowski, J., *et al.*, 1982, J. Phys. G **8**, 13.

Cieplý, A., M. Mai, U.-G. Meißner, and J. Smejkal, 2016, Nucl. Phys. A **954**, 17.

Cincioglu, E., J. Nieves, A. Ozpineci, and A. U. Yilmazer, 2016, Eur. Phys. J. C **76**, 576.

Cleven, M., H. W. Grießhammer, F.-K. Guo, C. Hanhart, and U.-G. Meißner, 2014, Eur. Phys. J. A **50**, 149.

Cleven, M., F.-K. Guo, C. Hanhart, and U.-G. Meißner, 2011a, Eur. Phys. J. A **47**, 120.

Cleven, M., F.-K. Guo, C. Hanhart, and U.-G. Meißner, 2011b, Eur. Phys. J. A **47**, 19.

Cleven, M., F.-K. Guo, C. Hanhart, Q. Wang, and Q. Zhao, 2015, Phys. Rev. D **92**, 014005.

Cleven, M., Q. Wang, F.-K. Guo, C. Hanhart, U.-G. Meißner, and Q. Zhao, 2013, Phys. Rev. D **87**, 074006.

Cleven, M., Q. Wang, F.-K. Guo, C. Hanhart, U.-G. Meißner, and Q. Zhao, 2014, Phys. Rev. D **90**, 074039.

Cleven, M., and Q. Zhao, 2017, Phys. Lett. B **768**, 52.

Close, F. E., and P. R. Page, 2004, Phys. Lett. B **578**, 119.

Close, F. E., and P. R. Page, 2005, Phys. Lett. B **628**, 215.

Close, F. E., and E. S. Swanson, 2005, Phys. Rev. D **72**, 094004.

Colangelo, G., J. Gasser, B. Kubis, and A. Rusetsky, 2006, Phys. Lett. B **638**, 187.

Colangelo, G., J. Gasser, and H. Leutwyler, 2001, Phys. Rev. Lett. **86**, 5008.

Colangelo, P., and F. De Fazio, 2003, Phys. Lett. B **570**, 180.

Coleman, S., and R. E. Norton, 1965, Nuovo Cimento **38**, 438.

Copley, L. A., N. Isgur, and G. Karl, 1979, Phys. Rev. D **20**, 768; **23**, 817(E) (1981).

Cotugno, G., R. Faccini, A. D. Polosa, and C. Sabelli, 2010, Phys. Rev. Lett. **104**, 132005.

Cui, C.-Y., Y.-L. Liu, W.-B. Chen, and M.-Q. Huang, 2014, J. Phys. G **41**, 075003.

Dalitz, R. H., and S. F. Tuan, 1959, Phys. Rev. Lett. **2**, 425.

Dalitz, R. H., and S. F. Tuan, 1960, Ann. Phys. (N.Y.) **10**, 307.

Danilkin, I. V., V. D. Orlovsky, and Yu. A. Simonov, 2012, Phys. Rev. D **85**, 034012.

Danilkin, I. V., and Y. A. Simonov, 2010a, Phys. Rev. Lett. **105**, 102002.

Danilkin, I. V., and Yu. A. Simonov, 2010b, Phys. Rev. D **81**, 074027.

Davoudi, Z., and M. J. Savage, 2011, Phys. Rev. D **84**, 114502.

Debastiani, V. R., F. Aceti, W.-H. Liang, and E. Oset, 2017, Phys. Rev. D **95**, 034015.

Debastiani, V. R., S. Sakai, and E. Oset, 2017, Phys. Rev. C **96**, 025201.

DeGrand, T. A., 1991, Phys. Rev. D **43**, 2296.

del Amo Sanchez, P., *et al.* (*BABAR* Collaboration), 2010, Phys. Rev. D **82**, 011101.

De Rujula, A., H. Georgi, and S. L. Glashow, 1977, Phys. Rev. Lett. **38**, 317.

Dias, J. M., F. Aceti, and E. Oset, 2015, Phys. Rev. D **91**, 076001.

Ding, G.-J., 2009, Phys. Rev. D **79**, 014001.

Ding, G.-J., J.-F. Liu, and M.-L. Yan, 2009, Phys. Rev. D **79**, 054005.

Di Pierro, M., and E. Eichten, 2001, Phys. Rev. D **64**, 114004.

Dong, Y., A. Faessler, T. Gutsche, S. Kovalenko, and V. E. Lyubovitskij, 2009, Phys. Rev. D **79**, 094013.

Dong, Y., A. Faessler, T. Gutsche, and V. E. Lyubovitskij, 2013a, J. Phys. G **40**, 015002.

Dong, Y., A. Faessler, T. Gutsche, and V. E. Lyubovitskij, 2013b, Phys. Rev. D **88**, 014030.

Dong, Y., A. Faessler, and V. E. Lyubovitskij, 2017, Prog. Part. Nucl. Phys. **94**, 282.

Döring, M., J. Haidenbauer, U.-G. Meißner, and A. Rusetsky, 2011, Eur. Phys. J. A **47**, 163.

Döring, M., C. Hanhart, F. Huang, S. Krewald, and U.-G. Meißner, 2009, Nucl. Phys. A **829**, 170.

Döring, M., B. Hu, and M. Mai, 2016, arXiv:1610.10070.

Döring, M., M. Mai, and U.-G. Meißner, 2013, Phys. Lett. B **722**, 185.

Döring, M., and U.-G. Meißner, **2012**, J. High Energy Phys. 01 009.

Döring, M., U.-G. Meißner, E. Oset, and A. Rusetsky, 2011, Eur. Phys. J. A **47**, 139.

Döring, M., U.-G. Meißner, E. Oset, and A. Rusetsky, 2012, Eur. Phys. J. A **48**, 114.

Du, M.-L., U.-G. Meißner, and Q. Wang, 2016, Phys. Rev. D **94**, 096006.

Dubynskiy, S., and M. B. Voloshin, 2008, Phys. Lett. B **666**, 344.

Dudek, J. J., R. Edwards, and C. E. Thomas, 2009, Phys. Rev. D **79**, 094504.

Dudek, J. J., R. G. Edwards, and D. G. Richards, 2006, Phys. Rev. D **73**, 074507.

Dudek, J. J., R. G. Edwards, and C. E. Thomas (Hadron Spectrum), 2013, Phys. Rev. D **87**, 034505; **90**, 099902(E) (2014).

Dudek, J. J., R. G. Edwards, and D. J. Wilson (Hadron Spectrum), 2016, Phys. Rev. D **93**, 094506.

Dürr, S., *et al.*, 2008, Science **322**, 1224.

Eden, R. J., P. V. Landshoff, D. I. Olive, and J. C. Polkinghorne, 1966, *The Analytic S-Matrix* (Cambridge University Press, Cambridge).

Edwards, R. G., J. J. Dudek, D. G. Richards, and S. J. Wallace, 2011, Phys. Rev. D **84**, 074508.

Eichten, E., S. Godfrey, H. Mahlke, and J. L. Rosner, 2008, Rev. Mod. Phys. **80**, 1161.

Eichten, E., K. Gottfried, T. Kinoshita, K. D. Lane, and T.-M. Yan, 1978, Phys. Rev. D **17**, 3090; **21**, 313(E) (1980).

Eichten, E., K. Gottfried, T. Kinoshita, K. D. Lane, and T.-M. Yan, 1980, Phys. Rev. D **21**, 203.

Eichten, E. J., K. Lane, and C. Quigg, 2006, Phys. Rev. D **73**, 014014; **73**, 079903(E) (2006).

Epelbaum, E., H.-W. Hammer, and U.-G. Meißner, 2009, Rev. Mod. Phys. **81**, 1773.

Esposito, A., A. L. Guerrieri, L. Maiani, F. Piccinini, A. Pilloni, A. D. Polosa, and V. Riquer, 2015, Phys. Rev. D **92**, 034028.

Esposito, A., A. L. Guerrieri, F. Piccinini, A. Pilloni, and A. D. Polosa, 2015, Int. J. Mod. Phys. A **30**, 1530002.

Esposito, A., A. L. Guerrieri, and A. Pilloni, 2015, Phys. Lett. B **746**, 194.

Esposito, A., F. Piccinini, A. Pilloni, and A. D. Polosa, 2013, J. Mod. Phys. **04**, 1569.

Esposito, A., A. Pilloni, and A. D. Polosa, 2016, Phys. Lett. B **758**, 292.

Esposito, A., A. Pilloni, and A. D. Polosa, 2017, Phys. Rep. **668**, 1.

Faessler, A., T. Gutsche, V. E. Lyubovitskij, and Y.-L. Ma, 2007, Phys. Rev. D **76**, 014005.

Fan, Y., J.-Z. Li, C. Meng, and K.-T. Chao, 2012, Phys. Rev. D **85**, 034032.

Fayyazuddin,, and O. H. Mobarek, 1994, Phys. Rev. D **50**, 2329.

Feijoo, A., V. K. Magas, A. Ramos, and E. Oset, 2015, Phys. Rev. D **92**, 076015; **95**, 039905(E) (2017).

Feijoo, A., V. K. Magas, A. Ramos, and E. Oset, 2016, Eur. Phys. J. C **76**, 446.

Feng, X., S. Aoki, S. Hashimoto, and T. Kaneko, 2015, Phys. Rev. D **91**, 054504.

Feng, X., K. Jansen, and D. B. Renner, 2011, Phys. Rev. D **83**, 094505.

Fernández-Caramés, T., A. Valcarce, and J. Vijande, 2009, Phys. Rev. Lett. **103**, 222001.

Ferretti, J., G. Galatà, and E. Santopinto, 2013, Phys. Rev. C **88**, 015207.

Ferretti, J., G. Galatà, and E. Santopinto, 2014, Phys. Rev. D **90**, 054010.

Ferretti, J., and E. Santopinto, 2014, Phys. Rev. D **90**, 094022.

Filin, A. A., A. Romanov, V. Baru, C. Hanhart, Y. S. Kalashnikova, A. E. Kudryavtsev, U.-G. Meißner, and A. V. Nefediev, 2010, Phys. Rev. Lett. **105**, 019101.

Flatté, S. M., 1976, Phys. Lett. B **63**, 224.

Fleming, S., M. Kusunoki, T. Mehen, and U. van Kolck, 2007, Phys. Rev. D **76**, 034006.

Fleming, S., and T. Mehen, 2008, Phys. Rev. D **78**, 094019.

Fleming, S., and T. Mehen, 2012, Phys. Rev. D **85**, 014016.

Flynn, J. M., P. Fritzsch, T. Kawanai, C. Lehner, B. Samways, C. T. Sachrajda, R. S. Van de Water, and O. Witzel (RBC, UKQCD Collaborations), 2016, Phys. Rev. D **93**, 014510.

Flynn, J. M., and J. Nieves, 2007, Phys. Rev. D **75**, 074024.

Fu, Z., 2012, Phys. Rev. D **85**, 014506.

Gamermann, D., J. Nieves, E. Oset, and E. Ruiz Arriola, 2010, Phys. Rev. D **81**, 014029.

Gamermann, D., and E. Oset, 2009, Phys. Rev. D **80**, 014003.

Gamermann, D., E. Oset, D. Strottman, and M. J. Vicente Vacas, 2007, Phys. Rev. D **76**, 074016.

Gao, X. Y., C. P. Shen, and C. Z. Yuan, 2017, Phys. Rev. D **95**, 092007.

Garcia-Recio, C., C. Hidalgo-Duque, J. Nieves, L. L. Salcedo, and L. Tolos, 2015, Phys. Rev. D **92**, 034011.

Garcia-Recio, C., M. F. M. Lutz, and J. Nieves, 2004, Phys. Lett. B **582**, 49.

Garcia-Recio, C., V. K. Magas, T. Mizutani, J. Nieves, A. Ramos, L. L. Salcedo, and L. Tolos, 2009, Phys. Rev. D **79**, 054004.

Garmash, A., *et al.* (Belle Collaboration), 2015, Phys. Rev. D **91**, 072003.

Garmash, A., *et al.* (Belle Collaboration), 2016, Phys. Rev. Lett. **116**, 212001.

Garzon, E. J., R. Molina, A. Hosaka, and E. Oset, 2014, Phys. Rev. D **89**, 014504.

Gasser, J., B. Kubis, and A. Rusetsky, 2011, Nucl. Phys. B **850**, 96.

Gell-Mann, M., 1964, Phys. Lett. **8**, 214.

Gell-Mann, M., R. J. Oakes, and B. Renner, 1968, Phys. Rev. **175**, 2195.

Geng, L., J. Lu, and M. P. Valderrama, 2017, arXiv:1704.06123.

Geng, L. S., and E. Oset, 2009, Phys. Rev. D **79**, 074009.

Göckeler, M., R. Horsley, M. Lage, U.-G. Meißner, P. E. L. Rakow, A. Rusetsky, G. Schierholz, and J. M. Zanotti, 2012, Phys. Rev. D **86**, 094513.

Godfrey, S., 2003, Phys. Lett. B **568**, 254.

Godfrey, S., 2005, Phys. Rev. D **72**, 054029.

Godfrey, S., and N. Isgur, 1985, Phys. Rev. D **32**, 189.

Godfrey, S., and K. Moats, 2015, Phys. Rev. D **92**, 054034.

Goebel, C. J., S. F. Tuan, and W. A. Simmons, 1983, Phys. Rev. D **27**, 1069.

Gokhroo, G., *et al.* (Belle Collaboration), 2006, Phys. Rev. Lett. **97**, 162002.

Gomez Nicola, A., and J. R. Peláez, 2002, Phys. Rev. D **65**, 054009.

Gong, Q.-R., Z.-H. Guo, C. Meng, G.-Y. Tang, Y.-F. Wang, and H.-Q. Zheng, 2016, Phys. Rev. D **94**, 114019.

Gong, Q.-R., J.-L. Pang, Y.-F. Wang, and H.-Q. Zheng, 2016, arXiv:1612.08159.

Gribov, V. N., Y. Dokshitzer, and J. Nyiri, 2009, *Strong Interactions of Hadrons at High Energies—Gribov Lectures on Theoretical Physics* (Cambridge University Press, Cambridge).

Gryniuk, O., and M. Vanderhaeghen, 2016, Phys. Rev. D **94**, 074001.

Guerrieri, A. L., F. Piccinini, A. Pilloni, and A. D. Polosa, 2014, Phys. Rev. D **90**, 034003.

Gülmez, D., U.-G. Meißner, and J. A. Oller, 2017, Eur. Phys. J. C **77**, 460.

Guo, F.-K., J. Haidenbauer, C. Hanhart, and U.-G. Meißner, 2010, Phys. Rev. D **82**, 094008.

Guo, F.-K., C. Hanhart, Y. S. Kalashnikova, P. Matuschek, R. V. Mizuk, A. V. Nefediev, Q. Wang, and J. L. Wynen, 2016, Phys. Rev. D **93**, 074031.

Guo, F.-K., C. Hanhart, Y. S. Kalashnikova, U.-G. Meißner, and A. V. Nefediev, 2015, Phys. Lett. B **742**, 394.

Guo, F.-K., C. Hanhart, S. Krewald, and U.-G. Meißner, 2008, Phys. Lett. B **666**, 251.

Guo, F.-K., C. Hanhart, G. Li, U.-G. Meißner, and Q. Zhao, 2010, Phys. Rev. D **82**, 034025.

Guo, F.-K., C. Hanhart, G. Li, U.-G. Meißner, and Q. Zhao, 2011, Phys. Rev. D **83**, 034013.

Guo, F.-K., C. Hanhart, and U.-G. Meißner, 2008, Phys. Lett. B **665**, 26.

Guo, F.-K., C. Hanhart, and U.-G. Meißner, 2009a, Phys. Rev. Lett. **102**, 242004.

Guo, F.-K., C. Hanhart, and U.-G. Meißner, 2009b, Eur. Phys. J. A **40**, 171.

Guo, F.-K., C. Hanhart, and U.-G. Meißner, 2009c, Phys. Rev. Lett. **103**, 082003.

Guo, F.-K., C. Hanhart, and U.-G. Meißner, 2010, Phys. Rev. Lett. **105**, 162001; **104**, 109901(E) (2010).

Guo, F.-K., C. Hanhart, U.-G. Meißner, Q. Wang, and Q. Zhao, 2013, Phys. Lett. B **725**, 127.

Guo, F.-K., C. Hanhart, Q. Wang, and Q. Zhao, 2015, Phys. Rev. D **91**, 051504.

Guo, F.-K., C. Hidalgo-Duque, J. Nieves, A. Ozpineci, and M. P. Valderrama, 2014, Eur. Phys. J. C **74**, 2885.

Guo, F.-K., C. Hidalgo-Duque, J. Nieves, and M. P. Valderrama, 2013a, Phys. Rev. D **88**, 054007.

Guo, F.-K., C. Hidalgo-Duque, J. Nieves, and M. P. Valderrama, 2013b, Phys. Rev. D **88**, 054014.

Guo, F.-K., and U.-G. Meißner, 2011, Phys. Rev. D **84**, 014013.

Guo, F.-K., and U.-G. Meißner, 2012a, Phys. Rev. Lett. **108**, 112002.

Guo, F.-K., and U.-G. Meißner, 2012b, Phys. Rev. Lett. **109**, 062001.

Guo, F.-K., U.-G. Meißner, J. Nieves, and Z. Yang, 2016, Eur. Phys. J. A **52**, 318.

Guo, F.-K., U.-G. Meißner, and C.-P. Shen, 2014, Phys. Lett. B **738**, 172.

Guo, F.-K., U.-G. Meißner, and W. Wang, 2014, Commun. Theor. Phys. **61**, 354.

Guo, F.-K., U.-G. Meißner, and W. Wang, 2017, Chin. Phys. C **41**, 053108.

Guo, F.-K., U.-G. Meißner, W. Wang, and Z. Yang, **2014**a, J. High Energy Phys. 05 138.

Guo, F.-K., U.-G. Meißner, W. Wang, and Z. Yang, 2014b, Eur. Phys. J. C **74**, 3063.

Guo, F.-K., U.-G. Meißner, W. Wang, and Z. Yang, 2015, Phys. Rev. D **92**, 071502.

Guo, F.-K., U.-G. Meißner, and Z. Yang, 2015, Phys. Lett. B **740**, 42.

Guo, F.-K., U.-G. Meißner, and Z. Yang, 2016, Phys. Lett. B **760**, 417.

Guo, F.-K., U.-G. Meißner, and B.-S. Zou, 2016, Commun. Theor. Phys. **65**, 593.

Guo, F.-K., P.-N. Shen, and H.-C. Chiang, 2007, Phys. Lett. B **647**, 133.

Guo, F.-K., P.-N. Shen, H.-C. Chiang, R.-G. Ping, and B.-S. Zou, 2006, Phys. Lett. B **641**, 278.

Guo, P., J. Dudek, R. Edwards, and A. P. Szczepaniak, 2013, Phys. Rev. D **88**, 014501.

Guo, P., and V. Gasparian, 2017, Phys. Lett. B **774**, 441.

Guo, Z.-H., L. Liu, U.-G. Meißner, J. A. Oller, and A. Rusetsky, 2017, Phys. Rev. D **95**, 054004.

Guo, Z.-H., U.-G. Meißner, and D.-L. Yao, 2015, Phys. Rev. D **92**, 094008.

Guo, Z.-H., and J. A. Oller, 2011, Phys. Rev. D **84**, 034005.

Guo, Z.-H., and J. A. Oller, 2013, Phys. Rev. C **87**, 035202.

Guo, Z.-H., and J. A. Oller, 2016a, Phys. Rev. D **93**, 096001.

Guo, Z.-H., and J. A. Oller, 2016b, Phys. Rev. D **93**, 054014.

Guo, Z.-k., S. Narison, J.-M. Richard, and Q. Zhao, 2012, Phys. Rev. D **85**, 114007.

Haidenbauer, J., G. Krein, U.-G. Meißner, and L. Tolos, 2011, Eur. Phys. J. A **47**, 18.

Hall, J. M. M., W. Kamleh, D. B. Leinweber, B. J. Menadue, B. J. Owen, A. W. Thomas, and R. D. Young, 2015, Phys. Rev. Lett. **114**, 132002.

Hammer, I. K., C. Hanhart, and A. V. Nefediev, 2016, Eur. Phys. J. A **52**, 330.

Hanhart, C., Y. S. Kalashnikova, A. E. Kudryavtsev, and A. V. Nefediev, 2007a, Phys. Rev. D **76**, 034007.

Hanhart, C., Y. S. Kalashnikova, A. E. Kudryavtsev, and A. V. Nefediev, 2007b, Phys. Rev. D **75**, 074015.

Hanhart, C., Y. S. Kalashnikova, P. Matuschek, R. V. Mizuk, A. V. Nefediev, and Q. Wang, 2015, Phys. Rev. Lett. **115**, 202001.

Hanhart, C., Y. S. Kalashnikova, and A. V. Nefediev, 2010, Phys. Rev. D **81**, 094028.

Hanhart, C., Y. S. Kalashnikova, and A. V. Nefediev, 2011, Eur. Phys. J. A **47**, 101.

Hanhart, C., B. Kubis, and J. R. Peláez, 2007, Phys. Rev. D **76**, 074028.

Hanhart, C., J. R. Peláez, and G. Ríos, 2008, Phys. Rev. Lett. **100**, 152001.

Hanhart, C., J. R. Peláez, and G. Ríos, 2014, Phys. Lett. B **739**, 375.

Hansen, M. T., and S. R. Sharpe, 2014, Phys. Rev. D **90**, 116003.

Hansen, M. T., and S. R. Sharpe, 2015, Phys. Rev. D **92**, 114509.

Hansen, M. T., and S. R. Sharpe, 2016a, Phys. Rev. D **93**, 014506.

Hansen, M. T., and S. R. Sharpe, 2016b, Phys. Rev. D **93**, 096006.

Hansen, M. T., and S. R. Sharpe, 2017, Phys. Rev. D **95**, 034501.

He, J., 2014, Phys. Rev. D **90**, 076008.

He, J., 2016, Phys. Lett. B **753**, 547.

He, J., X. Liu, Z.-F. Sun, and S.-L. Zhu, 2013, Eur. Phys. J. C **73**, 2635.

He, J., Y.-T. Ye, Z.-F. Sun, and X. Liu, 2010, Phys. Rev. D **82**, 114029.

He, Q., *et al.* (CLEO Collaboration), 2006, Phys. Rev. D **74**, 091104.

He, X.-G., X.-Q. Li, X. Liu, and X.-Q. Zeng, 2007, Eur. Phys. J. C **51**, 883.

Helminen, C., and D. O. Riska, 2002, Nucl. Phys. A **699**, 624.

Hemingway, R. J., 1985, Nucl. Phys. B **253**, 742.

Hidalgo-Duque, C., J. Nieves, A. Ozpineci, and V. Zamiralov, 2013, Phys. Lett. B **727**, 432.

Hidalgo-Duque, C., J. Nieves, and M. P. Valderrama, 2013, Phys. Rev. D **87**, 076006.

Hiller Blin, A. N., C. Fernández-Ramírez, A. Jackura, V. Mathieu, V. I. Mokeev, A. Pilloni, and A. P. Szczepaniak, 2016, Phys. Rev. D **94**, 034002.

Hofmann, J., and M. F. M. Lutz, 2004, Nucl. Phys. A **733**, 142.

Hofmann, J., and M. F. M. Lutz, 2005, Nucl. Phys. A **763**, 90.

Höhler, G., 1983, *Pion-Nucleon Scattering—Methods and Results of Phenomenological Analyses* (Springer-Verlag, Berlin).

Hosaka, A., T. Iijima, K. Miyabayashi, Y. Sakai, and S. Yasui, 2016, Prog. Theor. Exp. Phys. **2016**, 062C01.

Hu, B., R. Molina, M. Döring, and A. Alexandru, 2016, Phys. Rev. Lett. **117**, 122001.

Huang, F., W. L. Wang, Z. Y. Zhang, and Y. W. Yu, 2007, Phys. Rev. C **76**, 018201.

Huang, Y., J.-J. Xie, J. He, X. Chen, and H.-F. Zhang, 2016, Chin. Phys. C **40**, 124104.

Humphrey, W. E., and R. R. Ross, 1962, Phys. Rev. **127**, 1305.

Huo, W.-S., and G.-Y. Chen, 2016, Eur. Phys. J. C **76**, 172.

Hyodo, T., 2013a, Int. J. Mod. Phys. A **28**, 1330045.

Hyodo, T., 2013b, Phys. Rev. Lett. **111**, 132002.

Hyodo, T., and D. Jido, 2012, Prog. Part. Nucl. Phys. **67**, 55.

Hyodo, T., D. Jido, and A. Hosaka, 2012, Phys. Rev. C **85**, 015201.

Hyodo, T., S. I. Nam, D. Jido, and A. Hosaka, 2003, Phys. Rev. C **68**, 018201.

Ikeda, Y., S. Aoki, T. Doi, S. Gongyo, T. Hatsuda, T. Inoue, T. Iritani, N. Ishii, K. Murano, and K. Sasaki (HAL QCD Collaboration), 2016, Phys. Rev. Lett. **117**, 242001.

Ikeda, Y., T. Hyodo, and W. Weise, 2012, Nucl. Phys. A **881**, 98.

Inoue, T., E. Oset, and M. J. Vicente Vacas, 2002, Phys. Rev. C **65**, 035204.

Ioffe, B. L., 1979, Yad. Fiz. **29**, 1611.

Isgur, N., and M. B. Wise, 1989, Phys. Lett. B **232**, 113.

Jaffe, R. L., 1977a, Phys. Rev. D **15**, 267.

Jaffe, R. L., 1977b, Phys. Rev. D **15**, 281.

Jaffe, R. L., 2007, AIP Conf. Proc. **964**, 1.

Jansen, M., H.-W. Hammer, and Y. Jia, 2014, Phys. Rev. D **89**, 014033.

Jansen, M., H.-W. Hammer, and Y. Jia, 2015, Phys. Rev. D **92**, 114031.

Janssen, G., B. C. Pearce, K. Holinde, and J. Speth, 1995, Phys. Rev. D **52**, 2690.

Jido, D., J. A. Oller, E. Oset, A. Ramos, and U.-G. Meißner, 2003, Nucl. Phys. A **725**, 181.

Jimenez-Tejero, C. E., A. Ramos, L. Tolos, and I. Vidana, 2011, Phys. Rev. C **84**, 015208.

Jimenez-Tejero, C. E., A. Ramos, and I. Vidana, 2009, Phys. Rev. C **80**, 055206.

Kaiser, N., P. B. Siegel, and W. Weise, 1995, Nucl. Phys. A **594**, 325.

Kalashnikova, Y. S., and A. V. Nefediev, 2009, Phys. Rev. D **80**, 074004.

Kalashnikova, Y. S., and A. V. Nefediev, 2016, Phys. Rev. D **94**, 114007.

Kalashnikova, Yu. S., 2005, Phys. Rev. D **72**, 034010.

Kang, X.-W., Z.-H. Guo, and J. A. Oller, 2016, Phys. Rev. D **94**, 014012.

Kang, X.-W., and J. A. Oller, 2017, Eur. Phys. J. C **77**, 399.

Kaplan, D. B., M. J. Savage, and M. B. Wise, 1998a, Phys. Lett. B **424**, 390.

Kaplan, D. B., M. J. Savage, and M. B. Wise, 1998b, Nucl. Phys. B **534**, 329.

Karliner, M., and J. L. Rosner, 2015a, Phys. Rev. Lett. **115**, 122001.

Karliner, M., and J. L. Rosner, 2015b, Phys. Rev. D **91**, 014014.

Karliner, M., and J. L. Rosner, 2016, Phys. Lett. B **752**, 329.

Kawamura, H., and S. Kumano, 2014, Phys. Rev. D **89**, 054007.

Kawamura, H., S. Kumano, and T. Sekihara, 2013, Phys. Rev. D **88**, 034010.

Ke, H.-W., Z.-T. Wei, and X.-Q. Li, 2013, Eur. Phys. J. C **73**, 2561.

Kim, J. K., 1965, Phys. Rev. Lett. **14**, 29.

Kim, S.-H., H.-C. Kim, and A. Hosaka, 2016, Phys. Lett. B **763**, 358.

Klarsfeld, S., J. Martorell, and D. W. L. Sprung, 1984, J. Phys. G **10**, 165.

Klempt, E., and J.-M. Richard, 2010, Rev. Mod. Phys. **82**, 1095.

Klempt, E., and A. Zaitsev, 2007, Phys. Rep. **454**, 1.

Kolomeitsev, E. E., and M. F. M. Lutz, 2004, Phys. Lett. B **582**, 39.

König, S., D. Lee, and H.-W. Hammer, 2011, Phys. Rev. Lett. **107**, 112001.

König, S., D. Lee, and H.-W. Hammer, 2012, Ann. Phys. (N.Y.) **327**, 1450.

Körber, C., and T. Luu, 2016, Phys. Rev. C **93**, 054002.

Kou, E., and O. Pene, 2005, Phys. Lett. B **631**, 164.

Krehl, O., C. Hanhart, S. Krewald, and J. Speth, 2000, Phys. Rev. C **62**, 025207.

Kreuzer, S., and H.-W. Hammer, 2011, Phys. Lett. B **694**, 424.

Krokovny, P., *et al.* (Belle Collaboration), 2013, Phys. Rev. D **88**, 052016.

Kubarovsky, V., and M. B. Voloshin, 2015, Phys. Rev. D **92**, 031502.

Kubarovsky, V., and M. B. Voloshin, 2016, arXiv:1609.00050.

Lage, M., U.-G. Meißner, and A. Rusetsky, 2009, Phys. Lett. B **681**, 439.

Landau, L. D., 1959, Nucl. Phys. **13**, 181.

Lang, C. B., L. Leskovec, D. Mohler, S. Prelovsek, and R. M. Woloshyn, 2014, Phys. Rev. D **90**, 034510.

Lang, C. B., D. Mohler, S. Prelovsek, and M. Vidmar, 2011, Phys. Rev. D **84**, 054503; **89**, 059903(E) (2014).

Lang, C. B., D. Mohler, S. Prelovsek, and R. M. Woloshyn, 2015, Phys. Lett. B **750**, 17.

Larionov, A. B., M. Strikman, and M. Bleicher, 2015, Phys. Lett. B **749**, 35.

Lebed, R. F., 2015, Phys. Lett. B **749**, 454.

Lebed, R. F., R. E. Mitchell, and E. S. Swanson, 2017, Prog. Part. Nucl. Phys. **93**, 143.

Lee, I. W., A. Faessler, T. Gutsche, and V. E. Lyubovitskij, 2009, Phys. Rev. D **80**, 094005.

Lee, N., Z.-G. Luo, X.-L. Chen, and S.-L. Zhu, 2011, Phys. Rev. D **84**, 014031.

Lee, S.-h., C. DeTar, H. Na, and D. Mohler (Fermilab Lattice, MILC Collaborations), 2014, arXiv:1411.1389.

Lees, J. P., *et al.* (*BABAR* Collaboration), 2012, Phys. Rev. D **86**, 051102.

Lepage, G. P., 1990, in *From Actions to Answers: Proceedings of the 1989 Theoretical Advanced Study Institute in Elementary Particle Physics*, edited by T. DeGrand and D. Toussaint (World Scientific, Singapore), pp. 483–508.

Leskovec, L., C. Alexandrou, G. Koutsou, S. Meinel, J. W. Negele, S. Paul, M. Petschlies, A. Pochinsky, G. Rendon, and S. Syritsyn, 2016, *Proc. Sci.* LATTICE2016, 159.

Leskovec, L., and S. Prelovsek, 2012, Phys. Rev. D **85**, 114507.

Levinson, N., 1949, Phys. Rev. **75**, 1445.

Li, B.-Q., C. Meng, and K.-T. Chao, 2009, Phys. Rev. D **80**, 014012.

Li, G., 2013, Eur. Phys. J. C **73**, 2621.

Li, G., and X.-H. Liu, 2013, Phys. Rev. D **88**, 094008.

Li, G., X.-h. Liu, Q. Wang, and Q. Zhao, 2013, Phys. Rev. D **88**, 014010.

Li, G., F.-l. Shao, C.-W. Zhao, and Q. Zhao, 2013, Phys. Rev. D **87**, 034020.

Li, G., and W. Wang, 2014, Phys. Lett. B **733**, 100.

Li, G., and Q. Zhao, 2008, Phys. Lett. B **670**, 55.

Li, G., and Q. Zhao, 2011, Phys. Rev. D **84**, 074005.

Li, M. T., W. L. Wang, Y. B. Dong, and Z. Y. Zhang, 2012, Int. J. Mod. Phys. A **27**, 1250161.

Li, M.-T., W.-L. Wang, Y.-B. Dong, and Z.-Y. Zhang, 2013, arXiv:1303.4140.

Li, N., and C. Liu, 2013, Phys. Rev. D **87**, 014502.

Li, N., Z.-F. Sun, X. Liu, and S.-L. Zhu, 2013, Phys. Rev. D **88**, 114008.

Li, N., and S.-L. Zhu, 2012, Phys. Rev. D **86**, 074022.

Li, X., and M. B. Voloshin, 2013, Phys. Rev. D **88**, 034012.

Li, X., and M. B. Voloshin, 2014, Mod. Phys. Lett. A **29**, 1450060.

Liang, W. H., R. Molina, and E. Oset, 2010, Eur. Phys. J. A **44**, 479.

Liang, W. H., T. Uchino, C. W. Xiao, and E. Oset, 2015, Eur. Phys. J. A **51**, 16.

Lin, Y.-H., C.-W. Shen, F.-K. Guo, and B.-S. Zou, 2017, Phys. Rev. D **95**, 114017.

Lipkin, H. J., and S. F. Tuan, 1988, Phys. Lett. B **206**, 349.

Liu, B. C., and B. S. Zou, 2006, Phys. Rev. Lett. **96**, 042002.

Liu, C., 2017, *Proc. Sci.* LATTICE2016, 006.

Liu, C., X. Feng, and S. He, 2006, Int. J. Mod. Phys. A **21**, 847.

Liu, J.-F., and G.-J. Ding, 2012, Eur. Phys. J. C **72**, 1981.

Liu, L., G. Moir, M. Peardon, S. M. Ryan, C. E. Thomas, P. Vilaseca, J. J. Dudek, R. G. Edwards, B. Joo, and D. G. Richards (Hadron Spectrum Collaboration), **2012**, J. High Energy Phys. 07, 126.

Liu, L., K. Orginos, F.-K. Guo, C. Hanhart, and U.-G. Meißner, 2013, Phys. Rev. D **87**, 014508.

Liu, X., Z.-G. Luo, Y.-R. Liu, and S.-L. Zhu, 2009, Eur. Phys. J. C **61**, 411.

Liu, X., B. Zhang, and X.-Q. Li, 2009, Phys. Lett. B **675**, 441.

Liu, X.-H., 2014, Phys. Rev. D **90**, 074004.

Liu, X.-H., and G. Li, 2013, Phys. Rev. D **88**, 014013.

Liu, X.-H., and U.-G. Meißner, 2017, Eur. Phys. J. C **77**, 816.

Liu, X.-H., and M. Oka, 2016a, Phys. Rev. D **93**, 054032.

Liu, X.-H., and M. Oka, 2016b, Nucl. Phys. A **954**, 352.

Liu, X.-H., M. Oka, and Q. Zhao, 2016, Phys. Lett. B **753**, 297.

Liu, X.-H., Q. Wang, and Q. Zhao, 2016, Phys. Lett. B **757**, 231.

Liu, Y.-R., 2013, Phys. Rev. D **88**, 074008.

Liu, Y.-R., M. Oka, M. Takizawa, X. Liu, W.-Z. Deng, and S.-L. Zhu, 2010, Phys. Rev. D **82**, 014011.

Liu, Z. Q., X. S. Qin, and C. Z. Yuan, 2008, Phys. Rev. D **78**, 014032.

Liu, Z. Q., *et al.* (Belle Collaboration), 2013, Phys. Rev. Lett. **110**, 252002.

Long, B., 2016, arXiv:1609.08940.

Long, B., J. Wang, and S. Lyu, 2017, arXiv:1704.08935.

Longacre, R. S., 1990, Phys. Rev. D **42**, 874.

Lorenz, I. T., H.-W. Hammer, and U.-G. Meißner, 2015, Phys. Rev. D **92**, 034018.

Lu, J.-X., H.-X. Chen, Z.-H. Guo, J. Nieves, J.-J. Xie, and L.-S. Geng, 2016, Phys. Rev. D **93**, 114028.

Lu, J.-X., E. Wang, J.-J. Xie, L.-S. Geng, and E. Oset, 2016, Phys. Rev. D **93**, 094009.

Lu, J.-X., Y. Zhou, H.-X. Chen, J.-J. Xie, and L.-S. Geng, 2015, Phys. Rev. D **92**, 014036.

Lu, Y., M. N. Anwar, and B.-S. Zou, 2016, Phys. Rev. D **94**, 034021.

Lu, Y., M. N. Anwar, and B.-S. Zou, 2017, Phys. Rev. D **95**, 034018.

Lü, Q.-F., and Y.-B. Dong, 2016, Phys. Rev. D **93**, 074020.

Lü, Q.-F., X.-Y. Wang, J.-J. Xie, X.-R. Chen, and Y.-B. Dong, 2016, Phys. Rev. D **93**, 034009.

Lüscher, M., 1986, Commun. Math. Phys. **105**, 153.

Lüscher, M., 1991, Nucl. Phys. B **354**, 531.

Lutz, M. F. M., and E. E. Kolomeitsev, 2004a, Nucl. Phys. A **730**, 110.

Lutz, M. F. M., and E. E. Kolomeitsev, 2004b, Nucl. Phys. A **730**, 392.

Lutz, M. F. M., and M. Soyeur, 2008, Nucl. Phys. A **813**, 14.

Luu, T., and M. J. Savage, 2011, Phys. Rev. D **83**, 114508.

Ma, L., X.-H. Liu, X. Liu, and S.-L. Zhu, 2015, Phys. Rev. D **91**, 034032.

Ma, L., Z.-F. Sun, X.-H. Liu, W.-Z. Deng, X. Liu, and S.-L. Zhu, 2014, Phys. Rev. D **90**, 034020.

Magas, V. K., E. Oset, and A. Ramos, 2005, Phys. Rev. Lett. **95**, 052301.

Mai, M., and U.-G. Meißner, 2013, Nucl. Phys. A **900**, 51.

Mai, M., and U.-G. Meißner, 2015, Eur. Phys. J. A **51**, 30.

Maiani, L., F. Piccinini, A. D. Polosa, and V. Riquer, 2005, Phys. Rev. D **71**, 014028.

Margaryan, A., and R. P. Springer, 2013, Phys. Rev. D **88**, 014017.

Martínez Torres, A., L. R. Dai, C. Koren, D. Jido, and E. Oset, 2012, Phys. Rev. D **85**, 014027.

Martínez Torres, A., K. P. Khemchandani, F. S. Navarra, M. Nielsen, and L. M. Abreu, 2014, Phys. Rev. D **90**, 114023; **93**, 059902(E) (2016).

Martínez Torres, A., E. Oset, S. Prelovsek, and A. Ramos, **2015**, J. High Energy Phys. 05, 153.

McNeile, C., 2011, "Charmonium spectroscopy on $n_f = 2 + 1$ isotropic lattices," Talk given at the 8th International Workshop on Heavy Quarkonium, Darmstadt, Germany.

Mehen, T., 2015, Phys. Rev. D **92**, 034019.

Mehen, T., and J. Powell, 2013, Phys. Rev. D **88**, 034017.

Mehen, T., and J. W. Powell, 2011, Phys. Rev. D **84**, 114013.

Mehen, T., and R. Springer, 2011, Phys. Rev. D **83**, 094009.

Mehen, T., and D.-L. Yang, 2012, Phys. Rev. D **85**, 014002.

Meißner, U.-G., 1991, Comments Nucl. Part. Phys. **20**, 119.

Meißner, U.-G., and J. A. Oller, 2015, Phys. Lett. B **751**, 59.

Meißner, U.-G., G. Ríos, and A. Rusetsky, 2015, Phys. Rev. Lett. **114**, 091602; **117**, 069902(E) (2016).

Meng, C., and K.-T. Chao, 2007, Phys. Rev. D **75**, 114002.

Meng, C., and K.-T. Chao, 2008a, Phys. Rev. D **77**, 074003.

Meng, C., and K.-T. Chao, 2008b, Phys. Rev. D **78**, 074001.

Meng, C., Y.-J. Gao, and K.-T. Chao, 2013, Phys. Rev. D **87**, 074035.

Meng, C., H. Han, and K.-T. Chao, 2017, Phys. Rev. D **96**, 074014.

Meng, C., J. J. Sanz-Cillero, M. Shi, D.-L. Yao, and H.-Q. Zheng, 2015, Phys. Rev. D **92**, 034020.

Meng, G.-Z., *et al.* (CLQCD Collaboration), 2009, Phys. Rev. D **80**, 034503.

Meyer, H. B., 2011, Phys. Rev. Lett. **107**, 072002.

Migura, S., D. Merten, B. Metsch, and H.-R. Petry, 2006, Eur. Phys. J. A **28**, 41.

Mikhasenko, M., B. Ketzer, and A. Sarantsev, 2015, Phys. Rev. D **91**, 094015.

Mizuk, R., *et al.* (Belle Collaboration), 2009, Phys. Rev. D **80**, 031104.

Mizutani, T., and A. Ramos, 2006, Phys. Rev. C **74**, 065201.

Mohler, D., C. B. Lang, L. Leskovec, S. Prelovsek, and R. M. Woloshyn, 2013, Phys. Rev. Lett. **111**, 222001.

Mohler, D., S. Prelovsek, and R. M. Woloshyn, 2013, Phys. Rev. D **87**, 034501.

Moir, G., M. Peardon, S. M. Ryan, C. E. Thomas, and D. J. Wilson, **2016**, J. High Energy Phys. 10, 011.

Molina, R., and M. Döring, 2016, Phys. Rev. D **94**, 056010; **94**, 079901(E) (2016).

Molnar, D. A. S., R. F. Luiz, and R. Higa, 2016, arXiv:1601.03366.

Morgan, D., 1992, Nucl. Phys. A **543**, 632.

Morgan, D., and M. R. Pennington, 1993, Phys. Rev. D **48**, 1185.

Moriya, K., *et al.* (CLAS Collaboration), 2013, Phys. Rev. C **87**, 035206.

Moriya, K., *et al.* (CLAS Collaboration), 2014, Phys. Rev. Lett. **112**, 082004.

Moxhay, P., 1989, Phys. Rev. D **39**, 3497.

Nakamura, K., *et al.* (Particle Data Group), 2010, J. Phys. G **37**, 075021.

Nebreda, J., J. R. Peláez, and G. Ríos, 2011, Phys. Rev. D **84**, 074003.

Neubert, M., 1994, Phys. Rep. **245**, 259.

Nieves, J., and M. P. Valderrama, 2011, Phys. Rev. D **84**, 056015.

Nieves, J., and M. P. Valderrama, 2012, Phys. Rev. D **86**, 056004.

Nogga, A., and C. Hanhart, 2006, Phys. Lett. B **634**, 210.

Nowak, R. J., *et al.*, 1978, Nucl. Phys. B **139**, 61.

Ohkoda, S., Y. Yamaguchi, S. Yasui, and A. Hosaka, 2012a, Phys. Rev. D **86**, 117502.

Ohkoda, S., Y. Yamaguchi, S. Yasui, K. Sudoh, and A. Hosaka, 2012b, Phys. Rev. D **86**, 014004.

Ohnishi, S., Y. Ikeda, T. Hyodo, and W. Weise, 2016, Phys. Rev. C **93**, 025207.

Oller, J. A., and U.-G. Meißner, 2001, Phys. Lett. B **500**, 263.

Oller, J. A., E. Oset, and J. R. Peláez, 1998, Phys. Rev. Lett. **80**, 3452.

Oller, J. A., E. Oset, and J. R. Peláez, 1999, Phys. Rev. D **59**, 074001; **75**, 099903(E) (2007).

Oller, J. A., E. Oset, and A. Ramos, 2000, Prog. Part. Nucl. Phys. **45**, 157.

Olsen, S. L., 2015, Front. Phys. **10**, 121.

Olsen, S. L., T. Skwarnicki, and D. Zieminska, 2018, preceding article, Rev. Mod. Phys. **90**, 015003.

Ono, S., A. I. Sanda, N. A. Törnqvist, and J. Lee-Franzini, 1985, Phys. Rev. Lett. **55**, 2938.

Ono, S., and N. A. Törnqvist, 1984, Z. Phys. C **23**, 59.

Ortega, P. G., D. R. Entem, and F. Fernandez, 2013, Phys. Lett. B **718**, 1381.

Ortega, P. G., D. R. Entem, and F. Fernández, 2017, Phys. Lett. B **764**, 207.

Ortega, P. G., J. Segovia, D. R. Entem, and F. Fernandez, 2010, Phys. Rev. D **81**, 054023.

Oset, E., and A. Ramos, 1998, Nucl. Phys. A **635**, 99.

Oset, E., *et al.*, 2016, Int. J. Mod. Phys. E **25**, 1630001.

Ottnad, K., C. Michael, S. Reker, C. Urbach, C. Michael, S. Reker, and C. Urbach (ETM Collaboration), **2012**, J. High Energy Phys. 11, 048.

Owen, B. J., W. Kamleh, D. B. Leinweber, M. S. Mahbub, and B. J. Menadue, 2015, Phys. Rev. D **92**, 034513.

Ozaki, S., and S. Sasaki, 2013, Phys. Rev. D **87**, 014506.

Padmanath, M., C. B. Lang, and S. Prelovsek, 2015, Phys. Rev. D **92**, 034501.

Pakhlov, P., and T. Uglov, 2015, Phys. Lett. B **748**, 183.

Pakhlova, G., *et al.* (Belle Collaboration), 2008, Phys. Rev. Lett. **101**, 172001.

Pakhlova, G., *et al.* (Belle Collaboration), 2009, Phys. Rev. D **80**, 091101.

Pakvasa, S., and M. Suzuki, 2004, Phys. Lett. B **579**, 67.

Patrignani, C., *et al.* (Particle Data Group), 2016, Chin. Phys. C **40**, 100001.

Peláez, J. R., 2004, Phys. Rev. Lett. **92**, 102001.

Peláez, J. R., 2016, Phys. Rep. **658**, 1.

Peláez, J. R., and G. Ríos, 2006, Phys. Rev. Lett. **97**, 242002.

Peláez, J. R., and G. Ríos, 2010, Phys. Rev. D **82**, 114002.

Pennington, M. R., and S. D. Protopopescu, 1973, Phys. Rev. D **7**, 1429.

Pennington, M. R., and D. J. Wilson, 2007, Phys. Rev. D **76**, 077502.

Phillips, D. R., S. R. Beane, and M. C. Birse, 1999, J. Phys. A **32**, 3397.

Pilloni, A., C. Fernandez-Ramirez, A. Jackura, V. Mathieu, M. Mikhasenko, J. Nys, and A. P. Szczepaniak (JPAC Collaboration), 2017, Phys. Lett. B **772**, 200.

Pirjol, D., and T.-M. Yan, 1997, Phys. Rev. D **56**, 5483.

Polejaeva, K., and A. Rusetsky, 2012, Eur. Phys. J. A **48**, 67.

Polosa, A. D., 2015, Phys. Lett. B **746**, 248.

Prelovsek, S., C. B. Lang, L. Leskovec, and D. Mohler, 2015, Phys. Rev. D **91**, 014504.

Prelovsek, S., and L. Leskovec, 2013a, Phys. Rev. Lett. **111**, 192001.

Prelovsek, S., and L. Leskovec, 2013b, Phys. Lett. B **727**, 172.

Qin, W., S.-R. Xue, and Q. Zhao, 2016, Phys. Rev. D **94**, 054035.

Ramos, A., A. Feijoo, and V. K. Magas, 2016, Nucl. Phys. A **954**, 58.

Richard, J.-M., 2016, Few-Body Syst. **57**, 1185.

Roca, L., M. Mai, E. Oset, and U.-G. Meißner, 2015, Eur. Phys. J. C **75**, 218.

Roca, L., J. Nieves, and E. Oset, 2015, Phys. Rev. D **92**, 094003.

Roca, L., and E. Oset, 2013, Phys. Rev. C **87**, 055201.

Roca, L., and E. Oset, 2017, Phys. Rev. C **95**, 065211.

Roca, L., E. Oset, and J. Singh, 2005, Phys. Rev. D **72**, 014002.

Romanets, O., L. Tolos, C. Garcia-Recio, J. Nieves, L. L. Salcedo, and R. G. E. Timmermans, 2012, Phys. Rev. D **85**, 114032.

Rummukainen, K., and S. A. Gottlieb, 1995, Nucl. Phys. B **450**, 397.

Sakitt, M., T. B. Day, R. G. Glasser, N. Seeman, J. H. Friedman, W. E. Humphrey, and R. R. Ross, 1965, Phys. Rev. **139**, B719.

Samart, D., W.-h. Liang, and E. Oset, 2017, Phys. Rev. C **96**, 035202.

Schmid, C., 1967, Phys. Rev. **154**, 1363.

Sekihara, T., 2017, Phys. Rev. C **95**, 025206.

Sekihara, T., T. Hyodo, and D. Jido, 2015, Prog. Theor. Exp. Phys. **2015**, 063D04.

Shen, C. P., *et al.* (Belle Collaboration), 2014, Phys. Rev. D **89**, 072015.

Shen, C.-W., F.-K. Guo, J.-J. Xie, and B.-S. Zou, 2016, Nucl. Phys. A **954**, 393.

Shimizu, Y., D. Suenaga, and M. Harada, 2016, Phys. Rev. D **93**, 114003.

Shultz, C. J., J. J. Dudek, and R. G. Edwards, 2015, Phys. Rev. D **91**, 114501.

Sirunyan, A. M., *et al.* (CMS Collaboration), 2017, arXiv: 1712.06144.

Sjostrand, T., S. Mrenna, and P. Z. Skands, 2008, Comput. Phys. Commun. **178**, 852.

Suganuma, H., K. Tsumura, N. Ishii, and F. Okiharu, 2007, Prog. Theor. Phys. Suppl. **168**, 168.

Sun, Z.-F., J. He, X. Liu, Z.-G. Luo, and S.-L. Zhu, 2011, Phys. Rev. D **84**, 054002.

Sun, Z.-F., X. Liu, M. Nielsen, and S.-L. Zhu, 2012, Phys. Rev. D **85**, 094008.

Sun, Z.-F., Z.-G. Luo, J. He, X. Liu, and S.-L. Zhu, 2012, Chin. Phys. C **36**, 194.

Swanson, E. S., 2004a, Phys. Lett. B **598**, 197.

Swanson, E. S., 2004b, Phys. Lett. B **588**, 189.

Swanson, E. S., 2006, Phys. Rep. **429**, 243.

Swanson, E. S., 2015, Phys. Rev. D **91**, 034009.

Swanson, E. S., 2016, Int. J. Mod. Phys. E **25**, 1642010.

Szczepaniak, A. P., 2003, Phys. Lett. B **567**, 23.

Szczepaniak, A. P., 2015, Phys. Lett. B **747**, 410.

Szczepaniak, A. P., 2016, Phys. Lett. B **757**, 61.

Tamponi, U., *et al.* (Belle Collaboration), 2015, Phys. Rev. Lett. **115**, 142001.

Tawfiq, S., P. J. O'Donnell, and J. G. Korner, 1998, Phys. Rev. D **58**, 054010.

Törnqvist, N. A., 1994, Z. Phys. C **61**, 525.

Törnqvist, N. A., 2003, arXiv:hep-ph/0308277.

Törnqvist, N. A., 2004, Phys. Lett. B **590**, 209.

Torres-Rincon, J. M., L. Tolos, and O. Romanets, 2014, Phys. Rev. D **89**, 074042.

Tovee, D. N., *et al.*, 1971, Nucl. Phys. B **33**, 493.

Tsuchida, Y., and T. Hyodo, 2017, arXiv:1703.02675.

Uglov, T. V., and P. N. Pakhlov, 2016, Yad. Fiz. **79**, 174 [Phys. At. Nucl. **79**, 285 (2016)].

Valderrama, M. P., 2012, Phys. Rev. D **85**, 114037.

van Beveren, E., and G. Rupp, 2003, Phys. Rev. Lett. **91**, 012003.

Van Der Leun, C., and C. Alderliesten, 1982, Nucl. Phys. A **380**, 261.

Voloshin, M. B., 1983, Pisma Zh. Eksp. Teor. Fiz. **37**, 58 [JETP Lett. **37**, 69 (1983)].

Voloshin, M. B., 2004a, Phys. Lett. B **604**, 69.

Voloshin, M. B., 2004b, Phys. Lett. B **579**, 316.

Voloshin, M. B., 2006, Int. J. Mod. Phys. A **21**, 1239.

Voloshin, M. B., 2011, Phys. Rev. D **84**, 031502.

Voloshin, M. B., 2013, Phys. Rev. D **87**, 091501.

Voloshin, M. B., 2016a, Phys. Rev. D **94**, 074042.

Voloshin, M. B., 2016b, Phys. Rev. D **93**, 074011.

Voloshin, M. B., and L. B. Okun, 1976, Pisma Zh. Eksp. Teor. Fiz. **23**, 369 [JETP Lett. **23**, 333 (1976)].

Wang, B.-K., W.-Z. Deng, and X.-L. Chen, 2010, Chin. Phys. C **34**, 1052.

Wang, E., J.-J. Xie, W.-H. Liang, F.-K. Guo, and E. Oset, 2017, Phys. Rev. C **95**, 015205.

Wang, G.-J., L. Ma, X. Liu, and S.-L. Zhu, 2016, Phys. Rev. D **93**, 034031.

Wang, P., and X.-G. Wang, 2013, Phys. Rev. Lett. **111**, 042002.

Wang, Q., 2014, Phys. Rev. D **89**, 114013.

Wang, Q., M. Cleven, F.-K. Guo, C. Hanhart, U.-G. Meißner, X.-G. Wu, and Q. Zhao, 2014, Phys. Rev. D **89**, 034001.

Wang, Q., C. Hanhart, and Q. Zhao, 2013a, Phys. Rev. Lett. **111**, 132003.

Wang, Q., C. Hanhart, and Q. Zhao, 2013b, Phys. Lett. B **725**, 106.

Wang, Q., G. Li, and Q. Zhao, 2012, Phys. Rev. D **85**, 074015.

Wang, Q., X.-H. Liu, and Q. Zhao, 2011, Phys. Rev. D **84**, 014007.

Wang, Q., X.-H. Liu, and Q. Zhao, 2015, Phys. Rev. D **92**, 034022.

Wang, R.-Q., J. Song, K.-J. Sun, L.-W. Chen, G. Li, and F.-L. Shao, 2016, Phys. Rev. C **94**, 044913.

Wang, W., and Q. Zhao, 2016, Phys. Lett. B **755**, 261.

Wang, W. L., F. Huang, Z. Y. Zhang, and B. S. Zou, 2011, Phys. Rev. C **84**, 015203.

Wang, X. L., *et al.* (Belle Collaboration), 2007, Phys. Rev. Lett. **99**, 142002.

Wang, X. L., *et al.* (Belle Collaboration), 2015, Phys. Rev. D **91**, 112007.

Wang, Z.-G., 2014, Eur. Phys. J. C **74**, 2963.

Wang, Z.-G., and T. Huang, 2014, Eur. Phys. J. C **74**, 2891.

Wang, Z.-G., and X.-H. Zhang, 2010a, Eur. Phys. J. C **66**, 419.

Wang, Z.-G., and X.-H. Zhang, 2010b, Commun. Theor. Phys. **54**, 323.

Watson, M. B., M. Ferro-Luzzi, and R. D. Tripp, 1963, Phys. Rev. **131**, 2248.

Weinberg, S., 1963a, Phys. Rev. **130**, 776.

Weinberg, S., 1963b, Phys. Rev. **131**, 440.

Weinberg, S., 1965, Phys. Rev. **137**, B672.

Weinberg, S., 1979, Physica A (Amsterdam) **96**, 327.

Weinstein, J. D., and N. Isgur, 1982, Phys. Rev. Lett. **48**, 659.

Weinstein, J. D., and N. Isgur, 1990, Phys. Rev. D **41**, 2236.

Wiese, U. J., 1989, Nucl. Phys. B, Proc. Suppl. **9**, 609.

Wilbring, E., H.-W. Hammer, and U.-G. Meißner, 2013, Phys. Lett. B **726**, 326.

Wise, M. B., 1992, Phys. Rev. D **45**, R2188.

Wong, C.-Y., 2004, Phys. Rev. C **69**, 055202.

Wu, J.-J., T.-S. H. Lee, A. W. Thomas, and R. D. Young, 2014, Phys. Rev. C **90**, 055206.

Wu, J.-J., X.-H. Liu, Q. Zhao, and B.-S. Zou, 2012, Phys. Rev. Lett. **108**, 081803.

Wu, J.-J., R. Molina, E. Oset, and B. S. Zou, 2010, Phys. Rev. Lett. **105**, 232001.

Wu, J.-J., R. Molina, E. Oset, and B. S. Zou, 2011, Phys. Rev. C **84**, 015202.

Wu, J.-J., Q. Zhao, and B. S. Zou, 2007, Phys. Rev. D **75**, 114012.

Wu, Q., G. Li, F. Shao, Q. Wang, R. Wang, Y. Zhang, and Y. Zheng, 2016, Adv. High Energy Phys. **2016**, 3729050.

Wu, X.-G., C. Hanhart, Q. Wang, and Q. Zhao, 2014, Phys. Rev. D **89**, 054038.

Wu, X.-G., J.-J. Wu, Q. Zhao, and B.-S. Zou, 2013, Phys. Rev. D **87**, 014023.

Wu, X.-G., and Q. Zhao, 2012, Phys. Rev. D **85**, 034040.

Xiao, C. W., 2017, Phys. Rev. D **95**, 014006.

Xiao, C. W., J. Nieves, and E. Oset, 2013, Phys. Rev. D **88**, 056012.

Xiao, C.-W., and U.-G. Meißner, 2015, Phys. Rev. D **92**, 114002.

Xiao, T., S. Dobbs, A. Tomaradze, and K. K. Seth, 2013, Phys. Lett. B **727**, 366.

Xiao, Z., and Z.-Y. Zhou, 2016, Phys. Rev. D **94**, 076006.

Xiao, Z., and Z.-Y. Zhou, 2017a, J. Math. Phys. (N.Y.) **58**, 062110.

Xiao, Z., and Z.-Y. Zhou, 2017b, J. Math. Phys. (N.Y.) **58**, 072102.

Xie, J.-J., L.-S. Geng, and E. Oset, 2017, Phys. Rev. D **95**, 034004.

Yamaguchi, Y., S. Ohkoda, A. Hosaka, T. Hyodo, and S. Yasui, 2015, Phys. Rev. D **91**, 034034.

Yamaguchi, Y., S. Ohkoda, S. Yasui, and A. Hosaka, 2013, Phys. Rev. D **87**, 074019.

Yamaguchi, Y., and E. Santopinto, 2017, Phys. Rev. D **96**, 014018.

Yamazaki, T., K.-i. Ishikawa, Y. Kuramashi, and A. Ukawa, 2012, Phys. Rev. D **86**, 074514.

Yamazaki, T., K.-i. Ishikawa, Y. Kuramashi, and A. Ukawa, 2015, Phys. Rev. D **92**, 014501.

Yan, T.-M., H.-Y. Cheng, C.-Y. Cheung, G.-L. Lin, Y. C. Lin, and H.-L. Yu, 1992, Phys. Rev. D **46**, 1148; **55**, 5851(E) (1997).

Yang, Y., J. Ping, C. Deng, and H.-S. Zong, 2012, J. Phys. G **39**, 105001.

Yang, Y.-B., Y. Chen, L.-C. Gui, C. Liu, Y.-B. Liu, Z. Liu, J.-P. Ma, and J.-B. Zhang (CLQCD Collaboration), 2013, Phys. Rev. D **87**, 014501.

Yang, Y.-C., Z.-Y. Tan, J. Ping, and H.-S. Zong, 2017, arXiv:1703.09718.

Yang, Z., Q. Wang, and U.-G. Meißner, 2017, Phys. Lett. B **767**, 470.

Yang, Z.-C., Z.-F. Sun, J. He, X. Liu, and S.-L. Zhu, 2012, Chin. Phys. C **36**, 6.

Yuan, C. Z., *et al.* (Belle Collaboration), 2007, Phys. Rev. Lett. **99**, 182004.

Yuan, C. Z., *et al.* (Belle Collaboration), 2008, Phys. Rev. D **77**, 011105.

Yuan, C.-Z., 2014, Chin. Phys. C **38**, 043001.

Yuan, C.-Z., 2017, "e^+e^- annihilation cross section measurements at besiii," Talk given for the BESIII Collaboration at the 10th workshop of the France China Particle Physics Laboratory, Tsinghua University, Beijing, China.

Zhang, J.-R., 2013, Phys. Rev. D **87**, 116004.

Zhang, J.-R., 2014, Phys. Rev. D **89**, 096006.

Zhang, J.-R., and M.-Q. Huang, 2009, Phys. Rev. D **80**, 056004.

Zhang, J.-R., M. Zhong, and M.-Q. Huang, 2011, Phys. Lett. B **704**, 312.

Zhang, O., C. Meng, and H.-Q. Zheng, 2009, Phys. Lett. B **680**, 453.

Zhang, Y.-J., H.-C. Chiang, P.-N. Shen, and B.-S. Zou, 2006, Phys. Rev. D **74**, 014013.

Zhang, Y.-J., G. Li, and Q. Zhao, 2009, Phys. Rev. Lett. **102**, 172001.

Zhang, Y.-J., and Q. Zhao, 2010, Phys. Rev. D **81**, 074016.

Zhao, L., H. Huang, and J. Ping, 2017, Eur. Phys. J. A **53**, 28.

Zhao, L., L. Ma, and S.-L. Zhu, 2014, Phys. Rev. D **89**, 094026.

Zhao, Q., 2017, JPS Conf. Proc. **13**, 010008.

Zhong, X.-H., and Q. Zhao, 2008, Phys. Rev. D **77**, 074008.

Zhou, H.-Y., and Y.-P. Kuang, 1991, Phys. Rev. D **44**, 756.

Zhou, Z.-Y., and Z. Xiao, 2014, Eur. Phys. J. A **50**, 165.

Zhou, Z.-Y., and Z. Xiao, 2015, Phys. Rev. D **92**, 094024.

Zhou, Z.-Y., and Z. Xiao, 2017, Phys. Rev. D **96**, 054031; **96**, 099905 (E) (2017).

Zhu, S.-L., 2000, Phys. Rev. D **61**, 114019.

Zou, B. S., 2008, Eur. Phys. J. A **35**, 325.

Zychor, I., *et al.*, 2008, Phys. Lett. B **660**, 167.